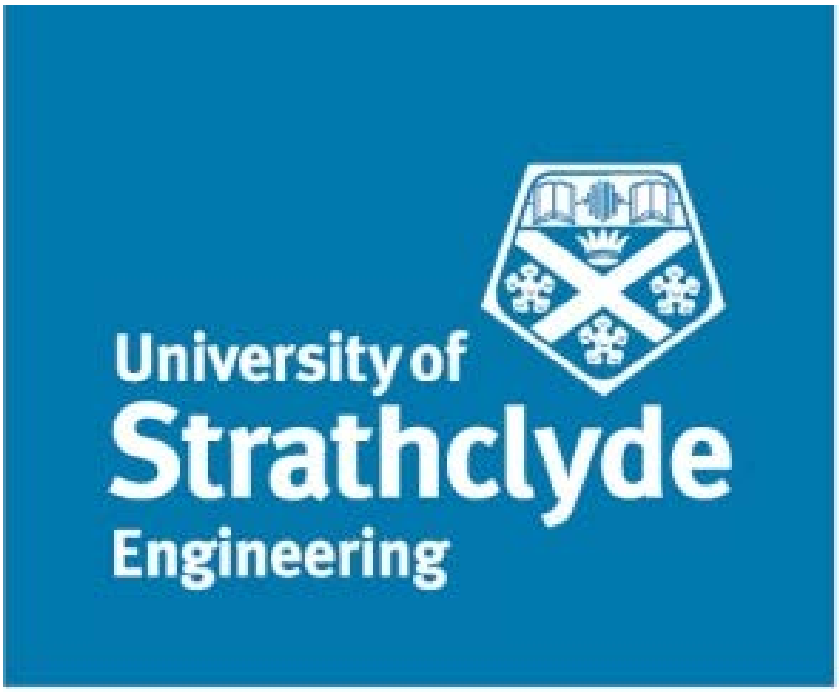

University of Strathclyde

Department of Chemical and Process Engineering

Developing Materials and Methods for Remediation of Metaldehyde from Drinking Water

Bing Tao

A thesis presented in fulfilment of the requirements for the degree of Doctor of Philosophy

2014

Declaration of Author Rights

This thesis is the result of the author's original research. It has been composed by the author and has not been previously submitted for examination which has led to the award of a degree.

Signed:

Date:

Dedication

This dissertation is dedicated to my daughter,

Zixin (Jasmine) Tao,

for inspiring and amazing me every day.

Acknowledgement

I would like to express my deepest appreciation to my principal supervisor Dr. Ashleigh J. Fletcher for her guidance and support throughout the project. She always made herself available for enlightening discussions when I needed help. Without her persistent help, this dissertation would not have been possible. Her influence on me is not only limited to academic aspects, but also her attitude to life and to people enlightens me all the time. I could not have imaged having a better mentor for my Ph.D project.

My sincerer gratitude also goes to Prof. Carl Schaschke for his continuous support and help for the whole duration. His good advice and help have been invaluable, for which I am extremely grateful.

Thanks are given to the technical staff: Mr. J. Murphy, Mr. I. Airdrie, Mr. S. Adams and Mr. L. Allan, at the Department of Chemical and Process Engineering. I also thank the departmental secretary staff: Mrs C. Rashid, Miss T.Knight, Miss M. O'Donnell and Miss L. Kane; and the IT support, Mr. M. Kidd.

Thank Department of Chemical and Process Engineering of University of Strathclyde and China Scholarship Council (CSC) for financial support.

I would like to acknowledge my fellow Ph.D students and friends I shared time with at the department. Thanks to Yuchen, Lei, Chris, Tiger, SherLeen, Ese, Stewart, Vitor and Claudia for making the last three years enjoyable.

I would also like to express my gratitude to the thesis examiners, Prof. Paul Younger and Dr. Lorraine Gibson, for their constructive advice on this thesis and very generous help.

Finally, I would like to thank my parents and my wife for their support and patience over the years. You are always my purpose and motivation.

Table of Contents

List of Figures

List of Tables

Abstract

Metaldehyde contamination of drinking water across the United Kingdom has raised extensive public attention since 2007. There is still no effective solution for this issue, despite all of the steps taken by different concerned parties. The proposed methods of removing metaldehyde either suffer from prohibitive energy costs and/or the by-product issue. In this project, adsorption, ion-exchange and heterogeneous catalysis were evaluated and employed to address the metaldehyde contamination issue.

Detailed investigation of metaldehyde sorption onto different activated carbons showed that the low adsorption capacity and high leaching tendency are the main reasons why the current method employed in water treatment works failed. The detailed investigation of metaldehyde removal by granular activated carbon (GAC), MN200 and S957 confirmed that strong acid functionalities (e.g. sulfonic acid) are desirable for metaldehyde removal. The non-functionalised MN200 or GAC both suffered high leaching tendency, which is the result of weak affinity between adsorbent and metaldehyde. The sulfonic and phosphonic acid functionalised S957 was showed to exhibit high adsorption capacity and no leaching at all, except suffering poor kinetics.

Sulfonic acid functionalised silica samples (SA-SBA-15) were synthesised to improve the kinetic performance. The nuclear magnetic resonance (NMR) study indicated that the mechanism of sulfonic acid functionality removing metaldehyde is a heterogeneous catalysis process, and acetaldehyde is the only by-product, with further confirmation by quantification study.

A variety of polymeric Macronets with tuneable sulfonic acid functionality and porosity were manufactured to optimize the materials development. Results showed that sample MN502 exhibits the best degrading performance and is also the most cost-effective one. Therefore, a novel dual-stage method was developed using MN502 as a heterogeneous catalyst to degrade metaldehyde into acetaldehyde. Experimental

demonstrations showed that acetaldehyde can be completely removed by amine functionalised ion-exchanger A830. The bench-scale column tests using both synthetic and real surface water confirmed that the developed dual-stage method is promising and of practical interest since it can adapt the current facilities in water treatment works, making the actual application easy to employ, and most importantly very cost-effective.

Chapter 1 Introduction

1.1 Emerging Contaminants in Drinking Water

Water is essential to life; 70% of the Earth is covered by water yet in 2002 more than 17% of the global population did not have access to safe and clean drinking water (L.S. Pereira, Ian Cordery et al. 2009) and the number of people lacking quality drinking water is expected to increase substantially with an ever increasing global population. Infectious waterborne diseases, such as cholera, typhoid fever and Legionellosis, are the main causes of death in children under five years old. It is a sobering statistic that ,according the World Health Organization (WHO), every year, the worldwide number of people dying from unsafe water exceeds that from all kinds of violence, including war (World Health Organization 2002). WHO propound that every person is entitled to access to safe and clean drinking water, since it is a basic need for human development, health and wellbeing.

Besides the uneven distribution of water resources across the globe, water pollution is also a major reason why hundreds of millions of people suffer from unavailability of quality drinking water. Every day, 2 million tonnes of sewage, and industrial and agriculture wastes are discharged into the world's water bodies (United Nations World Water Assessment Program 2003). The United Nations estimates that the amount of waste water produced annually is ~1,500 km^3, equivalent to more than six times the volume of water within all the rivers of the world (United Nations World Water Assessment Program 2003). The uneven distribution of water resources across the world is a natural occurrence which cannot be changed, yet the remediation of wastewater or sea water offers an excellent approach to combat the lack of availability as a consequence of water contamination. For example, electrodialysis of seawater produces clean potable water and brine, which is a notable industry. Most importantly,

quality water resource management and protection polices combined with high standards of water treatment processes should be engaged to achieve water reclamation from polluted waters. According to WHO and European water regulations, it is essential that available water should be properly treated and delivered before human consumption. Advances in water treatment technology have contributed significantly to remediation of contaminated water; for example, the emergence of water treatment technologies like activated sludge, adsorption, ion-exchange, membrane technology and advanced oxidation processes have seen large quantities of polluted supplies being treated to clean and safe potable water.

The term ‘emerging water contaminants’ generally refers to compounds that previously have not been considered or recognized as water contaminants, but are nowadays widely detected with the potential to cause known or suspected adverse ecological or human health effects (Stuart, Lapworth et al. 2012). There are many reasons for the detection of emerging contaminants: firstly, synthesis of new chemicals and changes in the use of existing chemicals creates new sources of contamination, for example, many compounds that are the main ingredients of personal care products, pharmaceuticals and cosmetics have been detected in recent years, including sex hormones (e.g. estrogens), veterinary and human antibiotics (e.g. ciprofloxacin) and prescription/nonprescription drugs (e.g. ibuprofen and salicylic acid); secondly, emerging contaminants also include substances that have existed in water for a long time but whose presence and significance are only now being recognized (Daughton 2004). Advancements in analytical technologies have revealed some contaminants whose concentration in water was previously too low to be detected, for instance, metaldehyde has existed in water sources for a significant period of time but its detection has only been reported since 2008, due to advancements in solid phase extraction and chromatography coupled mass spectrometric detection technologies (GC/HPLC-MS) (UK Environmetal Agency 2009; Richardson and Ternes 2011).

Emerging water contaminants are commonly derived from various municipal,

industrial and agricultural sources and pathways (Stuart, Lapworth et al. 2012) and there are many other currently unidentified compounds that escape detection as a result of existing analytical techniques; for instance, it is suggested that chlorinated solvent contamination has not been recognized historically due to a lack of technical paradigms relating the process of contamination and the identification of adverse effects (Jackson 2004).

Water regulations are of significant importance in terms of alleviating emerging water contaminants; and it is expected that the number of regulated contaminants will keep growing in future years (Stuart, Lapworth et al. 2012). In Europe, groundwater quality is currently regulated under the Water Framework Directives (European Commision 2000), groundwater under the Groundwater Daughter Directives (European Commision 2006) and Drinking Water under the Drinking Water Directives (European Commision 1998). Additionally, regulation may exist at a European level, for example several organic contaminants, including polycyclic aromatic hydrocarbons, chlorinated solvents and disinfection by-products, are regulated by the European Drinking Water Directives (European Commision 1998).

1.2 Classes of Emerging Contaminants

1.2.1 Pesticides

Pesticide pollution can be traced back decades with those pesticides posing the greatest threat to ecological and human health being banned, for instance, atrazine in 1993. Recently, the advancement of analytical techniques has allowed the identification of a number of pesticide compounds as present pollutants, for example, metaldehyde (UK Environmetal Agency 2009; Bristol Water 2013; Marshall 2013; MSG 2014), and this is compounded by the attention given, not only to the pesticide, but also to the related metabolites and degradates. In some cases, the concentrations of the metabolites detected in water are even higher than the parent pesticides with some

metabolites also determined to be more toxic than the parent compound (Kolpin, Thurman et al. 1998). These developments have prompted increased interest from researchers, including studies on the occurrence, source, fate and effects of pesticides in water (Pal, Gin et al. 2010).

1.2.2 Pharmaceuticals

The presence, and detection, of pharmaceutical chemicals in water has also been reported for a long time (Richardson and Bowron 1985; Halling-Sørensen, Nors Nielsen et al. 1998). The pathways by which these compounds enter water bodies include human excretion, inappropriate disposal of used products, and via agricultural usage. There are a variety of pharmaceutical compounds showing spikes in natural waters, including human antibiotics (e.g. tetracycline, erythromycin) and prescription and non-prescription drugs (e.g. codeine, salbutamol) (Stuart, Lapworth et al. 2012). In recent years, some researchers have reported the detection of drugs used in cancer treatment, such as 5-fluororcil and ifosfamide (Buerge, Buser et al. 2006; Johnson, Jürgens et al. 2008).

1.2.3 Personal Care and Life-style Products

The most common compounds associated with our consumerist daily life are caffeine and nicotine; while these compounds are presumed to be nontoxic, their metabolites are raising concerns (Seiler, Zaugg et al. 1999). For, example, cotinine, the metabolite of nicotine is widely detected in groundwater, while the compound triclosan, extensively used in toothpaste, soap and other household products, has been detected, along with its metabolite methyl triclosan, in surface water in Switzerland and these compounds are considered to be persistent (Lindström, Buerge et al. 2002).

1.2.4 Industrial Additives and By-products

There are a variety of organic compounds associated with global industries, including industrial additives and by-products. A number of these compounds have previously been considered as emerging contaminants, however, their now well-established associated issues have resulted in their re-classification as priority contaminants, and this category includes polycyclic aromatic hydrocarbons from the petroleum industry. Although these compounds are not considered emerging contaminants anymore, their metabolites or breakdown products may be considered as emergent (Stuart, Lapworth et al. 2012).

1.2.6 Disinfection By-products in Water Treatment

Disinfection by-products in water treatment processes refers to the compounds formed via the reaction of disinfectants (i.e. chlorine, chloramines, ozone, chlorine dioxide, *etc*.) with natural organic matters, and bromide, in source waters (Richardson and Ternes 2011). Disinfectants can also react with other organic contaminants, such as food additives, which are not toxic themselves, but the resulting by-products could be carcinogenic and/or toxic. This can be best illustrated by considering that high levels of N-nitrosodimethylamine have been detected in drinking water, where it is formed by the reaction between ozone and a fungicide widely used in Europe (Richardson and Ternes 2005). A recent review reported that more than 600 disinfection by-products have been identified in water supplies (Richardson 2011).

1.2.7 Hormones and Sterols

Sex hormones include androgens and estrogens which have subsets of androstenedione and testosterone for androgens, estrogens, oestrone and oestriol for estrogens. In addition to natural hormones, synthetic hormones such as 17α-ethinyl oestra-

diol and diethylstilbestrol have been used extensively as contraceptives. In recent years, both natural and synthetic compounds have been detected in natural waters (Standley, Rudel et al. 2008; Vulliet and Cren-Olivé 2011), with a recent study reporting that 11 out of 26 hormones were detected in water samples with contamination levels of 0.1 to a few ppb(Vulliet and Cren-Olivé 2011). Again, the metabolites or biodegradation by-products of some of these steroids are causing increasing concern.

1.3 Metaldehyde Contamination in Drinking Water

1.3.1 General Information for Metaldehyde

Metaldehyde is the tetramer of acetaldehyde, with IUPAC name r-2,c-4,c-6,c-8-tetramethyl-1,3,5,7-tetroxocane. Its solubility in water is approximately 200 mg/L at 20 °C and it is highly soluble in organic solvents, for instance its solubility in methanol is 1.73 g/L. The pure tetramer has the physical appearance of a colorless crystal powder; it is tasteless with a characteristically unpleasant odour similar to formaldehyde. The general properties of metaldehyde are summarised in Table 1.1. It is primarily used as a molluscicide to control slugs and snails but is also sometimes used to control fish, leeches and frogs (Organization 1996).

Figure 1.1a shows the structural formula of metaldehyde. Pure metaldehyde forms colorless crystals, which are easy to fracture such that it exhibits a powdery appearance. Research has demonstrated that metaldehyde molecules are hydrogen bonded to each other (Barnett, Hulme et al. 2005), as shown in Figure 1.1b; the four hydrogen atoms in each metaldehyde molecule can connect to four other metaldehyde molecules, bringing about the 3-dimensional structural stack. Figure 1.1c displays the hydrogen bonding in a 3-dimensional style with a view along the *a* axis.

Table 1.1 General information for metaldehyde

Molecular Formula	$C_8H_{16}O_4$
Molecular mass	176.21 g mol^{-1}
IUPAC name	2, 4, 6, 8-tetramethyl-1, 3, 5, 7-tetroxocane
Synonym	Acetaldehyde tetramer
Solubility	213 mg L^{-1}(25 °C in water) (University of Hertfordshire 2012) 1730 mg L^{-1} (20 °C in methanol) (University of Hertfordshire 2012)
Appearance	White or colourless crystalline solid
Uses	Used as a molluscicide bait to control slugs and snails
Toxicity	Moderately toxic, kidney and liver toxicant (University of Hertfordshire 2012)

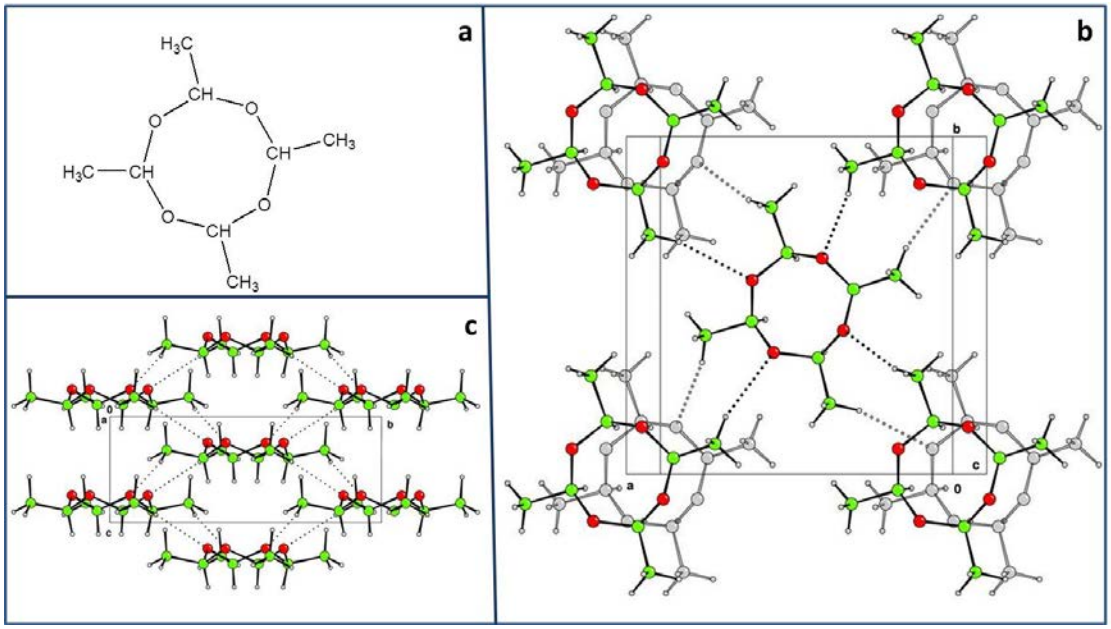

Figure 1.1 a): The structure of a single molecule of metaldehyde; b): A 2D c axis inclined view of metaldehyde molecules and the hydrogen bonding between them. The grey molecules are one unit cell lower than the colour ones. The dotted lines represent the hydrogen bonding, courtesy from Acta Crystallographica (Barnett, Hulme et al. 2005). c): A 3D view along the a axis, courtesy from Acta Crystallographica (Barnett, Hulme et al. 2005).

1.3.2 Toxicity of Metaldehyde

Metaldehyde is widely used as a selective molluscicide for the control of slugs and snails by farmers and gardeners across the world. The concentration of metaldehyde is usually 4% or less in commercial products, including liquids, powders and pellets, traded under a variety of commercial names, including Antimilice, Ariotox, Cekumeta, Meta, Metason, Deadline, Slug-death, Slug-Tox, *etc.*(Organization 1996). Metaldehyde is normally absorbed from the gastrointestinal tract but can be absorbed through the skin or lungs as well. Toxic effects extend to domestic animals, such as dogs and horses, and animals that ingest metaldehyde can suffer from vomiting, tachycardia and seizures, sometimes resulting in death (Dolder 2003).

Unfortunately, metaldehyde is easily ingested by dogs and horses; the oral LD_{50} of metaldehyde is 100 mg/kg in dogs and 60 mg/kg in horses (Dolder 2003) and it is recommended that decontamination need to be undertaken if any dose > 2 mg/kg occurs in animals. As a result, there are many instances of dog and horse intoxication by metaldehyde (Richardson, Welch et al. 2003; Steenbergen 2004; Gupta 2007; Sperling, Schoenfelder et al. 2010; Nolte 2012).

Since metaldehyde is classified as moderately toxic, and as little information about the effects on human health is available, several incidents of metaldehyde exposure have been reported, with the majority of these incidents resulting from erroneous ingestion of slug bait by children. Incidents of human poisoning, associated with the voluntary ingestion of tablets for use as a fuel, have been reported, where symptoms took a few hours to be observed, with survivors showing loss of memory up to a year later (Organization 1996).

1.3.3 Metaldehyde Contamination

Metaldehyde contamination of drinking water supplies was first reported in England in 2007; after this first detection, measurements of water catchments were per-

formed across the U.K., and the results showed that in 2008 and 2009, metaldehyde contamination levels were as high as four times those permitted by U.K. and E.U. regulations (Edwards 2010). The maximum concentration of metaldehyde in drinking water is regulated as 0.1 μg/L (ppb), according to water regulations in both the E.U. (The Council of The European Union 1998) and U.K. (Water England and Wales 2000). In 2008, 16 out of 22 water samples from the Forehill Water Treatment Works exceeded the limit of 0.1 ppb and, in 2009, another 26 of 70 water catchments breached the threshold value (Edwards 2010). In 2010, more water companies in the Midlands, Eastern, South East and South of England detected high levels of metaldehyde in raw waters, reaching levels as high as 1 ppb, i.e. ten times higher than the permitted value. Although many breaches have occurred since 2007, metaldehyde contamination was worst in 2012, as a result of the unseasonably dry spring and the subsequent over-application of pesticides to control the explosion in slug populations. This was exacerbated by the subsequent exceptionally wet summer and autumn, which increased the wash-off of metaldehyde into water streams (Marshall 2013).

With regard to the presence of metaldehyde in U.K. water supplies, various steps have been taken by the Environment Agency, Water companies, metaldehyde manufacturers, farmers and researchers in academia, with an aim to alleviate the problem. Water companies, such as Bristol Water, launched campaigns to raise public awareness and provide water consumers with up to date information. The *Metaldehyde Action Project* launched by Bristol Water monitors the metaldehyde concentration in their water supplies and frequently updates users (Bristol Water 2013). Severn Trent Water has funded research at Cranfield University into the feasibility of new technologies, such as advanced oxidation processes.

Besides the water companies, the water regulation authorities, metaldehyde manufacturers and farmers have taken part in this campaign to control metaldehyde levels. The Metaldehyde Stewardship Group, formed by metaldehyde manufacturers including Lonza, Certis, Chiltern Farm Chemicals, Des Sangosse, Doff Portland, Frunol

Delica and Makhteshim Agan (U.K.), aims to promote and encourage best practice with metaldehyde slug pellets to optimise the usage of metaldehyde pellets and minimise impacts on water quality (MSG 2014). The primary method of *Get Pelletwise* practice is to raise awareness of metaldehyde use to farmers and promote the accurate dose rates. They provide professional guidelines and machinery to achieve the goal. The effort has obvious effects, such as the determination of a maximum dosage, set at 700 g/ha (MSG 2014). Before this, there was no guideline for the accurate dosage for slug control using metaldehyde such that when slugs and snails prevailed in crops, farmers tended to use large excess of metaldehyde.

U.K. Water has also contributed to this practice. They proposed that alternative chemicals should be applied to protect crops from slugs and snails, for example, ferric phosphate based products including Sluxx or Derrex. U.K. agriculture could not switch completely to ferric phosphate though, as global supplies are insufficient to meet the demand that would be created. The combination of ferric phosphate products and metaldehyde can reduce the dosage of metaldehyde, thus alleviating the metaldehyde contamination issue (Bristol Water 2013).

1.4 Removal of Metaldehyde by Water Treatment Methods - Literature Review

The detection of metaldehyde in drinking water indicates that current methods applied in the water treatment industry, i.e. Granular Activated Carbon (GAC) beds, are not working. In 2010, there were 1103 water samples that failed to meet the drinking water standards in England and Wales, and more than 368 failures were caused by high levels of metaldehyde (Autin, Hart et al. 2012). An investigation into GAC adsorption of metaldehyde demonstrated that GAC has high initial adsorptive capacities while beds exhausted quickly. Research conducted by the Water Research centre (WRc) showed that a virgin GAC bed lasted only 44 days before metalde-

hyde breakthrough (reaching 0.1 ppb) (Hall 2010 March 23rd). Another concern for metaldehyde removal by GAC is that, although GAC can lower the concentration of metaldehyde in water, it can only remove approximately 30-50% of the total metaldehyde, which means that water streams with metaldehyde contamination levels > 0.15 ppb, even if treated, will definitely exceed the threshold of 0.1 ppb (Hall 2011 June 7-8th). Hence, alternative methods are urgently required to address metaldehyde contamination.

Cranfield University have been using advanced oxidation processes (AOP) to remove metaldehyde from drinking water (Autin, Hart et al. 2012; Autin, Hart et al. 2013; Autin, Hart et al. 2013); AOP comprise a category of destructive reaction processes, which have demonstrated promise for the removal of micro pollutants. One sub-category of AOP is UV irradiation to activate a variety of different chemicals to generate highly reactive hydroxyl radicals (• OH). These compounds include H_2O_2, TiO_2 and H_2O_2/ Fe^{3+} (Evgenidou and Fytianos 2002; Thomson, Roddick et al. 2002; Sharpless and Linden 2003; Parsons 2004; Toepfer, Gora et al. 2006; Sanches, Barreto Crespo et al. 2010). The group evaluated the feasibility of AOP for metaldehyde removal and the data showed that UV coupled with H_2O_2 is more effective than UV coupled with TiO_2, although large quantities of H_2O_2 are required to make this method work, since irradiation at 254 nm UV light does not activate H_2O_2 effectively (Autin, Hart et al. 2012; Autin, Hart et al. 2013). Furthermore, they evaluated the influence of competing organic substances on the performance of UV/H_2O_2 and UV/TiO_2. Their findings showed that hydrophobic matters had greater inhibitory effect than hydrophilic matters (Autin, Hart et al. 2013). Although it is was shown that AOP can remove metaldehyde from water, there are some serious issues to be addressed before it can be employed in water treatment works, for example the studies on AOP do not mention products or by-products of the processes. In recent years, disinfection by-products of ozone or chlorine treatment processes have raised severe concerns; hence, there is a possibility that the proposed AOP could generate toxic

by-products. It is also worth noting that this AOP method is prohibitively expensive at practicable scales, as acknowledged by the authors. Until the next generation of UV light source is developed, allowing very high UV doses to be delivered cost-effectively, the practical use of UV/H_2O_2 for the removal of metaldehyde is not realistic (Autin, Hart et al. 2012; Autin, Hart et al. 2013; Autin, Hart et al. 2013).

Researchers in University College London have also considered the feasibility of photocatalytic processes to remove metaldehyde. Nano-sized zinc oxide composites couple with UV were used to catalytically remove metaldehyde. The results showed that the method had some removal performance but similarly to AOP, the method suffers from the issues of low efficiency and high cost, as well as the fact that the mass production of nano-sized zinc oxide composites is a challenge that would have to be overcome before this method could be practically employed (Doria, Borges et al. 2013).

1.5 Project Objectives

The methods review detailed in this chapter illustrates that there is no effective and practicable method of water treatment available to address the current metaldehyde contamination issue. In tandem with this, steps taken by the Government and manufacturers showed that there was also no significant improvement achieved for management and regulation. There is, therefore, an urgent need to develop alternative water treatment methods which are efficient, cost-effective and practical to employ.

The main objective of this project is to develop and optimise materials and methods for the removal of metaldehyde from drinking water, where the developed method should be cost-effective and easy to put into practice.

To achieve the main objective, several key aims have been identified:

- To understand the reason why current methods fail: although research has shown that GAC had initial high performance, the bed exhausted rather quickly, and there is no detailed explanation for this failure. It is impractical

to develop alternative novel methods or materials without first understanding the exact reasons for previous failures. In order to determine the reason for GAC failure, detailed adsorption measurements for metaldehyde on GAC should be investigated, including determination of adsorption kinetics, adsorption capacities, adsorption mechanisms and, most importantly, leaching tendencies.

- To investigate the desirable characteristics of prospective materials. These characteristics include the porosity of the materials, surface area, pore volume, pore size distribution, and surface functionalities.
- To synthesise, optimise and evaluate novel materials for their performance in removing metaldehyde, according to the research findings of what are determined as desirable materials properties.
- To develop and optimise novel methods based on the optimal materials developed above. The developed method should be employed to remove metaldehyde from drinking water, using both batch and fixed-bed reactors. The impact of competing substances present in real water supplies should be investigated. This means that the developed fixed-bed reactor should be tested using real water samples.

Chapter 2 Principles of Liquid Phase Adsorption, Ion-Exchange and Heterogeneous Catalysis

2.1 Adsorption

Adsorption is the concentration of one, or more, species at an interfacial layer, involving intermolecular forces or even the formal attachment of molecules or particles to a surface. The application of adsorption dates back to as early as 1500BC, in Egypt, when charcoal was used to adsorb odorous vapours from putrefying wounds and from within the intestinal tract (Parsons and Jefferson 2006). Liquid phase adsorption processes involve the separation of a substance from a solution and its concentration at the surface of a solid material. The substance adsorbed onto the surface is termed an adsorbate (or solute) and the solid material is termed an adsorbent. An adsorbate may be any particle that has attraction for an adsorbent, such as macromolecules, virus, bacteria, colloidal particles, *etc*. An adsorbent may be any solid material which provides bonding sites. In fact, almost any solid substance can act as an adsorbent; the best-known and mostly used commercial adsorbent is activated carbon (AC) (Hendricks 2011).

The adsorption of organic molecules onto adsorbents usually occurs in four steps. Initially, the solute diffuses from the bulk liquid phase to the liquid film surrounding the adsorbent; secondly, the adsorbate diffuses through the liquid film surrounding the adsorbent particle to the interstitial pores (also known as film diffusion or external diffusion); thirdly, the adsorbate travels through the porous network of the adsorbent (also called particle diffusion or internal diffusion) before eventually, adsorbing onto the adsorbent.

Adsorption of organic solutes from aqueous phases is a very important applica-

tion of AC. It has been widely used in drinking water and waste water treatments as well as in the food, beverage, pharmaceutical and chemical industries. AC adsorption has been cited by the US Environmental Protection Agency as one of the best available environmental control technologies. In spite of the large market for AC, the specific mechanisms by which the adsorption of many compounds, especially organic species, occurs are still ambiguous, mainly due to the fact that liquid-phase adsorption is a more complicated process than gas or vapour-phase adsorption. The main differences between adsorption from gas and liquid phases are as follows (Moreno-Castilla 2004):

(i). A solution is typically a system of more than one component. In real cases, there are at least two substances that can adsorb. For a dilute solution, adsorption of one type of molecule (say A) involves replacement of the other (B). Thus, adsorption from solution is essentially an exchange process, hence, molecules adsorb not only because they are attracted by solids but also because the solution may reject them. A typical illustration is that the attachment of hydrophobic molecules on hydrophobic adsorbents from aqueous solutions is mainly driven by their dislike of water and not by their attraction to the surface.

(ii). Multilayer adsorption from solution is less common than from the gas phase, because of the stronger screening interaction forces in condensed fluids.

(iii). Isotherms from solution may exhibit non-ideality, not only because of lateral interactions between adsorbed molecules but also because of non-ideality in the solution.

2.1.1 Types of Adsorption and Intermolecular Forces

Adsorption can be classified as either a physical or chemical process. In physical adsorption (physisorption), solutes are held on the adsorbent surface by weak forces,

such as London dispersion or van der Waals forces, resulting from induced dipole-dipole interactions, or may be dependent on the physical configuration of the adsorbent such as the porosity of ACs. Dispersion forces are the result of rapid fluctuations in the electronic density of one adsorbent molecule inducing an electrical moment in a second atom (Gregg and Sing 1982). If the adsorbate possesses a permanent dipole, or even a multipole, then additional interactions may occur, as charge distributions are induced in the adsorbent and interactions of these moments with any permanent field of the solid. During physisorption, there is no significant redistribution of electron density in either the molecule or at the adsorbent surface and no chemical bonds are formed; the process being a very general one and analogous with that of condensation. Physisorption occurs to varying extents for all adsorbates, solutes, gases and vapours, with all adsorbing solids and the effect increases with decreasing temperature, as it is an exothermic process, or increasing pressure, i.e. increasing chemical potential. Physical adsorption is based on certain basic considerations and adsorption on a heterogeneous surface, that is a surface on which the sites are different, occurs at the sites of highest adsorption potential.

In chemical adsorption (chemisorption) the transfer of electrons usually occurs between adsorbent and adsorbate with the formation of chemical bonds by reaction between the two species, which results in adhesion of the adsorbate molecules. The nature of these bonds may be completely ionic, completely covalent or lie anywhere between these two extremes. Chemical adsorption is far less common than physical adsorption, requiring the capacity for chemical bonds to be formed, and, due to the chemical bonds formed, regeneration of the adsorbent for subsequent reuse is often difficult or impossible, and desorption of the adsorbed phase may yield products that are chemically different to the original adsorbate. For example oxygen may chemically bond to the surface of a carbon; forming only a monolayer of oxygen atoms on the exposed carbon surface, which upon desorption may evolve CO and CO_2 as products. Table 2.1 summarises the main differences between physi- and chemisorp-

tion.

Table 2.1 Characteristics associated with physical and chemical adsorption (Atkins and Paula 2009).

	Physical Adsorption	Chemical Adsorption
Heat of Adsorption ($kJmol^{-1}$)	20 - 40	> 80
Rate of Adsorption (at 273K)	Fast	Slow
Temp. Dependence of Uptake	Decreases with increasing T.	Increases with increasing T.
Desorption	Easy	Difficult
Desorbed Species	Adsorbate unchanged	Unchanged or Changed
Specificity	Non-specific	Very Specific
Monolayer Coverage	Monolayer or Multilayer	Monolayer

2.1.2 Adsorption Equilibria

Adsorption from aqueous solution involves concentration of a solute on a solid surface. The adsorbed solute then tends to desorb back into the solution, thus the adsorption and desorption processes proceed in tandem. Eventually, equal amounts of solute are adsorbed and desorbed simultaneously, hence the rates of adsorption and desorption attain an equilibrium state, called the *adsorption equilibrium*. At equilibrium, no change is observed in the concentration of solute on the solid surface or in the bulk solution. The position of the equilibrium is characteristic of the entire system, the solute, adsorbent, temperature, pH, *etc*. The adsorbed amounts of solute at equilibrium state usually increase with an increase in initial solution concentration. At constant temperature, the presentation of amount of solute adsorbed per unit of ad-

sorbent as a function of equilibrium concentration in bulk solution is defined as an *adsorption isotherm*.

All adsorption isotherms should fit at least one, or a combination of two or more, of the six recognised types as classified by the Brunauer, Deming, Deming and Teller (Brunauer, Deming et al. 1940) (B.D.D.T. system). Figure 2.1 shows expected profiles for the six types and the inference which may be subsequently drawn from each is outlined below:

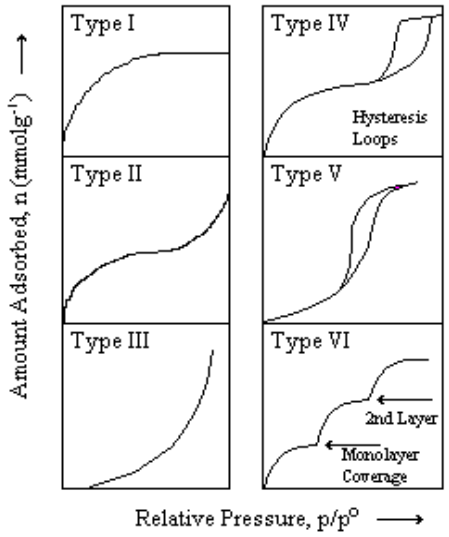

Figure 2.1 Typical shapes of isotherms for adsorption. Reproduced from Brunauer et al.(Brunauer, Deming et al. 1940) Courtesy of American Chemical Society.

Type I isotherms are associated with systems where adsorption does not proceed beyond a monomolecular layer; by contrast all other isotherm types involve multilayer formation. For gas/vapour adsorption systems, these isotherms are typical of adsorbents with predominantly microporous structures, as the majority of micropore filling will occur at relative pressures below 0.1. The adsorption process is usually complete at a partial pressure of ~0.5. Examples include adsorption of nitrogen on carbon at -193 ^{o}C and ammonia on charcoal at 0 ^{o}C. In the case of adsorption from an aqueous phase, the adsorption isotherms mostly follow a *Type I isotherm*, although under certain conditions multilayer adsorption may be encountered.

Normally, the surface of an adsorbent is heterogeneous, not only in surface structure but also in the distribution of surface energy; the heat of adsorption is, therefore, not constant for each incremental increase in uptake. Usually the initial uptakes of adsorbate show greater differential heats of adsorption than those at higher chemical potential. Hence, a steep initial drop in heat of adsorption occurs when the first molecules to arrive at the bare surface are preferentially adsorbed on the most attractive sites or on positions on the surface where their potential energy will be a minimum. As adsorption proceeds, the less active sites eventually become occupied, therefore, smooth adsorption isotherms are usually obtained for adsorption of solutes from liquid phase due to the presence of a sufficiently large numbers of sites that may occur in patches of equal energy or randomly distributed sites of unequal energy(Young and A.D.Crowell 1962). Consequently, several adsorption models can be used for the description of liquid phase adsorption data, which are shown in Figure 2.2, of which Langmuir and Freundlich adsorption isotherms are the most commonly used.

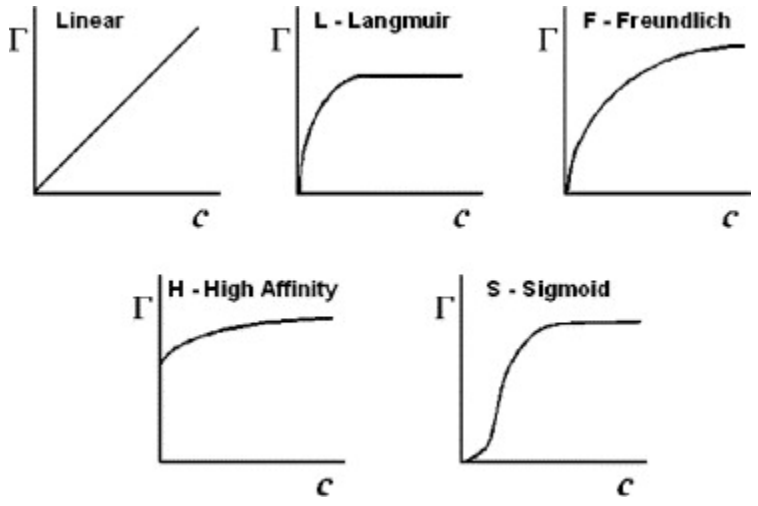

Figure 2.2 Most common adsorption isotherms found from aqueous solution on carbon materials. Reproduced from Carlos Moreno-Castilla(Moreno-Castilla 2004), courtesy of Elsevier B.V.

Completely linear isotherms are not common in adsorption on carbons but linearity is found in the initial part of all isotherms obtained on homogeneous surfaces. The Langmuir (L) type frequently occurs, even when the assumptions of Langmuir theory are not satisfied. Type F (Freundlich), typical of heterogeneous surfaces, is perhaps the most commonly observed. High-affinity (H) isotherms are characterised by a very steep initial rise, followed by a pseudo-plateau, while Sigmoidal (S) isotherms have also been obtained for homogeneous surfaces such as the graphitized carbon blacks: Graphon and V3G(Moreno-Castilla 2004).

Type *II-VI* isotherms are most often observed in gas/vapour adsorption systems, which are crucial in the evaluation of nitrogen adsorption data used to characterise porous materials including those used for water treatment; hence a brief discussion of these isotherms is made below. *Type II* isotherm typifies physical adsorption of gases on non-porous solids, where monolayer coverage is followed by multi-layering at higher relative pressures. Carbons with mixed micro- and meso-porosity often produce *Type II* isotherms.

Type III isotherms show a plot of uptake that is convex to the relative pressure axis. This class of isotherm is characteristic of weak adsorbate-adsorbent interactions (Kiselev 1968) and is most commonly associated with both non-porous and microporous adsorbents. The weak interactions between the adsorbate and the adsorbent lead to small uptakes at low relative pressures. However, once a molecule has become adsorbed onto a primary adsorption site, the adsorbate-adsorbate interaction, which is much stronger than the adsorbent-adsorbate interaction, becomes the driving force of the adsorption process, resulting in accelerated uptakes at higher relative pressures. This co-operative type of adsorption, at high partial pressures, is known as cluster theory, and examples include adsorption of water molecules on carbon where primary adsorption sites are oxygen based.

Type IV isotherms show a hysteresis loop, commonly associated with the presence of mesoporosity, the shape of which is unique to each adsorption system. Capillary

condensation gives rise to these hysteresis loops (Sing, D.H.Everett et al. 1985) and these isotherms also exhibit limited uptake at high relative pressures.

Type V isotherms, similar to *Type III*, have uptakes convex to the relative pressure axis; characteristic of weak adsorbate-adsorbent interactions (Kiselev 1968), the reasons behind the shape of this class of isotherm are the same as those for *Type III*, where water adsorption on carbon may also exhibit a *Type V* isotherm. Such isotherms are indicative of either microporous or mesoporous solids.

Lastly, the *Type VI* isotherm was introduced primarily as a hypothetical isotherm, where the shape is due to the complete formation of monomolecular layers before progression to a subsequent layer. It has been proposed, by Halsey (Halsey 1948), that these isotherms arise from adsorption on extremely homogeneous, non-porous surfaces where the monolayer capacity corresponds to the step height. One example known to exist is the adsorption of krypton at -183 °C on carbon black (graphitised at 2727 °C) (Krätschmer, Rathouský et al. 1999).

2.1.2.1 Langmuir Adsorption Isotherm

The Langmuir model is also called the *ideal localized monolayer model* and is based on three major assumptions (Langmuir 1916), these being:

(i). The surface of the adsorbent is a two-dimensional array of energetically homogenous sites.

(ii).Only one molecule may be adsorbed on any one site and saturation of adsorption occurs at monolayer coverage.

(iii). Adsorbed molecules cannot migrate across the surface and there are no interactions between any of the adsorbed molecules.

The Langmuir equation was originally derived from kinetic considerations (Langmuir 1915). But latterly, derivation were made on the bases of statistical mechanisms, thermodynamics, the law of mass action, theory of absolute reaction rates and the Maxwell-Boltzmann distribution law (Young and A.D.Crowell 1962).

The kinetic derivation considered the adsorbed layer to be in dynamic equilibrium with the bulk solution phase. A certain fraction of the molecules striking the bare sites are held by surface forces for a finite time and are regarded as adsorbed. Those molecules striking sites that are already occupied will immediately desorb. If the fraction of the site already covered is defined as θ, then:

$$\textbf{Rate of adsorption} = k_a C_e(1-\theta) \qquad \textbf{Eq. (2-1)}$$

$$\textbf{Rate of desorption} = k_d\theta \qquad \textbf{Eq. (2-2)}$$

Where:

k_a = rate constant of adsorption (S^{-1} L mol^{-1});

k_d =rate constant of desorption (S^{-1});

θ =coverage of active sites.

At equilibrium, the rate of adsorption equals the rate of desorption; therefore:

$$k_a C_e(1-\theta) = k_d\theta \qquad \textbf{Eq. (2-3)}$$

then:

$$\frac{\theta}{1-\theta} = \frac{k_a}{k_d} C_e \qquad \textbf{Eq. (2-4)}$$

Taking $\frac{k_a}{k_d} = K_L$, which is defined as the Langmuir adsorption equilibrium constant, and then the above equation becomes:

$$\frac{\theta}{1-\theta} = K_L C_e \qquad \textbf{Eq. (2-5)}$$

or

$$\theta = \frac{K_L C_e}{1+K_L C_e} \qquad \textbf{Eq. (2-6)}$$

which is known as the Langmuir adsorption isotherm.

If q_e is the amount of solute adsorbed per unit mass of adsorbent at a concentration of C_e, and q_m is the amount of solute adsorbed per mass unit of adsorbent when all sites are covered (monolayer capacity), then:

$$\theta = \frac{q_e}{q_m} \qquad \textbf{Eq. (2-7)}$$

Hence, the Langmuir equation becomes:

$$q_e = \frac{K_L C_e q_m}{1 + K_L C_e} \quad \textbf{Eq. (2-8)}$$

Which shows that q_e approaches q_m asymptotically as C_e approaches infinity.

Hence a plot of C_e/q_e against C_e should yield a linear graph from which q_m may be determined as the reciprocal of the gradient. Using the value obtained it is possible to determine the specific surface area, *S*, from:

$$S = q_m A_m L \quad \textbf{Eq. (2-9)}$$

where:

S = the specific surface area, ($m^2 g^{-1}$);

A_m = average area occupied by one molecule of the adsorbate at monolayer coverage (m^2);

L = Avogadro's constant, 6.0221367 x 10^{23} (molecules mol^{-1}).

Due to the basic assumptions made in the derivation of the Langmuir equation there are often limitations in the application of the relationship to some systems involving physical adsorption, however it is a useful tool in the determination of surface areas and approximations of other adsorption parameters from *Type I* isotherms.

It must be stressed that conformity to the algebraic form of the Langmuir equation does not constitute obedience to an ideal localized monolayer model, even if reasonable values of K_L and q_m are obtained as a constant value of K_L may be the result of minimal variation in adsorption heat (ΔH). In turn, non-variation of ΔH may be a result of internal compensation of opposing effects such as attractive lateral interactions and surface non-uniformity (Young and A.D.Crowell 1962; Faust and Aly 1987). One should be consider that the assumption that the number of sites and, in turn, q_m are determined solely by the nature of the solid hence, that they are independent of the nature of the solute, which is contrary to what is actually encountered in adsorption systems as orientation of solute molecules on the surface of AC has been shown to affect the monolayer capacity, as determined from the area occupied per molecule (Faust and Aly 1987). Although, these issues exist, nonconformity with the physical model should not detract from the usefulness of the Langmuir isotherm for analytical

description of adsorption systems that do not proceed beyond monolayers and produce Type *I* isotherms.

2.1.2.2 Freundlich Adsorption Isotherm

The Freundlich adsorption isotherm is, perhaps, the model most frequently used to describe adsorption data in aqueous systems; especially, when considering sorption of solutes onto surfaces with heterogeneity resulting from the presence of different functional groups (Hameed and El-Khaiary 2008), or several adsorbent-adsorbate interactions (Huo and Yan 2012). The Freundlich equation (Freundlich 1926) is expressed as:

$$q_e = K_F C_e^{\frac{1}{n}} \qquad \textbf{Eq. (2-10)}$$

where:

q_e = amount of solute adsorbed per unit mass of adsorbent (mg g^{-1});

C_e = concentration of solute at equilibrium (mg L^{-1});

K_F = Freundlich characteristic constant (L g^{-1} (mg L^{-1})$^{-1/n}$) ;

n = dimensionless constant related to adsorption affinity of system.

The Freundlich model is an empirical expression that takes into account an exponential distribution of the heterogeneity of surface sites and energies (Hill 1949; Young and A.D.Crowell 1962). Linearization of the data can be achieved by rewriting the Freundlich equation as:

$$\log q_e = \log K_F + \frac{1}{n} \log C_e \qquad \textbf{Eq. (2-11)}$$

Plotting $\log q_e$ versus $\log C_e$, gives a straight line with slope of 1/n and intercept $\log K_F$. n and K_F indicate the magnitude of the adsorption driving force, hence the favourability of sorption, and the distribution of the energy sites on the adsorbent surface, respectively. As a guide, the values of *n* in the range 2-10 represent good adsorption characteristics, 1-2 indicate moderate or difficult and <1 suggest poor sorption char-

acteristics (Chen, Zhao et al. 2011). As K_F refers to relative adsorption capacity, larger values of K_F imply higher adsorption capacities when C_e is equal. As the Freundlich equation indicates, the adsorptive capacity is a function of the equilibrium concentration of the solute; therefore, higher capacities are always obtained at higher equilibrium concentrations.

2.1.2.3 Linear Adsorption Isotherm

The linear isotherm is the simplest isotherm, where the amount of solute adsorbed is proportional to the equilibrium concentration of the solute. It is often called Henry's Law after the analogous isotherm for the solubility of gases in liquids. The isotherm is described by:

$$q_e = K_h C_e \qquad \textbf{Eq. (2-12)}$$

Where:

q_e= amount of solute adsorbed by unit of mass of adsorbent (mg g^{-1});

C_e = equilibrium concentration (mg L^{-1});

K_h = Henry's constant (L g^{-1}).

Linear isotherms are usually only obtained under conditions of very low solute concentration. In such systems, the adsorbed layer is extremely dilute i.e. only a fraction of the monolayer capacity and consequently, almost all the adsorption isotherms discussed reduce to Henry's law at low concentrations. For example, for the Langmuir adsorption isotherm (Eq.2-8) at very low concentrations, $K_L \cdot C_e$ is much smaller than 1 so that the equation reduces to:

$$q_e = q_m K_L C_e \qquad \textbf{Eq. (2-13)}$$

which is a linear isotherm.

2.1.2.4 BET Model

The Brunauer Emmett Teller (BET) adsorption model is rarely observed in aqueous systems but all the porous materials used in the thesis are characterised by nitrogen

adsorption for which the BET model is primarily used to determine the surface area and other key parameters, hence, its inclusion here. The BET equation(Brunauer, Emmett et al. 1938), is an extension of the Langmuir equation, which accounts for the existence of multilayers in an adsorption process (Brunauer, Deming et al. 1940). It is still the most frequently used model despite it being greatly criticized. The equation uses the assumptions of the Langmuir equation (Langmuir 1915), primarily the postulate that the rate of adsorption onto surface sites is equal to the rate of evapouration from occupied sites, but additionally it is that the energy of adsorption for the second and subsequent layers of adsorbed material is equal to the enthalpy of liquefaction, hence, the total number of molecules adsorbed is the sum of all the adsorbed layers.

Consequently, the BET theory is based on several assumptions:

(i). adsorbent consists of regular array of adsorption sites equal in energy, with a constant enthalpy of adsorption in the monolayer, ΔH_A

(ii). adsorption is localized to these sites

(iii). neighbouring adsorbed molecules do not interact

(iv). multilayer formation is unlimited

(v). enthalpy of adsorption in second and subsequent multilayers is equal to the enthalpy of liquefaction, ΔH_L

(vi). adsorption, or desorption, may only occur on, or from, exposed sites.

Type *II* and Type *IV* isotherms are often referred to as BET isotherms, where Type *II* describes unrestricted multilayer formation, whilst Type *IV* indicates restricted multilayer formation. The BET equation, for unrestricted multilayer formation, is usually expressed as:

$$\frac{P}{n(P^0-P)} = \frac{1}{n_m C} + \frac{(C-1)}{n_m C} \cdot \frac{P}{P^0} \qquad \textbf{Eq. (2-14)}$$

where:

p^o = saturation vapour pressure (Pa);

n = uptake, at pressure p, expressed as a molar quantity;

n_m = the complete monolayer coverage, expressed as a molar quantity;

C = dimensionless constant, related to the adsorption energy which can be expressed as:

$$C = exp\left(\frac{\Delta H_A - \Delta H_L}{RT}\right) \quad \textbf{Eq. (2-15)}$$

where:

ΔH_A = heat of adsorption of the first adsorbed layer (J mol^{-1});

ΔH_L = heat of adsorption of the second and subsequent multilayers (i.e. molar heat of condensation) (J mol^{-1});

Thus, (ΔH_A-ΔH_L) is the net heat of adsorption.

By plotting $p/n(p^o-p)$ versus p/p^o, a linear plot should be obtained with a gradient of $(c-1)/n_m c$ and an intercept of $1/n_m c$. Hence, the quantities c and n_m may be evaluated by solving the two simultaneous equations obtained. The surface area may be calculated using n_m, N_A, Avogadro's constant, and A_m, the area occupied by one molecule, as outlined for the Langmuir equation (Eq. 2-9).

2.1.3 Adsorption Kinetics

Predicting the rate at which solute adsorption takes place in a given solid/solution system is one of the most crucial factors for an effective adsorption system design. Many attempts have been made to formulate general, methodical expressions that would be able to properly describe the kinetics of sorption in such systems. Progress in this field appears to be limited by the fact that the description of sorption kinetics is much more complicated than the theoretical description of sorption equilibria. Normally, two aspects of kinetics are considered in these studies:

1) Adsorption reaction models: describe overall adsorption, considering it in a lumped process; including pseudo-first, pseudo-second order and Elovich equations.
2) Adsorption diffusion models: describe adsorption in different diffusive steps and the rate of these steps vary result of in the fact that there is a

slowest step controlling the whole adsorption rate; including Homogeneous Particle Diffusion Model (HPDM) and intra-particle diffusion model.

2.1.3.1 Pseudo-First Order Model

At the end of 19th century, Lagergren presented an empirical equation to describe the kinetic behaviour of the adsorption of oxalic and malonic acids onto charcoal; the model is a pseudo-first order equation, believed to be the earliest model describing the rate of adsorption in the solid-liquid phase that is based on adsorption capacity (Lagergren 1898). It assumes that the overall adsorption rate is proportional to the driving force, i.e. the difference between the average solid phase and equilibrium concentrations, q_e-q_t (Kumar and Sivanesan 2006; Sundaram, Viswanathan et al. 2008; Behnamfard and Salarirad 2009; Nemr 2009).

$$\frac{dq_t}{dt} = k_1(q_e - q_t) \qquad \textbf{Eq. (2-16)}$$

where:

q_t = amount of solute adsorbed at time t (mg g^{-1});

q_e= amount of solute adsorbed at equilibrium state (mg g^{-1});

k_1= pseudo-first order rate constant (s^{-1}).

Integrating Eq. (2-16) with the boundary conditions q_t= 0 at t= 0 and q_t at t = t gives:

$$\ln(q_e - q_t) = lnq_e - k_1 t \qquad \textbf{Eq. (2-17)}$$

or

$$q_t = q_e\left(1 - e^{-k_1 t}\right) \qquad \textbf{Eq. (2-18)}$$

The values of q_e and k_1 parameters are usually determined by applying the commonly accepted linear regression procedure based on Eq. (2-17) or by fitting the experimental data to Eq. (2-18). Numerous studies have since reported that the experimental data could be described using pseudo-first order kinetic model including the sorption of metals ions (Iftikhar, Bhatti et al. 2009; Riaz, Nadeem et al. 2009), dyes (Ma, Jia et al. 2010; Lee, Kim et al. 2011) and other organic molecules (Uc,

Alvarez-Idaboy et al. 2008; Hameed, Salman et al. 2009; Yuan, Lin et al. 2011) onto different adsorbents.

2.1.3.2 Pseudo-Second Order Model

In 1984, Blanchard *et al.* (Blanchard, Maunaye et al. 1984) studied the overall exchange reaction of NH_4^+ ions fixed in a zeolitic structure by divalent metallic ions and proposed a second order rate equation, where the reaction can be written:

$$\boldsymbol{Z_{(2NH_4^+)} + M^{2+} \rightarrow Z_{M^{2+}} 2NH_4^+} \qquad \textbf{Eq. (2-19)}$$

where:

$Z_{(2NH_4^+)}$= amount of ammonia ions fixed in zeolite (mg g^{-1});

$Z_{M^{2+}}$= amount of metallic ions fixed in zeolite (mg g^{-1});

M^{2+}= concentration of metallic ions in solution (mg L^{-1});

NH_4^+= concentration of ammonia ions in solution (mg L^{-1}).

The authors proposed that the metallic ion concentration stays almost un-changed during the first few hours, and the kinetic order is two with respect to the number (n_0-n) of sites available for the exchange. Hence, the rate can be expressed as:

$$-\frac{dn}{dt} = K(n_0 - n)^2 \qquad \textbf{Eq. (2-20)}$$

Integrating the above equation given the boundary conditions n = 0 at t = 0 and n = n at t = t, gives:

$$\frac{1}{n_0 - n} - \frac{1}{n_0} = Kt \qquad \textbf{Eq. (2-21)}$$

where:

n = amount of M^{2+} fixed in zeolite;

n_0 = exchange capacity;

K = rate constant.

By plotting $1/(n_0\text{-}n)$ versus time, a straight line should be obtained, the slope of which gives K while n_0 is obtained from the intercept of the line. This second-order rate equation was adopted by many studies to describe kinetic processes such as the

exchange between sodium ions from Zeolite A (Z_{Na+}) and cadmium, copper and nickel ions from solution (Biškup and Subotić 2004).

In 1995, a similar second-order adsorption kinetic equation was proposed by Ho (Ho and McKay 1998; Ho and McKay 1998; Ho and McKay 1999; Ho and McKay 2000; Ho 2006) in a study of divalent metal ion adsorptions onto peat; chemical bonding between divalent metal ions and the polar functional groups present on peat (aldehydes, ketones, acids, and phenolics) are responsible for the exchange capacity, hence, the reaction between peat and the divalent ions (M^{2+}) can be written as:

$$2P^{-} + M^{2+} \leftrightarrow MP_2 \qquad \textbf{Eq. (2-22)}$$

and

$$2HP + M^{2+} \leftrightarrow MP_2 + 2H^{+} \qquad \textbf{Eq. (2-23)}$$

where P^- and HP are the active sites on the peat surface.

The authors made two key assumptions to develop their model, namely that the adsorption process is second order and that adsorption follows a Langmuir equation (Ho and McKay 2000). As seen in the equations shown above, the rate of adsorption is dependent upon the quantity of divalent ions adsorbed on the surface of peat at time t and at equilibrium, hence, the rate is expressed as:

$$\frac{d(P)_t}{dt} = k_{p2}((P)_0 - (P)_t)^2 \qquad \textbf{Eq. (2-24)}$$

where:

$(P)_0$ = number of active sites available at equilibrium;

$(P)_t$ = number of active sites occupied at time t;

k_{p2} = second order rate constant.

Since the driving force (q_e-q_t) is proportional to the number of active sites that are available, the above rate equation can be written on the basis of adsorption capacity as follows:

$$\frac{dq_t}{dt} = k_2(q_e - q_t)^2 \qquad \textbf{Eq. (2-25)}$$

where:

q_t = amount of solute adsorbed at time t (mg g^{-1});

q_e = amount of solute adsorbed at equilibrium (mg g^{-1});

k_2 = pseudo-second order rate constant (g mg^{-1} s^{-1}).

This second order rate equation is referred to as a pseudo-second order rate equation in order to distinguish the kinetic equations based on adsorption capacity from concentration of solution. Integrating this equation with the boundary conditions $q_t = 0$ at t = 0, and $q_t = q_t$ at t = t, as for the pseudo first-order model, gives a relationship, which is expressed linearly as:

$$\frac{t}{q_t} = \frac{1}{k_2 q_e^2} + \frac{t}{q_e} \qquad \textbf{Eq. (2-26)}$$

Or in the non-linear form:

$$q_t = \frac{q_e^2 kt}{1 + q_e kt} \qquad \textbf{Eq. (2-27)}$$

The pseudo-second order model constants can be determined empirically by fitting experimental data to the equations stated above. A kinetic model is concerned only with the effect of observable parameters on the overall rate, although there are many factors that affects the adsorption capacity, including initial adsorbate concentration, adsorption temperature, solution pH, adsorbent particle size, dosage of adsorbent and nature of solute, *etc* (Ho 2006). This pseudo-second order equation has been successfully applied to describe the kinetic data for the sorption of organic and inorganic substances (Hameed 2009; Hameed, Salman et al. 2009; Iftikhar, Bhatti et al. 2009).

2.1.3.3 Elovich Model

In 1934, a rate equation was proposed by Zeldowitsch to describe the kinetic data for adsorption of carbon monoxide (CO) onto manganese dioxide (MnO_2) (Zeldowitsch 1934); the resulting equation is known as the Elovich equation and the model has been widely used to describe adsorption processes as groups of reaction mechanisms, including diffusion in the mass of dissolution, surface diffusion and activated catalytic surfaces in the following form (Zeldowitsch 1934; Low 1960;

Valderrama, Cortina et al. 2007; Valderrama, Barios et al. 2010):

$$\frac{dq_t}{dt} = a\exp(-bq_t) \qquad \textbf{Eq. (2-28)}$$

Which integrates, with the same conditions of $q_t = 0$ at $t = 0$, and $q_t = q_t$ at $t = t$, to the rearranged form:

$$q_t = \frac{1}{b}\ln(ab) + \frac{1}{b}\ln(t + t_0) \qquad \textbf{Eq. (2-29)}$$

Where a and b are the desorption constant and the initial adsorption rate, respectively; and t_0 is equal to $^1/_{(ab)}$. With the assumption of $a{\cdot}b{\cdot}t \geq 1$, equation 2-29 can be further simplified to (Chien and Clayton 1980):

$$q_t = \frac{1}{b}\ln(ab) + \frac{1}{b}\ln(t) \qquad \textbf{Eq. (2-30)}$$

Although the Elovich model was originally proposed for adsorption of gases onto solid surfaces, it has also recently been widely applied to describe the kinetic data obtained for sorption of pollutants from aqueous systems, such as removal of dyes and heavy metals from solutions, *etc*.(Tseng, Wu et al. 2003; Senthilkumaar, Varadarajan et al. 2005; Gupta and Bhattacharyya 2006).

2.1.3.4 Homogeneous Particle Diffusion Model

Homogeneous Particle Diffusion Model (HPDM) (Valderrama, Barios et al. 2010) considers the adsorption mechanism to involve diffusion of solute molecules from the bulk solution to the adsorbent particle phase, possibly passing through some point of resistance. The solute must (1) migrate from the bulk solution to the surface of the adsorbent, (2) diffuse across the liquid/solid interface surrounding the adsorbent particle, (3) diffuse into the bulk of the adsorbent particle, and (4) possibly interact with a moiety on the surface of adsorbent. This adsorption process can be rigorously described by Fick's law, and applies to the quasi-homogeneous media. The corresponding diffusion mass transfer rate equation (Boyd, Adamson et al. 1947) is represented by:

$$X(t) = 1 - \frac{6}{\pi^2}\sum_{Z=1}^{\infty}\frac{1}{Z^2}exp\left[\frac{-Z^2\pi^2 D_{et}}{r^2}\right] \qquad \textbf{Eq. (2-31)}$$

Where

X(t) = fractional attainment of equilibrium at time t, herein $\frac{q_t}{q_e}$,

q_t , q_e = metaldehyde uptakes at time t and at equilibrium, respectively (mg g^{-1}),

D_e = effective diffusion coefficient of the adsorbent phase (m^2/s),

r = radius of the adsorbent particle (m), assumed to be spherical.

By considering the particles as spheres, it is possible to apply Vermeulen's approximation (Vermeulen 1953) to the above equation over the whole range ($0 < X(t) < 1$); by assuming particle diffusion controls the adsorption rate, solving the equation , gives:

$$\boldsymbol{X(t) = \sqrt{1 - \exp\left(\frac{-2\pi^2 D_e}{r^2}\mathrm{t}\right)}} \qquad \textbf{Eq. (2-32)}$$

Conversely, if the adsorption rate is limited by liquid film diffusion, the equation becomes:

$$\boldsymbol{X(t) = 1 - \exp\left(-\frac{3DC}{rC_r}t\right)} \qquad \textbf{Eq. (2-33)}$$

2.1.3.5 Intra-Particle Diffusion Model

Intra-particle diffusion model (Weber and Morris 1963) is widely used to analyse whether the adsorption process is kinetically controlled by particle diffusion, and it is expressed:

$$\boldsymbol{q_t = K_i t^{0.5} + I} \qquad \textbf{Eq. (2-34)}$$

Where

q_t = uptake of metaldehyde at time t (mg g^{-1}),

K_i = intra-particle diffusion rate constant (mg g^{-1} h^{-1}),

I =indication of the thickness of the boundary layer (mg g^{-1}), i.e. larger values of *I* suggest a greater boundary layer effect. If *I* is equal to zero, then the rate of adsorption is only controlled by intra-particle diffusion for the entire adsorption process (Huo and Yan 2012). Previous studies have determined that multi-linear behaviour in a plot of q_t against $t^{0.5}$ indicates that the sorption process is affected by two or more steps, where the first slope is generally believed to be related to mass transfer of solute through the

solid/film interface, i.e. the external resistance, which is only significant in the early stages of adsorption; the second slope reflects adsorption dominated by intra-particle diffusion (Valderrama, Barios et al. 2010).

2.2 Ion-exchange

2.2.1 Fundamentals of Ion-Exchange

Ion-exchange is the reversible interchange of ions between a solid (ion-exchanger) and a liquid, which results in permanent change in the structure of the solid. Used in water treatment, it provides a method of separation for many processes involving other liquids, while also finding use in chemical synthesis, medical research, food processing, mining, agriculture, and a variety of other areas. The significant use of ion-exchange methods rests with the ability to use and reuse the ion-exchanging material.

Ion-exchange occurs in a variety of substances, and has been used on an industrial basis since around 1910 with the introduction of water softening using natural and, later, synthetic zeolites. Sulfonated coal, developed for industrial water treatment, was the first ion-exchange material that was stable at low pH. The introduction of synthetic organic ion-exchange resins in 1935 resulted from the synthesis of phenolic condensation products containing either sulfonic or amine groups that could be used for the reversible exchange of cations or anions.

In theory, ion-exchange is about the same as ‘adsorption’ as described previously but differs in that the species attaching to the solid are ions (e.g. Ca^{2+}, Cl^{-}), rather than molecules. Also, the solid ion-exchanger has charged sites within its own interior, rather than sites that exhibit molecular forces attraction.

Generally, there are two types of ion-exchange processes: ***cation exchange*** and ***anion exchange***. ***Cation exchange*** is most commonly used in water softening treatment; where calcium and magnesium ions are exchanged for sodium ions. The ‘so-

dium cycle' operation refers to regeneration of such exchange system via common salt, and overall, this is water softening in its simplest form. This reactions are shown below.

Operation:

$$2Na^{+}R^{-} + Ca^{2+} \leftrightarrow Ca^{2+}R_2^{-} + 2Na^{+} \quad \textbf{Eq. (2-35)}$$

$$2Na^{+}R^{-} + Mg^{2+} \leftrightarrow Mg^{2+}R_2^{-} + 2Na^{+} \quad \textbf{Eq. (2-36)}$$

Regeneration:

$$2NaCl + Ca^{2+}R_2^{-} \leftrightarrow 2Na^{+}R^{-} + CaCl_2 \quad \textbf{Eq. (2-37)}$$

$$2NaCl + Mg^{2+}R_2^{-} \leftrightarrow 2Na^{+}R^{-} + MgCl_2 \quad \textbf{Eq. (2-38)}$$

Where R is a strong acid cation exchange resin.

Alternatively, conditions may be used whereby all cations in water are exchanged for hydrogen ions. The 'hydrogen cycle' operation of cation exchangers is the term used when regeneration is accomplished with dilute acid, usually sulfuric (H_2SO_4) or hydrochloric (HCl) acid, via these reactions shown below.

Operation:

$$2H^{+}R^{-} + Ca^{2+} \leftrightarrow Ca^{2+}R_2^{-} + 2H^{+}0 \quad \textbf{Eq. (2-39)}$$

$$2H^{+}R^{-} + Mg^{2+} \leftrightarrow Mg^{2+}R_2^{-} + 2H^{+} \quad \textbf{Eq. (2-40)}$$

Regeneration:

$$2HCl + Ca^{2+}R_2^{-} \leftrightarrow 2H^{+}R^{-} + CaCl_2 \quad \textbf{Eq. (2-41)}$$

$$2HCl + Mg^{2+}R_2^{-} \leftrightarrow 2H^{+}R^{-} + MgCl_2 \quad \textbf{Eq. (2-42)}$$

Anion exchange is the exchange of anions present in water (SO_4^{2-}, HCO_3^{-},etc.) for hydroxide ions (OH^{-}). This exchange, which occurs after cation exchange, completely demineralizes water when carried to completion. An example of a typical anion exchange reaction is shown below.

Operation:

$$2R^{+}OH^{-} + {SO_4}^{2-} \leftrightarrow {R_2}^{+}{SO_4}^{2-} + 2OH^{-} \quad \textbf{Eq. (2-43)}$$

$$R^{+}OH^{-} + {NO_3}^{-} \leftrightarrow R^{+}{NO_3}^{-} + 2OH^{-} \quad \textbf{Eq. (2-44)}$$

Regeneration:

$$R^{+}NO_3^{-} + NaOH \leftrightarrow R^{+}OH^{-} + \mathrm{Na}NO_3 \qquad \textbf{Eq. (2-45)}$$

In this thesis, for simplification and discursive convenience, a generalized form of the stoichiometric reaction can be written as:

$$nR^{\pm}A^{\mp} + B^{n\pm} \leftrightarrow R_n{}^{\pm}B^{n\mp} + nA^{\mp} \qquad \textbf{Eq. (2-46)}$$

Where:

$R^{\pm}$= ionic group attached to an ion-exchange resin;

A, B = exchanging ions;

n = valence of exchanging ion.

2.2.2 Ion-Exchange Equilibria

Equilibrium theory can predict ideal process performance and is much less complex mathematically than kinetic theories, which will be discussed in a later section. Therefore, equilibrium theory is often used to predict the maximum amount of work that an ion-exchange can perform on a particular solution. The two most common theories that have been developed to quantify ion-exchange equilibrium are by analogy to a chemical reaction or by analogy to membrane exclusion phenomenon. If treated as a chemical reaction, the law of mass action can be used to describe the distribution of ions in the solution and resin phases (Montgomery 1985).

The Donnan equilibrium model describes the behaviour of ions based on the unequal distribution of ions across a membrane, with an electrolytic solution on one side of the membrane, containing ionic species, which cannot diffuse through the membrane. Donnan theory for ion-exchange equilibria gives a thermodynamic interpretation of the phenomena, which the law of mass action does not take into account; hence Donnan theory is more sophisticated and mathematically more rigorous. However, it should be noted that mass action derivations will ultimately give the same equilibrium expressions as membrane theory.

Ion-exchange reactions have proven to be well suited for interpretation by mass action (Montgomery 1985), and equilibrium expressions developed using this method,

for binary component systems, are presented in the following sections (John C. Crittenden, R. Rhodes Trussell et al. 2012).

In water treatment, ion-exchange applications most often involve dilute ionic solutions where the ions behave independently of one another and are, therefore, treated as ideal solutions (i.e. activity coefficients are assumed to be unity.) In the resin phase, the ion concentrations can be much larger, hence the activity is not unity but will be a function of ionic strength (John C. Crittenden, R. Rhodes Trussell et al. 2012). Working from Eq. (2-42), the equilibrium constants for all binary exchange reactions can be expressed as:

$$K_B^A = \frac{[A^{\pm}]^n [R^{\pm} B^{n\mp}]}{[B^{n\pm}][R^{\pm} A^{\mp}]^n} \qquad \textbf{Eq. (2-47)}$$

Where

K_B^A = apparent equilibrium constant or selectivity coefficient for either cation or anion A exchanging with ion B onto resin.

$[A^{\pm}]$, $[B^{n\pm}]$ = aqueous-phase concentrations of pre-saturant and counter-ions, respectively.

$\left[R^{\pm}A^{\mp}\right]$, $\left[{R_n}^{\pm}B^{n\pm}\right]$ = concentrations of resin-phase pre-saturant ion and counter-ions, respectively.

Normally, the concentrations of ions in solution are denoted as C, for example C_A signifies the concentration of A, and, the concentrations of ions in the resin phase are denoted as q, for example q_A indicates the concentration of A in the resin phase. Hence, Eq(2-43) can be simplified to:

$$K_B^A = \frac{{C_A}^n q_B}{C_B {q_A}^n} \qquad \textbf{Eq. (2-48)}$$

2.2.2.1 Equivalent Fractions

Before further discussing ion-exchange isotherms and selectivity coefficients, the concept of equivalent fraction should be introduced, as it is a highly convenient tool in understanding ion-exchange materials and ion-exchange systems because of the

equivalent character of ion-exchange and the fixed number of functional groups in the ion-exchanger. The equivalent fraction (X) of an ion is the ratio of the equivalent concentration of ion X and the sum of the equivalent concentrations of all ions present, as per:

$$X_{ion\ A} = \frac{Z_{ion\ A}\,[A]}{\sum_{A=1}^{n} Z_{ion\ A}\,[A]} \quad 0 \le X \le 1 \qquad \textbf{Eq. (2-49)}$$

where

Z = charge of ions;

[ ] = the molar ionic concentrations.

For example, if a solution contains sodium and hydrogen ions, the equivalent fraction of sodium is calculated as

$$X_{Na^+} = \frac{[Na^+]}{[Na^+]+[H^+]} \qquad \textbf{Eq. (2-50)}$$

The equivalent fraction can be calculated for any phase, and is especially useful for resin phase since the sum of equivalent concentrations of all ions present in resin phase can be represented as Q, i.e. the ion-exchange capacity. For example, in an exchange system where the resin only has affinity to sodium and hydrogen ion, then at certain stage, the equivalent fraction of sodium can be calculated as

$$X_{Na^+} = \frac{[Na^+]}{[Na^+]+[H^+]} = \frac{[Na^+]}{Q} \qquad \textbf{Eq. (2-51)}$$

where Q represents the total ion-exchange capacity, a fixed value that is defined by the nature of the materials, which can be determined by experimental techniques such as titration.

2.2.2.2 Ion-exchange Isotherms

As with other chemical processes, ion-exchange equilibria can be characterised by the corresponding equilibrium isotherms obtained. Generally, isotherms are graphical representations of the relationship between the equilibrium position achieved and all possible experimental conditions, at constant temperature. Thus, the general isotherm is a multi-dimensional surface with each point corresponding to a unique set of

conditions but this definition is too wide to be practicably plotted. Indeed, a plot covering all possible conditions would have an unlimited number of dimensions, in practice, two-dimensional plots are used, i.e. only one variable condition is used for the independent variable and all other factors are considered to be constant a given plot. Consequently, the same chemical equilibrium can be illustrated by an infinite number of plots with various selected x-axes, with all other conditions fixed.

The most common ion-exchange isotherm represents interdependence between ionic compositions of two phases: the ion-exchange material and the surrounding solution. Conventionally, represented as a plot of equivalent ionic fraction of one counter-ion in the ion-exchanger, for example, X_A, as a function of the equivalent fraction X_A of the same ion in the solution, such a plot is called a normalized ion-exchange isotherm because the scales of both axes are dimensionless with values between 0 and 1. As described earlier, all other variables are kept constant. Normalized ion-exchange isotherms are convenient for two reasons: firstly, the simplest case of ion-exchange means the presence of two ions in the system and, representation by equivalent fraction allows simplification as the fraction of the second ion (i.e. X_B) is calculated as $1-X_A$, hence, the same isotherm plotted for ion B is a mirror reflection of the isotherm plotted for ion A; secondly the equivalent fraction has a special meaning for ion-exchange materials because its maximum value (X = 1) corresponds to the ion-exchange capacity, Q.

The following example helps in understanding ion-exchange isotherms: Neagu *et, al.* (Neagu, Untea et al. 2003) investigated the retention of chromate ion (CrO_4^{2-}) by two anion exchange resins; the first a type of anion resin synthesised in their work (for convenience here denoted VPDVB) and the other a commercialized resin (Purolite A-400). The active structural units are shown in Figure 2.3.

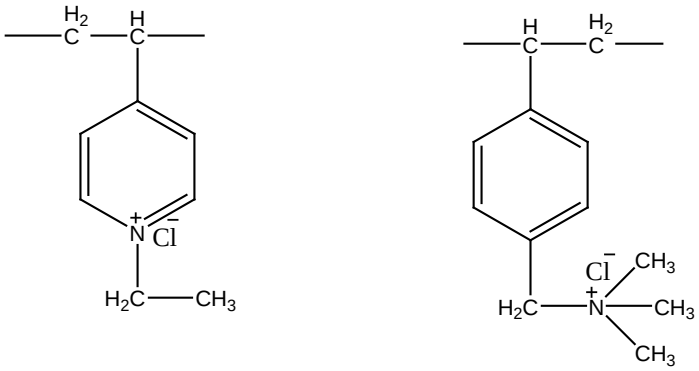

Figure 2.3 The active units of two strong anion exchange resins applied in the work.

In their work, the authors stated the reaction as:

$$2R^{+}Cl^{-} + CrO_4^{2-} \overset{K}{\leftrightarrow} R_2CrO_4^{2-} + 2Cl^{-} \qquad \textbf{Eq. (2-52)}$$

The ion-exchange isotherms for VPDVB and A-400 are shown in

Figure 2.4 Experimental isotherms for ion-exchange of chromate ion (CrO_4^{2-}) on chloride ion (Cl^-) for two anion exchangers: Purolite A-400(■) and VPDVB (●). Both X and Y axes represent the equivalent fractions of CrO_4^{2-}. Courtesy of Elsevier B.V.

, and it can be seen that both exchangers give similar isotherms, and that they both demonstrate a preference for CrO_4^{2-} over the Cl^- anions; hence, the results are in agreement with the rule that ion-exchange exchangers prefer higher value counter-ions, with the commercial resin showing a greater preference for CrO_4^{2-} than VPDVB.

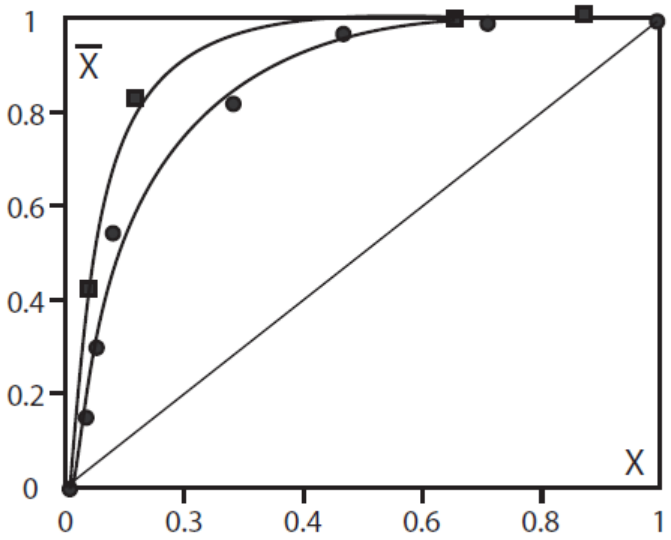

Figure 2.4 Experimental isotherms for ion-exchange of chromate ion (CrO_4^{2-}) on chloride ion (Cl^-) for two anion exchangers: Purolite A-400(■) and VPDVB (●). Both X and Y axes represent the equivalent fractions of CrO_4^{2-}. Courtesy of Elsevier B.V.

Ion-exchange isotherms are normally described by isotherm equations developed for processes other than stoichiometric exchange, and the most commonly used is the Langmuir equation:

$$q_e = Q\frac{K_L C_e}{1+K_L C_e} \qquad \textbf{Eq. (2-53)}$$

where

q_e = ion-exchange capacity (mg/g);

K_L = Langmuir constant;

Ce = equilibrium concentration of the target ion in the solution phase (mg/L);

Q = maximum ion-exchange capacity (eq/g).

Isotherms are a convenient way to summarise the equilibrium behaviour of an ion-exchange system, however, there are no fixed rules regarding which plot or quantification should be used for such characterisation. Researchers are free to choose the way which best fits to a particular purpose, resulting in multiple equilibrium characteristics throughout the literature. Different characteristics are often named in the same way; hence, it is important to provide definitions of discussed quantities to avoid

potential confusion.

2.2.3 Kinetics of Ion-Exchange

The theory of ion-exchange kinetics is akin to the theory of adsorption kinetics with three basic steps in each case, namely: (1) film diffusion, (2) particle diffusion, and (3) attachment. Within adsorption, substances of interest are molecules or small particles, while ion-exchange focuses on ions. A difference is that for ion-exchange process, mass transport of ions in one direction must be balanced by mass transport in the opposite direction to preserve electro-neutrality. In other words, ions exiting the resin must be balanced by the ions entering the resin.

As with adsorption, the rate-determining step for ion-exchange is either film or particle diffusion, and in simple cases, the rate of ion-exchange is determined by the slower of these steps. Dominance of one of the two mechanisms can be predicted using the following criterion (Helfferich 1995):

$\frac{Q \cdot \bar{D} \cdot \delta}{C \cdot D \cdot r_0} \cdot (5 + 2\alpha_A^B) \ll 1$ Particle diffusion control

$\frac{Q \cdot \bar{D} \cdot \delta}{C \cdot D \cdot r_0} \cdot (5 + 2\alpha_A^B) \gg 1$ Film diffusion control

Where

Q = concentration (eq/L) of fixed groups in the resin or ion-exchange capacity;

C = solution concentration (eq/L);

$\bar{D}$ = interdiffusion coefficient (cm^2/s) in the ion-exchanger;

D = interdiffusion coefficient (cm^2/s) in the film;

r_0 = bead radius (cm);

δ = film thickness (cm);

α_A^B = separation factor.

Practical estimation with this criterion is usually performed by taking known Q, C, r_0 and α_A^B; individual diffusion coefficients of the counter ions for D and $\bar{D}$; and $\delta = 10^{-3}$ to 10^{-2} cm (depending on the level of agitation). In the case of particle diffusion

control, concentration gradients exist only inside the exchanger beads; the momentary exchange flux is approximately proportional to the concentration of the fixed charges and to the inter-diffusion coefficient in the beads and is inversely proportional to the bead radius (Helfferich 1995).

2.2.4 Common Ion-Exchangers

An ion-exchanger is a solid substance having an open framework, which may be either crystalline or macromolecular, depending on the ion-exchanger material. As the framework is open, the exchanging sites are accessible by diffusion to any ions in a surrounding aqueous solution that are similar in size to the pores within the solid. As a rule, mineral ion-exchangers are granular, i.e. irregular, while resins are beads, with sizes approximating 0.5-1mm.

2.2.4.1 Mineral Ion-Exchangers

Most natural ion-exchangers are crystalline alumino-silicates with cation exchange properties,generally zeolites and clays. Zeolites have an open lattice structure with inter connecting channels, with the lattice carrying a negative charge for each aluminium atom balanced by cations free to move within the lattice. Clays on the other hand, have a loose layer structure that can swell, increasing the interlayer distance. Table 2.2 lists common zeolites and clay minerals (Hendricks 2011).

A clay is a mineral particle characterised by its small size, i.e. ≤1μm, with common mineral types including montmorillonite and kaolinite, the structures of which are displayed in Figure 2.5.

Table 2.2 Minerals having ion-exchange properties(Hendricks 2011).

Category	Name	Chemical Formula
Zeolites	Analeite	$Na[Si_2AlO_6]_2 \cdot H_2O$
	Chabezite	$(Ca, Na)[Si_2AlO_6]_2 \cdot 6H_2O$
	Harmotome	$(K, Ba)[Si_5Al_2O_{14}] \cdot 5H_2O$
	Natrolite	$Na_2[Si_3Al_2O_{10}] \cdot 2H_2O$
	Sadalite	$Na_8Al_6Si_6O_{24}C_{12}$
	Siliceous zeolite	$xNa_2O \cdot Al_2O_3 \cdot zSiO_2 \cdot aH_2O$
Clays	Montmorilonite	$Al_2[Si_4O_{10}(OH)_2] \cdot yH_2O$
	Illite	$(K_2H_3O)(Al, Mg, Fe)_2(Si, Al)_4O_{10}[(OH)_2, H_2O]$
	Kaolinite	$Al_2O_3 \cdot 2SiO_2 \cdot 2H_2O$

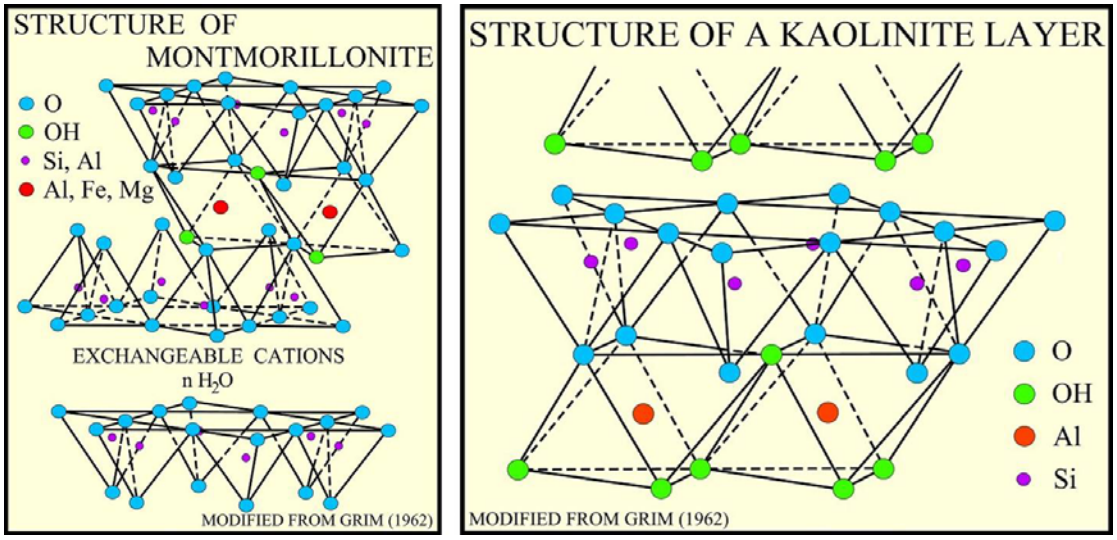

Figure 2.5 The structure of two common clays having ion-exchange properties (Costal and Marine Geology Program 2001).

Zeolites are microporous alumino-silicate minerals commonly used as adsorbents, but their open lattice structures with connecting channels and the free moving cations within the lattice, allow some zeolites to be used for ion-exchange. As a result, they are widely used in industry for water purification, as well as in catalysis, for the prep-

aration of advanced materials, and in nuclear reprocessing. Commercial applications also include nitrogen extraction from air, to increase the oxygen content for both industrial and medical purpose, while their biggest use is in the production of laundry detergents. To date, more than 206 unique zeolite frameworks have been identified and over 40 naturally occurring zeolite frameworks are recognized (Baerlocher and McCusker 2001). In the International Zeolite Association (IZA) system, each framework is designated a code consisting of three capital letters, e.g. ABW, ACO, AEI…….YUG,ZON, *etc*. Figure 2.6 displays a selection of zeolite frameworks with their corresponding codes.

Zeolites have unique crystal structures with a central channel of uniform size, within the range of 2.5-8 Å, and these pores may be three-dimensional, two-dimensional or one-dimensional (Haggerty and Bowman 1994). As a result of this structural versatility, zeolites have found a range of application areas including the water treatment industry, where they have been especially useful in removing inorganic ions such as NH_4^+ (Rožić, Cerjan-Stefanović et al. 2000) and heavy metals(Blanchard, Maunaye et al. 1984).

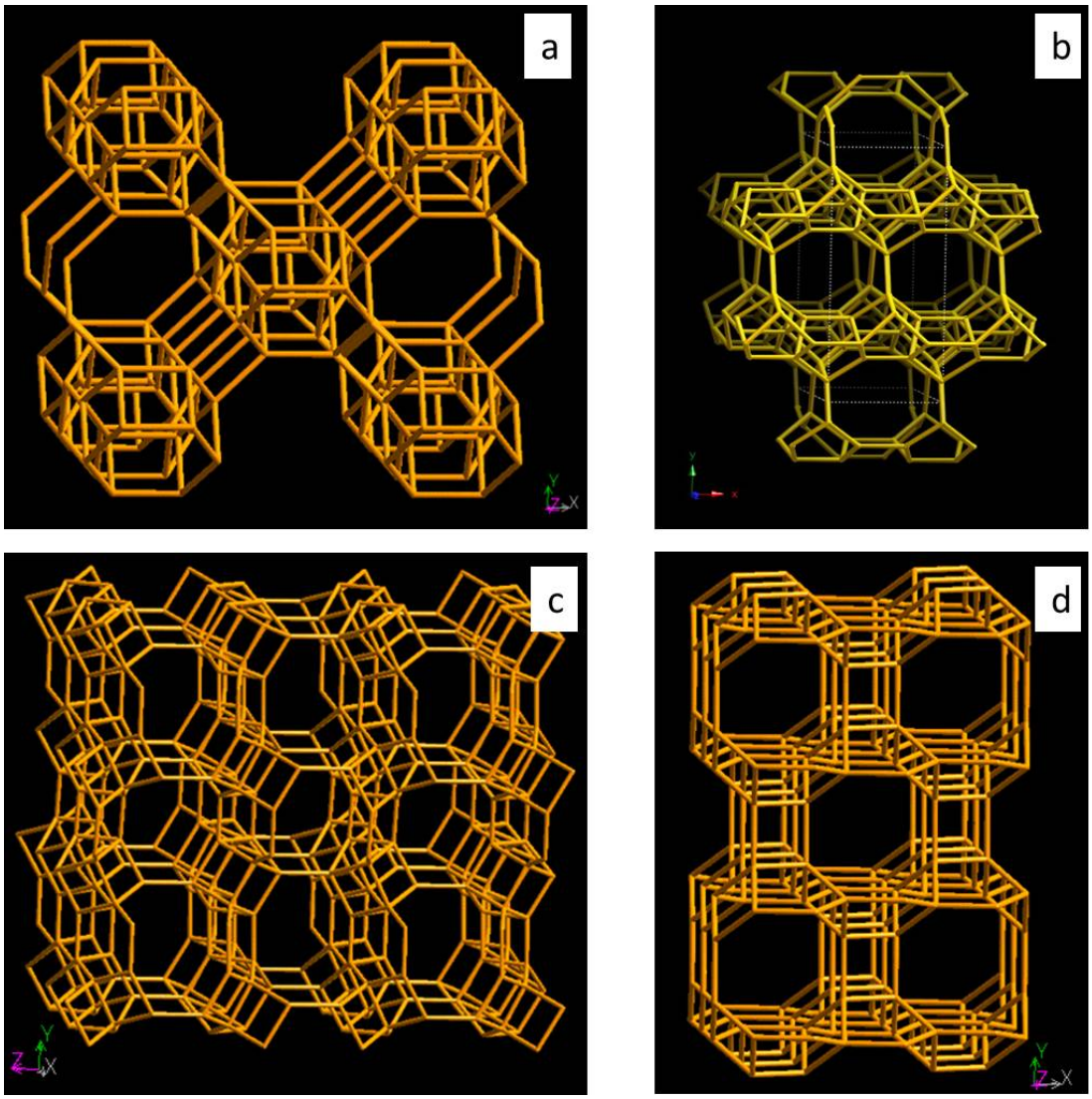

Figure 2.6 Examples of zeolites illustrating different framework types with codes of a) AEI, b) CDO, c) ZON, and d) YUG. Courtesy of International Zeolite Association (Baerlocher and McCusker 2001).

2.2.4.2 Synthetic Ion-Exchange Resins

A synthetic resin is a solid or liquid organic polymer, and the most common synthetic resin is based on a backbone of polystyrene cross-linked di-vinyl benzene. Normally, resins have a variety of functional groups with any ion-active groups located along the polymer chains. The mass as a whole appears as a solid homogeneous resin bead, made so by the interconnecting polymer chains, but with porous character. Microscopically, the mass is heterogeneous, i.e. the cross-linking is not uniform, nor

are the ion-active groups distributed uniformly.

Table 2.3 Common functional groups used to formulate four major categories of ion-exchange resins and their working pH ranges.

Cation exchangers		**Anion exchanger**	
Strong-acid	Weak-acid	Strong-base	Weak-base
4≤pH≤14	6≤pH≤14	1≤pH≤2	0≤pH≤7
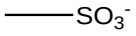		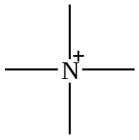	
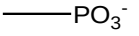	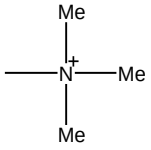	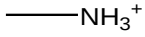	
	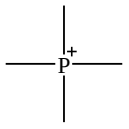		
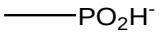			
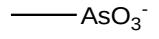			
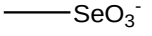			

The cross-linked polymer network discussed earlier forms the ion-exchange framework, with the degree of cross-linking being controlled by adjusting the di-vinyl benzene (DVB) proportion of the reactants, i.e. the molar ratio of DVB to styrene, and this determines the pore size of the network and the swelling propensity of the resin. For a highly cross-linked resin the mesh size within the polymers is only a few Angstroms but for one that is strongly cross-linked the mesh size may be as high as 100 Å after swelling. It should be noted that the cross-linking also serves to make the resin insoluble in water.

As mentioned above, a variety of functionalities may be attached to the styrene molecules with sulfonate is the most commonly used one for the formation of strong

acid ion-exchange resins and, quaternary amine the most common functionality for strong base exchangers. Figure 2.7 shows the building blocks of resins having frameworks of polystyrene cross-linked di-vinyl benzene, and Table 2.3 summarises the common functional groups in synthetic resins.

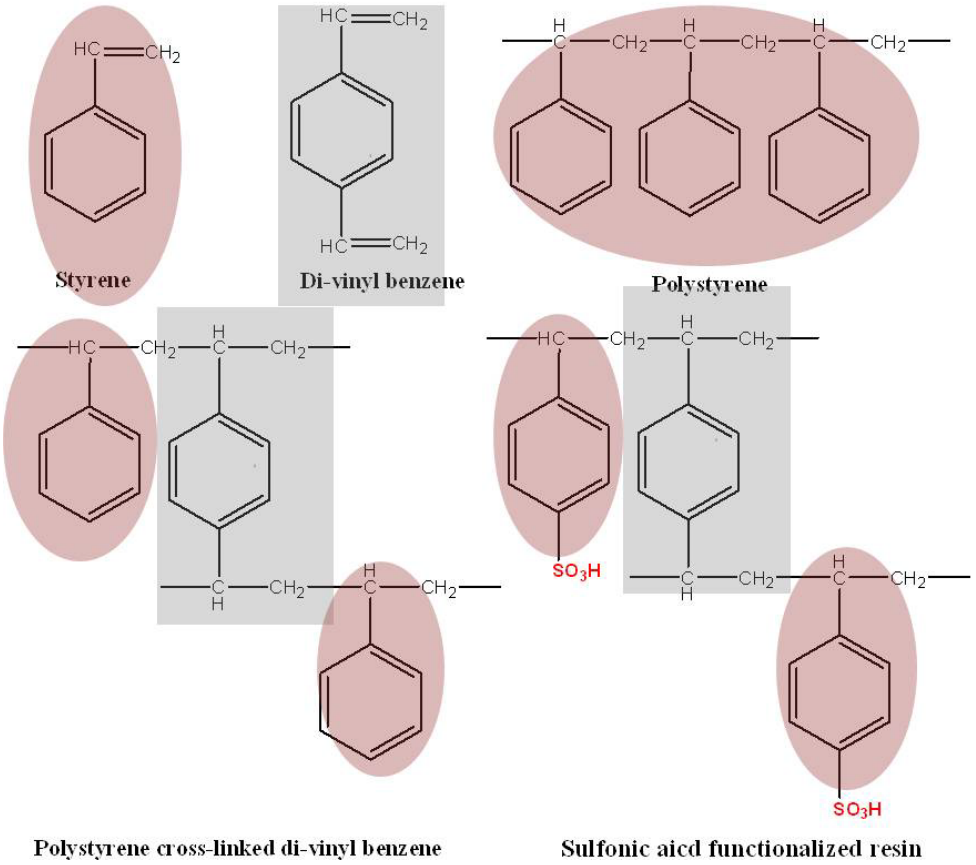

Figure 2.7 Chemical components of an ion-exchange resin with a backbone of polystyrene cross-linked di-vinyl benzene and a function group of sulfonic acid (grey shade represents styrene and pink shade represents di-vinyl benzene).

2.3 Heterogeneous Catalysis in Solutions

2.3.1 Introduction

A catalyst is a substance that alters the rate of a chemical reaction but is not con-

sumed in the reaction nor does it affect the final equilibrium position of the reaction (Gates 1991). There are two reasons for the use of a catalyst: (1) to accelerate the reaction rate and (2) to promote the production of a selected product and a catalyst cycle normally exists within the system, as illustrated in Figure 2.8.

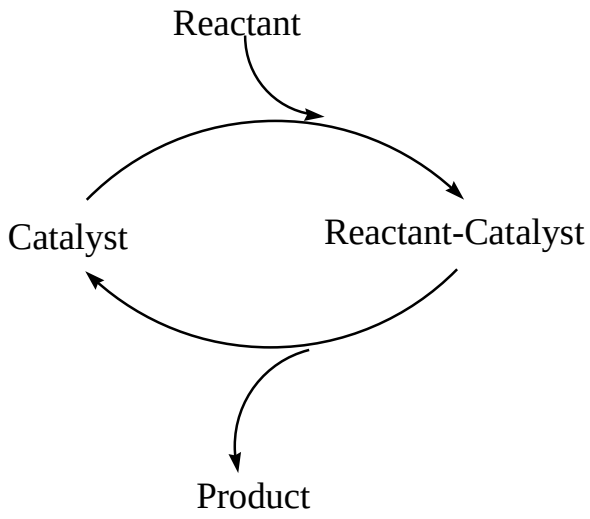

Figure 2.8 A simple illustration of a catalytic cycle.

The reason that a catalyst can accelerate a reaction is that it alters the activation energy of the reaction (E_a) by allowing the reaction to follow an alternative pathway, as demonstrated in Figure 2.9. Since k is related to E_a by the Arrhenius equation:

$$\boldsymbol{k = A \cdot e^{-E_a/(RT)}} \qquad \textbf{Eq. (2-54)}$$

where the pre-exponential factor A is a constant related to collision rates, and it is known that the rate of reaction is proportional to the rate constant (k) and the concentration of all reactants, a change in E_a alters the overall rate of reaction.

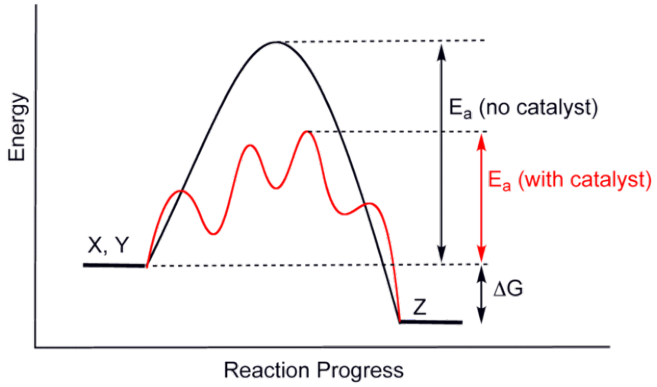

Figure 2.9 The reaction pathways and activation energies with (red line) and without (black line) a catalyst.

Catalysts can be classified into two categories: homogeneous and heterogeneous. Homogeneous catalysts have the same phase as the reactant and product, generally liquid or gas phase. For example, nitric oxide (NO) and nitrogen dioxide (NO_2) are used as homogeneous catalysts in the industrial catalytic process of converting sulfur dioxide (SO_2) into sulfur trioxide (SO_3) (Farnetti, Monte et al. 2011).

$$2SO_2 + O_2 \xrightarrow{NO/NO_2} 2SO_3 \qquad \textbf{Eq. (2-55)}$$

There is a great variety of homogeneous catalysts used, including acids, metal complex, metal ions, organometallic or coordination complexes *etc*. Homogeneous catalysts have high activities and selectivities since they can act as a single active site. However, the major disadvantage of homogeneous catalysts is that they are difficult to recover from the reaction system, since they are in the same phase as both the reactants and products, hence the process of recovering and reusing homogeneous catalyst is normally very expensive. This widely recognised, inherent limitation of homogeneous catalyst has driven extensive research in the field, for example, homogeneous rhodium phosphine catalysts are used on a large scale (4-5 MT/y) to catalyse the conversion of propene into butylaldehyde, where the product is removed from the reactor continuously by distillation. However, an increase in the chain length of the starting material (e.g. 1-octene), means the rhodium complex catalyst could no longer be utilised as the high distillation temperature of the product decomposes the structure of

the rhodium complex. Alternatively, cobalt carbonyl ($Co_2(CO)_8$) complexes may be used although the reaction conditions are more rigorous and selectivity is lower than those for the rhodium complex (Cole-Hamilton 2003), as rhodium complexes have higher selectivity to the desired linear aldehyde rather than the branched form (Figure 2.10).

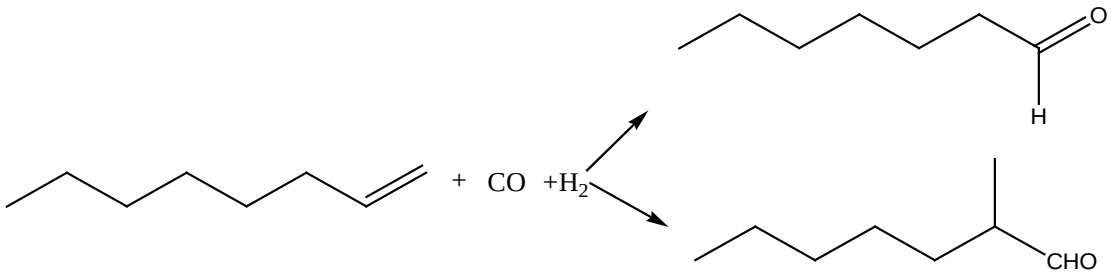

Figure 2.10 Hydroformylation of 1-octene (Cole-Hamilton 2003).

Heterogeneous catalysts have a different phase from the reactant(s). For example, the Haber process uses an iron-based catalyst to catalyse the synthesis of ammonia from nitrogen and hydrogen. Since heterogeneous catalysts are in a different phase to the reactant, there are normally several steps involved in a catalytic reaction. As illustrated in Figure 2.11, in the case of heterogeneous catalysis, it may involve:

1) external diffusion of reactant, i.e. diffusion of reactant towards the catalyst surface;
2) internal diffusion of reactant, i.e. reactant diffuses within the catalyst;
3) adsorption of reactant, which occurs due to the attractive forces between the reactant molecules and the catalyst;
4) surface reaction, which occurs when the reactant is brought close enough to the active sites;
5) desorption of products; when the product diffuses from the surface of the catalyst and leaves it unchanged;
6) internal diffusion of product;
7) external diffusion of product.

It can be seen that four of seven steps are connected with diffusion, thus the physical form and porosity of a catalyst is of crucial importance (Bowker 1998; Farnetti, Monte et al. 2011).

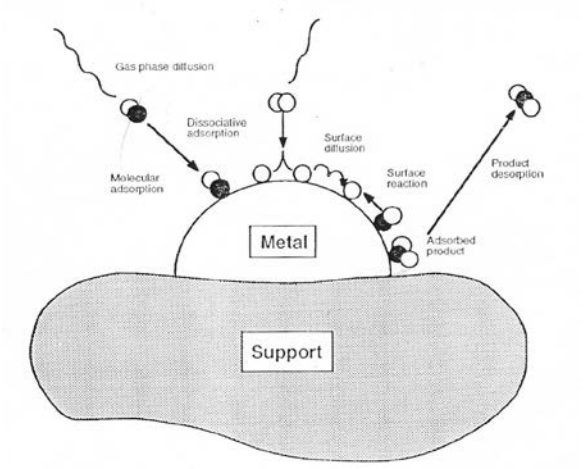

Figure 2.11 Steps involved in a heterogeneous catalysis reaction. Courtesy of Oxford University (Bowker 1998).

To evaluate the performance of a catalyst, there are four aspects normally considered. These are:

(i). activity - the quantitative measure of how quickly a catalyst works;

(ii).selectivity - the measure of a catalyst's ability to direct conversion to the desired products;

(iii). stability - demonstrates the robustness of the catalyst;

(iv). regenerability - how well the deactivated catalyst can be brought back to use.

The definitions of activity, selectivity and stability are all related to the reaction kinetics; therefore, it is important to explore the kinetics of catalytic reactions.

2.3.2 Kinetics of Catalysis

The kinetics of catalysis is a quantitative measure of how quickly a catalyst works and is usually defined as the reaction rate for converting reactant to product.

This can be understood more easily by considering the reaction examples mentioned in Figure 2.8. The overall reaction and elementary reactions can be presented as follows:

Overall reaction $$R \xrightarrow{C} P$$ **Eq. (2-56)**

Elementary reactions:

$$R \underset{k_2}{\overset{k_1}{\rightleftharpoons}} RC \xrightarrow{k_3} P$$ **Eq. (2-57)**

where R is the reactant; RC is the complex of the reactant and catalyst, and P is the product. The sequence of three steps shows that the intermediate form (RC) formed from R and C, is consumed either by decomposing back to C and R or by yielding product P. Since it is assumed that the three steps are elementary, the rate expression can be written directly from the equations:

$$r_1 = k_1[R] \cdot [C]$$ **Eq. (2-58)**

$$r_2 = k_2[RC]$$ **Eq. (2-59)**

$$r_3 = k_3[RC]$$ **Eq. (2-60)**

In the above rate expressions, r is the rate, [ ] denotes concentration[①] and k the rate constant. These equations can be solved by applying steady-state approximations, which assume that the concentration of the intermediate (RC) achieves a nearly time-independent value after a short induction period, hence, $\frac{d[RC]}{dt} = 0$. This approximation is most nearly correct when the intermediate is highly reactive and short-lived (Gates 1991). Therefore, according to the steady-state approximation, the mass balance of RC can be written:

$$\frac{d[RC]}{dt} = k_1[R] \cdot [C] - k_2[RC] - k_3[RC] = 0$$ **Eq. (2-61)**

$$[RC] = \frac{k_1[R] \cdot [C]}{k_2 + k_3}$$ **Eq. (2-62)**

[①] In elementary reactions, to be accurate, the concentration used to express kinetic equation should be activity. To simplify, here, in this thesis concentration is common used,

As soon as the concentration of RC is calculated, the rate of producing P can be calculated from Eq. (2-63):

$$\frac{d[P]}{dt} = r_3 = k_3[RC] = k_3 \cdot \frac{k_1[R]\cdot[C]}{k_2+k_3} = k'[R][C] \qquad \textbf{Eq. (2-64)}$$

This result shows that for a simple catalytic cycle, the reaction rate is dependent on the concentration of reactant and catalyst. In practical cases, the catalyst is always presented large excess and remains constant; therefore, the total rate of converting R to P is a first order kinetic process.

2.3.3 Selectivity of Catalysts

Selectivity is the most important property of a catalyst, and is defined as the catalytic reaction selecting one or more desirable products over many alternative reactions that could possibly occur (Misono 2013). If there are many possible products for a catalytic process, the selectivity of the catalyst may be superficially defined as the fraction of the desirable product over the total amount of product. Hence, a catalyst with selectivity refers to the situation where the desired product is produced in a satisfactory excess with respect to all by-products (Adriano Zecchina, Bordiga et al. 2011). This can be best illustrated by considering the case in Figure 2.12, where synthesis gas ($CO+H_2$) can be converted to methane if Ni is used as a catalyst. If Cu is applied as the catalyst, methanol is formed and higher alcohols can be produced using Cu alloys, and syngas can also be selectively converted into waxes if cobalt acts as the catalyst.

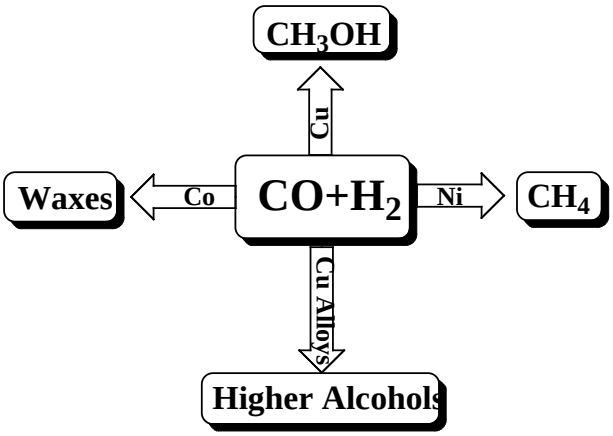

Figure 2.12 Syngas can be selectively converted into different products with various catalysts (Adriano Zecchina, Bordiga et al. 2011).

Another classical example is the catalytic conversion of ethanol, where the product is acetaldehyde and hydrogen with copper, ethylene and water with alumina, and a gasoline mixture and water with zeolite H-ZSM-5 (Adriano Zecchina, Bordiga et al. 2011).

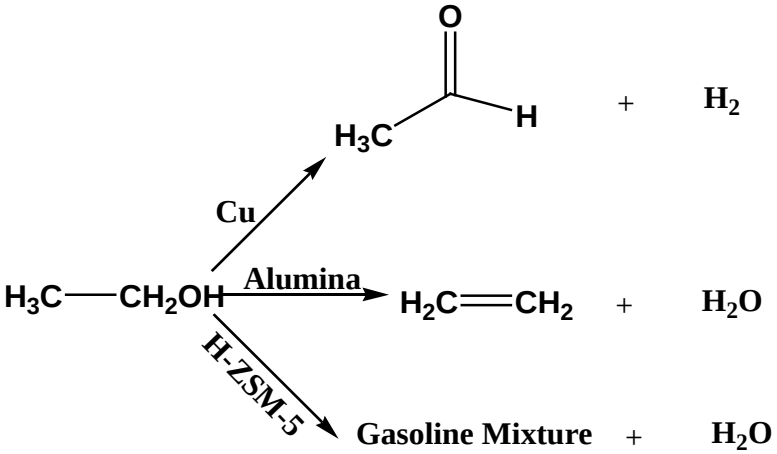

Figure 2.13 The catalytic conversion of ethanol into different compounds with various catalysts.

2.3.4 Stability and Regenerability of Catalysts

Stability is of vital importance to commercial catalysts. The definition of a catalyst states that the mass and property of a catalyst do not change during the catalytic process.

However, in reality it changes, usually in a gradual manner, and after a certain period, it has to be either replaced by fresh catalyst or reactivated by an appropriate method. Most commercial catalysts are prepared and activated through many elaborate steps and this is normally quite expensive. Therefore, the catalytic life of a catalyst should be sufficiently long; otherwise, the cost would be tremendous. In practice, the life of a commercial catalyst ranges from 10 months to 10 years (Misono 2013). Alternatively, a simple and effective continuous reactivation process is necessary for a commercial catalyst.

Chapter 3 Experimental Techniques

3.1 Materials Used

3.1.1 Activated Carbons

Granular Activated Carbon (GAC), DARCO® 20-40 mesh, was purchased from Sigma-Aldrich; herein GAC is used to refer to this material.

A further two AC samples were provided by CABOT Norit: Norit® CA1 and CNR 115. CA1 the Powdered Activated Carbon, herein referred to as PAC, is suitable for the purification of liquids in food, chemicals and pharmaceutics. Combining a significant adsorptive capacity with excellent filtration characteristics; it has a large surface area and is especially efficient in adsorbing high molecular weight organics such as large colour bodies (dyes) and proteins. Table 3.1summarises the characteristics of PAC, as published by Norit® (Norit 2014).

Table 3.1 The production specification and typical properties of PAC.

Product Specifications		Typical Properties	
Surface area (BET)	1400m^2/g	Apparent density	0.37g/mL
Particle size, d_{10}	7μm	pH range	2.0-3.5
Particle size, d_{50}	30μm	Particle size, d_{90}	75 μm

The second carbon sample supplied by Norit® is a pelletized chemically activated carbon, herein called CNR 115, produced from a renewable raw material source via a patented version of the phosphoric acid process (Norit 2010). It is produced as a dust free, 2mm diameter pellet to ensure reduced pressure drop when used in continuous fixed bed reactors. The physical appearance of these two carbons is shown in Figure 3.1.

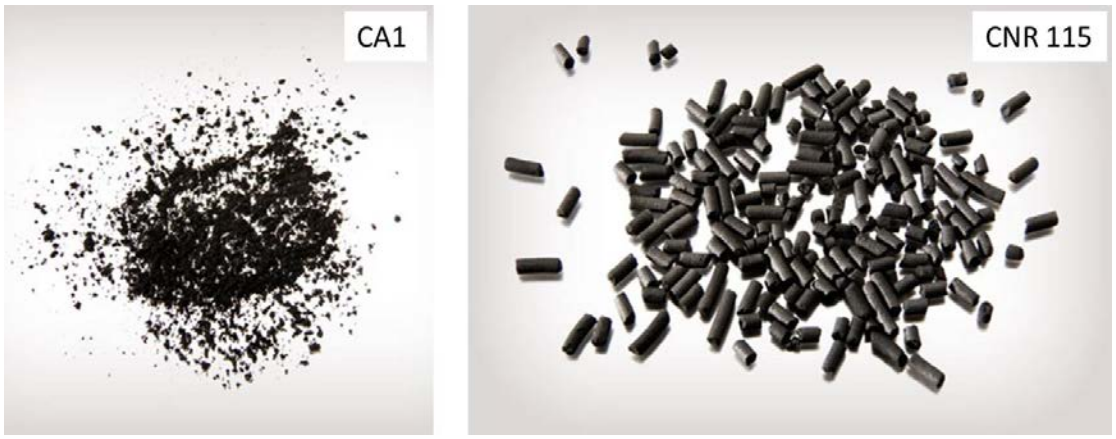

Figure 3.1 The physical appearance of powder and pelletized carbon samples from Norit®.

3.1.2 Polymeric Materials

In addition to activated carbons, 18 polymeric materials (including resins and Macronets) from Purolite® International were utilized within this work; these materials were divided into five categories and the properties of these samples is summarised in Table 3.2 (Purolite 2014).

- ***Unfunctionalised polymeric adsorbents***, including PuroSorb™ PAD300, PAD550 and PAD900. This range of adsorbents offer variations in their physical structure, i.e. pore volume, pore size, surface area and particle size range *etc*. Exhibiting very high surface areas (>1000 m^2/g) and unusual porosity, these materials are used in a wide range of applications in the food and pharmaceutical industries. The backbone of these materials is polystyrene cross-linked di-vinyl benzene.
- ***Cation exchange resins***, including weak acid, strong acid and sodium ionic forms of cation exchange resins. The ionic form of S950 and S930Plus is Na^+, where the sodium ion is readily exchanged with other cations from solution, such as Ca^{2+} and Mg^{2+}. Three weak-acid cation exchangers, with carboxylic acid functionalities: C104, C107 and C104Plus, were used in this work. A patented strong-acid exchanger with sulfonic

and phosphonic acid functional groups (Purolite 2014), S957, was also studied.

- ***Anion exchange resins,*** including weak base and strong base anion exchangers. Weak base exchangers normally have various amine functionalities, such as A830 and A111 used in this work. A830 has complex amine functionalities while A111 has tertiary amines as functional group. Strong base resins most commonly feature quaternary ammonium functionalities with the electro-neutrality balanced by Cl^-. A510Plus and A850 are good examples of strong base exchangers and both feature quaternary ammonium functionalities.
- ***Macronets***, featuring basic, neutral and acidic functionalities. Purolite® Macronets are highly and rigidly cross-linked sorbents supplied in the swollen state, and are, thus, characterised by very high internal surface areas, approaching those of ACs. As a result of their unique manufacturing technology, they will retain their swollen-state porosity, showing little or no change in swelling with change of the permeating liquid, unlike conventional polymeric sorbents. MN200 is a typical unfunctionalised Macronet with very high surface area (>1000 m^2/g). However, the performance in some specialized applications can be further enhanced by using Macronets with increased hydrophilicity, obtainable by the presence on the sorbent's internal surface of a minor amount of ion-exchange or other polar functional groups. Macronets with strong acid functional groups, such as sulfonic acid groups, were of special interest in this work and this thesis includes studies on Macronets with differing levels of sulfonic contents, specially developed by the R&D department of Purolite®. The detailed work is included in Chapter 7 of this thesis.

Table 3.2 The general information of the polymeric materials used in this work, all the information is provided by the manufacturer.

Category	Sample ID	Framework†	Functional Groups	meq/g	Moisture	pH	S_{BET} (m^2/g)	Pore Vol.(cm^3/g)	Particle Size
Polymeric Adsorbents	PAD300	C-L PS	None	NA	58-64%	8.10	700	0.7	350-1200μm
	PAD550	C-L PS	None	NA	58-64%	8.34	950	1.1	350-1200μm
	PAD900	C-L PS	None	NA	67-73%	8.07	800	1.5	350-1200μm
Cation Ex-changers	S950	PS C-L DVB	Aminophosphonic, Na^+	6.5	60-68%	9.71	<1	<0.01	350-1200μm
	S930Plus	PS C-L DVB	Iminodiacetic acid, Na^+	2.6	52-62%	10.5	<1	<0.01	800-1300 μm
	C104	C-L PA	Carboxylic acid, H^+	4.5	45-55%	5.62	<1	<0.01	350-1200μm
	C107	C-L PA	Carboxylic acid, H^+	10	45-55%	5.12	<1	<0.01	350-1200μm
	S957	PS C-L DVB	Phosphonic, sulfonic acids	10	55-70%	4.15	1.4	<0.01	350-1200μm
Anion Ex-changers	A830	PA	Complex amine	2.75	50-56%	9.01	1.82	0.01	300-1200μm
	A111	PS C-L DVB	Tertiary amine	1.7	56-62%	7.60	<1	<0.01	300-1200μm

Table3.2 The general information of the polymeric materials used in this work, all the information is provided by the manufacturer (Continued).

Category	Sample ID	Framework†	Functional Groups	meq/g	Moisture	pH	S_{BET} (m^2/g)	Pore Vol.(cm^3/g)	Particle Size
	A510	PS C-L DVB	Quaternary ammonium, Cl^-	1.15	48-56%	5.32	<1	<0.01	300-1200µm
	A850	PA C-L DVB	Quaternary ammonium, Cl^-	1.25	57-62%	5.29	<1	<0.01	300-1200µm
Macronets	MN200	PS C-L DVB	None	NA	57-61%	7.24	900	1.1	450-620µm
	MN500	PS C-L DVB	Sulfonic acid, H^+	2.771	52-57%	4.87	401	0.3095	450-620µm
	MN502	PS C-L DVB	Sulfonic acid, H^+	2.737	52-57%	4.65	355	0.3281	450-620µm
	D5564	PS C-L DVB	Sulfonic acid, H^+	2.881	52-57%	4.31	22.3	0.1325	450-620µm
	D5565	PS C-L DVB	Sulfonic acid, H^+	3.045	52-57%	4.01	21.1	0.0823	450-620µm
	D5566	PS C-L DVB	Sulfonic acid, H^+	3.342	52-57%	3.92	2.63	0.0004	450-620µm

† C-L = Cross-Linked; PS = Polystyrene; DVB = Di-vinyl benzene; PA = Polyacrylic;e.g. PS C-L DVB = polystyrene cross-linked Di-vinyl benzene.

3.1.3 Reagents and Chemicals Used

Analytical grade metaldehyde (98% purity) was purchased from Alfa-Aesar, U.K. Stock Solutions of metaldehyde (200 mg L^{-1}) were prepared in deionized water. Analytical standard grade dimethyl phthalate (99.6% purity) used as the internal standard for gas chromatography quantification was purchased from Sigma-Aldrich, U.K. Standard solutions of dimethyl phthalate (25 mg L^{-1}) were prepared by dissolving in methanol.

The ACs (i.e. GAC, PAC, CNR) used in this study were used as received. The polymeric materials provided by Purolite were dried in a vacuum oven at 45 °C for 6 h before use, to provide consistent mass bases for quantifiable comparison.

3.1.4 Synthesis of Ordered Mesoporous Silica with Sulfonic Acid and Amine Functionalities

Highly ordered mesoporous silica, first synthesised in 1998 (Zhao, Feng et al. 1998), especially materials incorporating different organic functional groups, have been explored for applications such as ion exchange (Ganesan and Walcarius 2004), heavy-metal-trapping (Feng, Fryxell et al. 1997) and solid acid catalysis (Van Rhijn, De Vos et al. 1998; Das, Lee et al. 2001). In the case of solid acid catalysts, sulfonic acid functionalised SBA-15 has been extensively synthesised and used in esterification reactions (Margolese, Melero et al. 2000; Shen, Herman et al. 2002; Mbaraka, Radu et al. 2003). The highly ordered uniform structure, high surface area and big pore volume (Bui and Choi 2009) have also allowed mesoporous silica to be applied as adsorbents and it has been reported that mesoporous SBA-15 is an effective adsorbent for the remediation of selected pharmaceuticals from surface water and wastewater, through the mechanism of hydrophilic reactions (Bui and Choi 2009). Moreover, mesoporous silica has been applied for removal of various organics such as phenolic compounds

(Cooper and Burch 1999; Burleigh, Markowitz et al. 2002), and cyanuric acid (Cooper and Burch 1999).

In this thesis, highly ordered mesoporous silica samples with sulfonic acid and amine functionalities were synthesised, characterised and applied for metaldehyde removal.

Synthesis of sulfonic acid functionalised mesoporous silica (SA-SBA-15) was similar to that described elsewhere (Margolese, Melero et al. 2000; Shen, Herman et al. 2002; Zeidan, Hwang et al. 2006). Typically, 4 g of pluronic acid 123 (Aldrich) was dissolved in 125 g of 1.9 M HCl and the resulting solution heated to 313 K before addition of tetraethoxysilane (TEOS), 3-mercaptopropyltrimethoxysilane (MPTMS) and 30 wt% H_2O_2 solution, all supplied by Sigma-Aldrich Co. The molar composition of the different mixtures for 4 g of copolymer was set as TEOS/MPTMS = 0.041(1-x)/0.041x, where x = 0.1, 0.2, 0.33, 0.5, 0.75, corresponding to functionalisation levels of 10, 20, 33, 50 and 75%. The molar amount of H_2O_2 was kept at 10 times that of MPTMS. The mixture was stirred at 313 K for 20 h, aged at 373 K for 24 h, then filtered and dried at room temperature overnight. Dried samples were extracted using absolute ethanol under reflux to remove the template.

Amine functionalised silicas (AF-SBA-15) were synthesised using a similar procedure, with TEOS and 3-aminopropyltrimethoxysilane, as described previously (Zeidan, Hwang et al. 2006).

3.2 Determination of Porosity of Materials

3.2.1 Nitrogen Adsorption/Desorption to Determine Porous Character

3.2.1.1 Introduction

The surface areas, porosities and pore volumes of all samples, detailed in Section

3.1, were determined by analysis of nitrogen adsorption/desorption isotherms. In this work, the measurements were conducted using a Micromeritics ASAP 2420 Surface Area and Porosity Analyser (Micromeritics), as shown in Figure 3.2. The Brunauer, Emmett and Teller (BET) method was utilized to determine surface area (Brunauer, Emmett et al. 1938). Barrett, Joyner and Halenda (BJH) adsorption/desorption analysis was utilized to determine the mesopore size distribution (Barrett, Joyner et al. 1951) . For micropore analysis, t-plot (Siminiceanu, Lazau et al. 2008) and α_s plot method (Sing 1989) were used as required. Mercury intrusion was used for the determination of macroporosity, as introduced in the following section. The total pore volume was evaluated from the volume of nitrogen adsorbed at the maximum pressure applied, i.e. just below the saturation point.

Figure 3.2 Micromeritics ASAP 14:20 Surface Area and Porosity Analyser

A porous solid is defined as a solid with pores, i.e. cavities, channels or interstices, which are deeper than they are wide (Rouquerol, Avnir et al. 1994). For materials with high specific areas it is useful to split the overall quantity into external and internal surface area. The external surface area is the surface area of the outer shell of the materials including the surface area of any cracks; whereas the internal surface area is the

area of all pores accessible to the adsorbate molecules. Pores can be classified into four categories: (a) open pores, (b) closed pores, (c) transport pores and (d) blind pores as shown in Figure 3.3.

Open pores are connected to the external surface of the material, whereas closed pores are voids and thus are not accessible. Transport pores connect internal areas to the external surface and are also known as through pores, blind pores are connected to transport pores but not to the external surface (Rouquerol, Avnir et al. 1994).

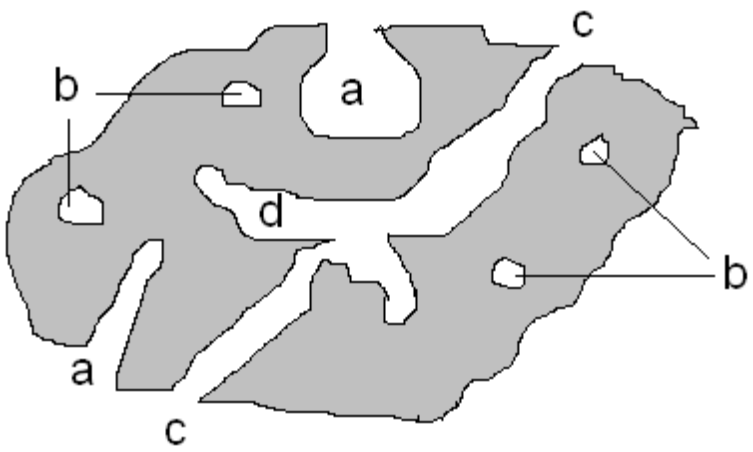

Figure 3.3 Schematic presentation of different types of pores.

To determine the internal pore size by gas adsorption the pores must be accessible to the gas molecules being used for analysis, hence, it is essential to classify pores by size. The IUPAC classification of pore size (Rouquerol, Avnir et al. 1994) is shown in Table 3.3.

Table 3.3 IUPAC classification of pores (Rouquerol, Avnir et al. 1994)

IUPAC Classification	Width of pore (nm)
Micropores	<2
Mesopores	2-50
Macropores	>50

3.2.1.2 Operating Procedure

Approximately 0.5 g of gel was transferred to a sample tube and fitted to a degas port within the analysis equipment. Prior to analysis all samples were degassed, initially by application of a slow vacuum at room temperature to 5 mmHg, before quick reduction of the pressure to 10 μmHg. Whilst under vacuum the samples were heated to 50 ºC (held for 30 minutes) before heating to 110 ºC (held for 120 min). For some samples that demonstrate thermal instability towards the second heating regime, the target temperature was reduced to 65ºC (held for an increased time of 360 min). This degassing process removed all adsorbed species; ensuring samples were clean for analysis. Degassed samples were cooled to room temperature and backfilled with inert gas (He) before being removed, reweighed and transferred to an analysis port. The reweighed mass was used as sample mass for analysis.

Adsorption/desorption isotherms were obtained at -196 ºC (critical temperature of N_2), through the use of a coolant (liquid N_2 held in Dewars surrounding the sample tube). Adsorption of N_2 (g), from a mixture of He/N_2, was monitored over 40 points between 0.1 - ~1.0 P/P_0 and desorption, from ~1.00 to 0.1 P/P_0 was recorded over 30 points. Prior to analysis a filler rod was placed within the sample tube and an isothermal jacket placed over the long sample tube neck, in order to reduce the volume of N_2 required and to ensure a constant sample temperature was maintained, respectively.

3.2.2 Mercury Intrusion Method

3.2.2.1 Introduction

Mercury intrusion is an extremely useful characterisation technique for porous materials, especially in the determination of the pore size distribution of macropores. By applying pressure to a sample immersed in mercury, the liquid metal is forced into pores and, by measuring the pressure required and the volume displaced, it is possible

to determine the size of the pores and cavities, as the pressure required to intrude mercury into the sample's pores is inversely proportional to the size of the pores. The method is called mercury porosimetry or, more often, 'mercury intrusion'. Mercury intrusion provides a wide range of information, for example, pore size distribution, total pore volume, skeletal and apparent densities and specific surface area. No other porosity characterisation technique can achieve this level of information. However, one of the greatest limitations lies in the fact that the method measures the largest entrance to a pore, but not the actual inner size of that pore, as depicted in Figure 3.4. For obvious reasons it can also not be used to analyse closed pores, since there is no entrance for mercury to enter (Giesche 2006), and the method is highly destructive of the sample analysed. Therefore, in this work, nitrogen adsorption/desorption is more frequently used and mercury intrusion is only applied when the BJH method is inappropriate for pore size distribution determination, i.e. for macroporous materials.

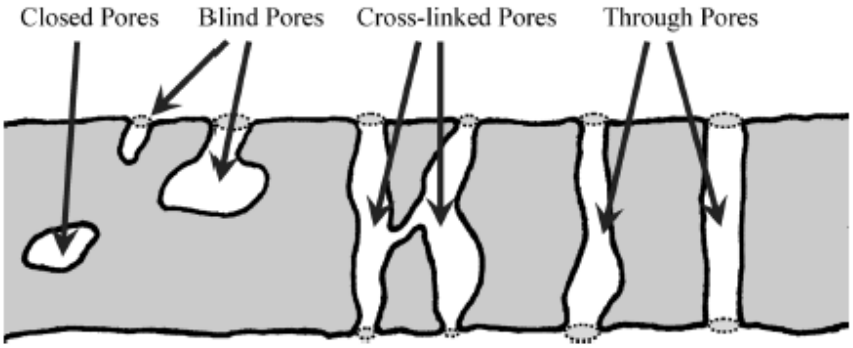

Figure 3.4 Schematic representation of pores, the dotted circle represents the pore size measured by mercury intrusion. Courtesy of Wiley-VCH 2006.

3.2.2.2 Operating Procedure

Mercury intrusion involves three main steps: sample preparation, filling and low pressure system analysis, and high pressure system analysis.

In order to achieve a good analysis, it is crucial to have a well-defined, unambiguous sample of sufficient mass to allow an accurate measurement. Porous materials also tend to adsorb water or other chemicals, which should be removed in the

sample preparation step, and filling of the material by mercury requires complete evacuation of the internal structure to avoid possible air pockets and contamination issues. Therefore, the sample is initially evacuated to remove any air and residual moisture from the pore system. After evacuation, the sample cell is filled with mercury with the entire cell still under reduced pressure. Slowly increasing the overall pressure allows mercury to penetrate the largest pores in the sample or any other void spaces. The first data point is usually taken at a pressure of 3-4 kPa or higher; thereafter, the pressure is increased to several bar, limited by the safety factors of the set-up.

After this low pressure measurement regime, the sample cell is transferred to the high-pressure system setting where the pressure is again increased, up to a maximum of 414 MPa (60, 000 psi), providing information about the smaller-sized pores.

The instrument used in this work is a PoreMaster® PM-60 produced by Quantachrome Instruments U.K. A glass test tube containing ~0.5g of materials was placed in the pressure vessel and evacuated to 6.7 Pa (50 μ m Hg). Then the pressure was increased to 60 psi, followed by transferring to high-pressure system and pressured increased to 20,000 psi.

3.3 pH Measurements

All pH measurements were conducted using a Hanna pH20 bench top meter equipped with an HI 1110B pH electrode probe. To ensure accurate measurements, the pH probe was calibrated before each batch of experiments, with both neutral (pH 7.1), and alkaline (pH 10) or acidic (pH 4.1) Hanna pH buffers, depending on the nature of specific samples.

3.4 Determination of Metaldehyde of Quantification of Concentration by Gas Chromatography

3.4.1 Introduction

Gas chromatography (GC) is a form of chromatography widely used in analytical chemistry for the separation and analysis of compounds that can be vapourized without decomposition. For those compounds with high boiling points (>350 °C) and/or compounds that are thermally sensitive, High Performance Liquid Chromatography (HPLC) is normally applied. The working mechanism of GC is akin to all other chromatographic techniques, with mobile and stationary phases required. The mobile phase (i.e. carrier gas) is an inert gas. The stationary phase consists of a packed column where either the packing or solid support itself acts as the stationary phase, or the solid support is coated with a liquid stationary phase (normally a high boiling point polymer). Commonly used in many instruments are capillary columns, where the stationary phase coats the walls of a small-diameter tube directly (e.g. 0.25 mm film in a 0.32 mm tube). A schematic representation of a typical GC setup is illustrated in Figure 3.5.

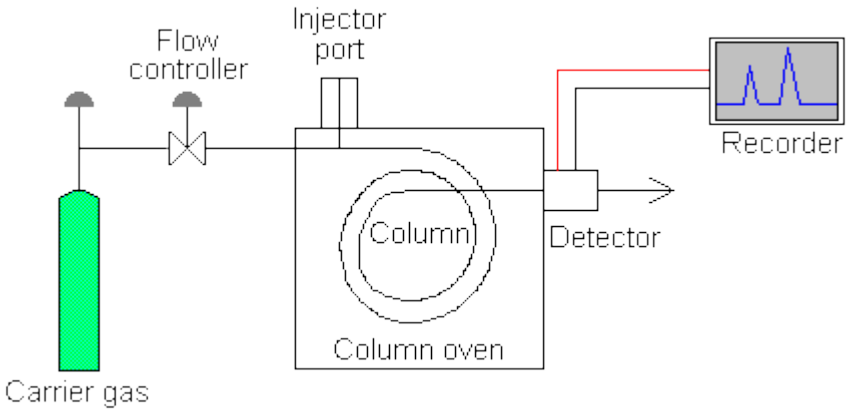

Figure 3.5 Schematic illustration of a typical GC setup.

As shown above, the arrangement normally consists of several components:

- ***Carrier gas***: as stated above, the carrier gas must be chemically inert.

Commonly used gases include nitrogen, helium, argon, and carbon dioxide. The choice of carrier gas is often dependent upon the type of detector used, and the gas supply system also contains a molecular sieve to remove water and other impurities.

- ***Sample injection port***: for optimum column efficiency, the sample volume should not be too large, and it should be introduced into the column as a 'plug' of vapour – as slow injection of large samples causes band broadening and loss of resolution. The most common injection method is via micro-syringe to injection through a rubber septum into a flash vapouriser port at the head of the column. The temperature of the sample port is usually ~50 °C higher than the boiling point of the least volatile component of the sample. For packed columns, sample size ranges from 0.1-20μL. Capillary columns, on the other hand, need much less sample, typically ~1μL. For capillary GC, split/splitless injection is normally used and Figure 3.6 shows a split/splitless injection port schematically.

  The injector contains a heated chamber containing a glass liner into which the sample is injected through the septum, and as the name suggests, the injector can be used in one of two modes: split or splitless. The carrier gas enters the chamber and can leave by three routes (when used in split mode). The sample vapourizes to form a mixture of carrier gas, vapourized solvent and vapourized solutes. A proportion of this mixture passes into the column, but most exits through the split outlet, and the septum purge outlet prevents septum bleed components from entering the column.

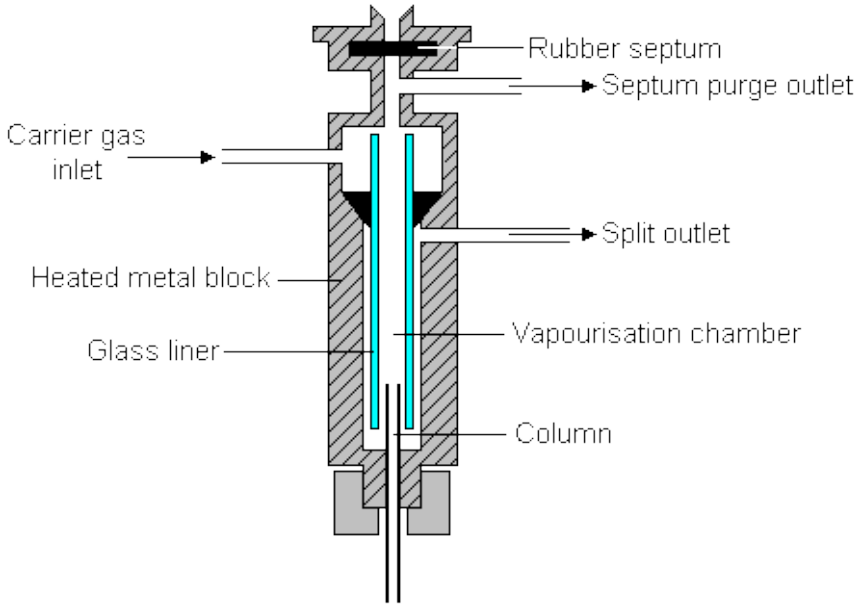

Figure 3.6 Schematic drawing of the split/splitless injection port of a GC.

- **Column**: There are two general types of column: packed and capillary. *Packed columns* contain a finely divided, inert, solid support material (commonly based on diatomaceous earth) coated with a liquid stationary phase. Most packed columns are ~1.5 - ~10m in length and have an internal diameter of 2 – 4 mm. *Capillary columns* are much narrower, with an internal diameter of a few tenths of a millimeter and are subdivided into two types: Wall-Coated Open Tubular (WCOT) or Support-Coated Open Tubular (SCOT). WCOT columns consist of a capillary tube with the walls are coated with liquid stationary phase. In SCOT columns, the inner wall of the capillary is lined with a thin layer of support material such as diatomaceous earth, onto which the stationary phase has been adsorbed. SCOT columns are generally less efficient than WCOT columns but both types of capillary column are more efficient than packed columns. In 1979, a new type of WCOT column was devised - the Fused Silica Open Tubular (FSOT) column (Figure 3.7), where its wall is strengthened by a polyimide coating, such that a FSOT column is flexible and can be wound into coils, which is now the main stream of the design.

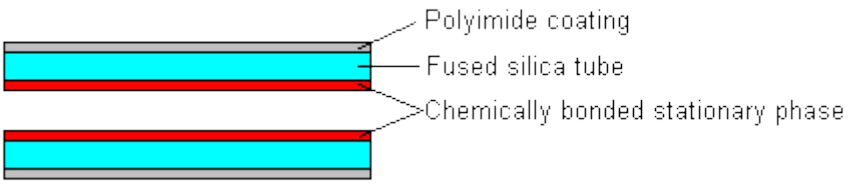

Figure 3.7 Cross-section of a fused silica open tubular column.

- ***Column oven***: used to control the temperature of the analysis process, the oven is of vital importance for analysis. Detailed oven temperature optimization will be outlined in the following section (Section 3.4.2).

  Detector: there are many detectors that can be used in gas chromatography, providing different types of selectivity. A non-selective detector responds to all compounds except the carrier gas (e.g. FID and TCD), a selective detector responds to a range of compounds with a common physical or chemical property, while a specific detector responds to a single chemical compound. Detectors can also be grouped into (1) *concentration dependent*, where the signal is related to the concentration of solute in the detector, this technique does not usually destroy the sample but dilution with make-up gas will lower the detector response; and (2) *mass flow dependent*, where the signal is related to the rate at which solute molecules enter the detector, this is a destructive technique and is unaffected by make-up gas. The following table summarises commonly used GC detectors.

  FID is the most common detector used in GC because it applies to every organic compound with C-H bonds, as shown in Figure 3.8. The effluent from the column is mixed with hydrogen and air before ignition; where the organic compounds burn to produce ions (C^+) and electrons, which can conduct electricity through the flame. A large electrical potential is applied at the burner tip, and a collector electrode located above the flame. The resulting current generated by this from the pyrolysis process is measured. FID is a useful general detector for the analysis of organic

compounds; due to its high sensitivity, large linear response range, and low noise, in addition to the fact that it is robust and easy to use; however, it does destroy the sample. Additionally, as seen in Table 3.4, FIDs are mass rather than concentration sensitive; giving the advantage that changes in mobile phase flow rate do not affect the detector's response.

Table 3.4 Summary of common detectors used in GC.

Detector	Type	Support gases	Selectivity	Detectability
Flame ionization (FID)	Mass flow	Hydrogen and air	Most organic compounds.	100 pg
Thermal conductivity (TCD)	Concentration	Reference	Universal	1 ng
Electron capture (ECD)	Concentration	Make-up	Halides, nitrates, nitriles, peroxides, anhydrides, organometallics	50 fg
Nitrogen-phosphorus	Mass flow	Hydrogen and air	Nitrogen, phosphorus	10 pg
Flame photometric (FPD)	Mass flow	Hydrogen and air possibly oxygen	Sulfur, phosphorus, tin, boron, arsenic, germanium, selenium, chromium	100 pg
Photo-ionization (PID)	Concentration	Make-up	Aliphatics, aromatics, ketones, esters, aldehydes, amines, heterocyclics, organosulfurs, some organometallics	2 pg

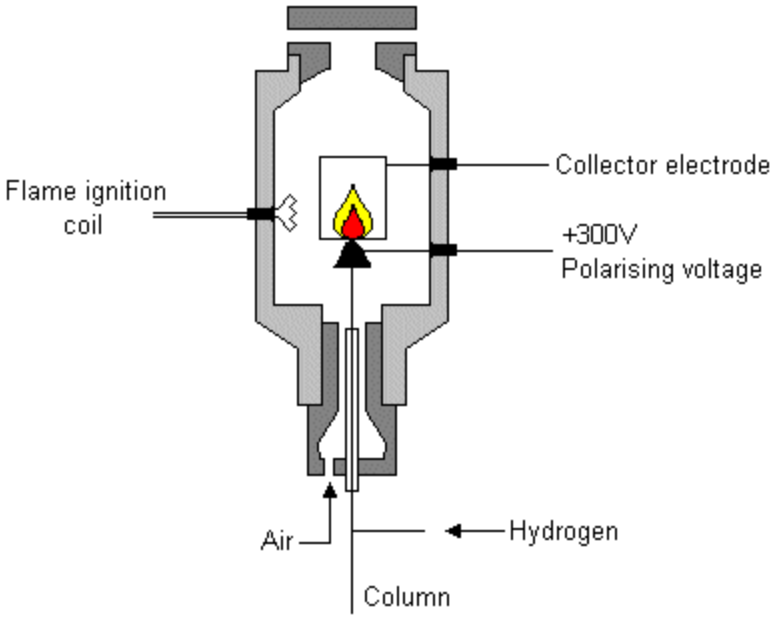

Figure 3.8 The schematic showing of a FID.

Different compounds can be separated by the column due to the various interactions the compounds experience with the stationary phase (‘like-dissolves-like’ rule); the stronger the interaction, the longer the compound remains attached to the stationary phase, hence the more time it takes to go through the column (i.e. longer retention time).

There are several factors affecting separation performance: polarity of the stationary phase; temperature, including injection temperature, detection temperature and, most importantly, the oven temperature program; flowrate of carrier gas; column characteristics including length, internal diameter and film thickness; and also amount of sample injected.

Polar compounds interact strongly with polar stationary phases; resulting in longer retention times than non-polar columns. Chiral stationary phases based on amino acid derivatives, (e.g. cyclodextrins, chiral silanes, etc.) are capable of separating enantiomers, as one form bonds slightly more strongly, often due to steric effects.

3.4.2 Developing Methods for GC Separation- Temperature Programming

3.4.2.1 Scouting Gradient

Higher temperatures increase the amount of the compound in the gas phase but as decrease its interaction with the stationary phase, hence, retention times are shorter but, consequently, the quality of separation deteriorates. As a result, the oven temperature program is of critical importance, thus, a scouting gradient (Crawford Scientific 2014) is normally employed when little information about the compounds are known. A good general scouting gradient is shown in Figure3.9.

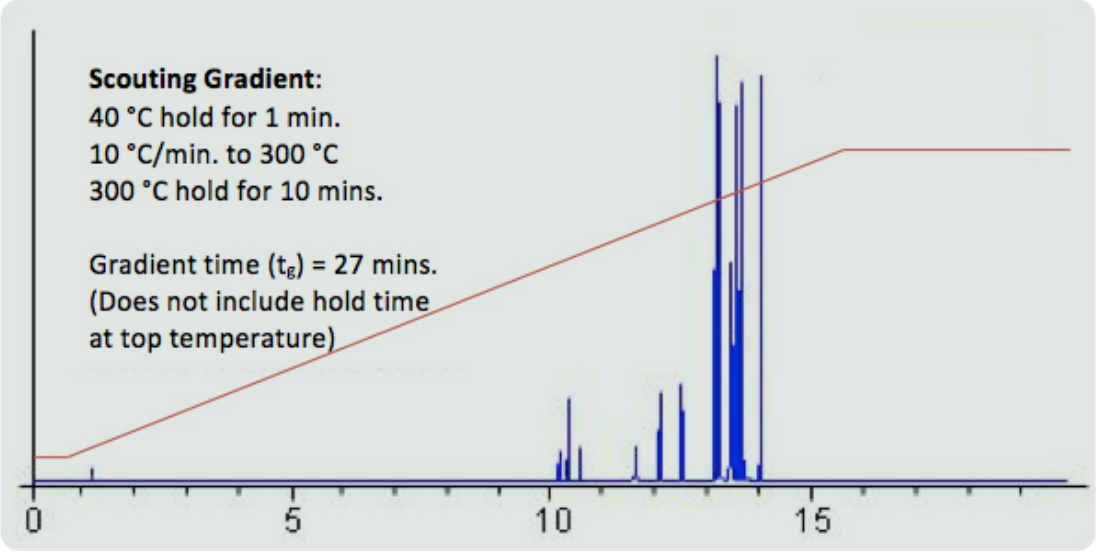

Figure3.9 Generic scouting gradient used to investigate the retention behaviour of compounds of interest when little information is available. Courtesy of Crawford Scientific (Crawford Scientific 2014).

The initial oven temperature should be as low as practicably possible (normally 35-40 °C, which is usually dictated by the ambient temperature of the laboratory where the instrument is housed), and the gradient rate is normally 10 °C/min, ending at the column gradient maximum temperature (the higher maximum operating tem-

perature as indicated on the column box or supplier specification) where a hold of at least 10 min should be employed. This program will ensure that all compounds of interest are eluted from the column with the relatively shallow temperature gradient resulting in a reasonable separation of peaks. Due to the investigative nature of this scouting run, it will likely be the longest performed during any method development activity and the final method will be shorter in the vast majority of cases.

3.4.2.2 Isothermal Elution

Following the use of a scouting gradient, it can easily be decided whether is is possible to use an isothermal method by considering the following rule:

If the peaks elute over less than 25% of the gradient time, then isothermal operation should be possible. For the scouting gradient shown in Figure3.9:

- t_g = gradient time = 27 min. (Holding at 40 °C for 1 min and increasing from 40-300 °C at a speed of 10°C in 26 min, thus the total gradient time is 27 min)
- t_i = elution time of initial peak = 10.08 min.
- t_f = elution time of final peak = 14.12 min.
- t_r = retention time window = $t_f - t_i$ = 14.12 – 10.08 = 4.04 min.
- 25% t_g = 6.75 min.

As shown above, all analytes elute in a period shorter than 25% of the gradient time, hence, isothermal operation can be used. The temperature of the isothermal method then can be calculated by:

$$T' = T_{target\ compound} - 45°C \qquad \textbf{Eq. (3-1)}$$

3.4.2. 3 Temperature Programmed Analysis

If isothermal elution is not possible, that is to say all compounds of interest cannot be eluted in less than 25% of t_g, a temperature programmed analysis must be carried out (Crawford Scientific 2014).

The parameters that should be optimised in temperature programmed GC are:

- initial temperature and hold time,
- ramp rate,
- final temperature and hold time.

In order to simplify this process, attention should be paid to the following:

Initial temperature:

Initial temperature and hold time affect the resolution of early eluting peaks. 40°C is often the lowest practical oven temperature that can be used without cryogenic cooling. If there is a problem resolving early eluting analytes, the initial oven temperature should be reduced instead of adding an initial hold time. This can be best illustrated by the following example shown in Figure 3.10.

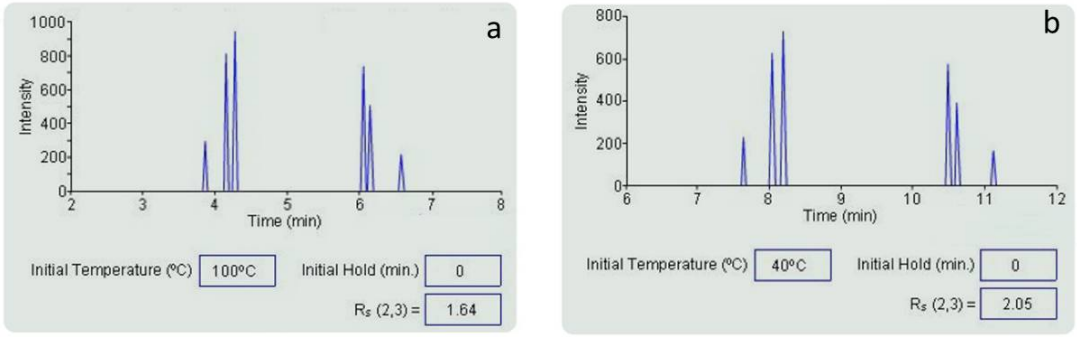

Figure 3.10 GC figures showing effect of initial temperature (Crawford Scientific 2014).

As can be seen above, decreasing the oven temperature from 100 °C to 40 °C increases the compound pair with retention time of 4.2 - 4.3 min. Figure 3.11 shows the effect of hold time at similar initial temperatures. An increase in hold time from 1–2 min (the initial oven temperatures are slightly different) does improve resolution of the compound pair but not to the same extent as decreasing the oven temperature. The analysing conditions in Figure 3.10 and Figure 3.11 (labeled a, b and c) are as follows:

- ***Column****:* 5% Diphenyl dimethylpolysiloxane, 30 m×0.25 mm ×0.5 µm.
- ***Injection****:* split 100:1, 1 µL, @180°C.
- ***Flow:*** constant linear velocity, 40 cm/sec.

- ***Carrier gas:*** hydrogen.
- ***Detector:*** FID @ 250 ^{o}C.
- ***Oven program***: initial temperature (b) 40 °C, (c) 50 °C or (a) 100 °C (no hold or hold for 1-2 min), before heating to 300 °C at a ramp of 10 °C/min, held at 300 °C for 20 min.

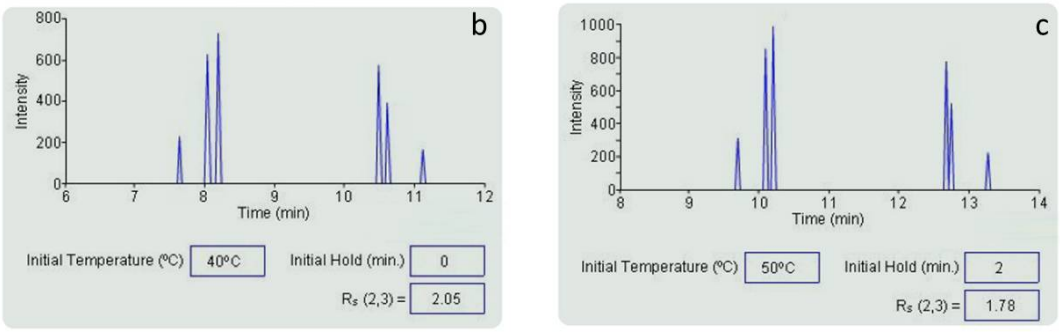

Figure 3.11 GC figures showing effect of hold time at similar initial temperatures (Crawford Scientific 2014).

Hold time at initial temperature:

The hold time at initial temperature is normally related to the sample injection method, depending on whether it is split or splitless. Split injection does not normally require an initial delay as holding at a low initial temperature for a prolonged period will broaden peaks, mitigating the efficiency of the split injection. However, a caveat to this is that, when operating at low initial oven temperatures (i.e. 30 °C less than the solvent boiling point), which may be required to improve the retention of very volatile analytes, a hold time may be necessary. In this case, an initial estimate of 30 s is advised and increased if necessary.

Splitless injection requires an initial hold time in order to 'cold trap' and/or 'solvent focus' the analytes. The hold time should be matched to the splitless time of the injection, typically it is 1 min.

Ramp rate:

Adjusting the rate at which the temperature increases during the thermal gradient

(ramp rate) has the most pronounced effect on the resolution of compounds that elute in the middle of the chromatogram.

There is an empirical equation proposed for the the optimization of the ramp rate (in °C/min), which is equal to 10 °C per void time (t_0, min), defined as the retention time of an unretained compound.

$$\boldsymbol{Optimum\ ramp\ rate}\ (°\boldsymbol{C/min}) = \mathbf{10°}\boldsymbol{C/t_0} \qquad \textbf{Eq. (3-2)}$$

Therefore, if:

- t_0=30 s; then ramp rate=20 °C/min;
- t_0=60 s; then ramp rate=10 °C/min
- t_0=120 s; then ramp rate=5 °C/min

Once this initial estimate has been made, the ramp rate can be further optimised by using adding or reducing 5 °C/min per step. If there is a critical pair of peaks that cannot be resolved by altering or using multiple ramp rates, then the following steps may be helpful:

- Step 1: Determine the elution temperature of the critical pair;
- Step 2: Using Eq. (3.1), determine the temperature at which to include an isocratic hold, i.e. subtract 45°C from the temperature at which the critical pair elutes.
- Step 3: Start with 1min hold time and increase if needed until separation occurs.

Final temperature and hold time:

The final temperature should be determined from the scouting gradient analysis. If there are no compounds left to elute after the scouting gradient, the final temperature should be set 10–30°C above the elution temperature of the final compound.

For example, if we have the following conditions:

- Initial temperature for the oven of scouting gradient =40 °C (T_i);
- Ramp rate= 10 °C;
- The retention time when the final compound is eluted = 14 min (t_f).

Then the final compound will elute at the temperature of 180°C (= T_i+ (rate × t_f) =40+10×14). Therefore, the final temperature should be in the range of 190-210 °C.

If a thermal burn is required to remove late eluting analytes or stationary phase bleed, and avoid possible carryover/contamination, a rapid gradient up to the gradient temperature maximum of the column should be included. The hold time should be optimised until no more peaks are seen in the chromatogram.

3.4.4 GC-FID Used

Concentrations of metaldehyde solutions in this work were determined by GC, and two types of detectors were used, depending on the concentration level of metaldehyde present. GC-FID was employed for the concentrations in ppm level, i.e. samples for the study of adsorption kinetics, isotherms and mechanisms prepared synthetically in the laboratory. The GC instrument used was a GC-2014, supplied by Shimadzu. Water samples provided by Scottish Water, were analysed using Solid Phase Extraction (SPE) and GC-MS, as detailed stated in the following section.

The analytical conditions used were as follows:

a. ***Column:*** SPB^{TM}-5 capillary column 30 m length ×0.53 mm internal diameter ×0.5 μm film thickness;
b. ***Temperature of injector:*** 100 °C
c. ***Temperature of detector:*** 180 °C
d. ***Oven Program:*** initial temperature 70 °C, held for 1 min; temperature increased to 100°C at 7.5°C/min, then to 180 °C at 15 °C/min, held for 6 min.
e. ***Carrier gas:*** helium (5.0 mL/min)
f. ***Combustion gas:*** hydrogen (30 mL/min) and air (300 mL/min)
g. ***Injection model:*** splitless
h. ***Injection volume:*** 1 μL

There are several types of quantification methods commonly used in GC and the

three most commonly used are the area percentage, external standard and internal standard methods. Area percentage is the simplest quantification method, which assumes that the detector responds identically to all compounds. This assumption is not valid in most cases; therefore, this method is only employed for rough estimations.

External standard method requires highly purified compounds of interest (analytical standard, normally >99.9% purity). For each compound of interest, calibration curves should be produced before analysis. The analytical standard is prepared at a minimum of five concentration levels and each level analysed by GC to obtain a linear relationship of mass injected (y axis) and peak area (x axis). Providing a calibration curve is available, the sample with unknown concentration is analysed and, as the peak area is therefore known, it is possible to calculate the mass injected, from the calibration curve. The external standard method is more accurate than area percentage method, but still greatly affected by instrumentation conditions.

Internal standard method is more reliable and affected less by instrumentation conditions, therefore, in this work; internal standard quantification method was employed. The compound used as internal standard was dimethyl phthalate (Sigma-Aldrich, 99.5% analytical standard grade). Before analysis, the calibration curve was produced by the following steps:

1. Preparation of five levels of metaldehyde standard calibration solutions. Since the concentration level in this work was 5-200 ppm (mg/L), the five levels were 5 ppm, 25 ppm, 50 ppm, 100 ppm and 200 ppm.
2. Prepare internal standard solution with a concentration of 25ppm.
3. Add 0.5 mL of internal standard solution to 0.5mL of each metaldehyde calibration solution. Mix well and prepare for analysis.
4. Inject 1µL of the mixed solution and analyse.
5. Plot peak area ratio (x axis) vs. concentration ratio (y axis).

Table 3.5 and Figure 3.12 show the internal standard calibration curve for the metaldehyde solutions prepared, with a concentration range of 5-200 ppm.

Table 3.5 Raw data for generating a typical internal standard method calibration curve.

$A_{sample}/A_{internal\ standard}$	$C_{sample}/C_{internal\ standard}$
0.1576	0.2 (5/25)
0.8225	1 (25/25)
1.4948	2 (50/25)
3.0154	4 (100/25)
6.2309	8 (200/25)

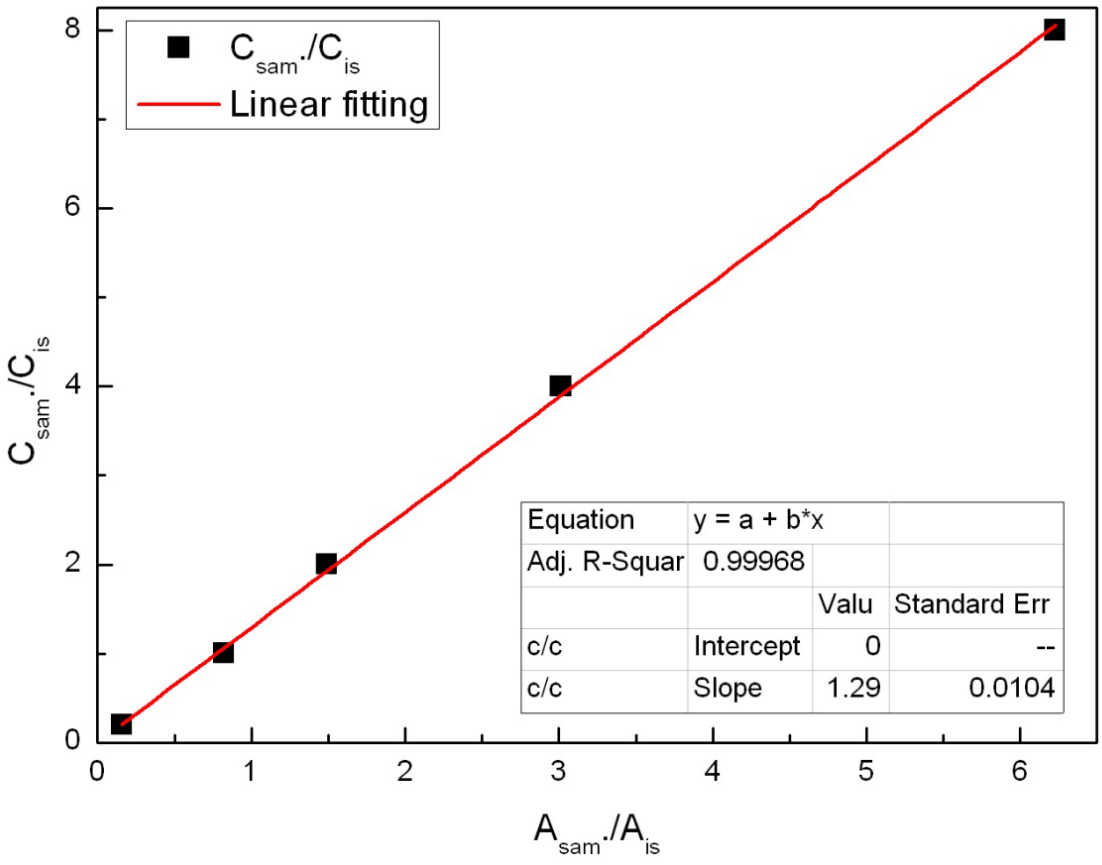

Figure 3.12 Calibration curve for metaldehyde GC analysis.

3.4.5 GC-MS Used

3.4.5.1 Solid Phase Extraction (SPE)

Since the metaldehyde level in real water samples is very low, normally ppb (µg/L) levels, which cannot be directly analysed by GC, it is therefore, necessary to accumulate the metaldehyde mass first by SPE, which is the most popular sample preparation technique for environmental and food samples. Due to its high versatility, SPE can be used for many purposes, such as purification and trace enrichment.

The general SPE procedure has to provide sample extracts free of interfering matrix components and concentrated enough for detection. The SPE process basically consists of four steps: conditioning, sample addition, washing and elution, as depicted in Figure 3.13.

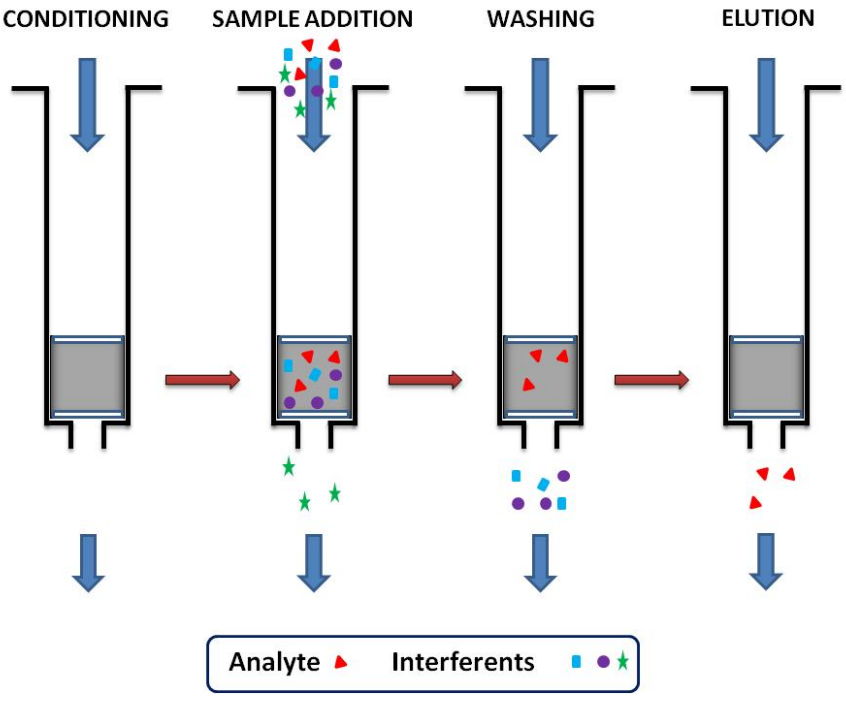

Figure 3.13 Schematic representation of SPE enrichment procedure, courtesy of INTECH (Lucci, Pacetti et al. 2012).

Firstly, the most suitable solid sorbent (cartridge) is selected and conditioned us-

ing an appropriate solvent. During conditioning, the functional groups of the sorbent bed are solvated to allow them to interact with the sample. The sample addition step consists of the percolation of the sample through the cartridge, during which, the analytes (compounds of interest), as well as some matrix components, are retained and thus concentrated on the SPE cartridge. Successively, the loaded cartridge is dried by passing air through it. The final dried cartridge is eluted using an appropriate solvent, before the solvent is vapourized to the desired volume, e.g.1 mL. The enrichment time is dependent on the initial volume of sample passed through the cartridge and the final volume of solvent. For example, 500 mL of metaldehyde contaminated water sample passed through a cartridge, followed by elution of the cartridge using 5 mL of dichloromethane (DCM), with the DCM vapourized to 1mL would result in an enrichment of 500 times.

3.4.5.2 GC-MS Analysis

Concentrated water samples were analysed by GC-MS, with analytical conditions adopted from the standard method proposed by the Environmental Agency U.K. (UK Environmetal Agency 2009). The instrumental arrangement comprised a Trace GC coupled with Polaris Q ion trap mass spectrometric detector, provided by Thermo Scientific.

SPE cartridges used for sample preparation were Strata-X polymeric reversed phase 200mg (3mL), purchased from Phenomenex.

The gas chromatograph was equipped with an auto-sampler and mass spectrometric detector capable of operating in selective ion monitoring mode. The analytical conditions used are as stated below:

a. ***Column:*** HP^{TM}-5 capillary column 30m length × 0.25 mm internal diameter × 0.25 μm film thickness
b. ***Temperature of injector:*** 300 °C
c. ***Oven Program:*** initial temperature 35 °C, held for 1 min; temperature in-

creased to 260 °C at 20 °C/min and held for 0.5 min.

d. ***Carrier gas:*** helium (5.0 mL/min)

e. ***Injection model:*** splitless

f. ***Injection volume:*** 1 µL

Quantification was achieved by use of an internal standard (analytical standard grade 1, 4, dichlorobenzene-d_4, supplied by Sigma-Aldrich) and same experimental procedure outlined in Section 3.4.4 was followed to generate the calibration curve. Figure 3.14 shows typical total ion and selective ion chromatographs for metaldehyde and the internal standard. The conditions shown in Table 3.6 were used for peak qualifications. A more detailed description of the experimental procedure for determination of metaldehyde concentrations by GC-MS is available from the Environmental Agency U.K. (UK Environmetal Agency 2009).

Table 3.6 Guiding table for determination of chromatographic peaks.

Compound	Retention time	Ions monitored (Target and Qualifier)	
1,4-dichorobenzene-d_4	9.26 min	150	152
Metaldehyde	9.04 min	45	89

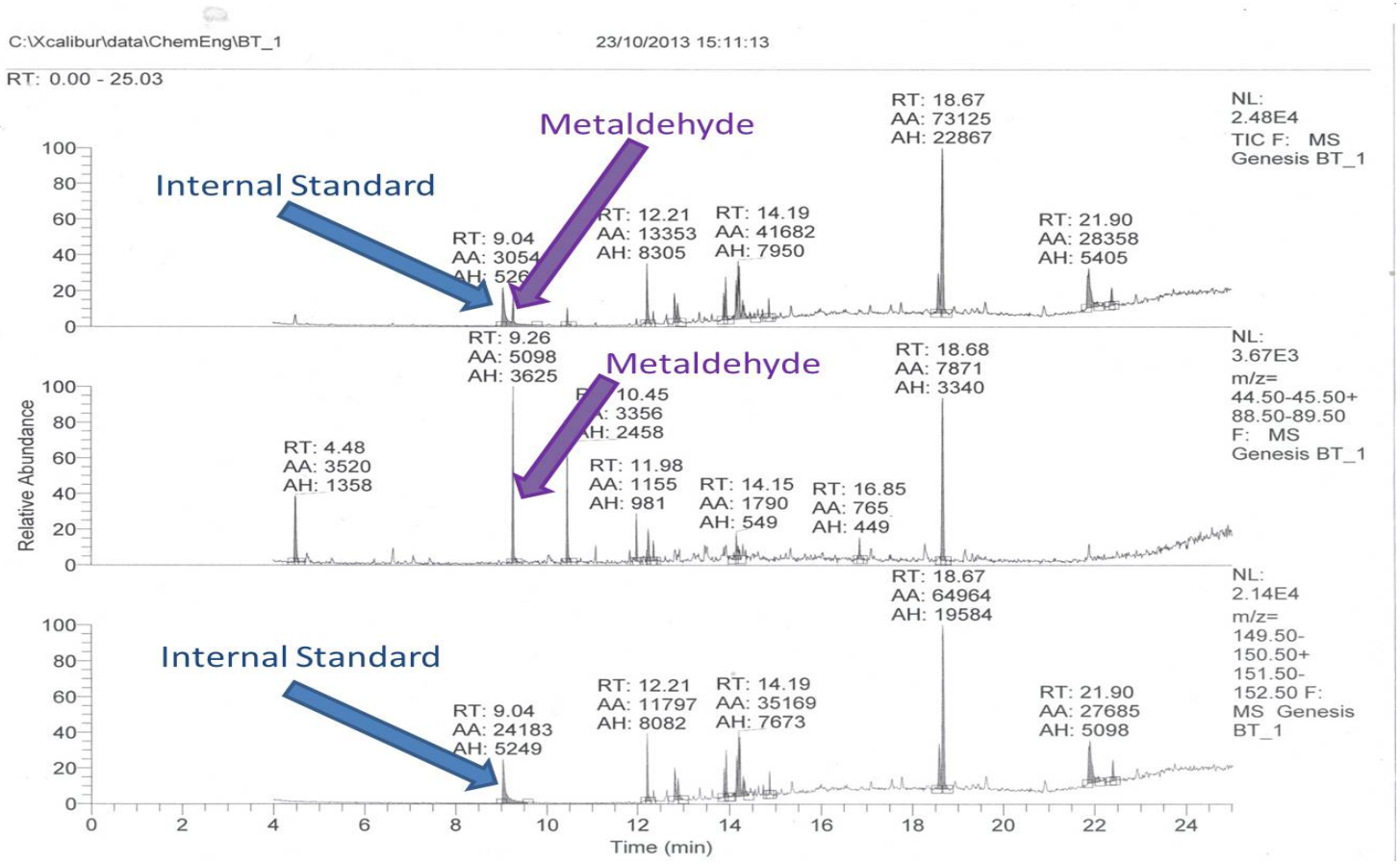

Figure 3.14 Typical chromatograph for metaldehyde and internal standard, the top chart shows total ion chromatography and the middle and bottom show selective ion chromatography for metaldehyde and internal standard, respectively.

3.5 Determination of Acetaldehyde Level by High Performance Liquid Chromatography

3.5.1 Introduction

Similar to gas chromatography, High Performance Liquid Chromatography (HPLC) is another type of column chromatography but highly improved as a result of the high pressure (up to 400 bar) applied to force the solvent through the column rather than the usual gravity driven drip. The increased pressure also allows narrow columns, packed by a fine particle size of material (higher surface area stationary phase) to be used, improving the interaction between the stationary phase and the analytes, hence, the separation performance. Most importantly, HPLC can be equipped with different detectors, used to detect the compounds as soon as they are eluted from the column. Figure 3.15 shows a schematic of the analytical flowchart for HPLC.

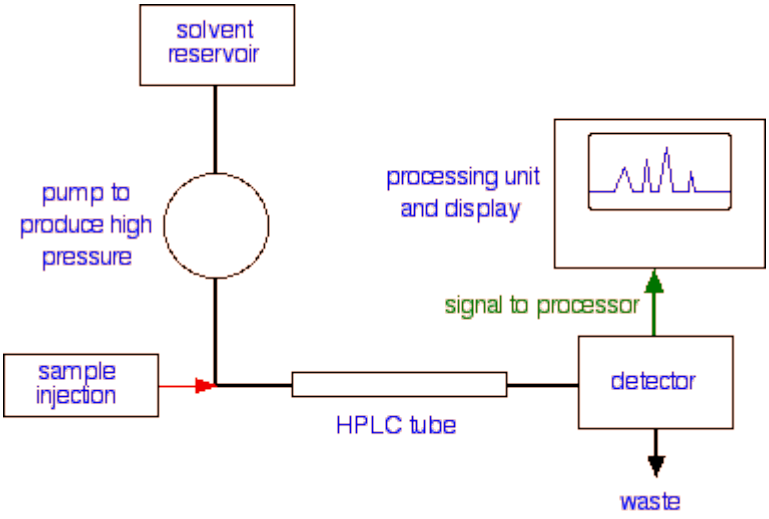

Figure 3.15 Schematic flowchart for a HPLC.

The operating procedure for HPLC is very similar to GC, normally consisting of sample injection, analysing and quantification, *etc*. (Douglas A. Skoog, Donald M. West et al. 2013).

3.5.2 HPLC Method Used

A Shimadzu Prominence equipped with an SPD-20A UV-Vis detector was employed to determine the concentration of acetaldehyde in the water samples studied.

The method used consisted of two steps: (1) sample preparation and (2) analysis. Sample preparation involved the water samples being reacted with 2, 4- dinitrophenyhydrazine (DNPH, 97% purity supplied by Sigma-Aldrich Co.), to yield acetaldehyde-DNPH, which was detected by UV-Vis (Kuwata, Uebori et al. 1983; Zhang, Lioy et al. 1994; Possanzini and DiPalo 1995). The mechanism of reaction between DNPH and aldehyde or ketone is shown in Figure 3.16.

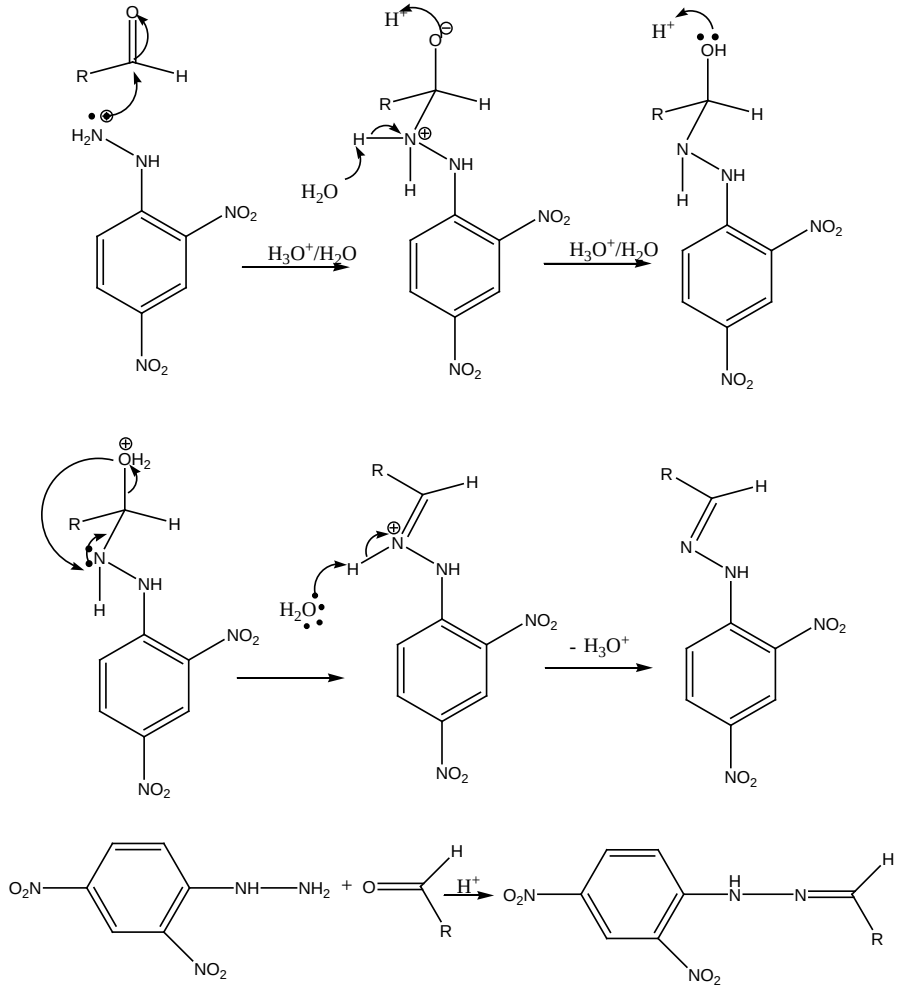

Figure 3.16 The mechanism of reaction between DNPH and aldehyde or ketone under the conditions of proton catalyst (Graham Hill and Holman 2011).

A VP-ODS column (150 mm L × 4.6 mm D), supplied by Shimadzu, was used for separation of compounds and the mobile phase was 50/50 v/v water/acetonitrile (both HPLC grade), with a flow rate 1.5 mL min^{-1}. The wavelength was set as 365 nm. An external standard quantification method was applied with analytical standard grade acetaldehyde-DNPH, supplied by Supelco, used as the external standard. A typical calibration curve is shown in Figure 3.17.

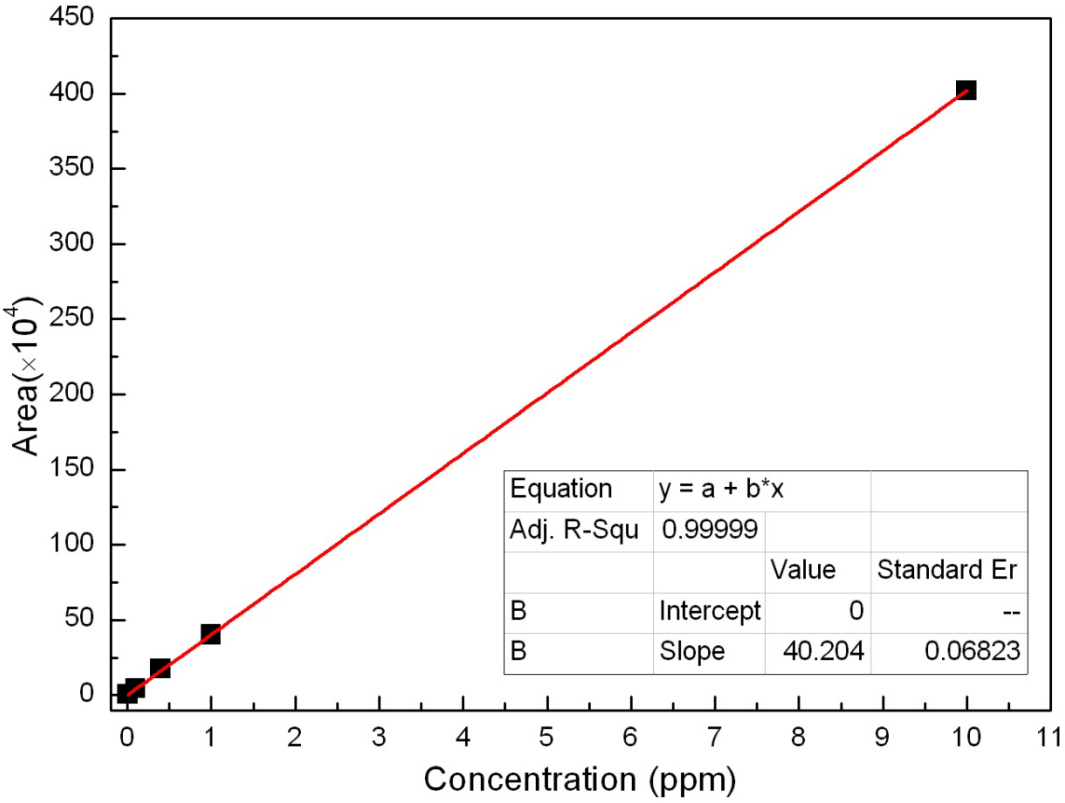

Figure 3.17 Calibration curve of the external quantification method for determining acetaldehyde using HPLC.

3.6 Determination of Materials Morphology using Scanning Electron Microscopy

3.6.1 Introduction

Scanning Electron Microscopy (SEM) is a very powerful technique used to determine the surface morphology of samples, which involves irradiating a sample with

a focused electron beam. The interactions between sample and electron beam produces signals, which are the results of different volumes within the sample and include backscattered electrons, secondary electrons and X-rays (shown in Figure 3.18), enabling the characteristics of the material (such as surface topography, morphology and composition) to be observed and characterised (Goldstein, Newbury et al. 2007).

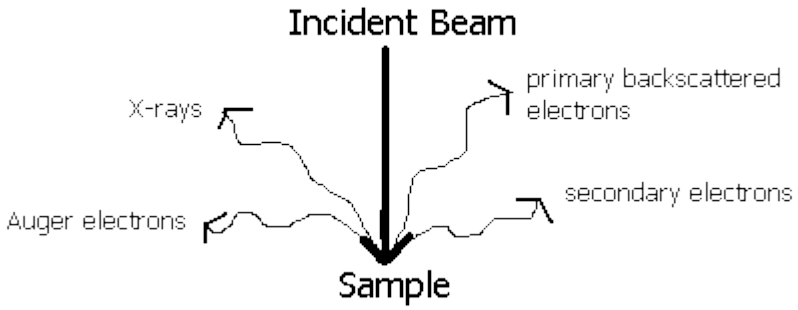

Figure 3.18 Electrons and X-rays ejected from the sample when the electron beam strikes the sample.

A schematic of an SEM instrument is shown in Figure 3.19, depicting the normal arrangement of electron gun, anode, magnetic lens, scanning system, sample chamber and electron and X-ray detectors, *etc* (Goldstein, Newbury et al. 2007). The electron gun fires a beam of electrons from the top of the microscope, and the electron beam follows a vertical path through the microscope, which is held within a vacuum. The beam travels through electromagnetic fields and lenses, which focus the beam toward the sample. Once the beam strikes the sample, electrons and X-rays are ejected from the sample, which are then detected and the resulting image of the sample observed.

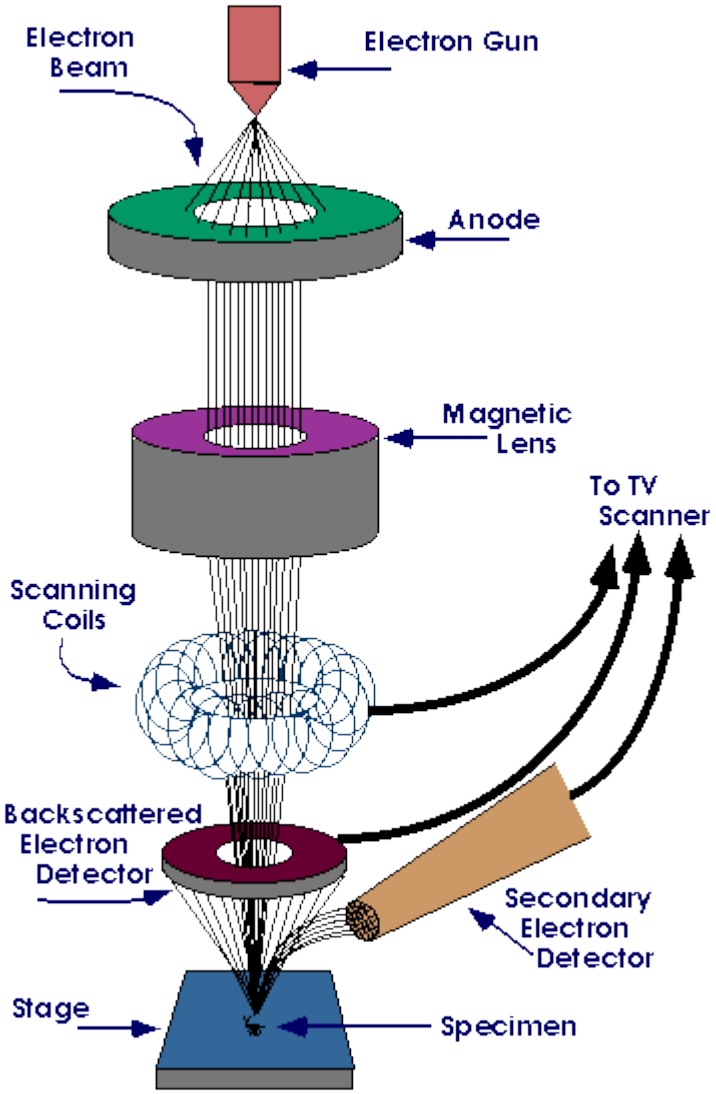

Figure 3.19 A diagram of an SEM instrument. Courtesy of Iowa State University(Iowa State University 2014).

3.6.2 SEM Used

The surface morphology of the porous materials was recorded using a Hitachi SU6600 analytical variable pressure field emission scanning electron microscope.

Since the materials used in this work are non-conductive, the samples were cold gold coated by an Edwards S150 sputter coater prior to analysis. The samples were crushed by mortar and pestle into small particle to be as homogeneous as possible so that an even coverage of gold could be achieved. After gold coating, the samples were

analysed and images were captured. Normally, each sample was analysed in 3 different surface sites at magnifications in the range of 30k - 300k.

3.7 Determination of Surface Chemistry by Boehm Titration

The acidic and basic properties resulting from the species present on the surface of carbons and polymeric materials may be evaluated using the scheme suggested by Boehm (Boehm and Voll 1970; Goertzen, Thériault et al. 2010; Oickle, Goertzen et al. 2010), which measures the volume of particular concentrations of acid and base required in a set of neutralising titrations.

The amounts of various acidic and basic functional groups may be determined by selective neutralisation by sodium hydrogen carbonate ($NaHCO_3$), sodium carbonate (Na_2CO_3) and sodium hydroxide (NaOH), for acidic groups, and hydrochloric acid (HCl), for basic species.

Typically, samples of ~1.0g of material were placed in four separate sample bottles already filled with 50 mL of 0.1 mol/L of each of the aforementioned reagents i.e. 1.0 g of material was reacted separately with each chemical agent. The sample bottles were left for 72 h, at room temperature, with occasional shaking to facilitate a uniform reaction. The resulting mixtures were separated by filtration and the remaining amount of each reagent neutralised by back titration using acid or base, using 0.1 mol/L hydrochloric acid or 0.1 mol/L sodium hydroxide, as required (Goertzen, Thériault et al. 2010; Oickle, Goertzen et al. 2010).

The quantities of specific species determined, using this method is outlined in Table 3.7.

Table 3.7 Determination of surface function groups by different reagents.

Reagent	Surface Species Reacted
HCl	Total Basic
NaOH	Phenolic + Carboxylic + Lactonic
Na_2CO_3	Carboxylic + Lactonic
$NaHCO_3$	Lactonic

Hence the quantities of each species may be calculated from the following relationship:

Total Basic = HCl

Total Acidic = NaOH

Carboxylic = Na_2CO_3 - $NaHCO_3$

Phenolic = NaOH - Na_2CO_3

Lactonic = $NaHCO_3$

3.8 Temperature Programmed Desorption

Temperature Programmed Desorption (TPD) is a powerful technique for the determination of surface reactions and adsorbed species in which a sample is heated with simultaneous detection of evolved gases using mass spectrometry in ultrahigh vacuum conditions. Species adsorbed on the surface of a material will escape and be detected as the temperature increases, and the method has also been extensively used for the characterisation of surface moieties of adsorbents (Salame and Bandosz 2001; Gorgulho, Mesquita et al. 2008) and to probe adsorbed species on catalyst surfaces (Cvetanović and Amenomiya 1972; Falconer and Schwarz 1983). The temperature at which a species is evolved from the sample is known as the desorption temperature, giving information on the binding energies of specific species. Using mass spectrometry, it is possible to determine the amounts of adsorbed molecules from the spectral peak intensities obtained.

Within this work, TPD was applied to determine the fragments of metaldehyde

attached to post-adsorption materials to provide evidence for the proposed adsorption mechanism (Chapter 5). Sorbents fully loaded with metaldehyde were dried and analysed using TPD to detect fragments of adsorbed metaldehyde molecules; the data were collected on a Hiden CATLAB micro-reactor system coupled with an online mass spectrometer QIC-20[②].

3.9 Nuclear Magnetic Resonance Spectroscopy

Nuclear Magnetic Resonance (NMR) is a physical phenomenon whereby electromagnetic radiation is adsorbed and re-emitted by nuclei in a magnetic field. The technique has many applications (e.g. medical NMR), and NMR spectroscopy is widely used in chemistry to determine the structure of organic compounds. In proton NMR (^{1}H-NMR), for a given radio frequency (e.g. 400 MHz), individual hydrogen atoms need slightly different magnetic fields to activate their resonance condition, depending on the species to which the hydrogen atom is attached; the specific resonant frequency of the hydrogen atom compared to that of a standard material (tetramethylsilane, TMS) is defined as the *chemical shift*, which acts as an indication of the chemical environment of the hydrogen atom under investigation. The number of peaks represents the variety of hydrogen environments within the structure, and the intensity of peaks can provide quantification information.

In this thesis, NMR was used to determine possible products of proposed catalytic reactions (Chapter 6). Metaldehyde was dissolved in deuterium oxide (D_2O), and the ^{1}H-NMR spectrum recorded, additional ^{1}H-NMR spectra were measured after the addition of catalysts. All NMR spectra were recorded on a Bruker AV400 NMR spectrometer[③].

---

② TPD data were collected in the Department of Pure and Applied Chemistry, University of Strathclyde, with the help of Dr. Leonard Berlouis and his group members.

③ NMR spectra were measured in the Department of Pure and Applied Chemistry, University of Strathclyde, with the help of Mr. Craig Irving.

Chapter 4 Adsorption of Metaldehyde onto Activated Carbons

4.1 Introduction

Activated Carbons (ACs) have been widely used as adsorbents to remove a variety of substances and the application of AC covers many areas such as drinking water and wastewater treatment, food and beverage industries and pharmaceutical and chemical sections (Moreno-Castilla 2004). Liquid phase adsorption processes are much more complex than those in gas phase and the mechanism is still not well defined, despite the AC market being very large. That said, there are a number of process descriptions in many publications, suggesting liquid phase adsorption could be initiated by electronic, dispersive interactions and reactivity of AC surface sites when placed in bulk solution, as well as being related to some of the characteristics of the bulk solution, and the adsorbate to be adsorbed.

During AC formation, pyrolysis of the carbonaceous material leads to formation of aromatic sheets of carbon micro-crystallites arranged in a random manner within the final material. It is reported that the randomised arrangement of the carbon micro-crystallites leads to various arrangements of electron clouds within the carbon skeleton, creating unpaired electrons and incompletely saturated valances on the AC surface (Roop Chand Bansal, ean-Baptiste Donnet et al. 1988), and the surface valence atoms form the adsorption sites on the surface of the AC adsorbent.

In addition to these surface valence atoms, the functional groups within the carbon structure play a vital role in adsorption. The functional groups are closely related to heteroatoms (majorly O and N), being derived either from the precursor material or from the activation process. This AC surface chemistry determines the charge of surface, the hydrophobicity and the electron density of the grapheme layers

(Moreno-Castilla 2004). The adsorption of ions by AC is normally related to the surface chemistry since immersion of AC in a bulk solution causes the surface groups to dissociate, altering the charge of the carbon. Common oxygen and nitrogen containing functional groups are presented in Figure 4.1 as neutral species but the surface charge depends on the pH level of the solution, e.g. the carboxylic groups will be presented as ArCOOH in acidic media and $ArCOO^-$ in basic; similarly amine groups present as $ArNH_3^+$ in acidic media and $ArNH_2$ in basic.

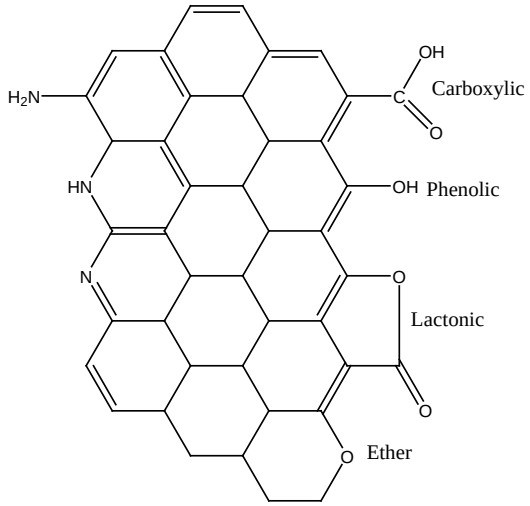

Figure 4.1 Schematic representation of oxygen and nitrogen containing functional groups commonly found in AC.

The final aspect that affects liquid adsorption is the porosity of the materials used. The adsorption potential of AC is related to their surface chemistry (as described above) and their porosity in complex ways. Essentially, adsorption is highly dependent on the accessibility of the active sites in ACs to the adsorptive sites. Hence, porous character, especially pore size is critical to adsorption processes, for instance, under appropriate experimental conditions, small molecules (e.g. phenol) can access micropores, Natural Organic Matter (NOM) can enter mesopores, and bacteria can access macropores (Moreno-Castilla 2004).

Currently, in the drinking water industry, AC is employed to remove various organic compounds, including metaldehyde, and physical adsorption of metaldehyde by AC has demonstrated good initial removal capacities but bed exhaustion is encoun-

tered after only a few weeks. This indicates that the current method is not wholly suitable for metaldehyde removal. In this section, the adsorption of metaldehyde onto ACs was investigated, including kinetics and leaching tendencies, with an aim to explain why AC is unable to efficiently remove metaldehyde.

4.2 Experimental

The general information of the three carbons is outlined in Section 3.1, and the textual properties of the samples were determined by nitrogen adsorption/desorption as discussed in Section 3.2.1.

The kinetics of metaldehyde sorption onto GAC, PAC and CNR were evaluated by batch reactor experiments: typically, 0.05 g of carbons was added to 500 mL of metaldehyde solution, with concentration 200 mg/L. The mixture was placed in an incubator-shaker (150 rpm) at a selected fixed temperature. At given contacting times, 0.2 mL aliquots of reacting solution were taken from the reactor for analysis.

Isotherms were determined by bottle-point method: at a selected temperature, 10 -100 mg samples of the chosen sorbent were added to several bottles containing fixed volumes of metaldehyde solution with varying initial concentrations, normally range from 2 mg/L to 200 mg/L. Once equilibrium was established, the final concentration of the solution was determined by GC as detailed in Section 3.4.

4.3 Results and Discussions

4.3.1 BET Characterisation Results

Figure 4.2 shows the nitrogen sorption isotherms for the three ACs used, at -196 ^{o}C. It is clear that all three isotherms fit Type IV with well-distinguished regions, including micropore filling, capillary condensation and the eventual plateauing at high relative pressures. The initial section corresponds to monolayer adsorption; and the

H2 type hysteresis loop indicates the presence of mesopores, i.e. the three ACs demonstrate a mix of porosity.

Figure 4.3 shows some similarity in the pore size distributions of the three ACs, and it is evident that all have significant porosity with width ~4nm. However, in the cases of GAC and PAC, besides the substantial volume of micropores, there is significant volume contributed by mesopores, as indicated by capillary condensation in the isotherms; this shifts the average pore diameters of GAC and PAC to 6.01 and 5.34 nm, respectively. In the case of CNR, besides the major pore volume contributed by ~4nm pores, a substantial portion of pore volume is contributed by pores with width ~2-3nm, reducing the average pore diameter of CNR to 2.83nm.

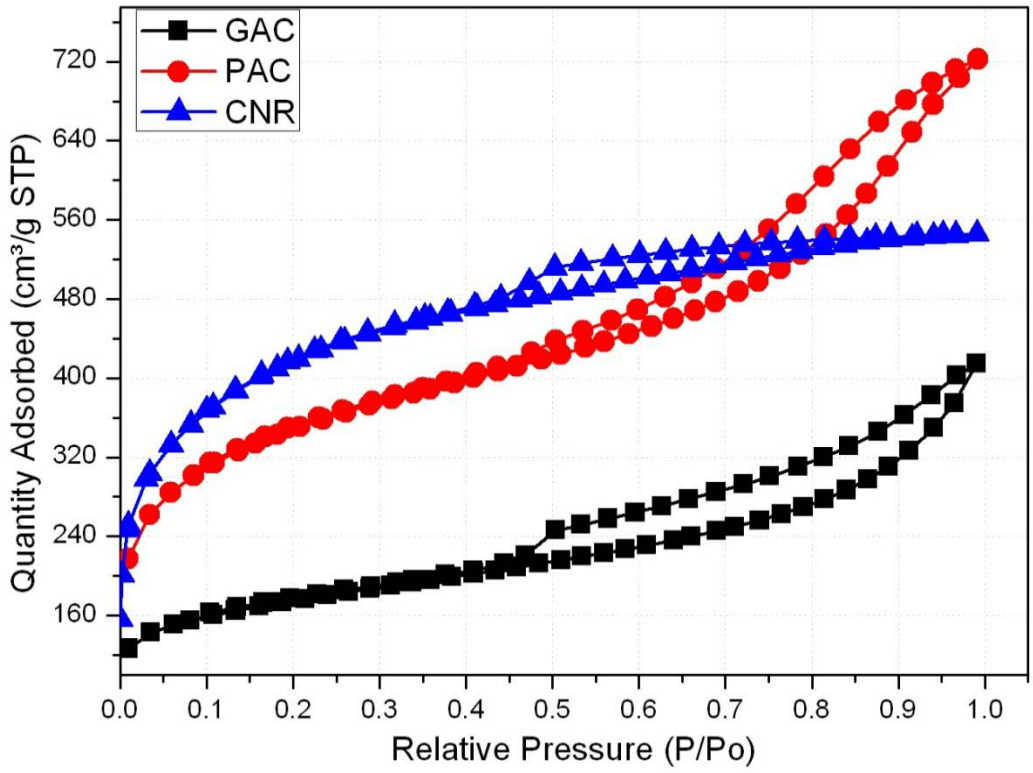

Figure 4.2 Nitrogen adsorption/desorption isotherms for the three ACs at -196 °C.

Table 4.1 summarises the porous characteristics of the three carbons. The micropore volume was determined by the t-plot method and the total pore volume was

determined from isotherm adsorption branch by single point method at P/P0=0.9916. It can be seen from Figure 4.2 and Table 4.1 that the pelletized carbon CNR has the biggest surface area, up to as high as 1403m^2/g. The surface areas of PAC and GAC are 1165 and 577 m^2/g, respectively; with GAC having the lowest surface area. Regards the pore volumes, PAC has a total pore volume of 1.11mL/g, with 17% of micropore volume. GAC and CNR have quite similar total pore volume and micropore volume percentage.

Table 4.1 Summary of porous characteristics of the three ACs.

Carbons	S_{BET} (m^2/g)	A.P.D. (nm)	M.P.V.(cm^3/g)	T.P.V. (cm^3/g)
GAC	577.7±8.7	6.01	0.11	0.641
PAC	1165.6±20.2	5.35	0.191	1.117
CNR	1403.3±26.9	2.83	0.197	0.843

A.P.D.: Average Pore Diameter; **M.P.V.:** Micropore Volume; **T.P.V.:** Total Pore Volume.

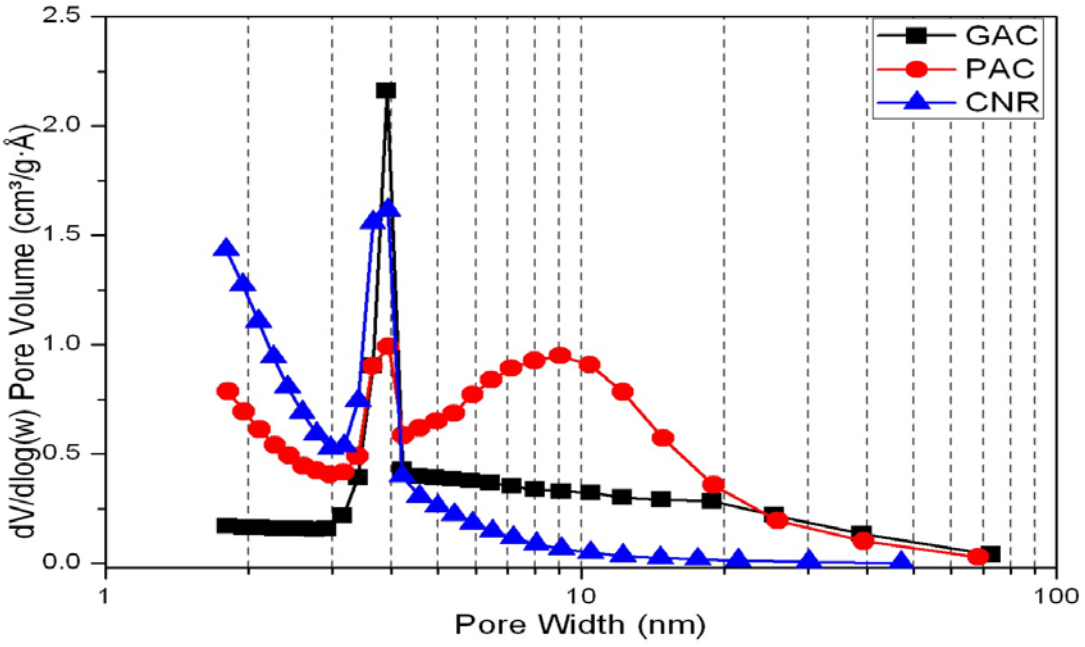

Figure 4.3 The BJH pore size distribution of the three ACs.

4.3.2 Kinetics of Metaldehyde Adsorption onto Activated Carbons

Figure 4.4 shows the data obtained for the kinetic studies of metaldehyde adsorption onto three ACs at 25 °C. The solid line represents the theoretical fitting of the experimental data to a pseudo-second order equation and Table 4.2 summarises the kinetic parameters determined from these fits.

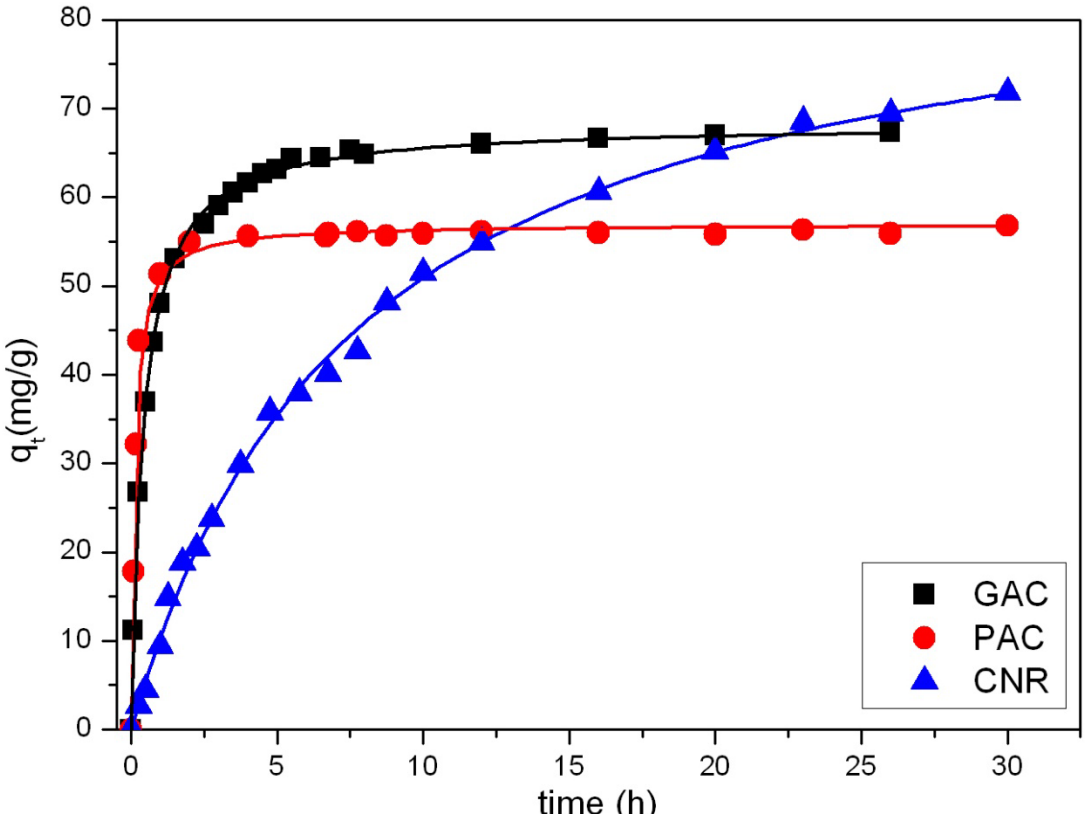

Figure 4.4 Kinetic profiles for metaldehyde sorption onto the three ACs used in this study and fits of the experimental data to a pseudo-second equation

PAC clearly shows the best kinetic performance, with a rate constant an order of magnitude higher than that of GAC and two orders higher than that of CNR. Kinetic performance is closely related to the physical and chemical properties of the sample and the exceptionally fast adsorption kinetics of PAC are most likely related to the large pore volume, especially mesoporosity present in the sample. Since only micro- and mesopores are present in all three ACs, and to simplify the situation here, the

mesopore volume is assumed to be the non-micropore volume, i.e. the mesopore volumes of the ACs are calculated by deducting the micropore volume from the total pore volume (TPV-MPV in Table 4.1). The resulting mesopore volumes of GAC, PAC and CNR are 0.523, 1.93 and 0.646 cm^3/g, respectively. It has been previously reported that metaldehyde molecules are linked to each other via hydrogen bonding, creating macromolecules, despite the small molecule size of single metaldehyde molecule (Barnett, Hulme et al. 2005), and the proposed hydrogen bonding between metaldehyde molecules is schematically shown in Figure 4.5. PAC may also perform well kinetically as a result of its average particle size (30 µm), which facilitates diffusive mass transfer of metaldehyde molecules into the carbon structure to be adsorbed.

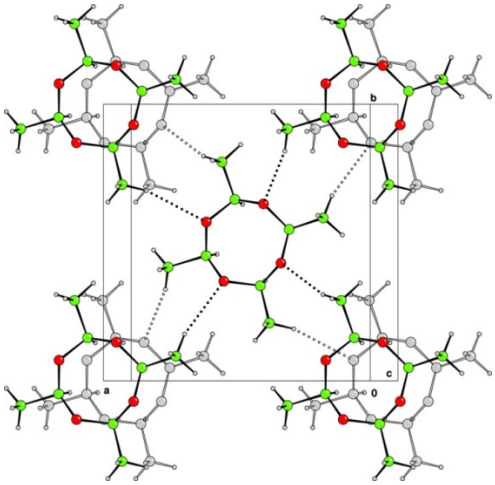

Figure 4.5 The schematic representation of hydrogen bonding between metaldehyde molecules. Courtesy of Acta Crystallographica (Barnett, Hulme et al. 2005).

CNR, however, has a greater surface area and larger total and mesopore volumes than GAC, yet the rate of adsorption for CNR is less than that of GAC, which can again be explained by the particle size of the ACs. As mentioned in Section 3.1.1, CNR is a pelletized carbon with 2 mm diameter and 5-10 mm length, while GAC has a particle size range of 20-40 mesh; this greater particle size creates significant diffusive resistance, hence, reducing the adsorption kinetics substantially.

Table 4.2 Calculated kinetic parameters of metaldehyde sorption onto ACs used in this study at 25°C.

Carbons	k_2 (g mg^{-1} h^{-1})	q_e(Experimental, mg/g)	q_e(Calculated, mg/g)
GAC	3.481×10^{-2}	68.269	69.548
PAC	0.1317	58.115	59.215
CNR	1.442×10^{-3}	90.123	92.358

4.3.3 Equilibrium Studies of Metaldehyde onto Activated Carbons

The equilibrium data obtained from the kinetic experiments gives some indications about adsorption capacity. It can be seen from Table 4.2 and Figure 4.4 that CNR had the highest adsorption capacity among the three samples, reaching 92.35 mg/g, despite its slow kinetics. GAC exhibited a lower capacity of 69.54 mg/g, which is slightly higher than that of PAC. In summary, CNR had the highest capacity while its pelletized physical form hindered the kinetics. PAC showed fastest kinetics with the lowest capacity; while GAC demonstrated both good kinetics and a reasonable capacity. Therefore, all follow-up studies used GAC as the typical AC material and is cited when comparisons are required.

In order to obtain more information regarding the removal metaldehyde using GAC, adsorption isotherms at selected temperatures were studied. Since this work is focused mainly on metaldehyde contamination in the United Kingdom, low temperatures were specifically considered when designing experiments. Figure 4.6 displays the adsorption isotherms of metaldehyde onto GAC obtained at 3, 22 and 32 °C.

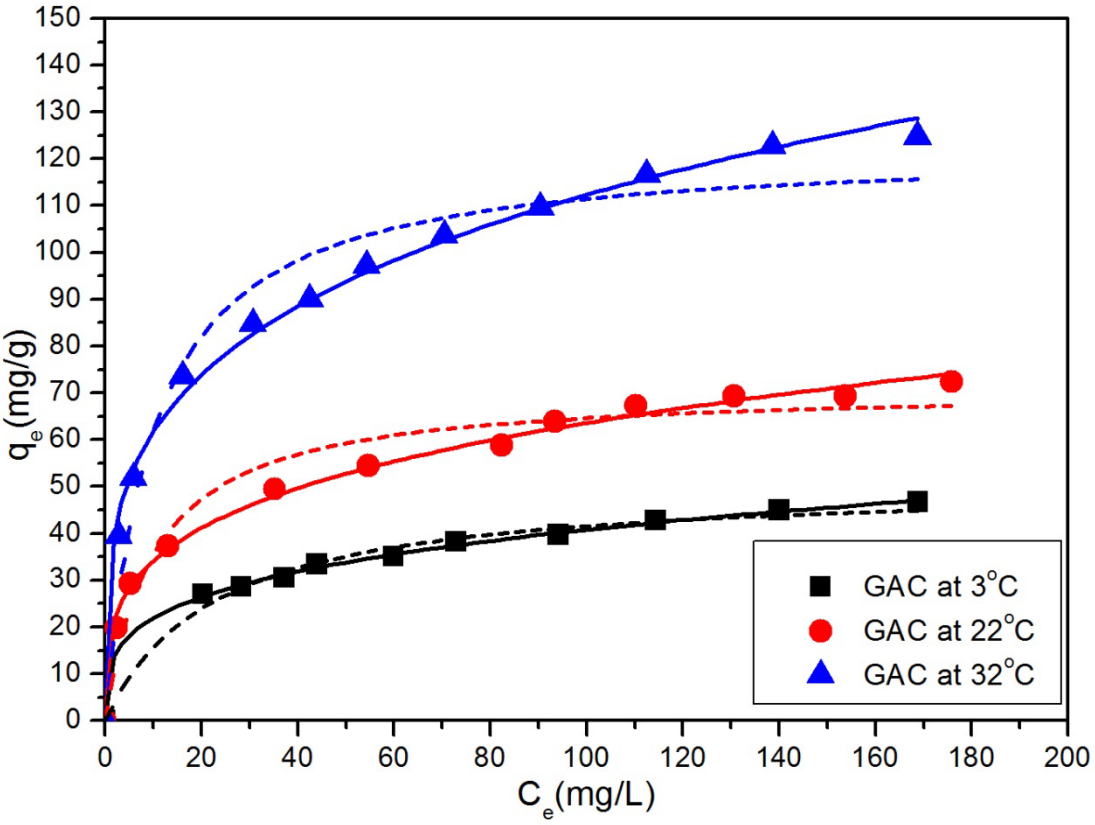

Figure 4.6 Adsorption isotherms for metaldehyde on GAC at different temperatures, and the fits of experimental data to Freundlich (solid line) and Langmuir (dotted line) equations

The experimental data were fitted to the Freundlich and Langmuir equations since these are the most commonly used isotherms equations in liquid phase adsorption (Section 2.1.2). The fitting parameters obtained are displayed in Table 4.3, and it can be seen that the Freundlich equation describes the experimental data more appropriately than the Langmuir equation; hence, the discussion is focus on the Freundlich isotherm. In the Freundlich equation, the value of *n* indicates the favourability of sorption; if $n = 2 – 10$ there should be a good favourability, $n = 1 - 2$ suggests moderate to difficult sorption, and $n < 1$ indicates poor sorption characteristics (Chen, Zhao et al. 2011). According to Table 4.3, all *n* values at different temperatures are greater than 2, indicating metaldehyde is favourably adsorbed onto GAC. The Freundlich adsorption constant, K_F, refers to the relative adsorption capacity, i.e. larger values of K_F imply

higher adsorption capacities. It is evident that the adsorption capacity of metaldehyde onto GAC increases with increasing of temperature, suggesting the adsorption process is endothermic. More detailed analysis and discussion about the process of metaldehyde adsorption onto GAC will be presented in the following Chapter when the performance of GAC is compared with other candidate materials.

Table 4.3 The parameters of Freundlich and Langmuir isotherms obtained by fitting the experimental data to the corresponding theoretical equations.

T (^{o}C)	Langmuir isotherm			Freundlich isotherm		
	q_m(mg/g)	K_L(L/mg)	R^2	K_F *	n	R^2
3	50.860	4.45×10^{-2}	0.98	11.770	3.70	0.99
22	71.098	9.98×10^{-2}	0.96	18.356	3.71	0.99
32	122.40	10.2×10^{-2}	0.95	33.903	3.84	0.99

* K_F: mg g^{-1} (L mg^{-1})$^{1/n}$

4.3.4 Leaching Tendency Tests for Metaldehyde Adsorbed onto Activated Carbons

Within a complete adsorptive process, adsorption is only one part of the study; the other critical part is desorption, or the leaching tendency test in water purification applications. Leaching tendencies demonstrate how much material will be desorbed from the sorbent and how quickly the molecules will desorb. A sorbent with excellent kinetics and capacity would not be of practical interest if high leaching tendency is observed, since this affects the breakthrough curve of a continuous fixed-bed reactor. Leaching tendencies give an indication of the strength of affinity between the sorbent and solute, therefore, desorption tests were performed to evaluate the leaching tendencies of the ACs. Samples fully loaded with metaldehyde were filtered and add-

ed to equivalent amounts of deionized water used for adsorption (i.e.500mL), followed by placing it in an incubator–shaker (i.e. 150 rpm). Samples were taken at given time intervals and the concentration of metaldehyde analysed by GC. Figure 4.7 shows the percentage of adsorbed metaldehyde leached out of the carbons as a function of time. It is evident that the adsorbed metaldehyde desorbed easily from all ACs, indicating the affinity between carbons and metaldehyde molecules is not strong enough to retain the solute. These leaching tests, in addition to the poor capacities, also give some explanation as to why AC beds used in water treatment factories had initial good performance but exhaustion only after a few weeks of implementation. Rapid loss without external stimuli indicates that metaldehyde removal by AC is a physical process, since intact metaldehyde molecules are detected during desorption. Consequently, novel removal process that either degrade or chemically bind metaldehyde molecules are desirable and of practical interest to improve existing technologies.

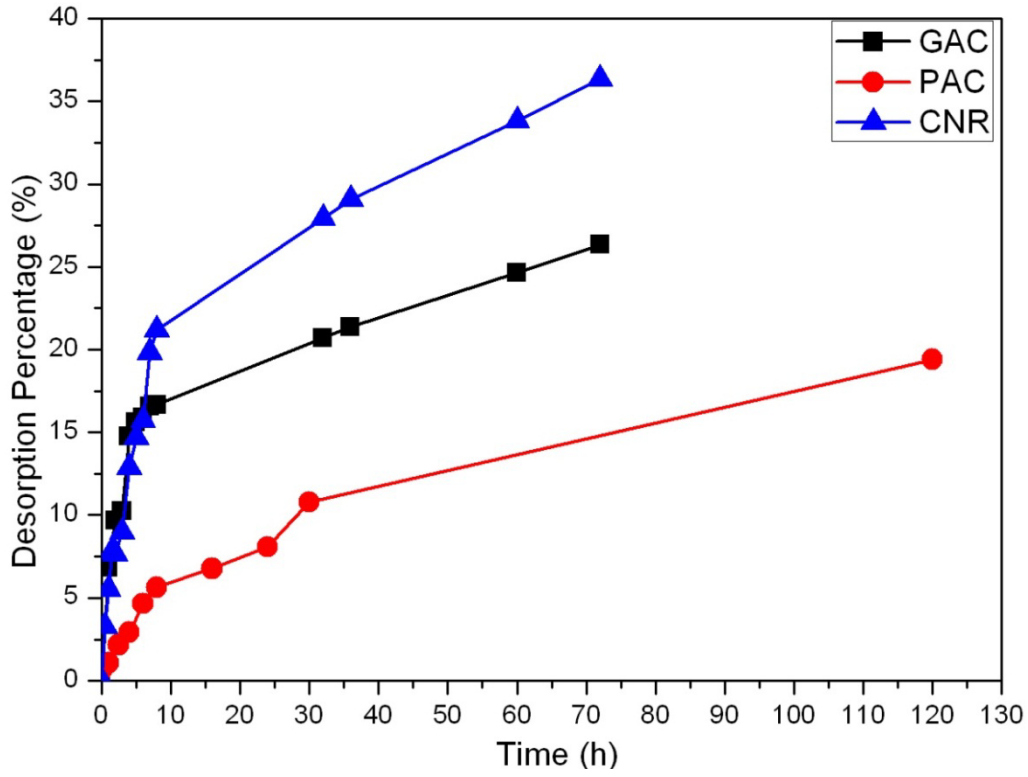

Figure 4.7 The percentage of adsorbed metaldehyde desorbed from carbons as a function of time.

4.5 Conclusions

In this Chapter, three ACs (i.e. GAC, PAC and CNR) were applied to adsorb metaldehyde from water samples. The kinetic studies showed that, to some extent, all three ACs were capable of removing metaldehyde from drinking water. PAC exhibited the fastest kinetics, with a rate constant 1-2 orders of magnitude higher than GAC or CNR, which could be associated with the very high surface area (>1165 m^2/g) and large, especially meso-, pore volume (>1.1 cm^3/g), for this sample. Moreover, the small particle size of PAC enhanced kinetic performance. CNR showed slow sorption kinetics, which is closely related to its porosity and large particle size. In terms of capacity, PAC was lowest while CNR was highest, reaching 92 mg/g. GAC exhibited both reasonable kinetics and uptake performance; therefore, the study focused on GAC and an isothermal study of metaldehyde adsorption onto GAC showed that the sorption system was endothermic and that the Freundlich equation was most appropriate to describing the experimental data. The leaching test results demonstrated that all the ACs were not practicable for use in the water treatment industry, since adsorbed metaldehyde molecules were easily and quickly desorbed from all ACs studied, which would lead to fast breakthrough times and quick bed exhaustion. Therefore, according to this study, it is advantageous to develop novel processes or materials to address metaldehyde contamination within U.K. water supplies.

Chapter 5 Metaldehyde Removal from Aqueous Solution by Adsorption and Ion-Exchange Mechanisms onto Activated Carbon and Polymeric Sorbents

5.1 Preliminary investigation of Removing Metaldehyde by Polymeric Materials

Investigation of metaldehyde adsorption onto different activated carbons (ACs) suggested reasons why AC materials fail to remove metaldehyde from drinking water in current treatment practices, namely low capacities and high leaching tendencies. It is, therefore, proposed that desirable materials should have fast removal kinetics, high adsorption capacities and low leaching tendencies. In order to develop materials with low leaching tendency or even zero leaching, desired material should contain functionalities that either demonstrate high affinity for and can chemically adsorb metaldehyde molecules, or can degrade metaldehyde into small non-toxic molecules. Hence, with these aims, preliminary studies were conducted to determine which functionalities have high affinity for metaldehyde.

18 polymeric samples were tested to adsorb/degrade metaldehyde. Initially, 1 g of each of the fully dried polymeric samples (supplied by Purolite) was added into test jars containing 500 mL of 200 ppm metaldehyde solution. The jars were placed in a shaker (150 rpm) to allow adsorption/degradation to occur. 24 h later, 0.5 mL of each post-reaction solution was taken and the level of metaldehyde analysed by GC, as described before. The detailed information for all these samples is summarised in Table 3.2, with the preliminary uptake results shown in Figure 5.1.

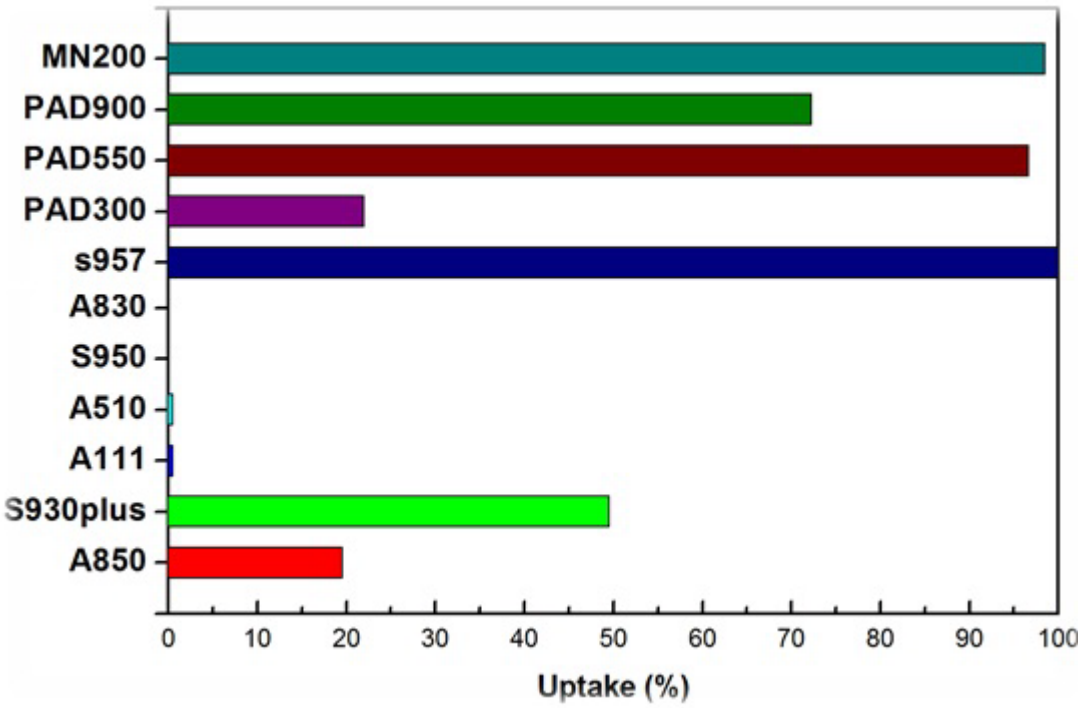

Figure 5.1 Preliminary results of metaldehyde adsorption onto polymeric samples

As outlined in Section 3.1, these polymeric samples can be classified into four categories:

Category 1. Non-functionalised polymeric materials

These materials including PAD300, PAD500, PAD900 and MN200, generally have high surface area and large pore volume. Preliminary results showed that all category 1 samples have significant adsorption capacities with the adsorption capacity increasing with increasing surface area (as demonstrated in Figure 5.2). The main issue with these samples is that they do not contain any surface functionalities, hence, the adsorbed metaldehyde molecules are highly likely to desorb easily from the adsorbent, resulting in the same scenario as for the ACs studied. Since MN200 has the greatest surface area and pore volume among these non-functionalised samples, it was selected for detailed study in the next section to represent this category for comparative purpose.

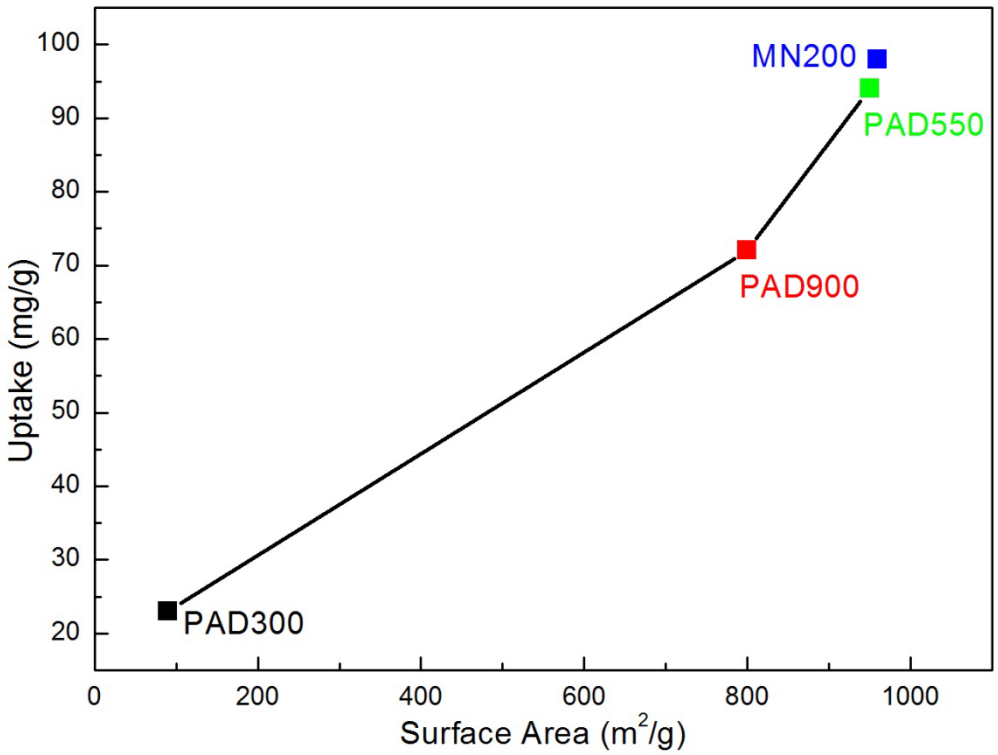

Figure 5.2 Metaldehyde uptakes as a function of a surface area for category 1 samples

Category 2. Cation exchange resins

Materials in this category include weak acid, strong acid and sodium ionic form of cation exchange resins. The ionic forms of S950 and S930Plus are Na^+, and the resulting weak-acid cation exchangers have carboxylic acid functionalities. A patented strong-acid exchanger, containing sulfonic and phosphonic acid functional groups, S957, was also utilized.

The preliminary results showed that the sodium form exchangers had no observable uptake, while the proton form exchangers had very high uptakes, especially the sulfonic and phosphonic acid functionalised S957, indicating strong affinity between H^+ and metaldehyde. Hence, S957 was studied in detail to obtain more information about the process.

Category 3. Anion exchange resins

Including weak base and strong base anion exchangers such as A830, A111, A510Plus and A850, the preliminary results for this category of materials, revealed

that basic functionalities had weak or no affinity at all with metaldehyde molecules.

Category 4. Macronets

Macronets are specially designed and manufactured polymeric samples,which were designed and prepared as guided by the research outcomes of the following Chapters for metaldehyde removal, hence, the results are not included here but in Chapter 7 .

Preliminary results showed that materials with high degree of porosity had increased adsorption capacities for metaldehyde. The capacity is closely related to surface area and pore volume. However, non-functionalised materials will potentially suffer from the same high leaching tendencies observed for AC. The H^+ form cation resins showed promising results and the strong acid cation exchange resin exhibited a better performance than its weak acid counterparts. The following Chapters, therefore, focus on strong acid cation exchangers.

5.2 Introduction

This study focuses on understanding the interactions driving the adsorption and/or degradation of metaldehyde within a water treatment process, to allow such interactions to be tailored, potentially via the incorporation of key functionalities into optimised adsorbent bed materials. As outlined previously, such sorbents are required to exhibit fast kinetics of adsorption, high adsorption capacities and low leaching tendencies; it may also be advantageous for these materials to degrade metaldehyde as a result of their inherent functionalities. Here, we evaluate the adsorption performance of non-functionalised hyper-cross-linked Macronet MN200 due to its high surface area (> 950 m^2 g^{-1}) and suitable pore sizes, additionally, as the cyclic structure of metaldehyde should be cleaved in the presence of strong acids, ion exchange resin S957, which contains sulfonic and phosphonic functionalities was also evaluated. These two materials were compared with a commercially available Granular Activated Carbon (GAC). Adsorbent performance was evaluated via adsorption kinetics, isotherms, thermody-

namic parameters and leaching tendencies.

5.3 Experimental

The stock solutions of metaldehyde and internal standard were prepared as outlined in Section 3.1.3, and textural characterisations of GAC, MN200 and S957 were performed using nitrogen adsorption/desorption analysis, as outlined in Section 3.2.1. The experimental procedures for kinetic and isothermal were similar as outlined in Section 4.2, and the leaching tendency tests were conducted as Section 4.3.4. Regarding regeneration tests, the kinetic of original S957 was tested and then the loaded samples were treated by 1.9mol L^{-1} HCl, followed by shaking the mixture for 24h, filtering, washing and drying before obtaining the regenerated S957, and finally, the kinetic of regenerated S957 was investigated as well.

Table 5.1 Characteristics of GAC, Macronet MN200 and ion-exchange resin S957.

	GAC	**MN200**	**S957**
Polymer structure	Activated carbon	Polystyrene cross-linked with DVB	
Appearance	Granules	Spherical beads	Spherical beads
Particle size(μm)	420-840	450-620	425-845
Pore structure	Microporous	Macroporous	Macroporous
$S_{BET}(m^2 g^{-1})$	560	950	1.4
$V_{Total}(cm^3 g^{-1})$	0.5155	0.66718	0.00974
Functional group(s)	Phenolic, carboxylic lactonic ,*etc*	Non-functionalised	Phosphonic Sulfonic acid
H^+ equ.(mmol/g)	0.8875	-	11.25

The characteristics of the sorbents used in this section are summarised in Table 5.1, for ease of reference.

To better understand the adsorption kinetics, pseudo-first, pseudo-second order and Elovich equations were applied to describe the kinetics of metaldehyde adsorption onto GAC, MN200 and S957 (Section 2.1.3).

- Pseudo-first order equation:

$$q_t = q_e\left(1 - e^{-k_1 t}\right) \quad \textbf{Eq. (5-1)}$$

- Pseudo-second order equation:

$$q_t = \frac{{q_e}^2 kt}{1 + q_e kt} \quad \textbf{Eq. (5-2)}$$

- Elovich model:

$$q_t = \frac{1}{b}\ln(ab) + \frac{1}{b}\ln(t) \quad \textbf{Eq. (5-3)}$$

Homogeneous Particle Diffusion Model (HPDM, Section 2.1.3.4) and intra-particle diffusion model (Section 2.1.3.5) were applied for the determination of the rate-limiting step in an adsorption process.

- HPDM particle diffusion:

$$X(t) = \sqrt{1 - \exp\left(\frac{-2\pi^2 D_e}{r^2}\mathrm{t}\right)} \quad \textbf{Eq. (5-4)}$$

- HPDM film diffusion:

$$X(t) = 1 - \exp\left(-\frac{3DC}{rC_r}t\right) \quad \textbf{Eq. (5-5)}$$

- Intra-particle diffusion:

$$q_t = K_i t^{0.5} + I \quad \textbf{Eq. (5-6)}$$

5.4 Results and Discussion

5.4.1 Adsorption Kinetic Studies

The adsorption rate ($\frac{dq_t}{dt}$) expresses the amount of metaldehyde adsorbed from the liquid phase onto an adsorbent per unit time. In Figure 5.3 the metaldehyde adsorption

rate is plotted as $q_e = f(t)$. Thus, the tangent to the curve between consecutive points represents the instantaneous adsorption rate. It can be seen that MN200 and GAC both reach equilibrium adsorption capacity at 6 h, and that the final capacity of MN200 is higher than GAC, at 89.83 and 64.46 mg g^{-1}, respectively. In contrast, S957 achieved equilibrium at ~24 h with a final capacity of 181.34 mg g^{-1}.

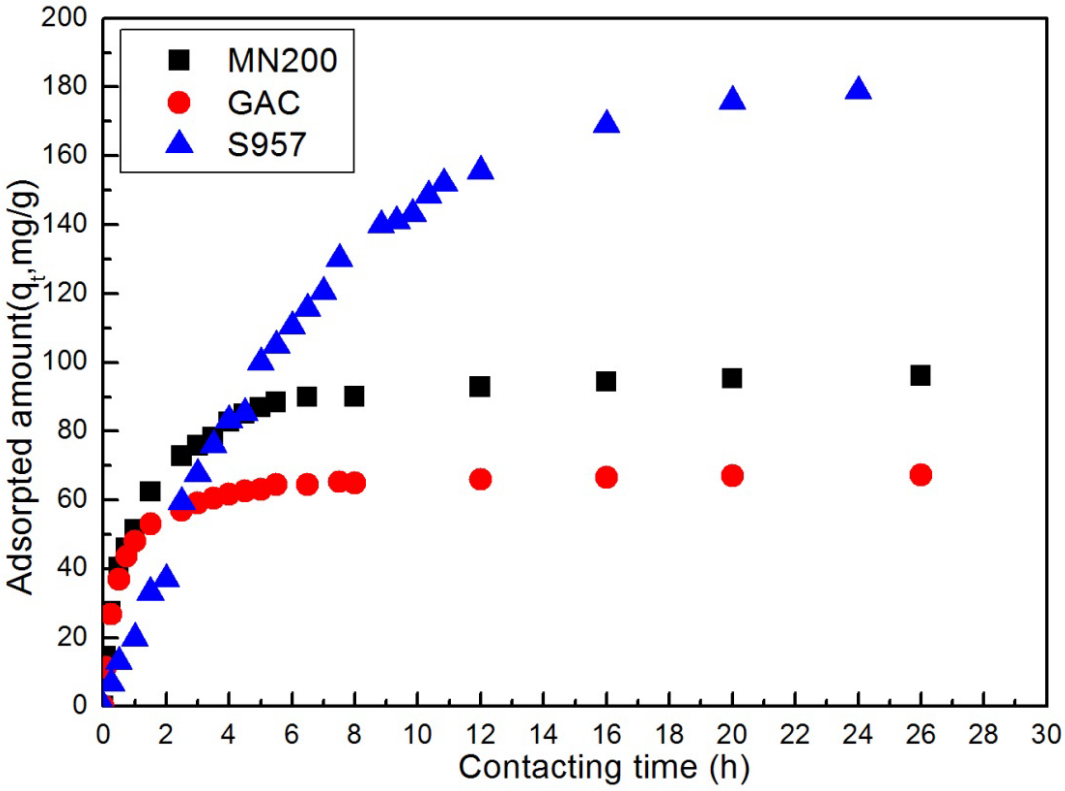

Figure 5.3 Metaldehyde uptake as a function of time to MN200 (■), GAC (●) and S957 (▲)

Figure 5.4 shows fits of experimental data obtained for GAC, MN200 and S957 to the three kinetic models described above; the kinetic parameters determined from these fits are summarised in Table 5.2. From Figure 5.4, it can be seen that the pseudo-second order model provides an excellent fit for metaldehyde adsorption on both MN200 and GAC, S957 is best described by a pseudo-first order model. Moreover, it can be observed from Table 5.2 that the adsorption rates for GAC and MN200 are much faster than for S957, which can be attributed to the large differences in surface area between MN200/GAC (560/950 m^2 g^{-1}, respectively) and S957 (1.4 m^2 g^{-1}).

Table 5.2 Kinetic parameters obtained by fitting kinetic data for metaldehyde adsorption to pseudo-first order, pseudo-second and Elovich models for MN200, GAC and S957.

Model	MN200	GAC	S957
Pseudo-first order			
$q_{e,\,cal}$ (mg g^{-1})	89.39	63.48	187.5
k_1 (h^{-1})	0.8682	1.594	0.1472
R^2	0.964	0.973	0.996
Pseudo-second order			
$q_{e,\,cal}$ (mg g^{-1})	99.10	68.27	253.2
k_2 (x 10^{-3} g mg^{-1} h^{-1})	12.35	34.81	0.4982
R^2	0.993	0.999	0.989
Elovich			
a (mg g^{-1} h^{-1})	496.1	946.8	89.92
b (x 10^{-2} g mg^{-1})	6.264	10.28	2.171
R^2	0.968	0.944	0.938

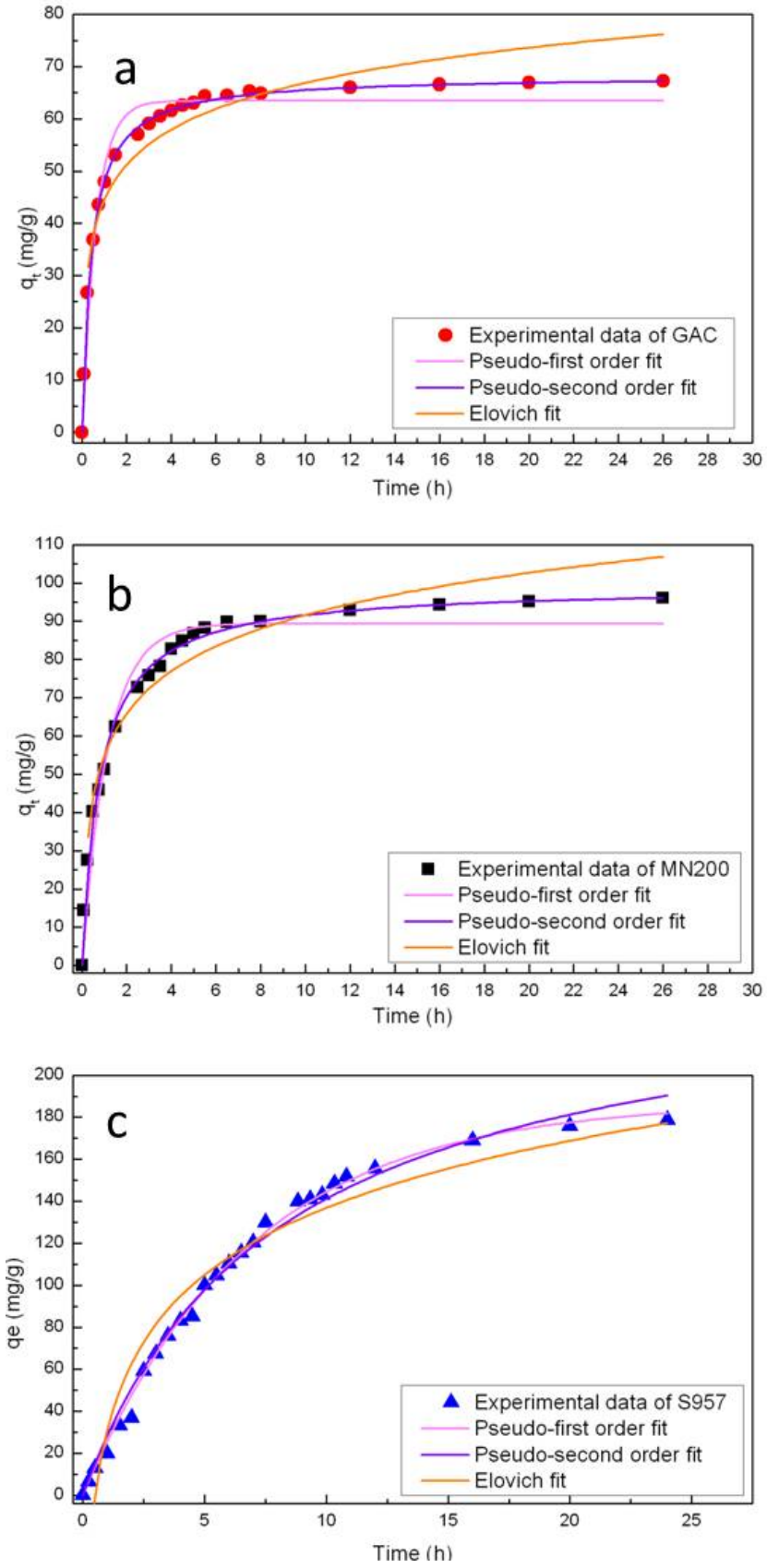

Figure 5.4 Kinetic data for metaldehyde adsorption onto GAC (●), MN200 (■) and S957 (▲) and fits obtained using pseudo-first, pseudo-second order and Elovich models.

Comparison of the kinetic parameters for MN200 and GAC indicates that GAC exhibits a faster rate of metaldehyde adsorption despite its relatively smaller surface area. According to the data in Table 5.2, the rate of adsorption for GAC is three times faster than that of MN200, which can be explained by consideration of the interaction forces between the adsorbents and metaldehyde, as determined by the surface chemistry of the material. As GAC has a variety of oxygen containing functionalities, including carboxylic, lactonic and phenolic groups, the interactions will be stronger than for non-functionalised MN200.

The adsorption of organic pollutants onto sorbents is commonly understood to involve different sequential stages that determine the adsorption rate (Valderrama, Cortina et al. 2007; Valderrama, Barios et al. 2010), namely: (a) diffusion of solute through the liquid film surrounding the particle, also known as liquid film diffusion control or the external diffusion step; (b) diffusion of solute through the polymeric matrix of the resin, also known as particle diffusion control or the internal diffusion step; and (c) actual adsorption, or chemical reaction. The pseudo-first order, pseudo-second order and Elovich models describe the overall adsorption rate by considering all adsorption processes as a lumped term; it is, therefore, necessary to deconvolute the predominant step among the three stages that actually govern the adsorption rate. Usually step (c), adsorption, is relatively fast, finishing in minutes, hence, it is generally not the rate limiting step; unless chemical modifications occur during adsorption (Doğan, Alkan et al. 2004), whereupon, deconvolution of the rate controlling step is more complex.

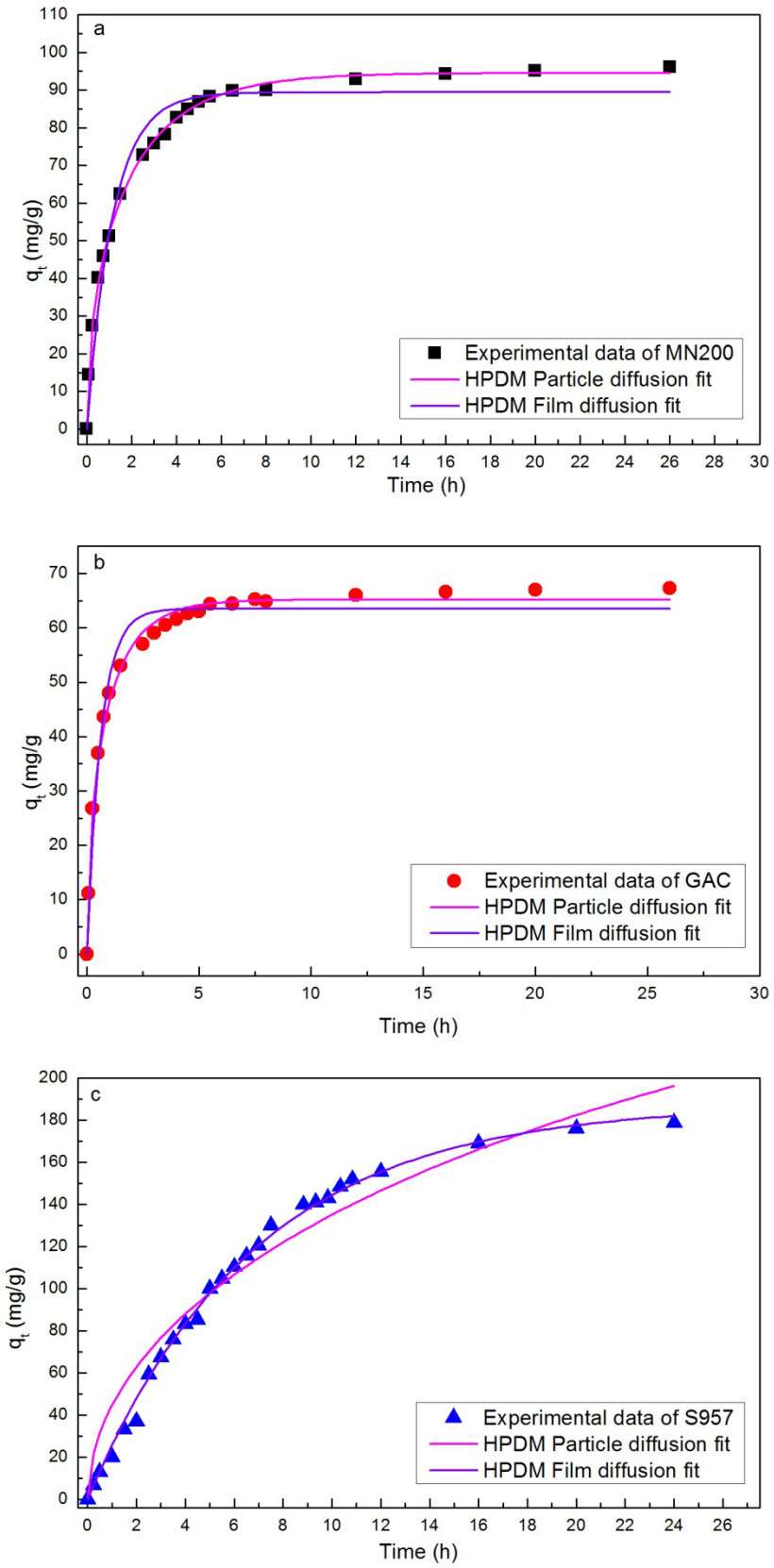

Figure 5.5 Metaldehyde uptakes on MN200 (■), GAC (●) and S957 (▲), shown with theoretical curves obtained by kinetic analysis using HPDM model

Figure 5.5 demonstrates the fitting of experimental data to the HPDM model and the parameters calculated from fitting are summarised in Table 5.3. Linear regression analysis supports the use of the HPDM model for treatment of the experimental data obtained for MN200 and GAC, which suggests particle diffusion as the rate limiting diffusion control for the removal of metaldehyde by MN200 and GAC. In the case of S957, however, linear regression analysis shows that the adsorption on S957 is controlled by film diffusion, indicating the rate is dominated by the diffusion of metaldehyde through the solid/liquid interface.

Table 5.3 Parameters obtained for fitting of metaldehyde adsorption kinetic data for GAC, MN200 and S957 to the HPDM diffusion model

	HPDM parameters			
	$-\ln(1-X^2)$(Particle)		**$-\ln(1-x)$(Film)**	
	R^2	$D_e(m^2/s)$	R^2	$D(m^2/s)$
MN200	0.998	2.3×10^{-12}	0.964	5.1×10^{-8}
GAC	0.992	4.5×10^{-12}	0.973	9.7×10^{-8}
S957	0.946	1.1×10^{-12}	0.996	1.9×10^{-8}

To confirm whether metaldehyde adsorption on both MN200 and GAC is dominated by particle diffusion, the experimental data were further analysed using the intra-particle diffusion model.

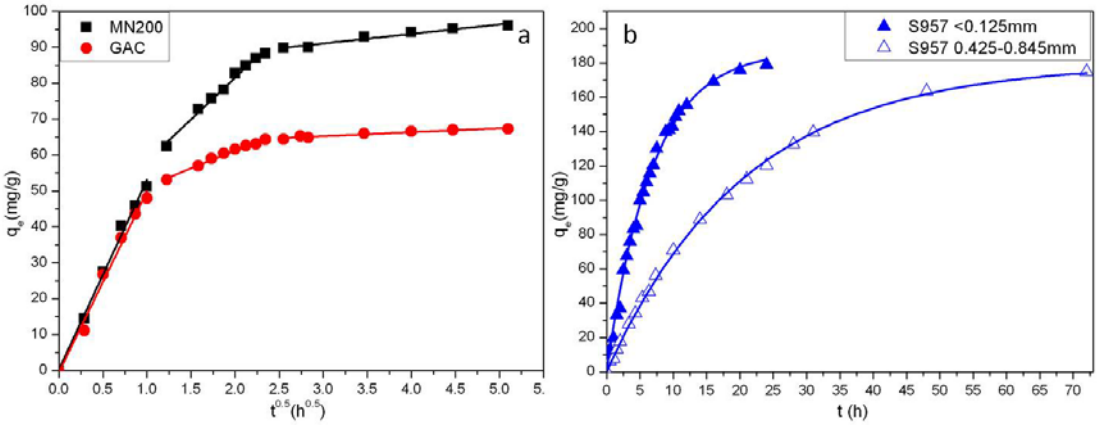

Figure 5.6 a) Intra-particle diffusion kinetics of metaldehyde adsorption onto MN200 (■) and GAC (●); b) Kinetics of metaldehyde adsorption on S957 (▲), with two particle sizes

Figure 5.6(a) shows plots of metaldehyde uptake (q_t) against $t^{0.5}$ for MN200 and GAC. The plots display multi-linear forms, rather than straight lines with intercepts of zero; indicating that adsorption is influenced by two or more steps. The initial linear part, of film diffusion, lasts only for a short time compared to the entire adsorption process. The second linear portion depicts metaldehyde diffusion in the larger pores of MN200 and GAC; while the final portion is due to micropore diffusion.

The kinetic profile of S957 is markedly different from those of MN200 and GAC; the whole sorption process conforms to a pseudo-first order model, with diffusion dominated by film diffusion instead of being limited by particle diffusion, as for MN200 and GAC. This is the result of the small surface area within S957, which practically makes the resin impermeable to the fluid reactant; hence the external resistance becomes the rate limiting step. Moreover, the comparative differences in the kinetic profile of S957 are caused by the sorption mechanism, since an ion exchange mechanism plays a significant role in the sorption of metaldehyde onto S957. Boyd *et al.* (Boyd, Adamson et al. 1947) developed a rate equation that includes a term for ion-exchange adsorption for the sorption of ions from aqueous solutions by organic zeolites. The authors proposed that the mass action rate and diffusion equations for diffusion through a boundary liquid film are the same as the pseudo-first order equation

of Lagergren (Lagergren 1898), if the adsorption process is regarded as a chemical phenomenon, as describes sorption of metaldehyde on S957.Thus, the rate is dominated by film diffusion and overall sorption is best described by a pseudo-first order equation, and the theory and mechanism proposed previously can be applied to the system studied in this work.

Boyd *et al.* also concluded that if film diffusion controls the rate, then the rate constant would vary inversely with particle size (Boyd, Adamson et al. 1947). As the rate of adsorption for S957 appears to be limited by film diffusion, the effect of particle size was investigated to confirm this hypothesis; the results of these experiments are shown in Figure 5.6(b), and these confirm the theory discussed above, as is evident that the rate constant increases (0.0482 h^{-1} to 0.1472 h^{-1}) with decreasing S957 particle size (0.425 - 0.845 mm to < 0.125 mm). Systems comparable to metaldehyde adsorption on the ion-exchange resin used in this study have previously shown similar adsorption mechanisms, such as arsenic adsorption onto granular hydroxide (Banerjee, Amy et al. 2008) and adsorption of acid blue 113 onto ACs (Gupta, Gupta et al. 2011).

5.4.2 Adsorption Equilibria Studies

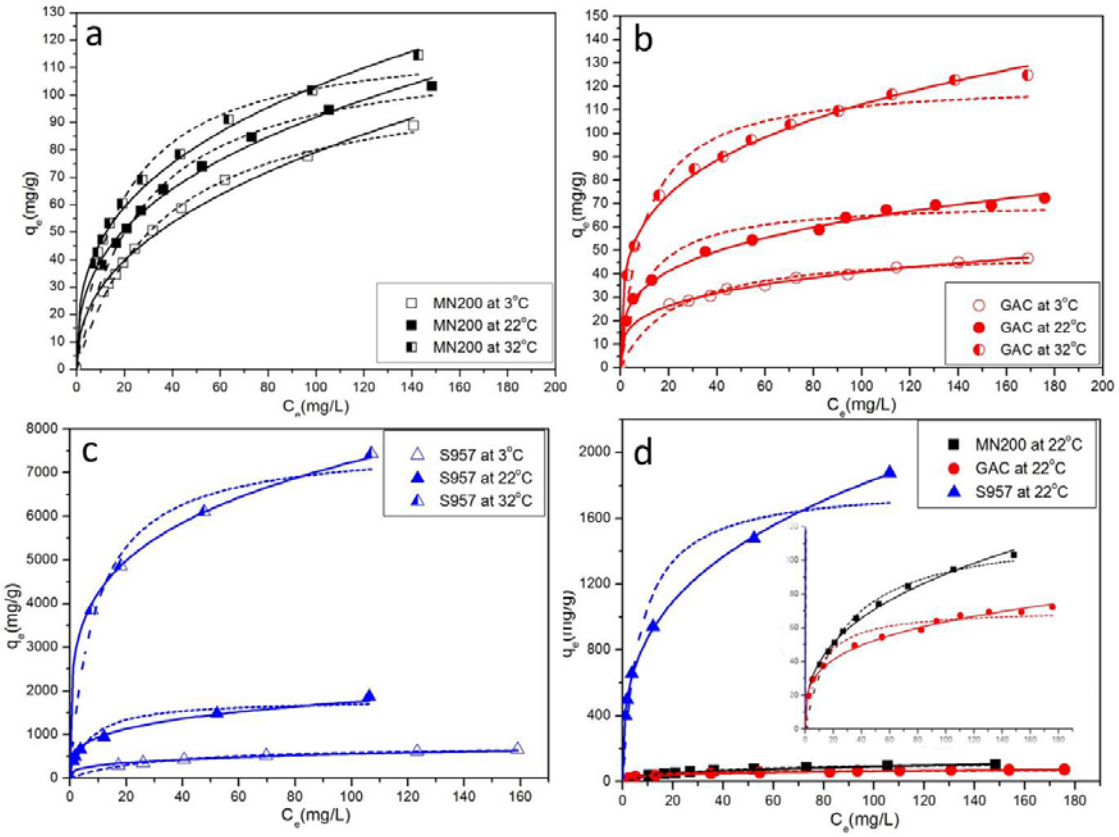

Figure 5.7 Adsorption isotherms for metaldehyde onto (a) MN200, (b) GAC and (c) S957 at selected temperatures and corresponding fits to the Freundlich (solid lines) and Langmuir (dash lines) equation; (d) adsorption isotherms of MN200 (■), GAC (●) and S957 (▲) at 22 °C, and corresponding fits (solid lines) to the Freundlich equation.

An understanding of the mechanism of adsorption can also be determined by analysing adsorption isotherms for the systems under study. Hence, the isotherms for metaldehyde adsorption on MN200, GAC and S957 were determined, at various temperatures, as a function of equilibrium concentration (C_e, mg L^{-1}), and the corresponding isotherms are shown in Figure 5.7. The Freundlich and Langmuir isotherm equations are widely used to describe sorption of solutes onto heterogeneous surfaces involving surface functionalities (Hameed and El-Khaiary 2008) and adsorbate-adsorbent interactions (Huo and Yan 2012), hence, the two equations were used to

fit the experimental data obtained for metaldehyde sorption.

The Langmuir and Freundlich equations were applied to analysis the isotherms, as outlined in Section 2.1.2.1 and 2.1.2.2, and fittings of the data to the two models are shown in Figure 5.7, with the parameters obtained summarised in Table 5.4.

Langmuir model:

$$q_e = q_m K_L C_e / (1 + K_L C_e) \qquad \textbf{Eq. (5-7)}$$

Freundlich model:

$$q_e = K_F C_e^{\frac{1}{n}} \qquad \textbf{Eq. (5-8)}$$

Table 5.4 Isotherm parameters obtained by fitting metaldehyde adsorption data for MN200, GAC and S957 to the Freundlich and Langmuir equation

Sorbents	Temp(°C)	Langmuir isotherm			Freundlich isotherm		
		q_m(mg/g)	K_L(L/mg)	R^2	K_F*	n	R^2
GAC	3	50.8597	4.45×10^{-2}	0.98	11.770	3.70	0.99
	22	71.0976	9.98×10^{-2}	0.96	18.356	3.71	0.99
	32	122.397	10.2×10^{-2}	0.95	33.903	3.84	0.99
MN200	3	108.078	2.85×10^{-2}	0.99	10.985	2.33	0.98
	22	118.34	3.63×10^{-2}	0.99	17.068	2.74	0.99
	32	121.667	5.30×10^{-2}	0.98	21.035	2.90	0.97
S957	3	769.801	3.22×10^{-2}	0.99	153.87	3.57	0.98
	22	1807.12	14.3×10^{-2}	0.93	504.39	3.71	0.99
	32	7669.71	11.2×10^{-2}	0.98	2492.5	4.32	0.99

* K_F: mg g^{-1} (L mg^{-1})$^{1/n}$

It can be seen from Figure 5.7 and Table 5.4 that the Freundlich isotherm model describes the experimental data more appropriately than the Langmuir isotherm model; therefore, subsequent discussions are focussed on the Freundlich analysis. In the

Freundlich equation, as outlined previously, the value of n indicates the favourability of sorption; if $n = 2 – 10$ there should be a good favourability, $n = 1 - 2$ suggests moderate to difficult sorption, and $n < 1$ indicates poor sorption characteristics (Chen, Zhao et al. 2011) for that system. From Table 5.4, it can be seen that all three adsorbents have n values greater than 2, indicating that metaldehyde is favourably adsorbed is all cases. The values are larger for both of the functionalised sorbents (GAC and S957) indicating stronger interactions between metaldehyde and their surfaces, than for non-functionalised MN200.

The Freundlich adsorption constant, K_F, refers to the relative adsorption capacity, i.e. larger values of K_F imply higher adsorption capacities. As shown in Table 5.4, the K_F values for S957 are in the range 153.87 - 2492.5 mg g^{-1} (L mg^{-1})$^{1/n}$, which far exceed those of MN200 (10.985 - 21.035 mg g^{-1} (L mg^{-1})$^{1/n}$) and GAC (11.770 - 33.903 mg g^{-1} (L mg^{-1})$^{1/n}$), showing that S957 has the greatest adsorption capacity of the three adsorbents. From the experimental data obtained, the maximum sorption capacity was indeed achieved for S957, at 32 °C, (7.5g g^{-1}). The isotherms shown in Figure 5.7 also show an increase in uptake with increasing temperature for set equilibrium concentrations, indicating that the adsorption processes are endothermic.

To further understand the energetics of the adsorption processes, thermodynamic parameters: standard free energy change (ΔG^0, kJ mol^{-1}), enthalpy change (ΔH^0, kJ mol^{-1}) and entropy change (ΔS^0, J mol^{-1}) were determined using the following relationships:

$$\Delta \boldsymbol{G^0} = -\boldsymbol{RTlnK_0} = \Delta \boldsymbol{H^0} - \boldsymbol{T}\Delta \boldsymbol{S^0} \qquad \textbf{Eq. (5-9)}$$

$$\boldsymbol{lnK_0} = \frac{\Delta \boldsymbol{S^0}}{\boldsymbol{R}} - \frac{\Delta \boldsymbol{H^0}}{\boldsymbol{RT}} \qquad \textbf{Eq. (5-10)}$$

where K_0 is the adsorption equilibrium constant; q_e and C_e are as defined previously; R is the universal gas constant and T (K) is temperature. As the concentration of metaldehyde decreases and approaches zero, K_0 can be obtained by plotting $\ln(q_e/C_e)$ against q_e and extrapolating q_e to zero (Li, Di et al. 2005). Once K_0 is known for several temperatures, ΔH^0 and ΔS^0 can be obtained from the slope and intercept of a plot of

$\ln K_0$ against 1/T. Values of K_0 and the subsequently determined thermodynamic parameters are presented in Table 5.5.

Table 5.5 Thermodynamic data for metaldehyde adsorption onto MN200, GAC and S957 at various temperatures

	3 °C		22 °C		32 °C		ΔH^0 †	ΔS^0 ‡
	K_0	ΔG^0 *	K_0	ΔG^0 *	K_0	ΔG^0 *		
MN200	1.5494	-1.0048	2.1611	-1.8851	2.6232	-2.4455	12.571	49.119
GAC	2.1567	-1.7637	3.2761	-2.9104	3.9424	-3.4786	14.617	59.336
S957	3.9632	-3.1601	6.6179	-4.6361	8.3232	-5.3735	17.972	76.542

*** ΔG^0: (kJ mol^{-1}); †ΔH^0: (kJ mol^{-1}); ‡$\Delta S^{0:}$ (J mol^{-1}).**

From the data shown in Table 5.5, it is evident that the standard free energy changes are negative for all adsorbents, indicating spontaneous adsorption of metaldehyde on all samples at all temperatures studied. Furthermore, the standard free energy changes for S957 are much greater than those of GAC and MN200, supporting the theory of strong interaction forces between metaldehyde and the ion exchange resin, as the free energy changes indicate adsorbate-adsorbent affinity, providing excellent agreement with the values determined for *n* in the Freundlich equation. As stated above, metaldehyde uptake increases with increasing temperature for all three sorbents, and the positive enthalpy changes, shown in Table 5.5, support this observation, demonstrating that the adsorption processes are endothermic. Values of ΔS^0 are also positive for all three adsorption systems, thus the randomness at the solid/liquid interface is increased during the adsorption processes, possibly the result of either the release of previously adsorbed surface water molecules upon metaldehyde adsorption on the adsorbent (Huo and Yan 2012), or reactions between functional groups and metaldehyde occurring during the sorption process (Li, Di et al. 2005). The unfavourable na-

ture of positive ΔH^0, which would make a reaction non-spontaneous, is counteracted by the positive ΔS^0 values, resulting in spontaneous adsorption. Hence, the driving force for adsorption is entropic rather than enthalpic, as supported by similar findings for alternative adsorption systems in previous studies (Li, Di et al. 2005; Cestari, Vieira et al. 2008; Tan, Ahmad et al. 2008; Hong, Wen et al. 2009; Gupta, Gupta et al. 2011; Hanafiah, Ngah et al. 2012; Huo, Lin et al. 2012; Huo and Yan 2012).

5.4.3 Adsorption Mechanisms

Interactions between neutral organic compounds and adsorbents normally involve three forces: van der Waals; hydrophobic interactions (hydrophobicity) and hydrogen bonding (Huo and Yan 2012). Of these, two forces are key in the adsorption of a non-polar molecule such as metaldehyde onto a non-functionalised polymer, e.g. MN200: van der Waals and the thermodynamic gradient determined by adsorbent hydrophobicity, which drives the solute out of solution (Valderrama, Barios et al. 2010). The interactions between metaldehyde and MN200 are enhanced by electronic interactions between the *p*-orbital of the metaldehyde oxygen functionalities and the delocalized π-electrons of the benzene rings; such interactions have been observed previously (Valderrama, Cortina et al. 2007; Valderrama, Gamisans et al. 2007; Valderrama, Barios et al. 2010; Valderrama, Barios et al. 2010).

Table 5.6 Quantification of functional groups for GAC and S957.

	GAC	**S957**
Total acidic groups (mmol g^{-1})	0.8875	11.25
Carboxylic groups (mmol g^{-1})	0.5267	-
Lactonic groups (mmol g^{-1})	0.3133	-
Phenolic (mmol g^{-1})	0.0475	-
Sulfonic(Phosphonic) groups (mmol g^{-1})	-	11.25

Adsorption of metaldehyde onto functionalised adsorbents, such as GAC and S957, again involve van der Waals interactions and the thermodynamic gradient; additionally the interaction forces between metaldehyde and these sorbents may involve other stronger forces such as hydrogen bonding and the formation of loosely bonded chemical complexes. Table 5.6 summarises the quantification of functional groups for GAC and S957, determined by Boehm titration methods (Section 3.7) (Goertzen, Thériault et al. 2010; Oickle, Goertzen et al. 2010). As indicated before, the interaction forces between GAC and metaldehyde are much stronger than those for MN200, which could be attributed to the surface chemistry of GAC. It is known that hydrogen bonding plays a significant role in adsorption (Moreno-Castilla 2004) and, according to previous work, metaldehyde molecules associate by hydrogen bonds (Gupta, Gupta et al. 2011), as indicated in Figure 5.8(a). Hence, it is reasonable to suggest that metaldehyde molecules will form hydrogen bonds with the oxygen functionalities, such as the phenolic, lactonic and carboxylic groups, present on the surface of GAC, as depicted in Figure 5.8(b).

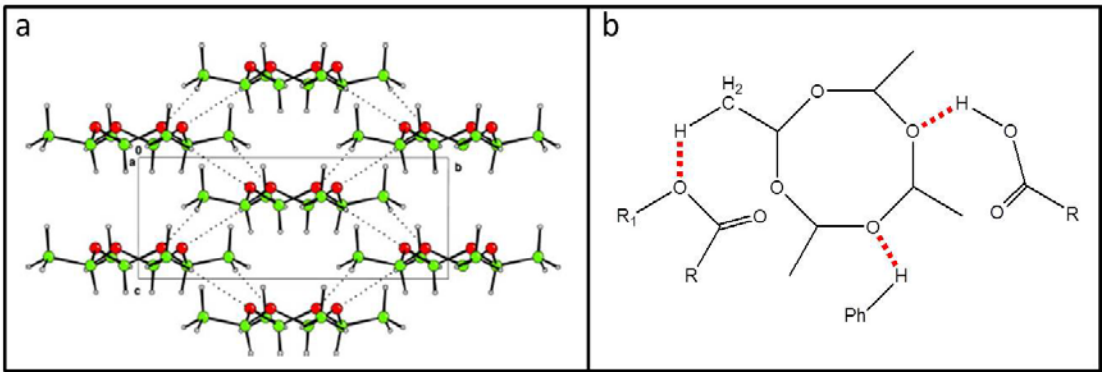

Figure 5.8 (a) Metaldehyde structure View along the axis, showing the C—H---O hydrogen-bonded network. Hydrogen bonds are shown as dotted lines. (Red: Oxygen atom; Green: carbon atoms; Grey: Hydrogen atoms) (©2005 International Union of Crystallography (Gupta, Gupta et al. 2011)); (b) Schematic illustration of possible bonding between GAC and metaldehyde, hydrogen bonds are shown in red dash lines.

The polymeric structure of S957 includes large quantities of sulfonic and phos-

phonic functional groups (11.25 mmol equivalent H^+ per g of material, according to Boehm titration results shown in Table 5.6); as it is known that sulfonic acids cleave dialkyl ethers, moieties that exist in the structure of metaldehyde (Michael Smith 2007), it is reasonable to propose that reactions occur between metaldehyde and the sulfonic functionalities in S957. The sulfonic acid groups cleave the ring of metaldehyde into long chain alcohols with ether functionalities. Moreover, since there are four ether structures within each metaldehyde molecule and the concentration of sulfonic functionalities is quite high, there might be second, third or even fourth step reactions between the long chain alcohols and sulfonic acid groups. These reactions are in agreement with the pKa values of CH_3SO_3H and H_3O^+, which are -2.6 and -1.7, respectively(D.H. Ripin 2005); these values indicate that sulfonic acid could ionize protons which subsequently break down the ether groups. It is also known that phosphonic acid groups form chemically bonded complexes with ether(Penczek, Kaluzynski et al. 2007); in 1978, Edwards *et al.* discovered an ether phosphoric acid compound (H_3PO_4 $(CH_3)_2CHO_2O$) formed (Edwards, Williams et al. 1978) during the purification of phosphoric acid contaminated water (Paul Otto Schallert 1968). It is, therefore, reasonable to assume that similar complex compounds could be formed between phosphonic acid groups and metaldehyde. Proposed adsorption mechanisms between metaldehyde and sulfonic and phosphonic acid groups are schematically illustrated in Figure 5.9.

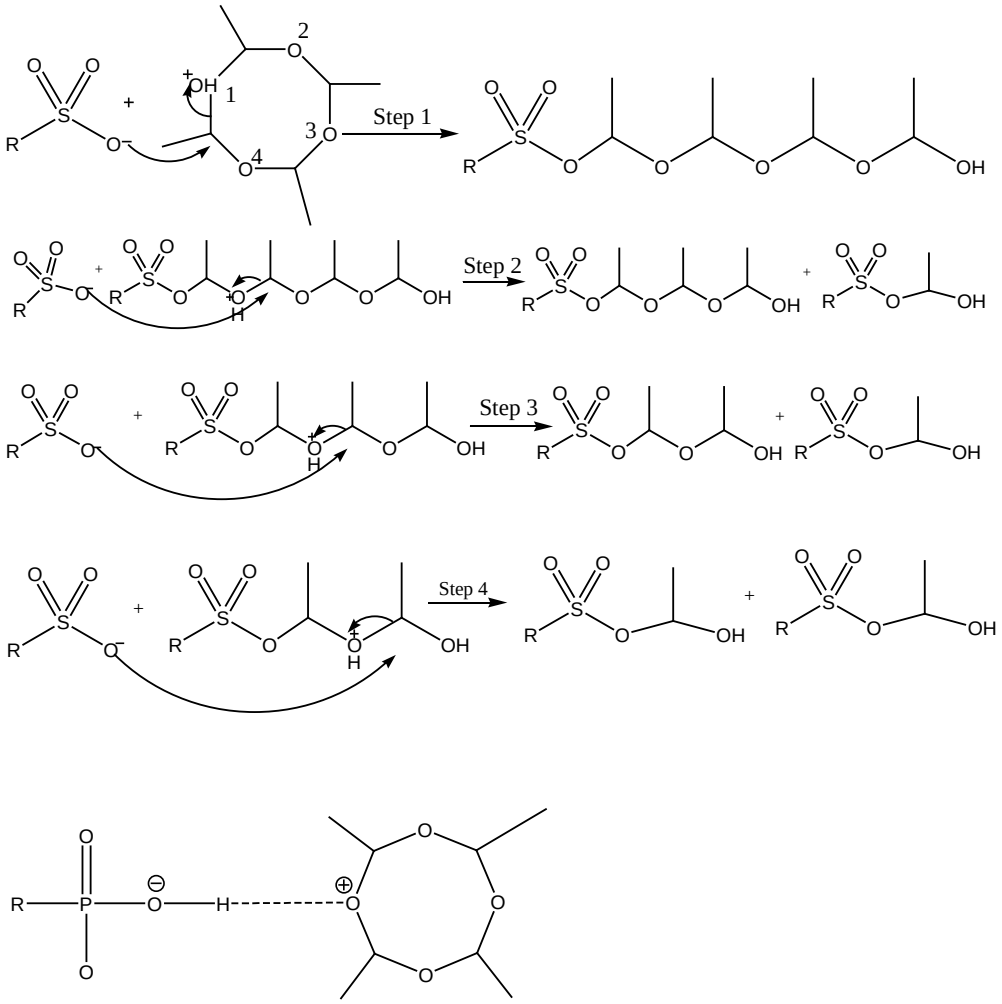

Figure 5.9 Schematic illustration of sorption mechanism of metaldehyde on S957

In order to gather further evidence to support these proposed mechanisms, the pH values of the ion exchange resin were measured before and after sorption by mixing 0.1g of each sample with 20mL water. The pH value increased from 3.68 at the beginning of the reaction to 4.94 after adsorption, supporting the above mechanism since the reaction of metaldehyde with the resin is proton-consumed, increasing basicity. Furthermore, Temperature Programmed Desorption (TPD) was performed on both original S957 and resin after adsorption, as outlined in Section 3.8. The TPD spectra of CO_2 are shown in Figure 5.10, and it is evident that the reacted resin generates much more CO_2 than original S957. This could be due to the fact that after adsorption degraded metaldehyde molecule fragments are attached to the polymer structure of the

resin, forming sulfonic acid ester structures (the products shown in Figure 5.9). These sulfonic acid esters decompose during TPD, as the material is heated (Barclay, Medeiros et al. 1995), thus the intensity of CO_2 is much stronger than that of original S957.

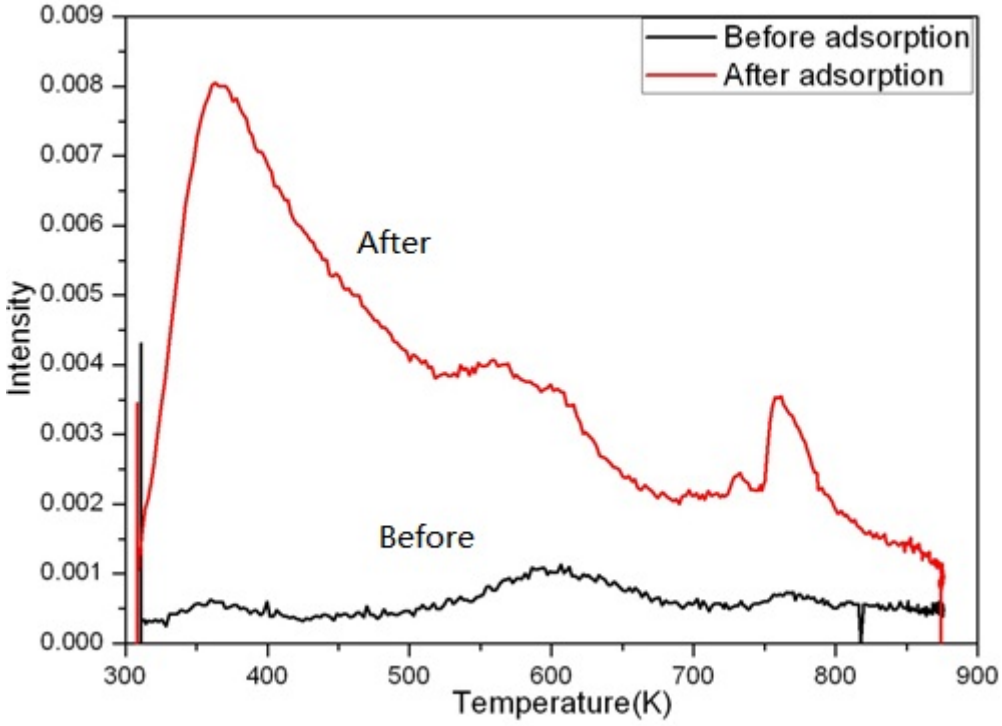

Figure 5.10 TPD spectra of CO_2 for both original and loaded S957

5.4.4 Leaching Tendency Tests and Recyclability Studies

Within water purification applications, adsorption of a contaminant is only one part of the required system, it is also necessary to study the leaching tendency of a potential adsorbent, as high leaching tendencies result in ameliorative failure even if the kinetics are fast and the adsorption capacity high. In this work, materials fully loaded with metaldehyde were thoroughly mixed with known quantities of deionized water to test how much of the adsorbed metaldehyde leached from the adsorbent.

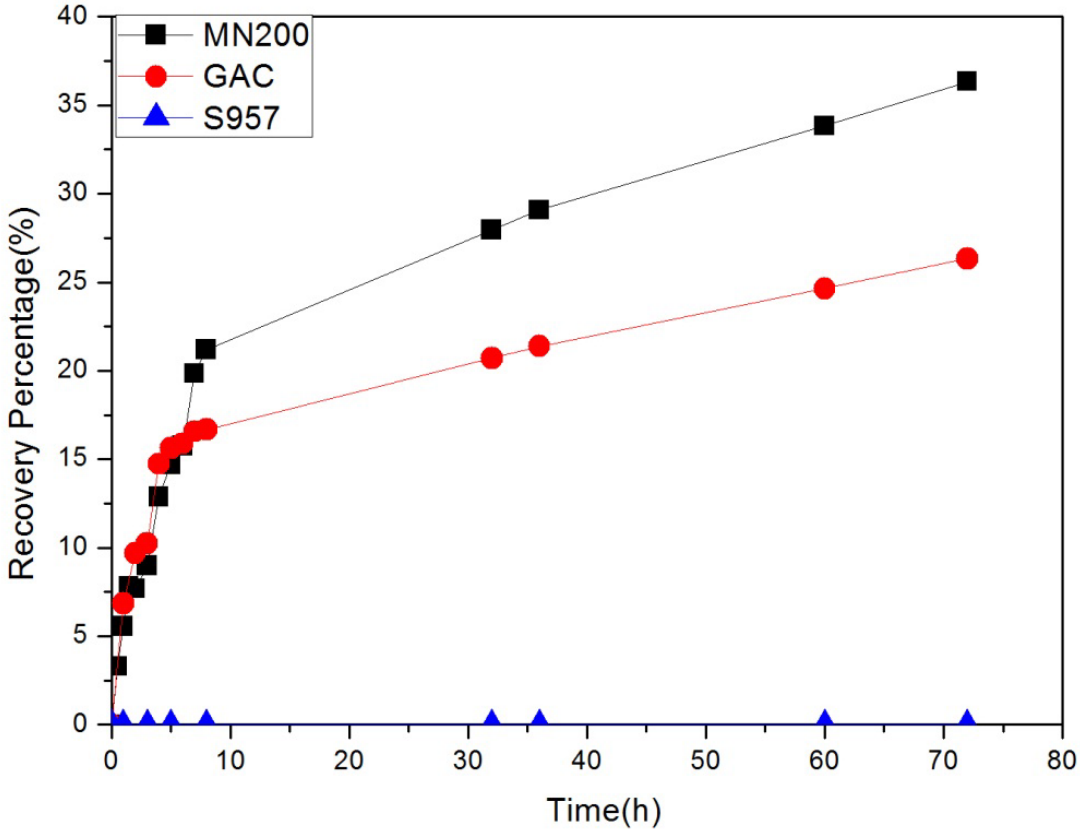

Figure 5.11 The percentage of adsorbed metaldehyde leached out of MN200 (■), GAC (●) and S957 (▲) as a function of time

Figure 5.11 shows the percentage of adsorbed metaldehyde leached from each adsorbent as a function of time. It is can be seen that 36% of adsorbed metaldehyde is leached from MN200 in only 72 h, while 26% of metaldehyde is leached from GAC in the same time period. Moreover, desorption rates for metaldehyde leaching from MN200 and GAC were both initially fast, with a decrease in rate as leaching time progressed. Conversely, metaldehyde desorption from S957, showed no measurable metaldehyde leaching within the studied time period. It is likely that these leaching tendencies are related to the adsorption mechanisms discussed above, as significant amounts of metaldehyde were leached from both MN200 and GAC, as a consequence of the failure of these materials to break down or chemically attach the adsorbed metaldehyde, in comparison to the destruction of metaldehyde by interactions with the polymeric surface functionalities within S957.

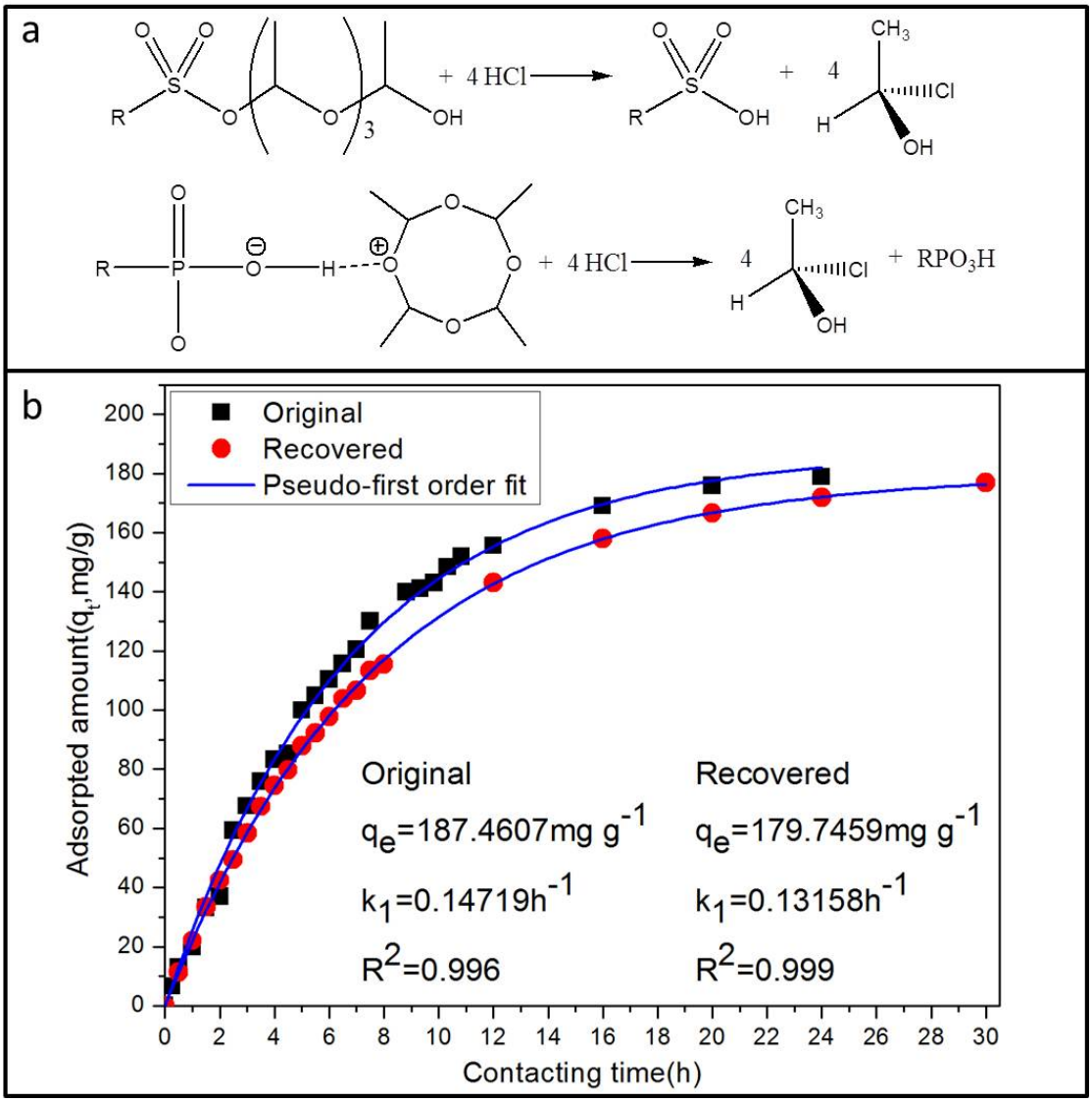

Figure 5.12 (a) Schematic illustration of the regeneration reactions between S957 and HCl; (b) the kinetic data of original and recovered S957 and their fitting to pseudo-first order equation.

Based on the proposed mechanism, the fully loaded resin should be regenerated by treatment with HCl, following the reactions depicted in Figure 5.12(a). Therefore, a regeneration study was performed, as described previously. Figure 5.12(b) shows the kinetics data obtained for original and recovered S957 resins, with fits to pseudo-first order equations. The calculated parameters (shown in Figure 5.12(b)) clearly show that the resin can be easily regenerated and the recovery rate is quite promising (89.4% in terms of k_1).

5.5 Conclusions

Metaldehyde removal was successfully performed by non-functionalised polymeric resin MN200, functionalised commercial GAC and ion exchange resin S957, which contains high sulfonic and phosphonic acid group contents. Kinetic studies revealed that the rate of metaldehyde adsorption is affected by surface area and the presence of surface functional groups. Metaldehyde adsorption on GAC showed the fastest kinetics, while the ion exchange resin exhibited the slowest adsorption rate. Analysis of kinetic data obtained showed adsorption on GAC and MN200 to be limited by particle diffusion, while the rate determining step of S957 was diffusion of metaldehyde through the solid/liquid interface as a consequence of the low surface area of the material. Isothermal studies showed GAC and MN200 to have similar adsorption capacities; comparatively S957 exhibited a capacity two orders of magnitude greater. This may be related to the greater affinity of S957 for metaldehyde, than either GAC or MN200, according to parameters determined using the Freundlich equation. Thermodynamic data were consistent with both kinetic and isothermal studies, and, using these findings, it was possible to propose adsorption mechanisms for these adsorbents. During metaldehyde removal using MN200 and GAC, the solute molecules were not destroyed but physically adsorbed, resulting in high leaching tendencies of intact metaldehyde from these materials. S957 demonstrated destruction of metaldehyde molecules by sulfonic and phosphonic functionalities, which subsequently become part of the polymeric structure through chemisorption of the resulting degradation products; this is supported by the results of leaching tendency test, which were negligible. The results of this work indicate that ion exchange resin S957 has superior performance than current water treatment adsorbents and is promising for melioration of metaldehyde from drinking water.

Chapter 6 Catalytic Degradation and Adsorption of Metaldehyde from Drinking Water by Functionalised Mesoporous Silica and Ion-Exchange Resin

6.1 Introduction

The findings in Chapter 5 suggested sulfonic acid functionalities are desirable for removing metaldehyde but adsorption kinetics of S957 were slow, which is kilely because of the poor porosity of S957. Hence, materials with both sulfonic acid functionalities and good porosities should be developed to improve the kinetics. Mesoporous silica (SBA-15) is a type material possessing good mesoporosity and can be incorporated with various functionalities, as outlined in Section 3.1.4. In this Chapter, we report the synthesis, characterisation and application of sulfonic acid functionalised SBA-15 materials as effective catalysts for the depolymerisation of metaldehyde into acetaldehyde, and subsequent optimization of the chemisorption of this single by-product to achieve the ultimate goal of complete removal of metaldehyde from drinking water.

6.2 Experimental

Sulfonic acid functionalised silica (SA-SBA-15) and amine functionalised silica (AF-SBA-15) were synthesised following the procedures outlined in Section 3.1.4, and characterisations, including textural, morphological and crystal structural, were performed as outlined in Chapter 3.

Heterogeneous catalytic degradation of metaldehyde using SA-SBA-15, with varied SA loadings, was performed by adding 200 mg of catalyst to 200 mL of metaldehyde solution with initial concentration 200 mg g^{-1} (5.6812 mmol L^{-1}). Samples were taken at predetermined time intervals and the concentration of metaldehyde and acetaldehyde determined. The kinetic investigation of acetaldehyde chemisorption onto AF-SBA-15 and A830 was performed by adding 100 mg of adsorbent to 200 mL acetaldehyde solution, with initial concentration of 20 mg L^{-1}. Samples were taken at selected time intervals. The adsorption isotherm of acetaldehyde onto A830 at 20 ^{o}C K was determined by bottle-point method, where 50 mg of A830 was added to 200 mL of acetaldehyde solutions with varying concentrations and the system allowed equilibrating.

The concentration determination of metaldehyde and acetaldehyde were performed using GC and HPLC, as outlined in Section 3.4.4 and 3.5.2.

6.3 Results and Discussion

6.3.1 Synthesis and Characterisation

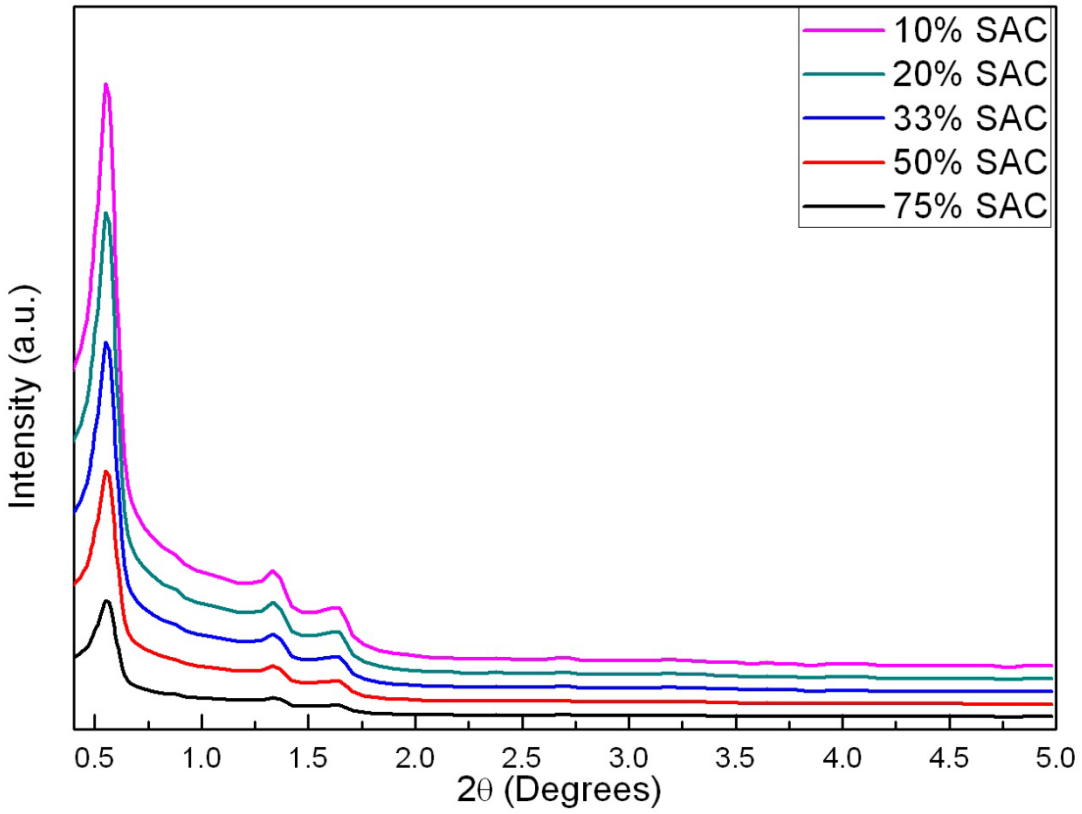

Figure 6.1 Low-angle powder X-ray diffraction patterns of as-synthesised sulfonic acid and AF-SBA-15 with different extent of functionalisation.

Figure 6.1 shows the small-angle Powder X-ray Diffraction (PXRD) pattern of five functionalised silica samples synthesised in this study. Three of the five SA-SBA-15 samples, i.e. those at 10%, 20% and 33%, exhibited three well-resolved peaks, indexed as (1 0 0), (1 1 0) and (2 0 0); these are known diffractions associated with the highly ordered two-dimensional hexagonal symmetry (space group p6mm) of mesoporous silica SBA-15. Although it has been reported that functionalisation could go as high as 60% (Kruk, Asefa et al. 2002; Tsai, Pan et al. 2009), in this work silica with SAC > 75% failed to form solids, and samples with SACs of 50% and 75% formed solids but failed

to show well-resolved PXRD peaks. Regarding amine functionalised SBA-15; both AF-SBA-15 samples exhibited well resolved peaks, indicating highly ordered mesoporous structures for these samples.

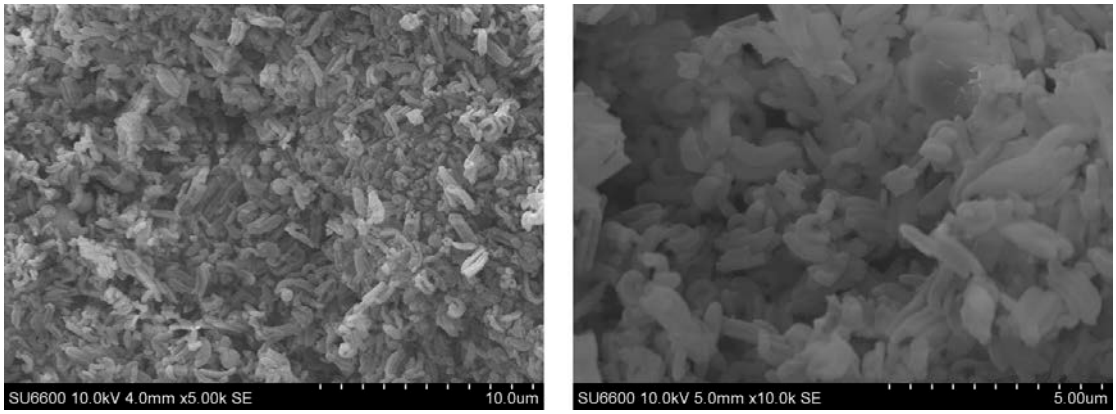

Figure 6.2 SEM images of as-synthesised 10% SA-SBA-15 with magnification of 5k (Left) and 10k (Right)

SEM images, shown in Figure 6.2, reveal that the as-prepared silica samples consist of many rope-like domains with relatively uniform sizes, aggregated into wheat-like macrostructures, which are similar to those found for conventional unmodified SBA-15 (Zhao, Feng et al. 1998; Margolese, Melero et al. 2000).

Figure 6.3 shows the isotherms of nitrogen adsorption and desorption onto the silica samples measured at -196 ^{o}C. It can be seen that all five isotherms fit Type IV isotherms, with well-distinguished regions identified as micropore filling, capillary condensation, as evidenced by H2 hysteresis loops, and eventual plateauing at high relative pressures.

Figure 6.4 displays the pore size distributions of the silica samples. It is clear that significant shrinkage in mesopore diameter is observed as SAC increases, coupled with the broader hysteresis loops observed for samples with higher SAC, as seen in Figure 6.3, this indicates partial blockage of the pores. Such phenomena have been observed previously for SBA-15, with partial pore blocking by organic functional groups (Kruk,

Jaroniec et al. 2000; Mori and Pinnavaia 2001; Kruk, Asefa et al. 2002; Vinu, Murugesan et al. 2004; Shieh, Hsiao et al. 2013), and is notable at pore entrances (Tsai, Pan et al. 2009). It is also reported that the observation of a H2 hysteresis loop in highly functionalised samples confirms the presence of blocking effects (Thommes, Köhn et al. 2002), and the observed decrease in pore volumes and surface areas for high SAC materials, shown in Table 6.1, is also ascribed to pore blocking.

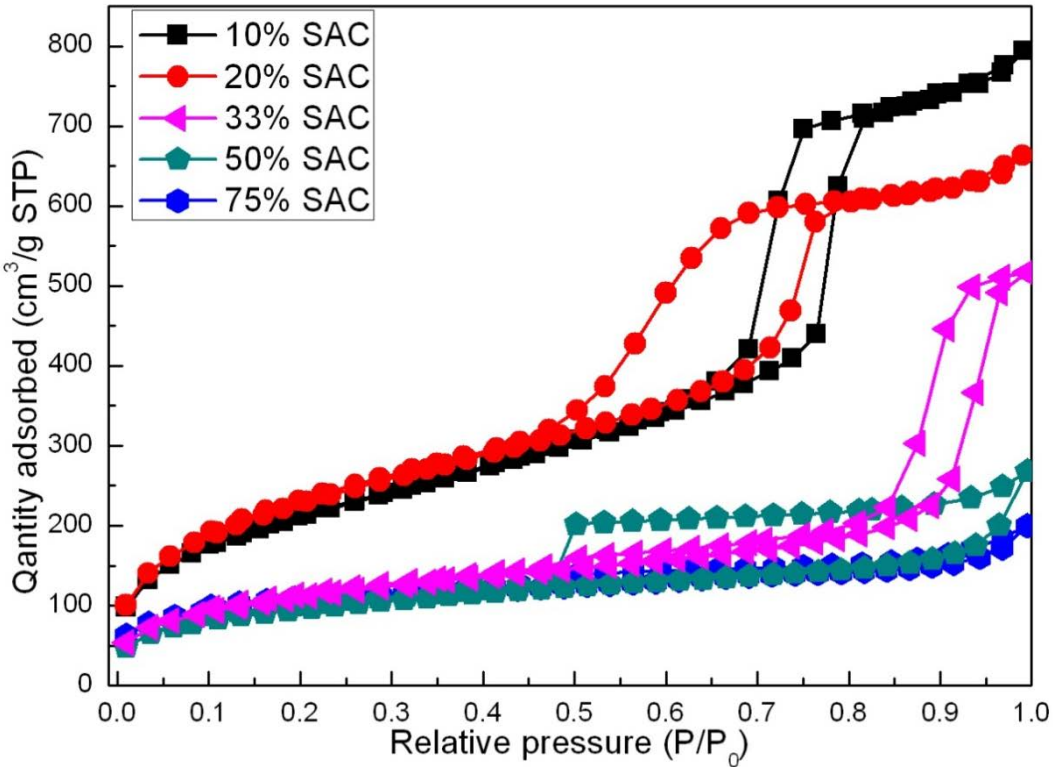

Figure 6.3 Nitrogen adsorption/desorption isotherms of the silica samples with different SAC

Table 6.1 summarises the characterisation results, including porosity parameters and titration results for all SA-SBA-15 samples synthesised in this study. BET surface areas were obtained from appropriate analysis of adsorption isotherms as described in Chapter 3. Pore volumes were determined from the final adsorption point (p/p_0 = 0.985). Pore size distributions were calculated using BJH analysis.

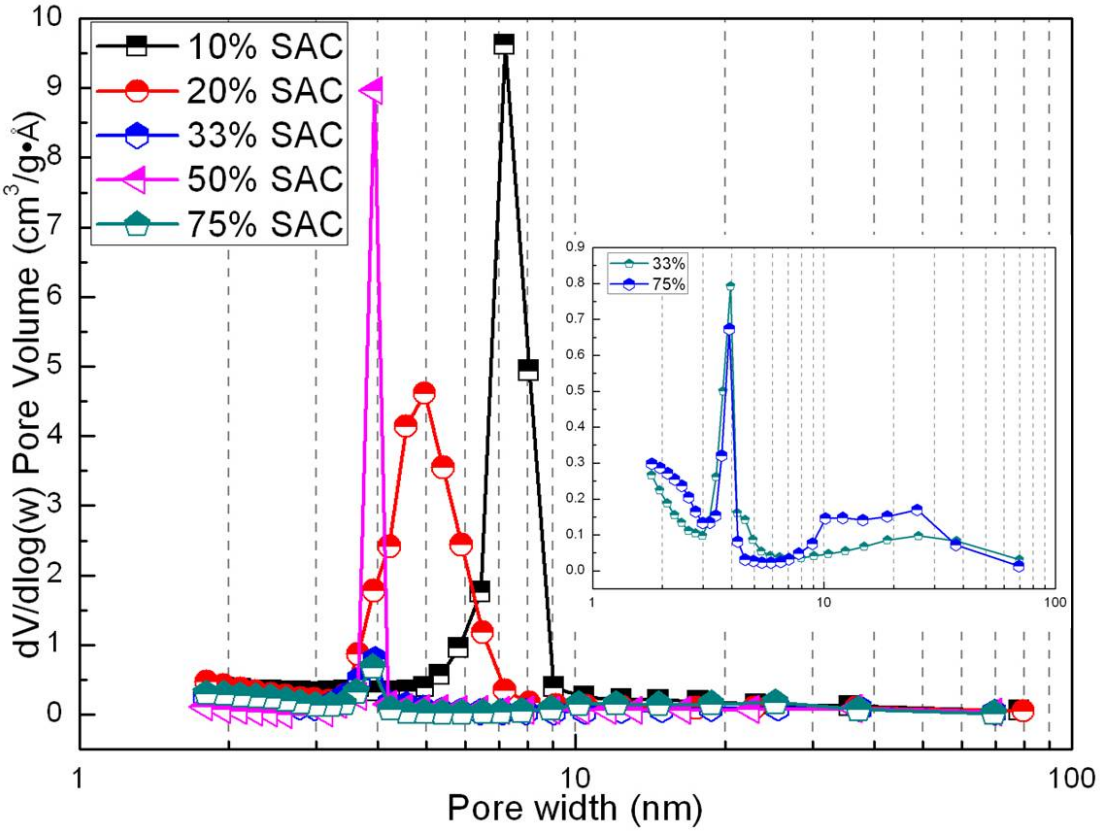

Figure 6.4 Pore size distributions of as-prepared SA-SBA-15 samples

Table 6.1 Porosity parameters, titration results and first order rate constants for as-synthesised SA-SBA-15 silica.

I.D.	S_{BET} (m^2 g^{-1})	APD (nm)	PV(cm^3 g^{-1})	SAC(mmol g^{-1})	k(min^{-1})
10%	828 ± 6.5	7.18	1.23	1.28	3.2 x 10^{-3}
20%	770 ± 4.5	5.82	1.03	1.71	2.4 x 10^{-3}
33%	350 ± 6.8	5.50	0.31	1.94	1.5 x 10^{-4}
50%	334 ± 3.8	4.91	0.41	2.05	1.3 x 10^{-4}
75%	394 ± 3.5	4.90	0.79	2.09	1.2 x 10^{-4}

APD = Average Pore Diameter; PV = Pore Volume; SAC = Sulfonic Acid Content; k = first-order rate constant.

6.3.2 Mechanism of Metaldehyde Removal by Sulfonic Acid Functionalities

There are two categories of literature reporting the interactions between metaldehyde and sulfonic acid functionality. The first considers metaldehyde as a compound with ether functionality, the removal mechanism should be as demonstrated (Michael Smith 2007) in the previous Chapter. In this mechanism, a very important assumption is that RSO_3^- is similar to Cl^- in that it is completely mobile, such that it attacks the carbon atom, allowing reaction to happen.

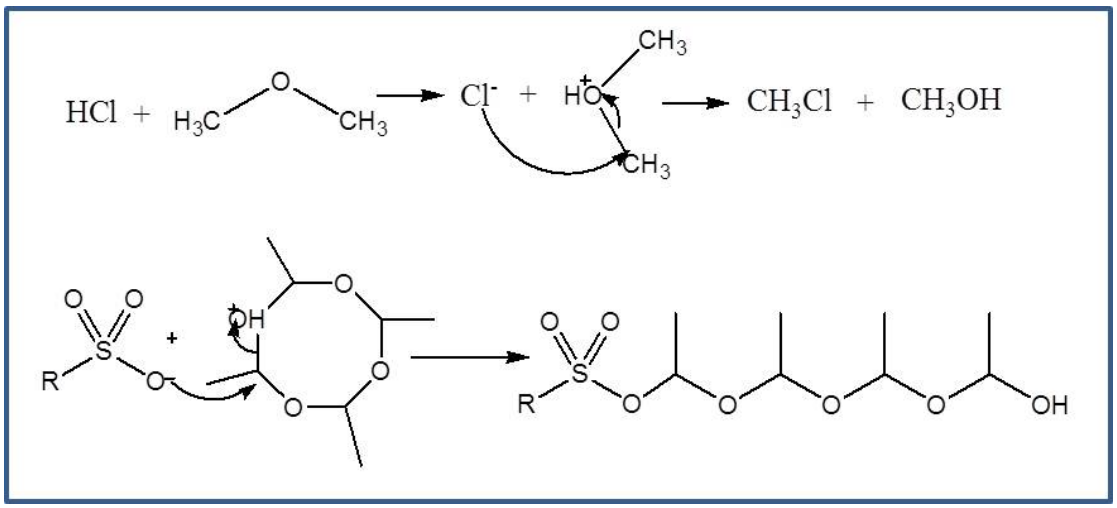

Figure 6.5 Reaction mechanisms between sulfonic acid and ethers

It has also been reported that metaldehyde can be degraded by the presence of strong acids (e.g. HCl) (Bevington 1952; Selim and Seiber 1973), although no detailed mechanism has yet been presented. Since $-SO_3H$ has very similar properties to HCl, it is reasonable to propose that $-SO_3H$ can similarly catalyse the depolymerisation reaction of metaldehyde. Here, a detailed mechanism for sulfonic functionalities tethered to silica promoting the depolymerisation of metaldehyde into acetaldehyde is proposed.

In order to confirm the exact mechanism, several additional experiments were conducted to provide supporting evidence.

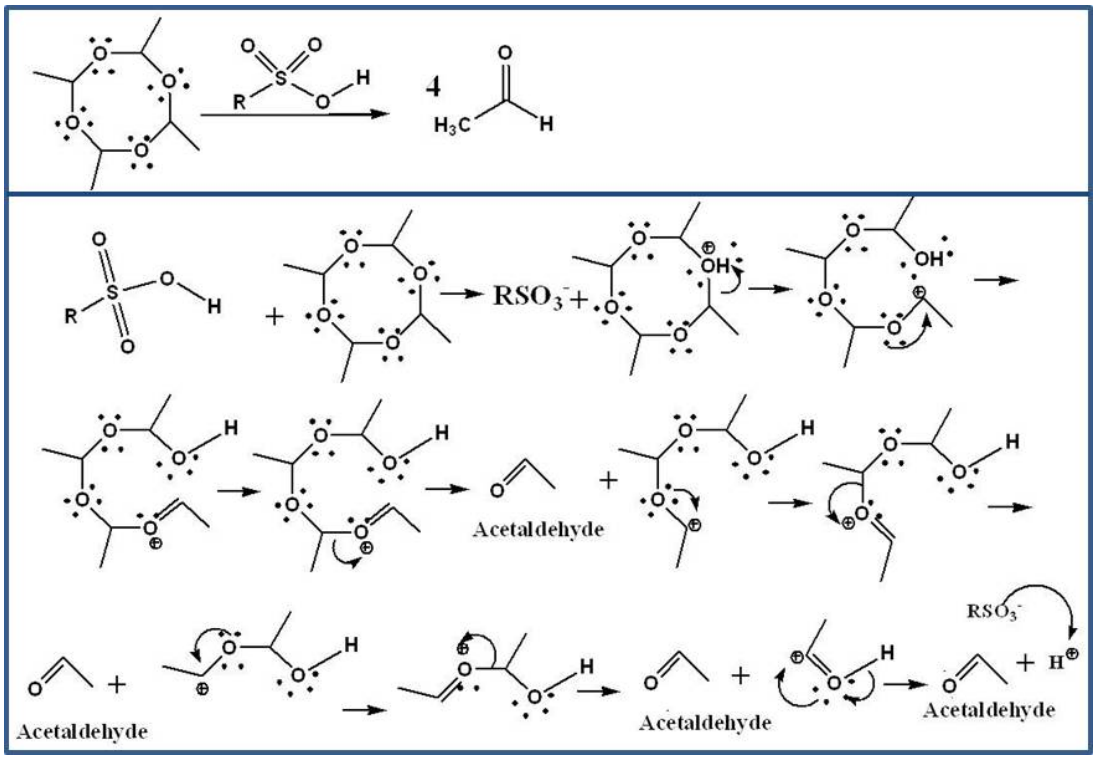

Figure 6.6 Depolymerising mechanism of metaldehyde by sulfonic acid functionality

6.3.2.1 Quantitative Determination by NMR

Firstly, Nuclear Magnetic Resonance (NMR) was employed to identify the possible products of the reactions taking place. Metaldehyde (1 mg) was dissolved in D_2O (10 mL) and the NMR spectrum of the solution (100 mg/L) recorded. Then, sulfonic acid functionalised silica (1 mg) was added to the solution. After a recorded reaction time, the NMR spectrum of the solution was recorded. This was repeated for a range of reaction times. Figure 6.7 shows the NMR spectra of the initial metaldehyde solution before the addition of 10% SA-SBA-15 and Figure 6.8 shows the spectrum of the solution 2 h after addition. It is clear that before the addition of SA-SBA-15, there are only two peaks observed: double-peak with chemical shift 1.3 ppm corresponding to the hydrogen atoms of $–CH_3$ groups present in metaldehyde, and the quadruple-peak located at 5.2 ppm, corresponding to the –CH group. As time evolves, the peaks corresponding to metaldehyde (d at 1.3 ppm, q at 5.2 ppm) decreased to almost negligible levels. In the meantime, only characteristic peaks for acetaldehyde (d at 2.2

ppm, s at 9.6 ppm) were observed. The peak with a chemical shift of 2.2 ppm corresponds to the hydrogen atoms of $–CH_3$ groups in acetaldehyde and the single located at 9.6 ppm corresponds to hydrogen atoms of –CHO groups. No other peaks for intermediates or any other by-products were observed.

The NMR studies only provide qualitative indications, providing that depolymerisation is involved in the removal process. It is also possible that a cleavage mechanism could be involved as there are no products with all metaldehyde molecular parts attached to the material, becoming part of the resin. Thus, in order to confirm whether the cleavage mechanism is involved, the quantification was performed using concentration determination for metaldehyde and acetaldehyde.

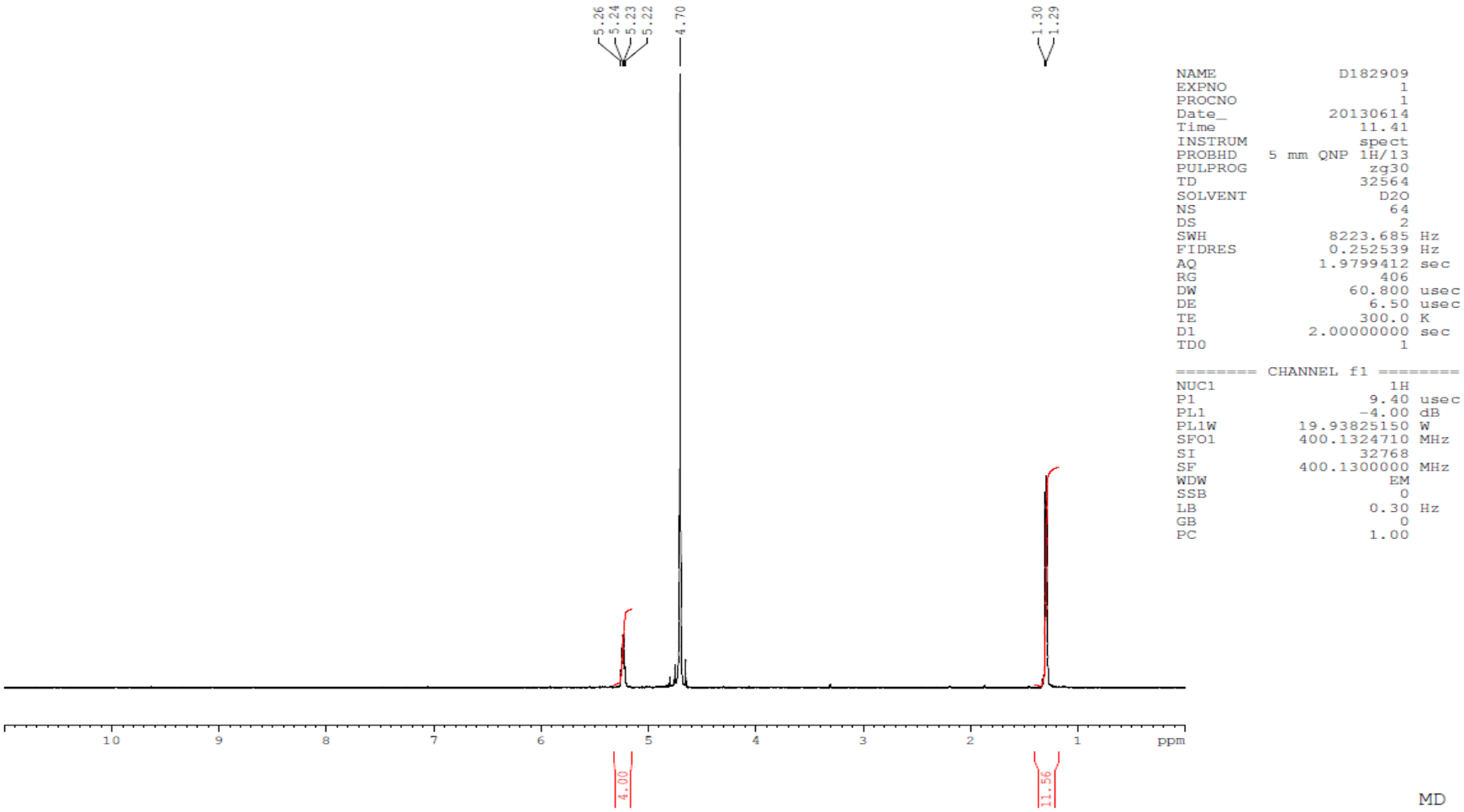

Figure 6.7 NMR spectrum of metaldehyde solution before addition of SA-SBA-15.

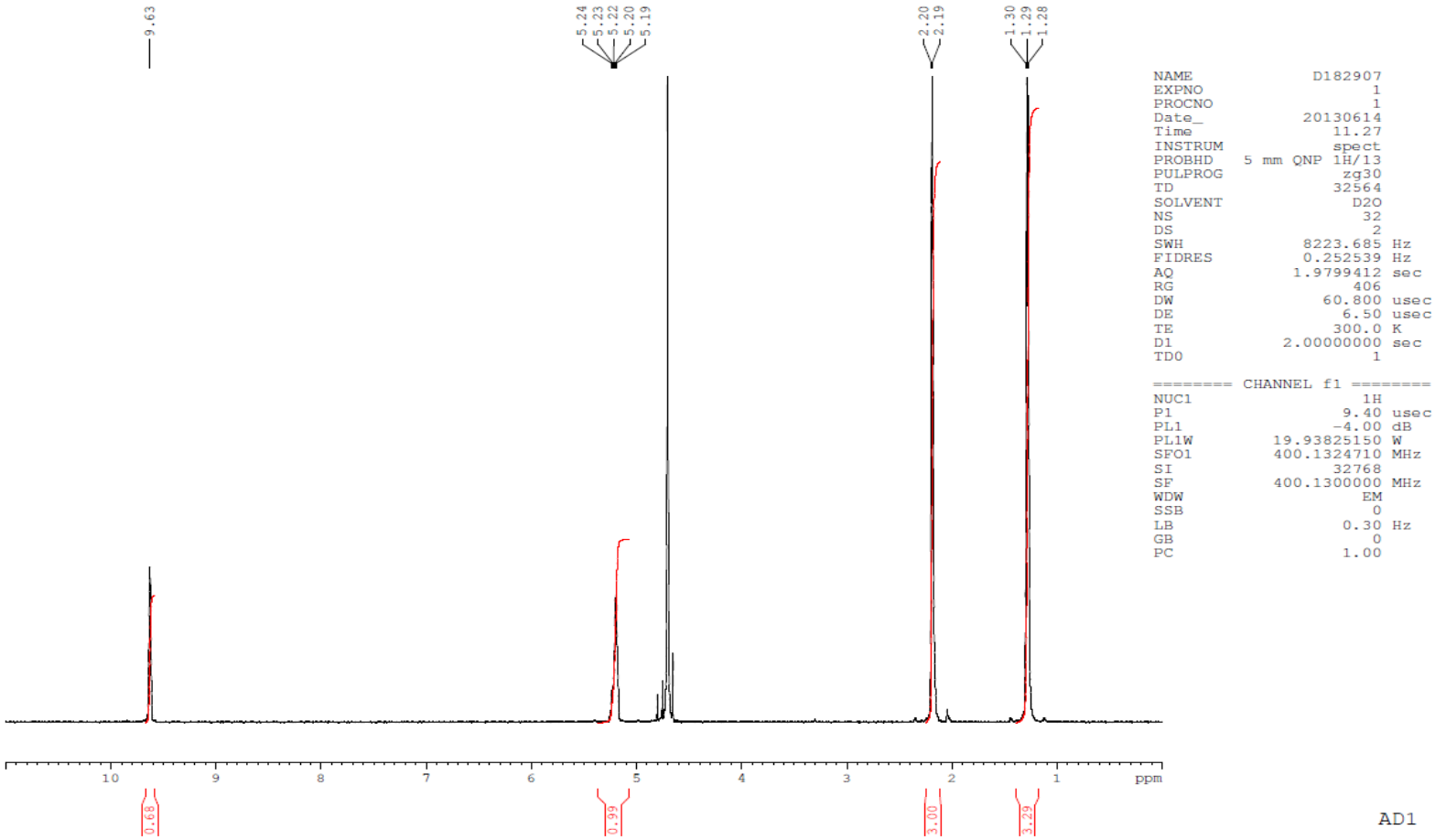

Figure 6.8 NMR spectrum of metaldehyde solution 2 h after addition of SA-SBA-15.

6.3.2.2 Quantification Determination

According to the depolymerisation reaction, 4 moles of acetaldehyde (AD) should be produced per 1 mole of metaldehyde (MD) consumed. Therefore, if only the depolymerisation process is involved in the removal process, then the concentration ratio of AD/MD should be 4.

$$\textbf{Metaldehyde}\ (\textbf{MD},\ C_8H_{16}O_4,) \xrightarrow{\text{Catalyst}\ (C,\ RSO_3H)} \textbf{Acetaldhyde}\ (\textbf{AD},\ C_2H_4O) \qquad \textbf{Eq. (6-1)}$$

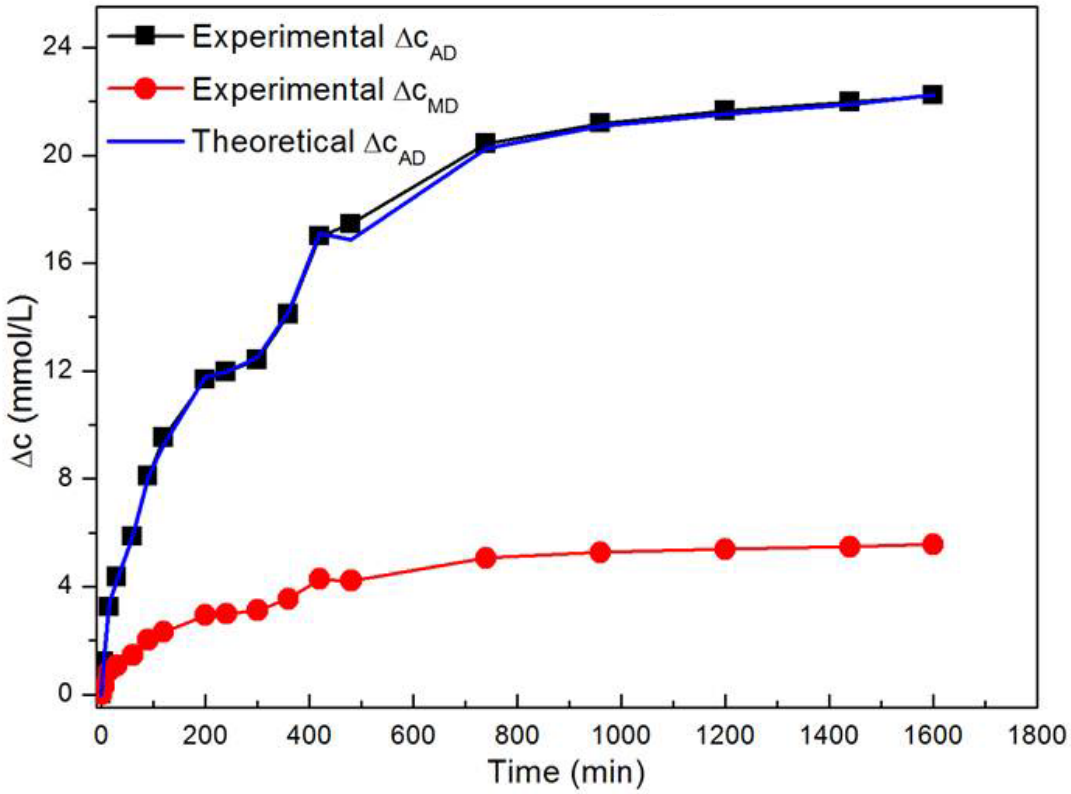

Figure 6.9 Molar concentration change of metaldehyde and acetaldehyde as a function of time using 10% SA-SBA-15 as catalyst; $\Delta c_{AD} = c_{t,AD}$, $\Delta c_{MD} = c_{0,MD} - c_{t,MD}$.

Figure 6.9 shows the change in molar concentrations of metaldehyde and acetaldehyde as a function of time. In the following equations, c_0 denotes initial concentration and c_t is the concentration at time t.

Change in acetaldehyde concentration: $\Delta c_{AD} = c_{t,AD}$;

Change in acetaldehyde concentration: $\Delta c_{MD} = c_{0,MD} - c_{t,MD}$.

It is shown in Figure 6.9 that the experimental data fits the theoretical data extremely well, indicating the metaldehyde molecules were almost totally converted into acetaldehyde. It is, therefore, clear that only depolymerisation occurs during the removal process.

6.3.3 Kinetic Study of the Catalyst

As a consequence of the improved understanding of the underlying mechanism, it was possible to determine the efficiency of the process. Catalytic activity is a significant parameter that measures the efficiency of a catalyst in converting reactants to products; the activity of a catalyst is defined as the rate of consumption of reactant, hence, the kinetics of the catalytic reactions were investigated, using:

$$\text{Metaldehyde (MD, } C_8H_{16}O_4,) \xrightarrow{\text{Catalyst (C, } RSO_3H)} \text{Acetaldhyde (AD, } C_2H_4O)$$

$$\mathbf{r = -\frac{d[MD]}{dt} = k_{MD,C} \times [MD] \times [C] = k'_{MD} \times [MD]} \qquad \textbf{Eq. (6-2)}$$

where r is the reaction rate of metaldehyde removal, [ ] denotes molar concentrations, $k_{MD,C}$ represents the second-order rate constant (mol^{-1} s^{-1}) and k'_{MD} is the first-order rate constant (s^{-1}). Since the concentration of the catalyst is constant, and in significant excess, the rate of reaction is only dependent on the concentration of metaldehyde; hence, a first-order rate equation can be employed:

$$\frac{C_t}{C_0} = e^{-k'_{MD}t} \qquad \textbf{Eq. (6-3)}$$

where C_t is the concentration at time t, and C_0 is initial concentration. Figure 6.10 shows the concentration evolution of metaldehyde as a function of time for silica samples with increasing SAC, and the resulting fits to a first-order kinetic equation; the rate constants, k, obtained are shown in Table 6.1.

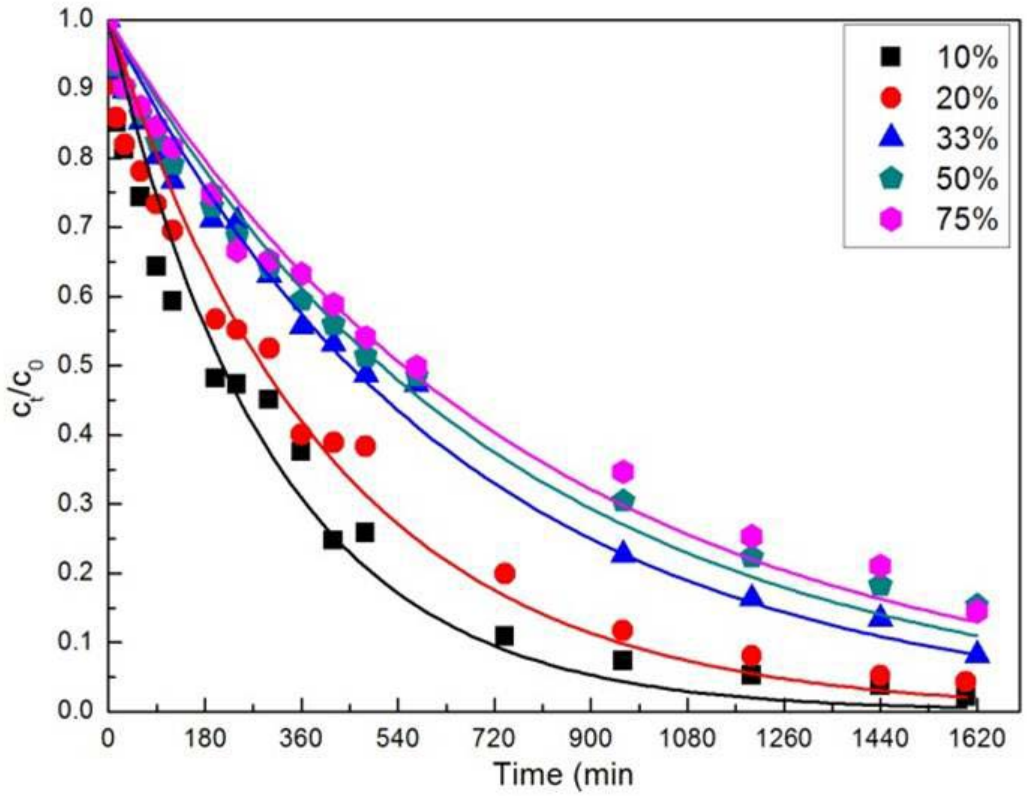

Figure 6.10 Kinetics data and first-order fits of metaldehyde depolymerisation using as-synthesised SA-SBA-15

It is clear that the rate of reaction decreases with increasing SAC, with 10% SA-SBA-15 showing the best kinetic performance, and a rate constant one order of magnitude higher than all other samples studied. It may be expected that increasing quantities of active acid groups would enhance the rate of degradation but, as stated earlier, higher SAC reduces the surface area, pore size and pore volume, such that the most important step of the catalytic reaction, reactant diffusion from the bulk solution to reactive catalyst sites, is hindered by increased diffusive resistance, reducing the reaction rate. Furthermore, the blocking of well-ordered pores by organic functional groups, especially significant blockage at pore entrances, also impedes access of metaldehyde molecules to reactive sites.

6.3.4 Adsorption of Acetaldehyde

It has been reported that vapour phase acetaldehyde can be adsorbed by amine functionalised materials via the following condensation reaction (Hayashi, Kumita et al. 2005; Ewlad-Ahmed, Morris et al. 2012):

$$\mathbf{H_2N - R + CH_3CHO \rightarrow CH_3CH = N - R + H_2O} \qquad \textbf{Eq. (6-4)}$$

It was assumed, by the authors, that a similar reaction would be possible in the aqueous phase; hence, in order to remove the single by-product of the catalytic degradation of metaldehyde, materials with amine functionality were applied to treated aqueous phase samples. As stated earlier, SBA-15 has a tuneable, highly ordered, uniform structure, high surface area, large pore volume and, most importantly, the ability to host various organic functionalities. Hence, it was possible to synthesise SBA-15 with amine functionalities (AF-SBA-15) as described earlier, which were applied for the removal of acetaldehyde. The amine content was kept low at only 2.6% and 10% as a result of the expected pore blocking effect for higher concentrations, as observed for SA-SBA-15. Small-angle powder XRD patterns of the AF-SBA-15 samples exhibited similar characteristic peaks to SA-SBA-15. Nitrogen adsorption characterisation data of these two samples is shown in Table 6.2, as well as the nitrogen contents determined by CHN analysis. It can be clearly seen from Table 6.2 that the inclusion of amine functionalities partially reduces the silica porosity, causing a decrease in surface area from 420 $m^2 g^{-1}$ (2.6%) to 291 $m^2 g^{-1}$ (10%). A similar trend in pore volume was observed for pore volume, with a decrease from 0.41 $cm^3 g^{-1}$ to 0.23 $cm^3 g^{-1}$ as amine content increased.

As-synthesised AF-SBA-15 samples were applied to remove acetaldehyde from prepared samples and Figure 6.11 shows the kinetic profiles of sorption at 20 ^oC. The experimental data were fitted to pseudo-first order and pseudo-second kinetic equations (Tao and Fletcher 2013). The modelling showed that the pseudo-second order equation describes the kinetic process better than the pseudo-first order equation, with the

pseudo-second order rate constants presented in Table 6.2.

Table 6.2 Textural parameters, nitrogen contents and pseudo-second order rate constants for as-synthesised AF-SBA-15 and ion exchange resin A830

Sample code	S_{BET}(m^2 g^{-1})	APD(nm)	PV(cm^3 g^{-1})	NC(%)	k_2(min^{-1})
AF-SBA-152.6%	420 ± 1.1	3.5	0.41	0.23	5.37×10^{-3}
AF-SBA-15 10%	291 ± 1.9	3.4	0.23	1.39	1.33×10^{-2}
A830	1.82 ± 0.06	>100	0.01	2.14	3.04×10^{-3}

APD = Average Pore Diameter; PV = Pore Volume; NC = Nitrogen Content, determined by elemental analysis; k_2 = pseudo-second-order rate constant (Tao and Fletcher 2013).

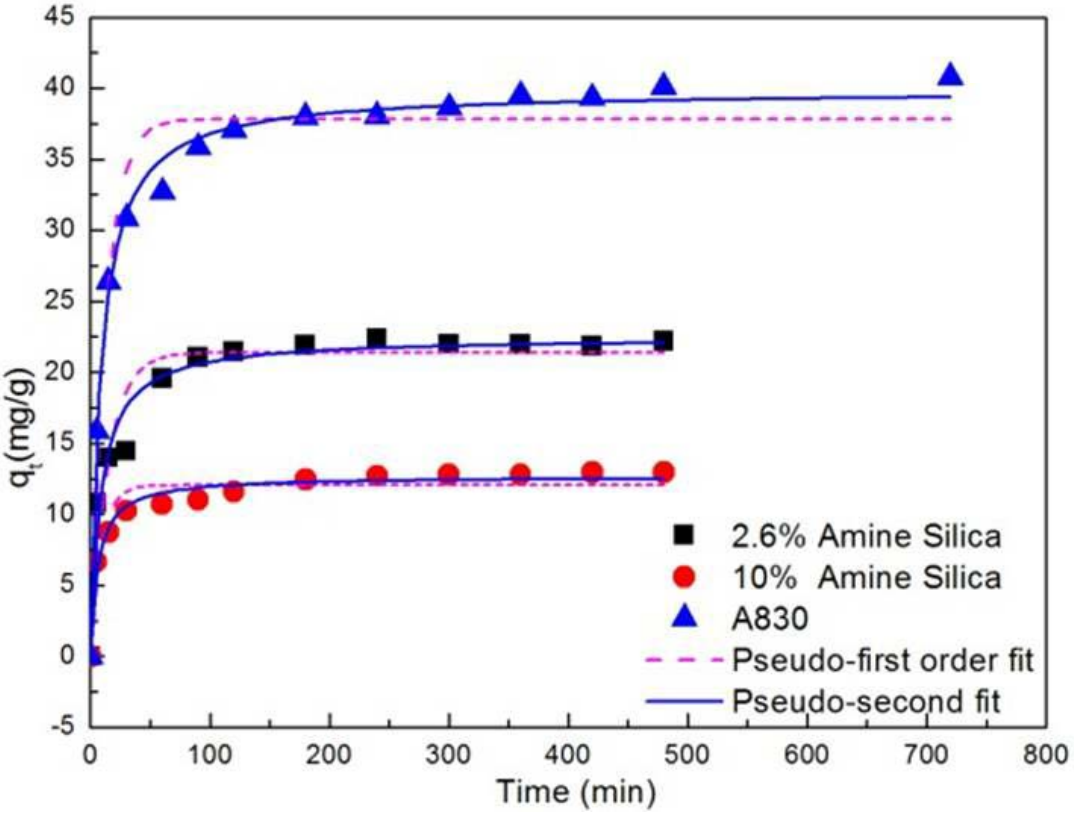

Figure 6.11 Adsorption kinetics of acetaldehyde onto AF-SBA-15 and A830 and the fitting of experimental data to different adsorption kinetic equations

It is clear that the sorption rate of 10% AF-SBA-15 was significantly faster than that of 2.6% AF-SBA-15. However, the adsorption capacities showed the opposite trend, i.e. 2.6% AF-SBA-15 demonstrated a greater capacity than that of 10% AF-SBA-15. These contradictory results are closely related to the pore structure of the samples and the adsorption mechanism. Increasing amine content increases the density of active sites, enabling 10% AF-SBA-15 a higher efficiency for capturing acetaldehyde; hence, this sample showed better kinetic performance. However, as stated above, the pore size and pore volume of 10% AF-SBA-15 were already reduced comparative to 2.6% AF-SBA-15, and as adsorption progressed, the pores became blocked further by the products of the condensation reaction, as illustrated in Eq.(6-4). This significantly increases blocking effects in the sample with greater functionalisation, which eventually hinders access of acetaldehyde molecules to the reactive sites. So, even though 10% AF-SBA-15 has a greater number of reactive sites overall, only those sites at the pore entrance are accessible, resulting in a faster kinetic performance yet lower adsorption capacity than 2.6% AF-SBA-15.

It is notable that both AF-SBA-15 samples showed low adsorption capacities, which is an impractical aspect for use in the water treatment industry. As the results obtained for these samples suggested lack of accessibility to reactive sites is limiting to the adsorption capacity, it is reasonable to propose that materials with larger pores, such as macroporous resins may exhibit an increased capacity, where reactive site number is still significant. To test this hypothesis, a macroporous ion exchange resin (A830) with an acrylic matrix and complex amine functionalities was applied for the removal of acetaldehyde. Data for the kinetics of acetaldehyde sorption onto A830 are displayed in Figure 6.11, together with comparative data for AF-SBA-15 samples. The capacity of A830 is much greater than the as-prepared mesoporous silicas; although the rate constant was much reduced, which is possibly due to the low surface area and pore volume of the resin. Figure 6.12 shows the isotherm for acetaldehyde adsorption on A830 at 20 ^{o}C and the subsequent fit to the Langmuir equation, because the Langmuir equation

is more appropriate to be used to describe chemisorption. The maximum capacity of A830 was obtained at 441 mg g^{-1}, indicating that materials with similar properties to A830 could be promising candidates for acetaldehyde removal. Hence, it is proposed that a novel two-stage method consisting of an initial step to degrade metaldehyde into acetaldehyde, and a second stage to adsorb the acetaldehyde formed could be developed and operated subject to further optimisation.

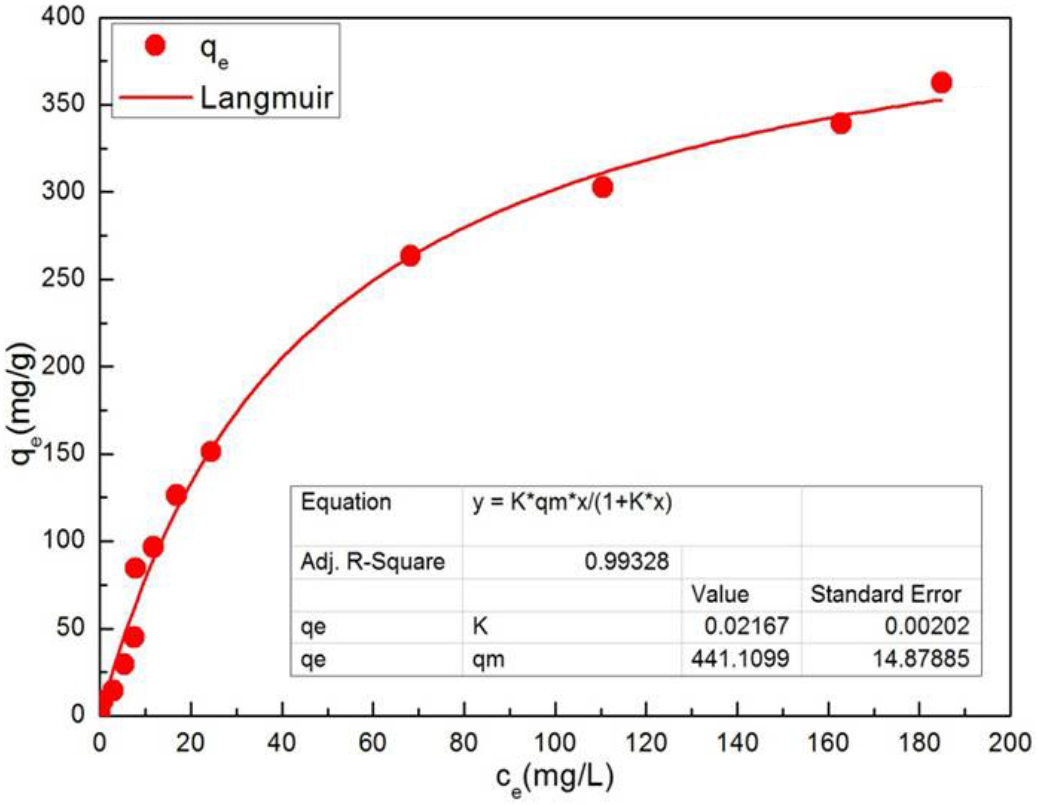

Figure 6.12 Isotherm of acetaldehyde sorption onto A830 at 20 °C and the fitting of experimental data to Langmuir equation

6.4 Conclusions

Well-ordered mesoporous sulfonic acid and amine functionalised SBA-15 has been synthesised via tri-block copolymer template reactions. Sulfonic acid functionalised SBA-15 showed excellent catalytic performance for the degradation of metaldehyde, with acetaldehyde as the only by-product. Kinetic studies showed that the rate of degradation is related to accessibility of metaldehyde molecules to the active sites present

within the pores of the catalyst; such that pore size and pore volume have a dramatic effect on kinetic performance. Degradation of metaldehyde was shown to produce stoichiometric quantities of acetaldehyde and amine functionalised SBA-15 was shown to be capable of chemically adsorbing acetaldehyde through surface condensation reactions, akin to vapour phase studies, indicating that high amine content would increase adsorption capacity. However, increasing amine content decreased both pore size and pore volume of the as-made silica samples, such that acetaldehyde molecules cannot access to the functional sites, which is exacerbated by the fact that the product of the surface condensation reaction blocks the pore entrances further. Application of a macroporous adsorbent with high amine content (A830), to reduce the influence of pore blockage, showed an improved performance compared to the amine functionalised mesoporous silica supporting the conclusion that pore blocking reduces capacity and suggesting routes to materials development. The combined results of metaldehyde degradation and acetaldehyde adsorption indicate that a dual-stage column method could achieve total removal of metaldehyde from drinking water, via catalytic depolymerisation of metaldehyde into acetaldehyde and subsequent chemical adsorption.

Chapter 7 Development and Optimization of a Novel Dual-Stage Method for Metaldehyde Removal from Water

7.1 Introduction

The investigation of sulfonic acid functionalised silica has demonstrated that it can efficiently degrade metaldehyde into acetaldehyde (Chapter 6). Acetaldehyde is a natural organic compound, which in practical cases, increases in concentration by ppb levels upon metaldehyde degradation will not cause any further pollution. However, future legislation may reduce permitted levels for acetaldehyde, hence, developing technologies should address any secondary pollution created during the application. Additional investigations have showed that amine functionalised ion-exchanger can chemically adsorb acetaldehyde for this purpose. Therefore, a dual-stage process was proposed at the end of the last Chapter. However, there are some obstructions which hinder the installation and evaluation of this novel dual-stage method. Initially, the massive production and commercialisation of the prepared silica samples are challenging and, most importantly, it would take time to commercialise such a product, especially obtaining regulatory permits for potable water. Moreover, the silica samples as-synthesised in Chapter 6 were in the form of very fine particles (<10 μm), which would cause tremendous pressure drop if used in fixed-bed columns. Therefore, the column proposed here was developed in cooperation with Purolite International, which is a world renowned polymeric material manufacturer specialising in water treatment media. Upon recommendations from this work, Purolite synthesised and supplied bespoke and already commercialised sulfonic acid functionalised polymeric resins, herein referred to as Macronets. Based on the outcomes of the work SA-SBA-15, a series of Macronets were synthesised with controlled porosity and ex-

tent of functionality so that the most suitable candidate material could be pinpointed. For optimisation, the following aspects of the samples were taken into consideration:

1) Macronet porosity, including the surface area, total pore volume, pore size distribution, *etc.*;
2) extent of functionalisation;
3) cost of manufacture.

Supplied with kilograms of sulfonic acid functionalised Macronets and amine functionalised ion-exchanger A830, it was possible to fabricate the dual-stage method for evaluation. Before undertaking bench-scale column tests, the detailed working mechanism and kinetic performance of the processes were investigated.

7.2 Experimental

7.2.1 Degradation of Metaldehyde and Chemisorption of Acetaldehyde

The Macronet samples were synthesised at Purolite® International, U.K. and are commercially available now. Six Macronet samples in total were prepared with different porosity textures and various acid capacities to optimize the desirable characteristics. They are divided into two categories: Macronet (MN) series and D code (DC) series. The MN series has three Macronets: MN500, MN501 and MN502. The DC series has three samples as well, including D5564, D5565 and D5566. The main difference between The MN and DC series is the sulfonic acid content. The acid capacities among MN series re very close (~2.72 mmol/g), while DC series are in the range of 2.88-3.34 mmol/g.

Textural characterisation was performed as outlined in Section 3.2.1, and the pore size distributions of Macronets were determined by mercury intrusion porosimetry, as outlined in Section 3.2.2. Quantification of extents of surface functionalisation was

performed using Boehm titration methods as described in Section 3.7. The concentration of metaldehyde and acetaldehyde in water samples were determined by GC and HPLC as described in Section 3.4.4 and 3.5.2).

The catalysis selectivity and activity of Macronets and acetaldehyde adsorption on A830 were performed as stated in Chapter 6.

7.2.2 Dual-Stage Column Tests

Performances of the dual-stage method were evaluated by rapid small scale column tests (RSSCTs) as depicted by Figure 7.1. 1 g of MN502 with mean particle size of 180 µm was packed in a small column (5 cm bed length × 8mm I.D.) acting as the heterogeneous catalyst. For treatment of acetaldehyde, 2g of A830 (5 cm bed length × 8mm I.D.) with the same particle size was packed in the second column. For comparison, a dual-column apparatus was fabricated using MN502 as catalyst and GAC as the adsorbent for acetaldehyde removal. All other parameters of the MN502/GAC column were the same as MN502/A830. Moreover, a third single column apparatus was setup , this time without using MN502 as catalyst, packing 2 g of GAC, with the same particle size, to remove metaldehyde as comparator to traditional treatment method. The flowrates for the three sets of apparatus were set at 7 mL/min resulting in Empty Bed Contact Times (EBCTs) of: column 1- 21.5 s and column 2 - 43s. The initial concentration of the feed solution was 2 mg/L and the effluents from each column were sampled and analysed by GC, to determine the concentration of metaldehyde, and HPLC, to determine the concentration of acetaldehyde.

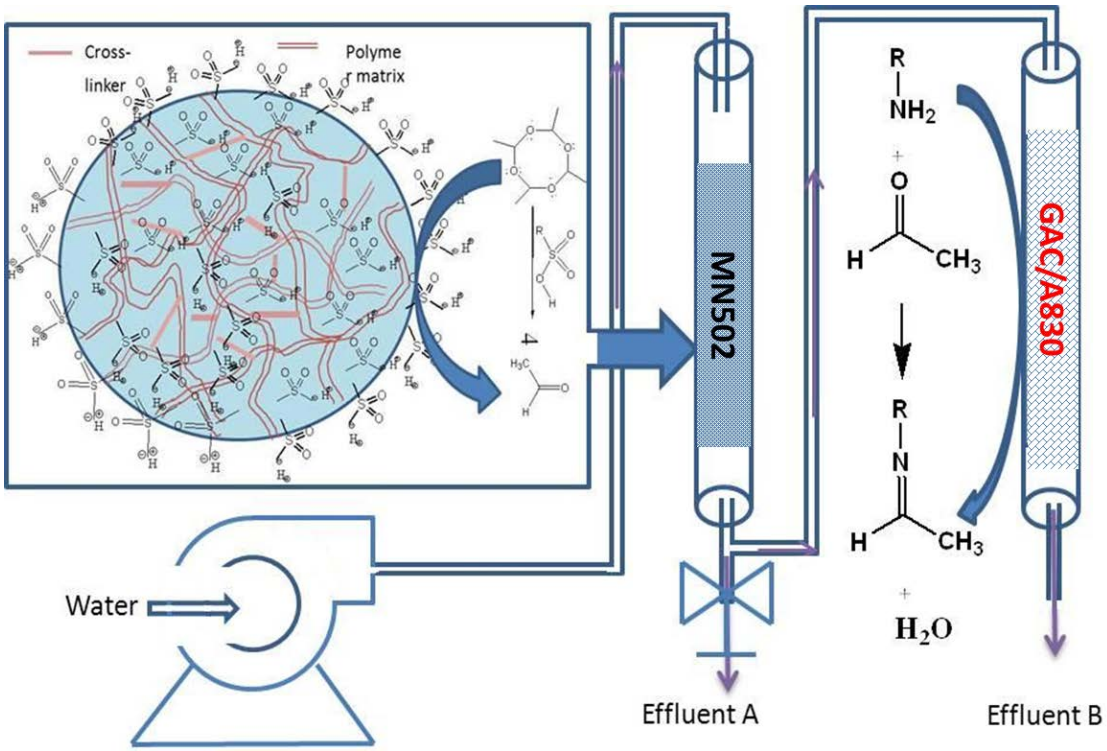

Figure 7.1 Schematic illustration of the setup of the novel dual-stage column tests

7.3 Results and Discussion

7.3.1 Characterisation of Materials

Table 7.1 Summary of the textural properties and acid capacities of the Macronet samples determined, as determined by nitrogen sorption, mercury porosimetry and Boehm titration, respectively.

I.D	Series	S_{BET} (m^2/g)	S_{Micro}(m^2/g)	$S_{Meso-Macro}$ (m^2/g)	V_{Total} (cm^3/g)	V_{Micro} (cm^3/g)	$V_{Meso-Macro}$(cm^3/g)	Acid Capacity (mmol/g)
MN500		331.8±7.92	233.5	98.30	0.2596	0.1206	0.1390	2.771
MN500DR	MN	401.8±9.79	293.2	108.6	0.3095	0.1514	0.1581	2.639
MN502		355.7±8.35	242.1	113.6	0.3281	0.1248	0.2033	2.737
D5564		22.34±0.39	5.162	17.18	0.1325	0.0026	0.1299	2.881
D5565	DC	21.15±0.25	4.905	16.24	0.0823	0.0025	0.0798	3.045
D5566		2.638±0.02	0.154	2.484	0.0066	0.0004	0.0062	3.342

S_{Micro}: Micropore surface area; $S_{Meso-Macro}$:Mesopore and macropore surface area; V_{Micro}: Micropore volume;

Table 7.1 summarises the textural properties and acid capacities of the Macronet samples and Figure 7.2 shows the pore size distributions of these samples, as determined by mercury intrusion. The introduction of sulfonic acid destroys the porosity of the samples; the un-functionalised matrix of these Macronets has a total pore volume of 0.667 mL/g and a surface area of 950 m^2/g, slightly functionalising the matrix (MN series) decreases both the surface area and pore volume substantially (surface areas range from 330-400 m^2/g). Further functionalising (DC series) caused additional decrease of the surface area (2.6-22 m^2/g) and a similar trend in pore volume.

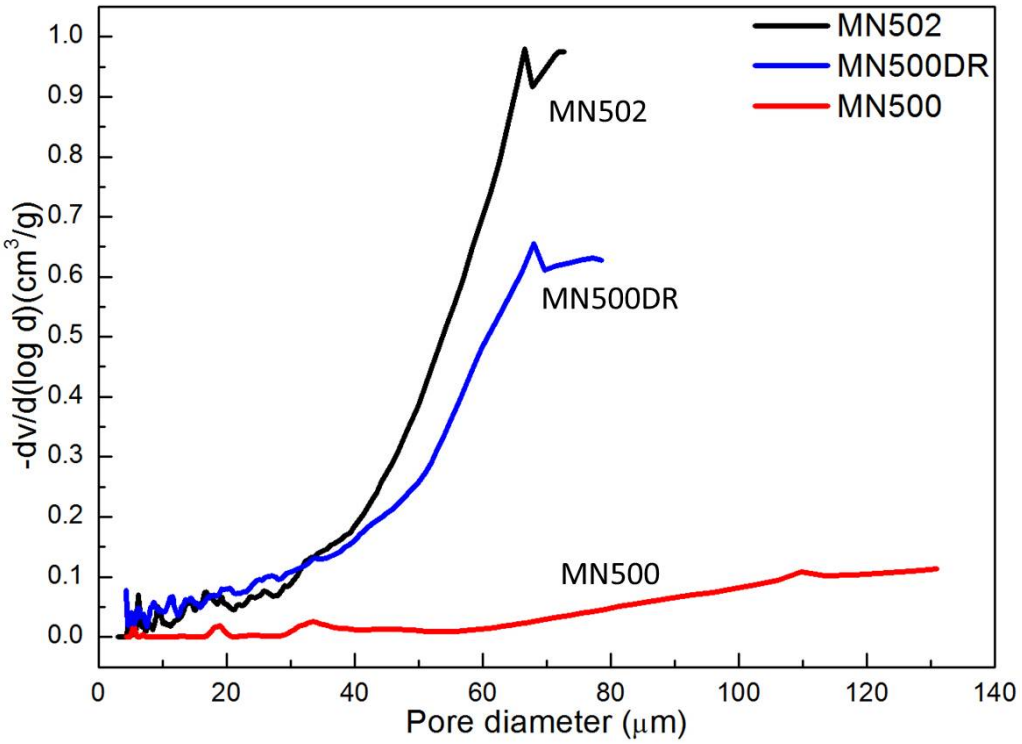

Figure 7.2 Pore size distributions of MN series Macronets

It is also important to consider the trend in pore size, since metaldehyde molecules tend to assemble via hydrogen bonding to form macro molecular structures, the surface area and pore volume contributed by meso- and macropore are the sites that will facilitate diffusion. Hence, the percentage of meso and macropore volume ($V_{Meso\text{-}Macro}$) compared to the total pore volume (V_{Total}) should be calculated. It is noted

that among the MN series, MN502 has the largest pore volume and meso- and macropore volume percentage, reaching 0.3281 mL/g and 62%, respectively. While for MN500DR, they are only 0.3095 mL/g and 51%, even though it has the highest surface area. In the case of MN500, it has the lowest total pore volume (0.2596 mL/g), meso- and macropore volume percentage (56%) and surface area (331 m^2/g).

7.3.2 Catalysis Selectivity Study

Sulfonic acid functionalised silica (SA-SBA-15) was demonstrated to degrade metaldehyde into acetaldehyde efficiently and completely. Therefore, in this Chapter, NMR tests were conducted to confirm that sulfonic acid functionalised polymeric resins have the same performance. Similar results were observed as in the silica study with peaks corresponding to metaldehyde (d at 1.4 ppm, q at 5.4 ppm) decreasing to almost negligible levels as reaction time elapsed, and only characteristic peaks for acetaldehyde (d at 2.2 ppm, s at 9.6 ppm), and no other intermediates or by-products, observed (Figure 7.3).

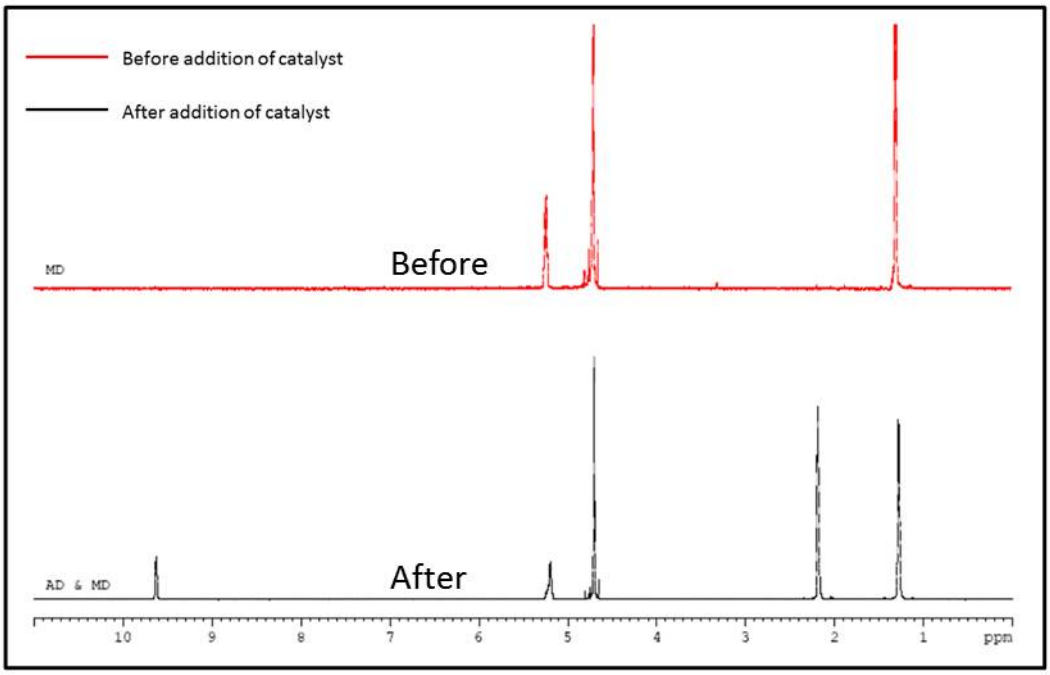

Figure 7.3 NMR spectra of metaldehyde (in D2O) before and after addition of Macronet MN502

Therefore, the mechanism for degradation of metaldehyde by Macronets is the same as in the case of SA-SBA-15 with the Macronet acting as a heterogeneous catalyst, effectively depolymerising metaldehyde into acetaldehyde (as presented in Chapter 6).

7.3.4 Catalysis Kinetic Study

It is also important to consider kinetic performance of the catalyst for heterogeneous catalytic reactions; hence, comparative kinetic experiments were conducted. The depolymerisation reaction can be described by the following kinetic equations:

$$C_8H_{16}O_4 \xrightarrow{RSO_3H} 4\,CH_3CHO \qquad \textbf{Eq. (7-1)}$$

$$r = -\frac{d[MD]}{dt} = k[MD][RSO_3H] \qquad \textbf{Eq. (7-2)}$$

Since the concentration of sulfonic acid is constant and in significant excess, the rate of the reaction is only dependent on the concentration of metaldehyde and a first order rate equation can be employed.

$$\frac{c_t}{c_0} = e^{-kt} \qquad \textbf{Eq. (7-3)}$$

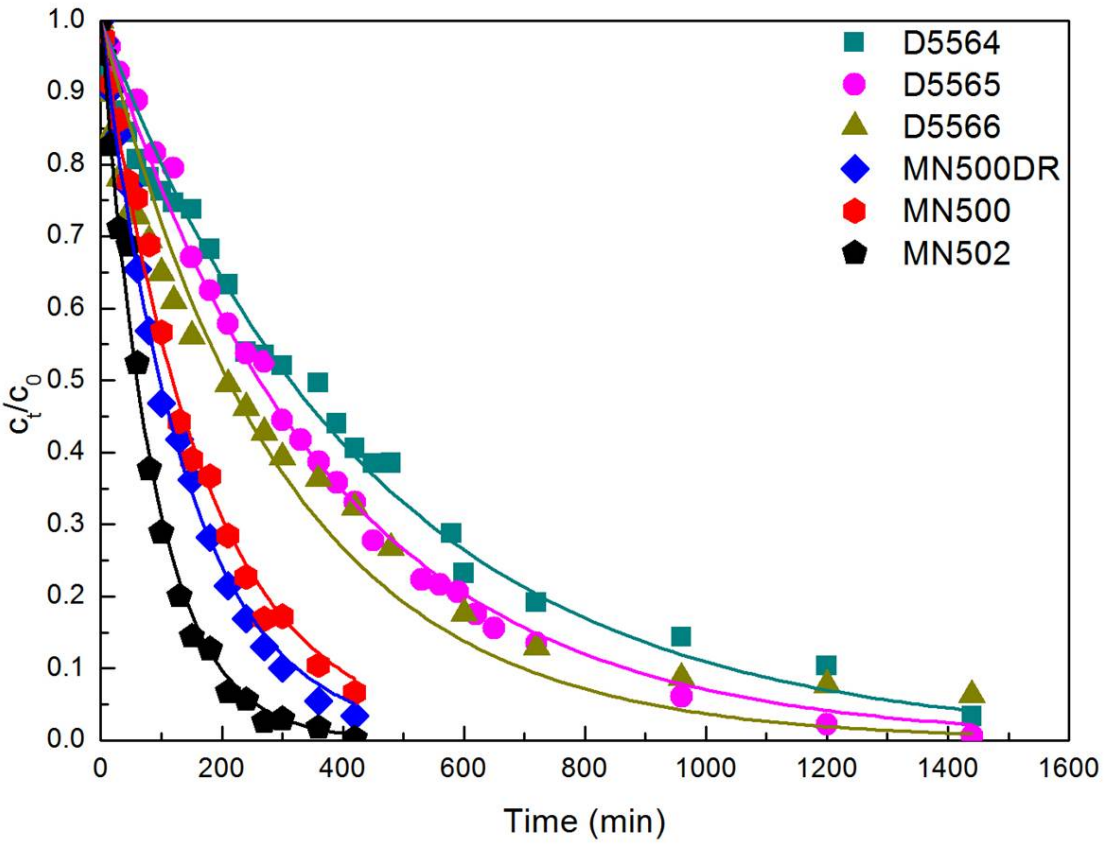

Figure 7.4 Kinetics of metaldehyde degradation by different catalysts at 22 °C and fits to first order rate equations (solid lines)

Figure 7.4 displays the concentration degradation of metaldehyde as a function of time by the catalytic action of different Macronets under the same experimental conditions, and the fits obtained using a first order rate equation. It can be seen that the three MN samples exhibited much faster kinetics than the three DC samples; due to the fact that the MN samples have much higher surface areas than the DC samples, which increases the permeability of the sample, facilitating the path of metaldehyde molecules to the active sites. Table 7.2 displays the kinetic parameters calculated from the fitting of experimental data to first order kinetic models, showing that the rate constants obtained for MN samples were much higher than the DC samples, indicating high acid content is not necessary to improve the rate constant. For a heterogeneous catalysis process, the diffusion step is always the rate-limiting step and the reaction step is, by comparison, very fast. The high acid capacity in DC samples significantly decreases

the porosity, resulting in the increase of the diffusive resistance of metaldehyde to the active sites. Therefore, the catalysis rates are quite slow even though the densities of active sites are high.

Table 7.2 Parameters obtained for fitting of experimental data to first order equation

Macronets	MN500	MN500DR	MN502			D5564	D5565	D5566
Series		MN	MN			DC		
Temp (^{o}C)	22	22	22	25	30	22	22	22
k ($\times10^{-3}$min^{-1})	5.86	7.11	11.6	16.3	24.8	2.22	2.65	3.31
R^2	0.99	0.98	0.99	0.99	0.99	0.98	0.99	0.93

It is also noted that for the MN samples, the best kinetic performance was observed for MN502 which possesses the greatest pore volume. MN500DR has the highest surface area, while the rate constant was only 7.11×10^{-3} min^{-1}, approximately a half of that of MN502 (1.16×10^{-2} min^{-1}). By examining the kinetics of the MN samples, pore volume, it can be seen that especially meso and macropore volume is more important than surface area. Figure 7.5 presents the correlations between rate constant and surface area, total pore volume and meso- and macropore volume among the MN samples. It can be seen that the rate constant correlates well with meso- and macropore volume, with the larger pores playing a significant role in the catalytic process since metaldehyde molecules hydrogen bonded into larger macromolecular structures. As a result of the extended molecular network of metaldehyde, the micropores in these resins are not desirable for metaldehyde degradation due to their size, which explains why GAC had such poor performance for metaldehyde removal, as the majority of the porosity present is microporous.

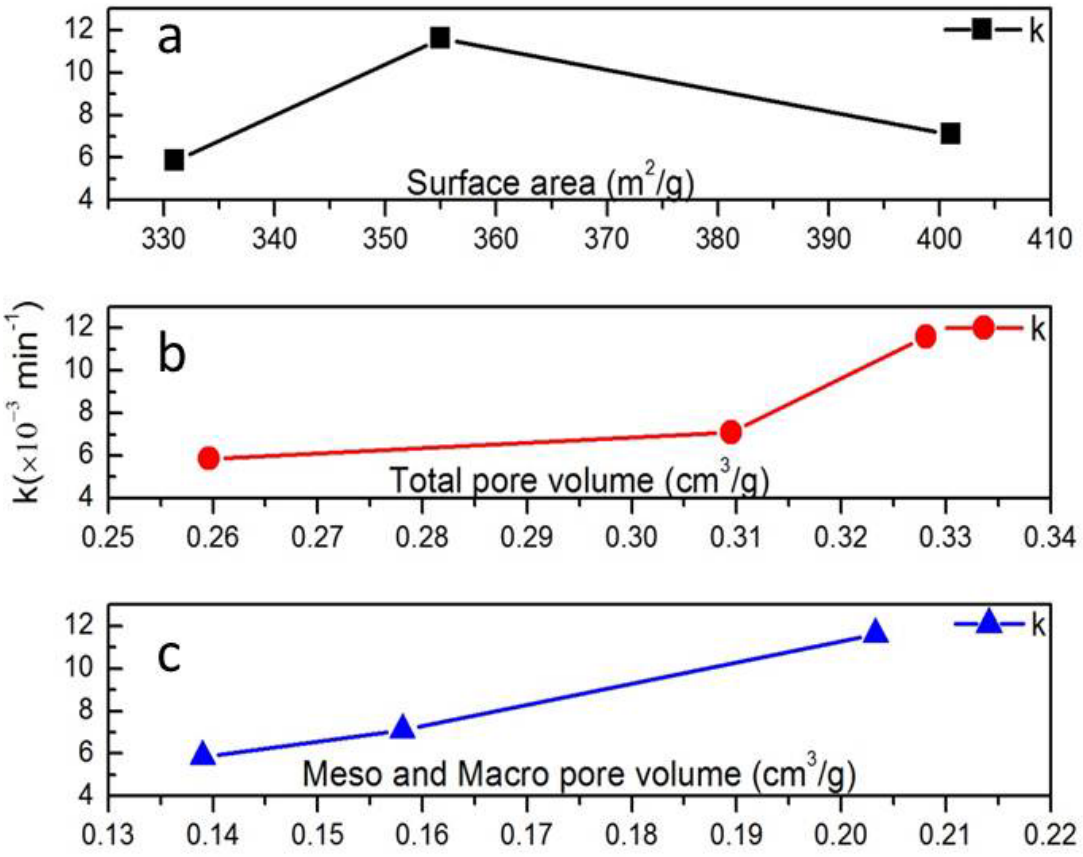

Figure 7.5 Relationships between rate constant and (a) surface area, (b) total pore volume and (c) meso- and macropore volume for MN samples

The Arrhenius equation (Eq.7-4) states the temperature dependence of associated rate constants, from which the activation energy of a catalytic process (E_a, kJ mol^{-1}) can be estimated.

$$\boldsymbol{ln}\mathbf{k} = \boldsymbol{lnA} - \frac{\boldsymbol{E_a}}{\boldsymbol{RT}} \qquad \textbf{Eq. (7-4)}$$

Figure 7.6 presents the catalytic kinetics for MN502 at different temperatures and the rate constants for each temperature, are shown in Table 7.2, having been calculated by fitting the data to first order rate equations. The gradient of a plot ln*k* against 1/T determines that the activation energy of metaldehyde sorption on MN502 to be 75.4 kJ/mol, hence, the process is endothermic.

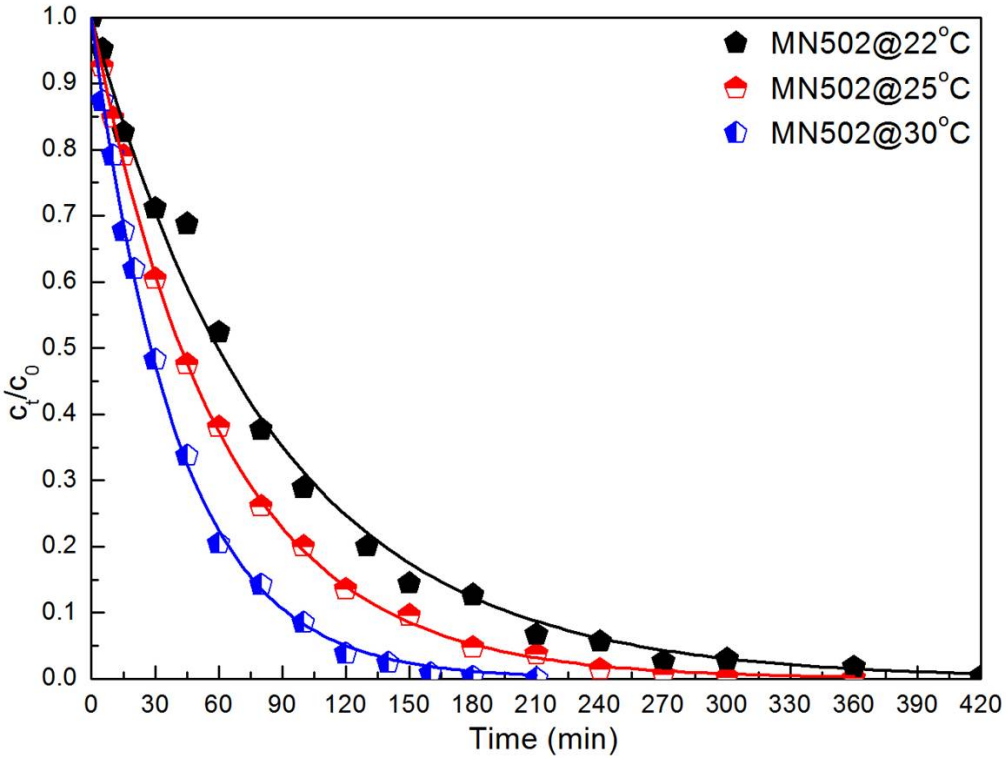

Figure 7.6 Temperature dependence of catalytic performance of MN502 and fits of experimental data to first order equations

7.3.5 Effect of Inorganic Ions on Catalytic Performance

It is generally recognised that the presence of inorganic ions could cause significant effect on adsorption and catalytic processes in water treatment. The effect of Ca^{2+} on the degradation of metaldehyde reaction was investigated since Ca^{2+} is the major inorganic ion, especially in U.K. regions that experience high levels of metaldehyde. **Figure 7.7** shows the effect of different concentrations of Ca^{2+} on the kinetics and capacities of the depolymerisation reaction. It is evident that the presence of calcium ions compromised both the reaction rate and capacity. However, the effect plateaued with increasing concentration ratio of Ca^{2+}/metaldehyde as high as 100 times.

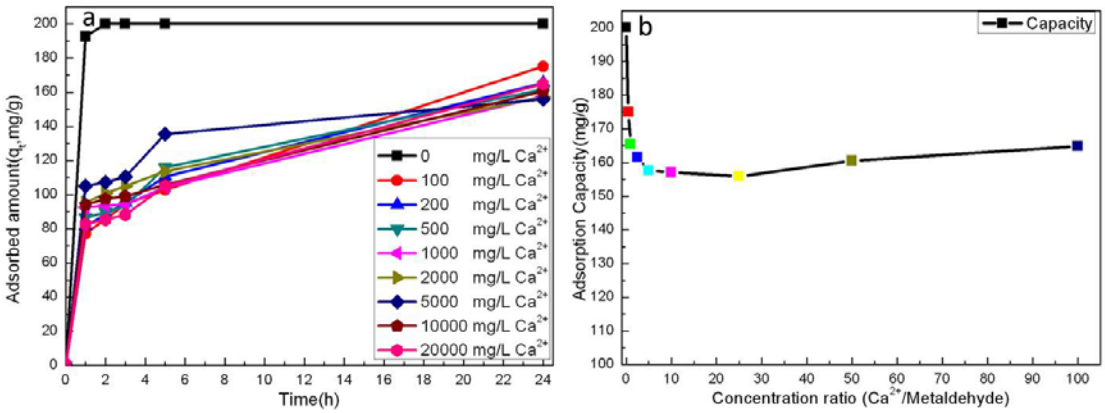

Figure 7.7 (a) Competing effects of Ca^{2+} on metaldehyde degradation kinetic performance by MN502; (b) Degradation capacities of metaldehyde in the presence of Ca^{2+} at 24h.

The observed experimental results demonstrated that the presence of inorganic ions decreased the kinetics and capacities of the material, which can be explained by considering the different working mechanisms of sulfonic acid group interactions with metaldehyde and inorganic ions. For inorganic ion remediation processes, the working mechanism is ion-exchange, while for metaldehyde removal; the process is a catalytic reaction (Figure 7.8). As is well recognized, every ion-exchange reaction is reversible and the equilibrium constant is highly dependent on the ion pairs. In industrial water treatment processes, sodium forms of resins are normally used to soften water instead of using the proton form as the bonding energy between RSO_3^- and H^+ is much stronger than that between RSO_3^- and Na^+, such that breaking RSO_3-H is more difficult than breaking RSO_3-Na. Hence, regards the ion-exchange process between MN502 and Ca^{2+}, the rate constant is expected to be lower, which means that even at equilibrium significant amount of RSO_3H remain. As long as some RSO_3H is available, it will catalysse the degradation of metaldehyde, hence even at high ratios of Ca^{2+}/metaldehyde, the performance is still good. Using these results as a basis, it is possible to predict that for implemented fixed-bed columns packed with Macronets, inorganic ions initially will be adsorbed by the column and metaldehyde degraded, the bed will then reach capacity for the inorganic ion and unable to adsorb further Ca^{2+}

ions but will still be able to degrade metaldehyde, as the remaining RSO_3H will degrade metaldehyde albeit with slower kinetics.

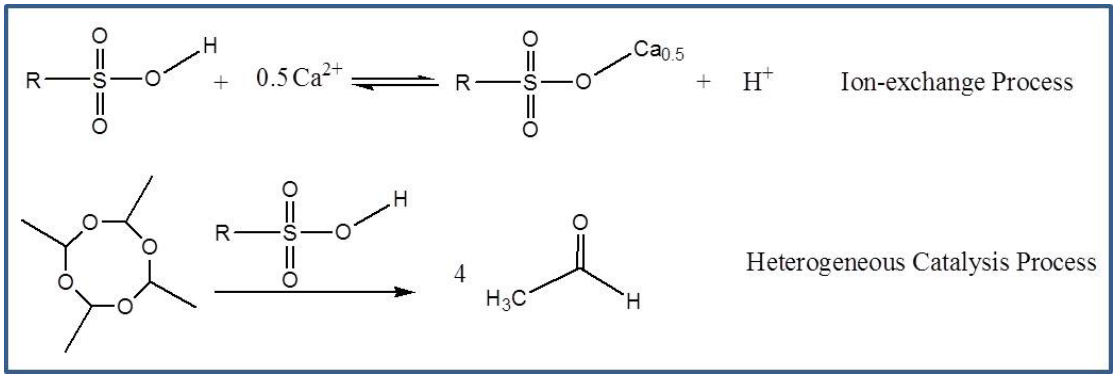

Figure 7.8 Working mechanism of sulfonic acid groups removing inorganic ions by ion-exchange and metaldehyde by heterogeneous catalysis

7.3.6 Removal of Acetaldehyde by Ion-Exchanger A830

It has been previously described that aldehydes can be removed by primary amines by the following condensation reaction (Hayashi, Kumita et al. 2005; Ewlad-Ahmed, Morris et al. 2012):

$$\boldsymbol{R - NH_2 + CH_3CHO \xrightarrow{yields} CH_3CH = N - R + H_2O} \qquad \textbf{Eq. (7-5)}$$

Therefore, in this work, a special amine functionalised resin with acrylic matrix has been applied to remove acetaldehyde produced in the first step of the process. Figure 7.9 shows the kinetic studies of acetaldehyde adsorption onto A830 and GAC, included for comparison. It is clear that the kinetics of acetaldehyde adsorption onto A830 is much faster than on GAC, with a pseudo-second order rate constant of 0.170 g mg^{-1} min^{-1}. Moreover, it is evident that the experimental data were better described by a pseudo-second order equation rather than a pseudo-first order equation. With regards to the adsorption of acetaldehyde onto GAC, the performance was quite poor, which is ascribed to the weak interactions between GAC and acetaldehyde.

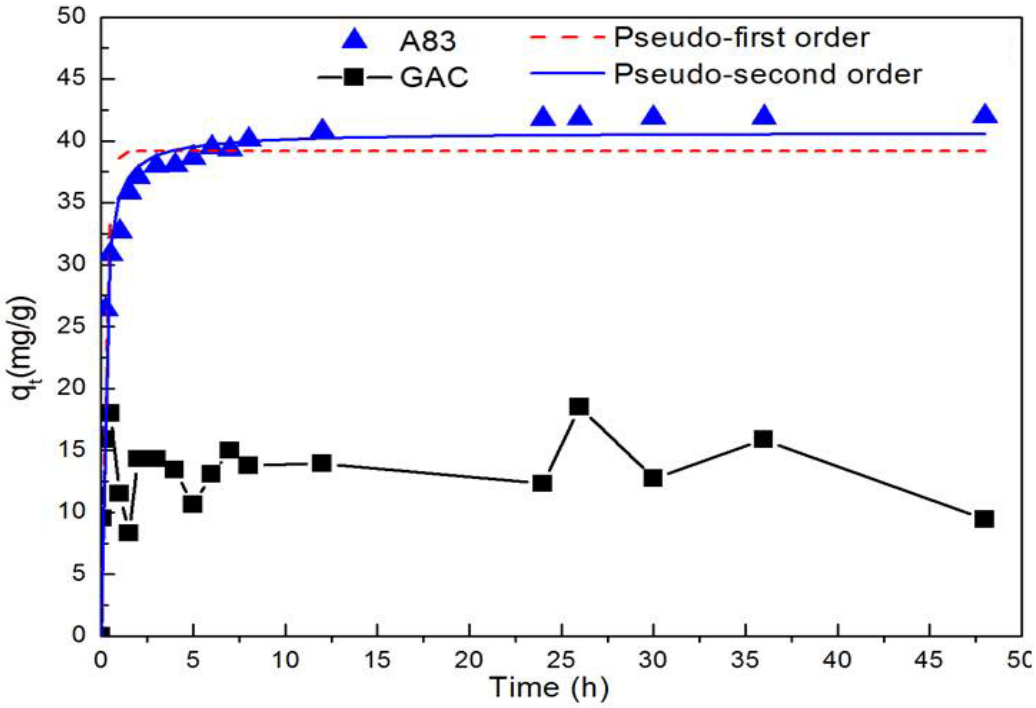

Figure 7.9 The adsorption kinetics of acetaldehyde onto A830 and GAC at 20 °C

Since the adsorption performance of A830 is much better than that of GAC, the isotherm of acetaldehyde sorption onto A830 was investigated. Figure 7.10 shows the isotherm obtained at 20 °C and the theoretical curve generated by the Langmuir equation. The Langmuir equation provides a good fit, and assumes monolayer adsorption, hence it is suited to this work as the mechanism requires acetaldehyde molecules to diffuse to the adsorbent surface and react with surface functional groups through the condensation reaction shown above. It is widely used to describe sorption of solutes onto heterogeneous surfaces which involves surface functionalities and adsorbate-adsorbent interactions, which is presented as follow:

$$q_e = q_m K_L C_e / (1 + K_L C_e) \qquad \textbf{Eq. (7-6)}$$

The fitting of the experimental data showed that the maximum capacity (q_m, mg/g) was as high as 441mg/g. The excellent fit of the experimental data to the Langmuir equation is in a good agreement with the proposed mechanism. The relatively high sorption capacity indicates A830 is good candidate to adsorb acetaldehyde.

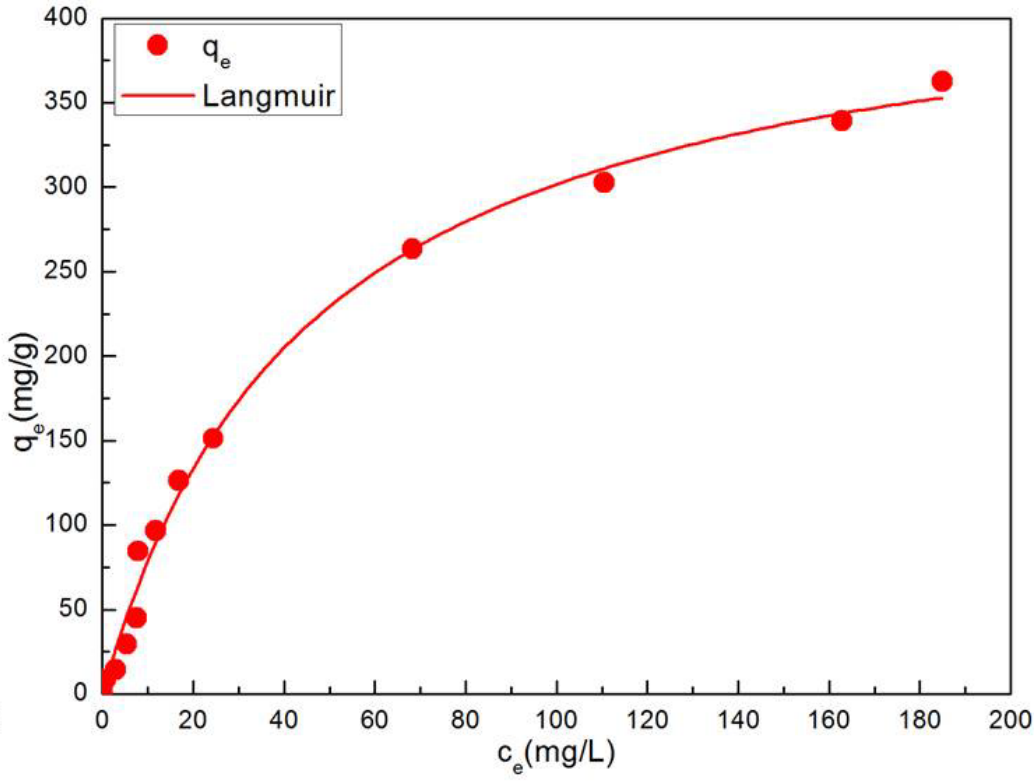

Figure 7.10 Isotherm of acetaldehyde sorption onto A830 at 20 °C and the fit of experimental data to the Langmuir equation.

7.3.7 Dual-Stage Column Tests-Synthetic Water Samples

The batch experiments showed that metaldehyde can be efficiently degraded into acetaldehyde by sulfonic acid and acetaldehyde can be removed by amine functionalised ion exchange resins. Therefore, a dual-column Fixed-Bed Adsorber (FBA) was fabricated with the first column packed with catalyst MN502 and the second one packed with adsorbent A830 or GAC, for comparison. For comparison, there three column tests were conducted: the first a single-column setup, where the column was packed with GAC; the other two arrangements were dual-column setups, with the same first column packed with Macronet MN502, the only difference between these two setups was the material packed in the second column, either A830 or GAC. The operating conditions and parameters were kept the same and are detailed in the experimental section.

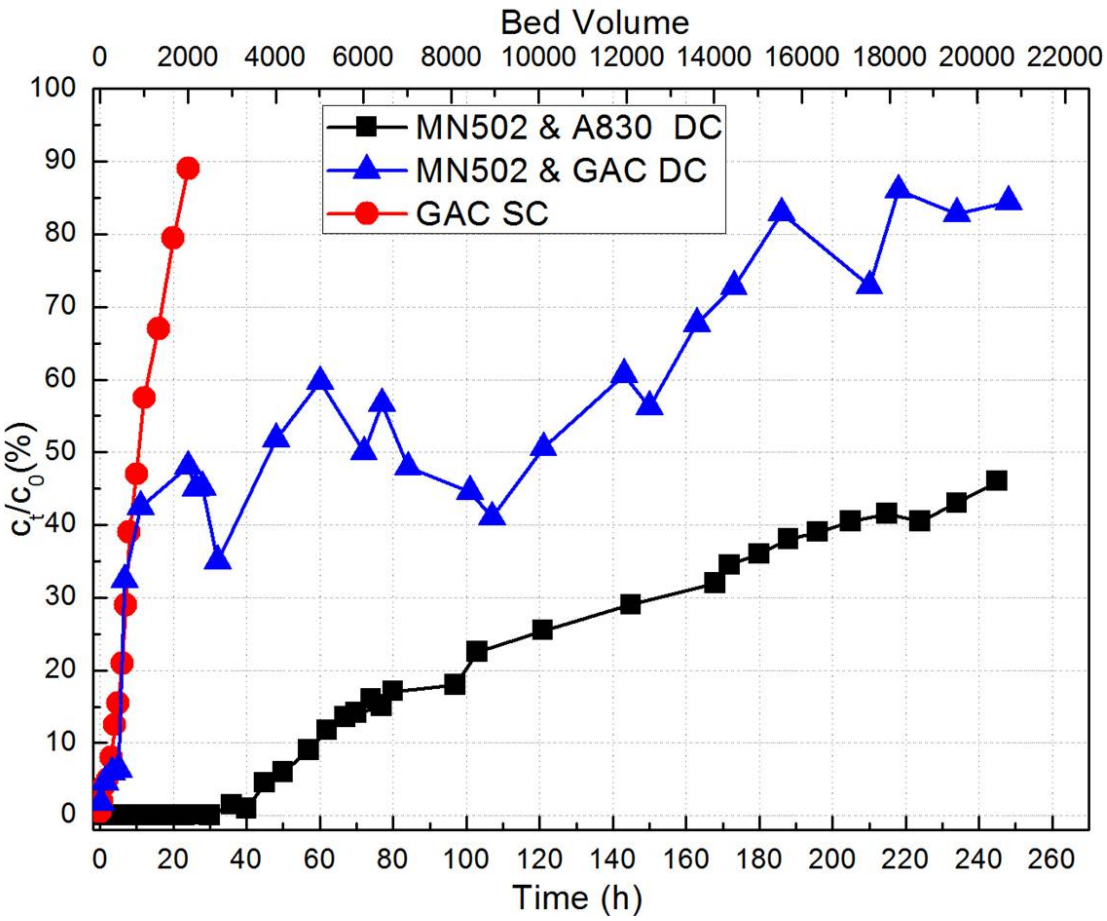

Figure 7.11 The breakthrough curves of the dual-column adsorber and single-column adsorber

Figure 7.11 demonstrates the breakthrough curves of the three column tests. For the single column setup, it can be seen that the bed was exhausted after 24 h of operating. This agrees with the results obtained from application of GAC in the water treatment industry, and is due to the low adsorption capacity and high leaching tendency of metaldehyde adsorption onto GAC. The dual-columns showed, no metaldehyde detected over the whole running time, indicating good degradation performance of MN502. In the case of GAC used to remove acetaldehyde, the breakthrough of the GAC bed was quickly observed, suggesting GAC is not appropriate to adsorb acetaldehyde, and lending weight to the development of alternative methods for its removal should legislation require a reduction in acetaldehyde concentration. The dual-column

setup consisting of MN502 and A830 showed excellent removal performance. It took 60 h (5,000 bed volumes (BV)) to reach the 10% of c_t/c_0 threshold. In this experiment, the initial concentration of metaldehyde was 2 ppm which is 2,000 times higher than the maximum concentration (1 ppb) detected in water catchments. Therefore, in practical cases, the breakthrough point of the dual-column should be expected to be much better than 5,000 BV, hence, this dual-column configuration showed very promising results. The bed completely removed acetaldehyde for the first 3,000 BV of water before breakthrough was detected. The bed was not exhausted after 10 d running and the concentration ratio was only reach 40%. The column tests are in good agreement with the batch experiment results. The dual-column test results showed robust performance, as expected, and the method developed here is of practical interest for the removal of metaldehyde from drinking water supplies.

7.3.8 Feasibility Tests of the Dual-Stage Method using Surface Water Supplied by Scottish Water

The feasibility of the developed and optimised dual-stage method was further tested by operating the system with a real water sample. The experimental setup and configuration were unchanged from those used to test the synthetic water samples. 20 L of surface water was supplied by Scottish Water, collected after the filtration operating unit in a water treatment works, hence, untreated by activated carbon fixed-beds or by ozone and chlorine. This provided a representative sample of influent water that would be treated using the developed technology if applied in a water treatment works. Due to instrumentation limits and the specific focus of the research presented here, the water quality was not characterised in detail. Previous studies have shown that inorganic ions are the main competing species for reaction with the Macronet used here, hence, the concentration levels of inorganic ions present in the supplied water sample were measured by Inductively Coupled Plasma with Optical Emission Spectrometry

(ICP-OES)[④]. The concentrations of the inorganic ions determined by ICP-OES are summarised in Table 7.3.

Table 7.3 Initial concentrations of inorganic ions of surface water sample supplied by Scottish Water

Ion	Ca	Na	Mg	Zn	P	Cd	Cr	Cu	Fe	Mn	Ni	Pb
Conc. µg/L	2835	2887	1135	7	4.7	<0.2	<1	<11	<13	<2	<1	<2.8

The intrinsic metaldehyde level in this water sample was negligible, so the water was contaminated within the laboratory by the addition of a known quantity of metaldehyde. The contamination level used was 1ppb, i.e. the highest concentration that has been reported in U.K. water supplies.

The concentration of metaldehyde was determined by GC-MS, with SPE used to prepare samples. Typically, 250 mL of water sample was passed through the SPE cartridge and the dried cartridge eluted by 1-2 mL of dichloromethane (DCM). The resulting metaldehyde/DCM solution was vapourised to 1 mL and analysed by GC-MS. The detailed experimental procedure is presented in Section 3.4.5. The operating parameters of the dual-column reactor are as follows:

- Empty Bed Contact Time (EBCT): 2.5 min;
- Bed length (L): 10 cm (~2 g of material packed);
- Mean particle size (d_p): 400 µm;
- Column I.D.: 8 mm;
- Flow rate: 2 mL/min;
- Bed Volume (B.V.): 5.024 mL;
- Treatability: 24 BV/h
- Water treated: 19 L=3782 BV

[④] ICP-OES measurements were performed by the Scottish Environmental Technology Network (SETN), University of Strathclyde. Website: www.setn.org.uk.

Samples were taken at t = 0 and every 12 hours thereafter with 14 samples taken in total. The samples were named as SW01-SW14, where SW01 is the initial contaminated water sample without treatment.

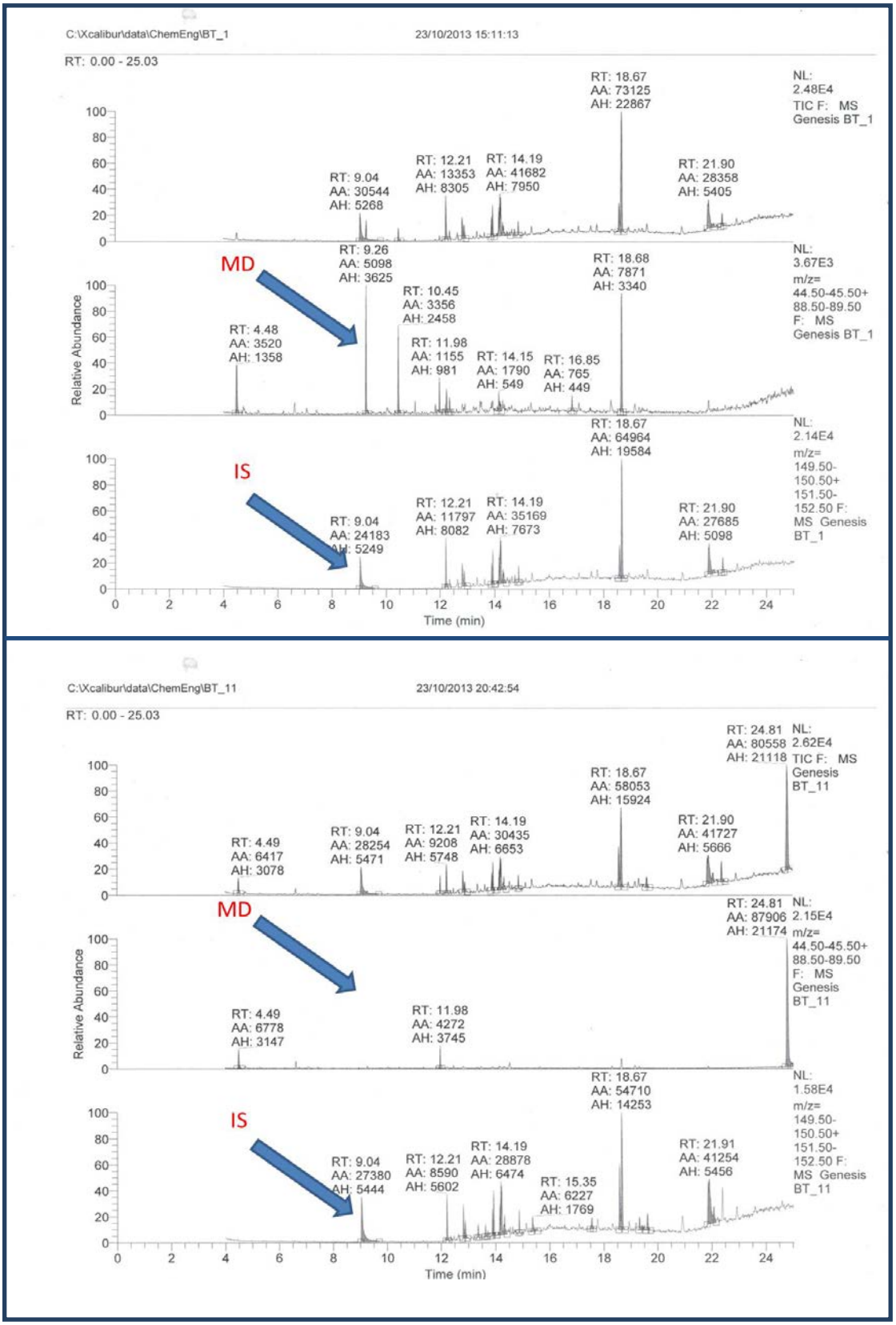

Figure 7.12 GC-MS chromatographs of the initial contaminated water sample (top), and a typical treated water sample (bottom)

As shown in Figure 7.12 (top), the retention time of metaldehyde in the GC-MS arrangement used was 9.26 min and the internal standard (1, 4-dichorobenzene-d_4) was 9.04 min. An internal standard quantification method was used and the detection limit was 0.001 ppb. The initial concentration of metaldehyde determined by GC-MS was 1.1 ppb. Metaldehyde was not detected for all samples treated using the dual-column system; Figure 7.12 (bottom) indicates metaldehyde was completely degraded and the trend with treatment volume is shown in Figure 7.13. Since ppb levels of acetaldehyde are acceptable in U.K. water supplies and should not cause any issue, coupled with the fact that the detection limit of the HPLC method employed in this work is 10 ppb level, concentrations of acetaldehyde were not determined for this part of the study.

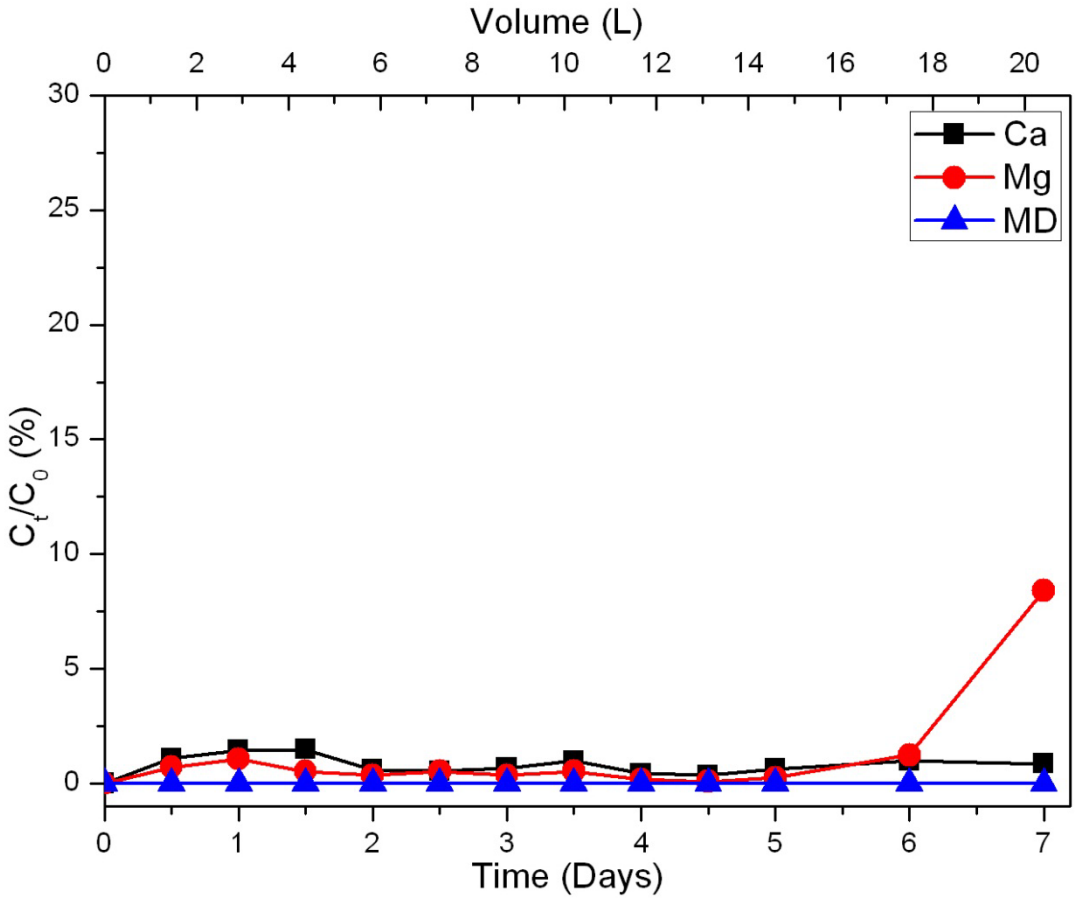

Figure 7.13 The partial breakthrough curve of Ca^{2+}, Mg^{2+} and metaldehyde.

Table 7.4 Concentration evolution of inorganic ions as a function of time (12 hr per sample).

Ions	SW01	SW02	SW03	SW04	SW05	SW06	SW07	SW08	SW09	SW10	SW11	SW12	SW13	SW14
Ca	2.835	0.009	0.031	0.041	0.042	0.017	0.015	0.019	0.028	0.012	0.010	0.018	0.028	0.024
Cr	<0.001	<0.001	<0.001	<0.001	<0.001	<0.001	<0.001	<0.001	<0.001	<0.001	<0.001	<0.001	<0.001	<0.001
Cu	<0.011	<0.011	<0.011	<0.011	<0.011	0.030	0.025	0.012	<0.011	<0.011	<0.011	<0.011	<0.011	<0.011
Fe	<0.013	<0.013	<0.013	<0.013	<0.013	<0.013	<0.013	<0.013	<0.013	<0.013	<0.013	<0.013	<0.013	<0.013
Mg	1.135	0.001	0.008	0.012	0.006	0.004	0.006	0.004	0.006	0.002	0.001	0.003	0.014	0.099
Mn	<0.002	<0.002	<0.002	<0.002	<0.002	<0.002	<0.002	<0.002	<0.002	<0.002	<0.002	<0.002	<0.002	<0.002
Na	2.887	0.012	0.026	0.182	<0.026	<0.026	<0.026	0.259	1.342	3.208	4.259	4.912	5.376	5.218
Ni	<0.001	<0.001	<0.001	<0.001	<0.001	<0.001	<0.001	<0.001	<0.001	<0.001	<0.001	<0.001	<0.001	<0.001
P	0.0047	0.0023	<0.0023	<0.0023	<0.0023	<0.0023	<0.0023	<0.0023	<0.0023	<0.0023	<0.0023	<0.0023	<0.0023	<0.0023
Pb	<0.0028	0.0029	0.3700	0.1253	0.0279	0.0513	0.0563	0.0364	0.0315	0.0199	0.0203	0.0147	0.0071	0.0046

Table 7.4 displays the evolution of inorganic ions as a function of time (or treated bed volume). It is evident that the concentration level of Ca^{2+} and Mg^{2+} decreased significantly. More than 95% of Ca^{2+} and Mg^{2+} were removed by the ion-exchange process as shown in Figure 7.8, confirming that inorganics do indeed compete with metaldehyde for reaction with the sulfonic acid functionalities on the Macronet used. However, as discussed previously, the removal mechanisms are completely different for these two processes and the performance of metaldehyde removal is only partially affected by the removal of inorganic ions by the sorbent. Even though the bed is exhausted in terms of removing inorganic ions, the performance of metaldehyde removal is still high. It is notable that Na^{+} was completely removed at the mid-point of the treatment studied, before a significant increase in concentration was observed, exceeding the initial concentration. This is caused by the fact that adsorbed and inherent Na^{+} will be exchanged, out of the resin, by divalent ions (Eq. 7-7), such as Ca^{2+} and Mg^{2+}:

$$RSO_3Na + Ca^{2+} \overset{liquid\ phase}{\longleftrightarrow} RSO_3Ca_{0.5} + Na^{+} \qquad \textbf{Eq. (7-7)}$$

As a consequence, sodium ions are initially adsorbed by the Macronet, resulting in almost complete removal before exchange with other inorganics, i.e. divalent ions, causes the adsorbed sodium and that already present within the Macronet to be desorbed.

In summary, the real surface water tests confirmed the proposed working mechanisms, while demonstrating that the developed method is of practical interest and a promising candidate for application in water treatment works.

7.4 Conclusions

Efficacious metaldehyde removal was achieved by the application of a combination of macroporous sulfonic functionalised Macronet as catalyst and amine functionalised ion-exchange resin as adsorbent. The heterogeneous catalyst selectivity test

confirmed that metaldehyde was efficiently degraded and acetaldehyde is the only product. Kinetic studies revealed that the rate of metaldehyde degradation is determined by the diffusion step. A high extent of functionality is not necessarily required to obtain good catalytic performance since the introduction of functional groups compromises the porosity significantly. The kinetic study also revealed that the rate is closely related to the total pore volume, especially to the meso and macro pore volume. Macronet sample MN502, with considerable surface area and large pore size and volume showed the best kinetic performance. The fast kinetics are related to the effective accessibility of metaldehyde molecules to the sulfonic acid groups present in the samples. Competing ion tests showed that the presence of inorganic ions (Ca^{2+}) decreased the performance to some degree, while the catalytic performance maintained a good level even with the Ca^{2+} concentration 100 times that of metaldehyde. This limited influence of inorganic ions was observed as a result of the interaction between sulfonic acid groups and Ca^{2+} being an ion-exchange process while that between sulfonic acid groups and metaldehyde is a heterogeneous catalytic process. The kinetic and isothermal studies of acetaldehyde onto resin A830 demonstrated that the only by-product, acetaldehyde, can be effectively removed. The breakthrough curve of the dual-column study confirmed the effective degradation of metaldehyde by MN502 and the complete removal of acetaldehyde by the second bed packed with ion exchange resin A830. The results of the real surface water tests confirmed the proposed mechanisms and indicate that the developed method is also effective in treating actual water samples. The method developed in this work is very promising since it can be used in conjunction with the existing infrastructure in U.K. water treatment works by only adding MN502 packed beds into their process; making the process cost-effective and easy to apply.

Chapter 8 Conclusions and Future Work

8.1 Conclusions

Contamination of U.K. water supplies by metaldehyde has attracted increasing interest in recent years. Despite the measures taken by different parties, there is still no effective solution to address this issue. Proposed advanced oxidation processes have demonstrated some degradation performance but costs are prohibitive and by-product issues (Autin, Hart et al. 2012; Autin, Hart et al. 2013) are yet to be fully determined, and may impede practical application at the large scale. Therefore, novel materials and/or methods are required to address this issue.

A detailed investigation into metaldehyde adsorption by Activated Carbons (ACs) was performed, using three different ACs, to understand why this current method of treatment fails to remove metaldehyde. The results showed that due to the low adsorption capacity, the adsorptive bed exhausts only after a few weeks of running; additionally, the high leaching tendency exacerbates the inefficiency of this method, as adsorbed metaldehyde easily desorbs from ACs, resulting in the same scenario as no adsorption at all. Both the low adsorption capacity and high leaching tendency are related to the adsorption mechanism, which is due to the low level of functionalization that leads to weak van der Waals forces between the GAC and metaldehyde. Hence, novel materials with embedded functionalities, which can degrade metaldehyde, were developed.

The ether functionalities present within the structure of metaldehyde indicate it could have strong interactions with acidic species. Preliminary screening results demonstrated that polymeric adsorbents and ion-exchange resins with basic functionalities cannot degrade metaldehyde, while ion-exchange resins with both weak and

strong acid functionalities showed notable degradation performance, especially strong acid functionalised ion-exchangers, such as S957. Hence, a detailed investigation into metaldehyde removal by polymeric ion-exchange resin S957 was conducted, while comparative data were obtained by studying non-functionalised MN200 and GAC. Kinetic results indicated that the rate of metaldehyde adsorption is affected by surface area and the presence of surface functional groups; adsorption on GAC showed the fastest kinetics, while the ion-exchange resin S957 exhibited the slowest adsorption rate because of the very small surface area. Analysis of the kinetic data showed adsorption on GAC and MN200 to be limited by particle diffusion, while the rate determining step of S957 was diffusion of metaldehyde through the solid/liquid interface. In contrast, isothermal studies showed GAC and MN200 to have similar adsorption capacities; comparatively S957 exhibited a capacity two orders of magnitude greater. This may be related to the greater affinity of S957 for metaldehyde, than either GAC or MN200, according to parameters determined using the Freundlich equation. Leaching tendency experiments showed that complete degradation of metaldehyde was achieved by S957, confirming strong acid functionality is a desirable property; however, the kinetic performance of S957, directly related to the porous character, was too poor for practical application.

Mesoporous SBA-15 silica samples with different degree of sulfonic acid functionalities (SA-SBA-15) were, therefore, synthesised using the tri-block template method. SA-SBA-15 samples showed excellent catalytic performance for the degradation of metaldehyde, with acetaldehyde as the only by-product. Kinetic studies showed that the rate of degradation was related to accessibility of metaldehyde molecules to the active sites present within the pores of the catalyst; such that pore size and pore volume have a significant effect on kinetic performance. Experimental results demonstrated that high extent of functionalities were not desirable since this compromises the porosity of the silica samples, resulting in slower kinetics. The only by-product, acetaldehyde, could be chemically adsorbed by amine functionalised sili-

ca samples (AF-SBA-15) or ion-exchanger A830, with A830 exhibiting much better adsorption capacity due to its porous structure; this suggested the development of a novel dual-stage method, with the first stage efficiently degrading metaldehyde into acetaldehyde and the second stage adsorbing acetaldehyde by amine functionalised ion-exchangers.

Although SA-SBA-15 samples exhibited excellent catalytic performance for metaldehyde degradation, their very small particle size (<10 μm) hinders practical application due to significant pressure drop when applied in fixed-bed reactors. Furthermore, mass production or commercialization of SA-SBA-15 would require considerable research. This project was furthered by working with Purolite International, a world leading manufacturer of polymeric adsorbents, ion-exchange resins and catalysts to produce and evaluate a novel category of Macronets with both good porosity and a range of extents of functionalisation. The results demonstrated that efficacious metaldehyde removal was achieved by using macroporous sulfonic functionalised Macronets as catalysts and amine functionalised ion-exchange resin as adsorbent. Heterogeneous catalyst selectivity tests confirmed that metaldehyde was efficiently degraded to only acetaldehyde. Again, a high degree of functionality is not necessarily required to obtain good catalytic performance, since the introduction of functional groups compromises the porosity significantly. Macronet sample MN502, with considerable surface area, large pore size and volume, showed the best kinetic performance and is the most cost-effective in this category of materials. Competing ion effects studies showed that event in the presence of significant quantities of competing ions (Ca^{2+} concentration is 100 times higher than metaldehyde); the catalytic performance maintained quite good levels. This limited influence of inorganic ions was observed because the interaction between sulfonic acid and Ca^{2+} is an ion-exchange process while that between sulfonic and metaldehyde is a heterogeneous catalytic process, meaning that even when the bed is exhausted in terms of removing inorganic ions, it is still capable of degrading metaldehyde. The breakthrough curve of the dual-column

study confirmed this effective degradation of metaldehyde by MN502 and the complete removal of acetaldehyde by the second bed packed with ion-exchange resin A830. The real surface water demonstration experiments confirmed the proposed mechanisms and indicated that the developed method was also effective in treating actual water samples.

In summary, this project identifies the reason why current GAC treatment methods fail to remove metaldehyde from water supplies, leading to the design and synthesis of novel materials. A dual-stage method was developed in this work, demonstrating that it effectively removes metaldehyde from synthetic water samples and actual surface water samples. The method developed in this work is especially promising because it can be adapted to current facilities in water treatment works simply packing the developed materials in the fixed-bed reactors; making it very cost-effective and easy to apply at large scale.

8.2 Future Work

The lab work conducted in this work demonstrated that the developed materials and method are promising to address the metaldehyde issue across UK. However, there are some aspects required to be considered and investigated before it is actually deployed in water treatment works. The pilot-scale column test are undertaking by ACWA Services Ltd to optimise the design of adding the MN502 packed column to the existing method flow. Furthermore, the treatability under evaluating is set as evaluated in the lab, namely, 20-30 bed volumes per hour. This treatability gives the basic engineering information when design the pilot column, that is the empty bed contacting time is 2-3 min, which is used to calculate the flow rate given the dimensions of the column. Eventually, every design should consider the cost of the process. MN502 is the cheapest of all the investigated Macronets but the cost of the whole method should be calculated when optimisation is finished.

Time, funding and instrumentation limits experienced in this project restricted the

full scope of the work that could be performed, hence, it is suggested that the study could be expanded and developed to probe the following themes in the future:

- Metaldehyde removal performance in a fixed-bed reactor could be investigated, by determining the effects of water quality (such as pH, initial concentrations of metaldehyde and competing species), as well as empty bed contact time (EBCT) on degradation performance.
- More detailed rapid small-scale column tests could be conducted with controlled water qualities and EBCTs to inform the modelling of the performance of large-scale or full-scale fixed-bed reactors.
- Pilot-scale tests could be carried out to test the stability of the developed method, with comparison of the performance with that of the rapid small-scale column tests, or the modelled performance, to fully evaluate the accuracy of the developed model.

References

Adriano Zecchina, S. Bordiga, et al. (2011). Selective Nanocatalysts and Nanoscience. UK, Wiley-VCH.

Atkins, P. and J. d. Paula (2009). Physical Edition, 9th Edition. United Kingdom, W.H. Freeman.

Autin, O., J. Hart, et al. (2012). "Comparison of UV/H_2O_2 and UV/TiO_2 for the degradation of metaldehyde: Kinetics and the impact of background organics." Water Research **46**(17): 5655-5662.

Autin, O., J. Hart, et al. (2013). "Comparison of UV/H_2O_2 and UV/TiO_2 processes in an annular photoreactor for removal of micropollutants: Influence of water parameters on metaldehyde removal, quantum yields and energy consumption." Applied Catalysis B: Environmental **138**: 268-275.

Autin, O., J. Hart, et al. (2013). "The impact of background organic matter and alkalinity on the degradation of the pesticide metaldehyde by two advanced oxidation processes: UV/H_2O_2 and UV/TiO_2." Water Research **47**(6): 2041-2049.

Baerlocher, C. and L. B. McCusker. (2001). "Database of zeolite structures." from http://www.iza-structure.org/databases/.

Banerjee, K., G. L. Amy, et al. (2008). "Kinetic and thermodynamic aspects of adsorption of arsenic onto granular ferric hydroxide (GFH)." Water Research **42**(13): 3371-3378.

Barclay, G., D. Medeiros, et al. (1995). "Thermal Stability of Sulfonate Ester Photoacid Generators in Phenolic Matrixes." Chemistry of Materials **7**(7): 1315-1324.

Barnett, S. A., A. T. Hulme, et al. (2005). "A low-temperature redetermination of metaldehyde." Acta Crystallographica Section E: Structure Reports Online **61**(4): o857-o859.

Barrett, E. P., L. G. Joyner, et al. (1951). "The determination of pore volume and area distributions in porous substances. I. Computations from nitrogen isotherms." Journal of the American Chemical Society **73**(1): 373-380.

Behnamfard, A. and M. M. Salarirad (2009). "Equilibrium and kinetic studies on free cyanide adsorption from aqueous solution by activated carbon." Journal of Hazardous Materials **170**(1): 127-133.

Bevington, J. (1952). "The polymerisation of aldehydes." Quarterly Reviews, Chemical Society **6**(2): 141-156.

Biškup, B. and B. Subotić (2004). "Kinetic analysis of the exchange processes between sodium ions from zeolite A and cadmium, copper and nickel ions from solutions." Separation and Purification Technology **37**(1): 17-31.

Blanchard, G., M. Maunaye, et al. (1984). "Removal of heavy metals from waters by means of natural zeolites." Water Research **18**(12): 1501-1507.

Boehm, H. and M. Voll (1970). "Basische Oberflächenoxide auf Kohlenstoff—I. Adsorption von säuren." Carbon **8**(2): 227-240.

Bowker, M. (1998). The Basis and Applications of Heterogeneous Catalysis Oxford, Oxford University Press.

Boyd, G., A. Adamson, et al. (1947). "The exchange adsorption of ions from aqueous solutions by organic zeolites. II. Kinetics1." Journal of the American Chemical Society **69**(11): 2836-2848.

Bristol Water. (2013). "Metaldehdye Action Project " Retrieved 12/03/2014, 2014, from http://www.bristolwater.co.uk/environment/catchment-protection/metaldehyde-action-project/.

Brunauer, S., L. S. Deming, et al. (1940). "On a theory of the van der Waals adsorption of gases." Journal of the American Chemical Society **62**(7): 1723-1732.

Brunauer, S., P. H. Emmett, et al. (1938). "Adsorption of gases in multimolecular layers." Journal of the American Chemical Society **60**(2): 309-319.

Buerge, I. J., H.-R. Buser, et al. (2006). "Occurrence and fate of the cytostatic drugs cyclophosphamide and ifosfamide in wastewater and surface waters." Environmental Science & Technology **40**(23): 7242-7250.

Bui, T. X. and H. Choi (2009). "Adsorptive removal of selected pharmaceuticals by mesoporous silica SBA-15." Journal of Hazardous Materials **168**(2): 602-608.

Burleigh, M. C., M. A. Markowitz, et al. (2002). "Porous polysilsesquioxanes for the adsorption of phenols." Environmental Science & Technology **36**(11): 2515-2518.

Cestari, A. R., E. F. S. Vieira, et al. (2008). "The removal of the indigo carmine dye from aqueous solutions using cross-linked chitosan—Evaluation of adsorption thermodynamics using a full factorial design." Journal of Hazardous Materials **153**(1): 566-574.

Chen, H., J. Zhao, et al. (2011). "Isotherm, thermodynamic, kinetics and adsorption mechanism studies of methyl orange by surfactant modified silkworm exuviae." Journal of Hazardous Materials **192**(1): 246-254.

Chen, H., J. Zhao, et al. (2011). "Isotherm, thermodynamic, kinetics and adsorption mechanism studies of methyl orange by surfactant modified silkworm exuviae." Journal of Hazardous Materials.

Chien, S. and W. Clayton (1980). "Application of Elovich equation to the kinetics of phosphate release and sorption in soils." Soil Science Society of America Journal **44**(2): 265-268.

Cole-Hamilton, D. J. (2003). "Homogeneous catalysis--new approaches to catalyst separation, recovery, and recycling." Science **299**(5613): 1702-1706.

Cooper, C. and R. Burch (1999). "Mesoporous materials for water treatment processes." Water Research **33**(18): 3689-3694.

Costal and Marine Geology Program. (2001). "U.S.Geological Survey Open File Report-01-041." from

http://pubs.usgs.gov/of/2001/of01-041/htmldocs/clays/smc.htm.
Crawford Scientific. (2014). "Optimising GC Temperature Programming." Retrieved 12 Feb, 2014, from http://www.chromacademy.com/chromatography-Optimising-GC-Temperature-Programming.html.
Cvetanović, R. and Y. Amenomiya (1972). "A temperature programmed desorption technique for investigation of practical catalysts." Catalysis Reviews **6**(1): 21-48.
D.H. Ripin, D. A. E. (2005). "pKa's of Inorganic and Oxo-Acids Substrate." Chemistry 206.
Das, D., J.-F. Lee, et al. (2001). "Sulfonic acid functionalized mesoporous MCM-41 silica as a convenient catalyst for Bisphenol-A synthesis." Chemical Communications(21): 2178-2179.
Daughton, C. G. (2004). "Non-regulated water contaminants: emerging research." Environmental Impact Assessment Review **24**(7): 711-732.
Doğan, M., M. Alkan, et al. (2004). "Kinetics and mechanism of removal of methylene blue by adsorption onto perlite." Journal of Hazardous Materials **109**(1): 141-148.
Dolder, L. K. (2003). "Metaldehyde toxicosis." Veterinary Medicine **98**(3): 213-215.
Doria, F. C., A. Borges, et al. (2013). "Removal of metaldehyde through photocatalytic reactions using nano-sized zinc oxide composites." Water, Air, & Soil Pollution **224**(2): 1-9.
Douglas A. Skoog, Donald M. West, et al. (2013). Fundamentals of Analytical Chemistry (9th Edition). Hampshire, Brooks/Cole Cengage Learning.
Edwards, R. (2010) "Slug-killing pellets blamed for Scottish water contamination."
Edwards, R. H., T. A. Williams, et al. (1978). Ether Phosphoric acid compound. U. S. P. Office, United States Patents 4,093,622.
European Commision (1998). Drinking Water Directive 98/83/EC, European Commission.
European Commision (2000). Water Framework Directives 2000/60/EC, European Commission.
European Commision (2006). Groundwater Daughter Directive 2006/118/EC, European Commission.
Evgenidou, E. and K. Fytianos (2002). "Photodegradation of triazine herbicides in aqueous solutions and natural waters." Journal of agricultural and food chemistry **50**(22): 6423-6427.
Ewlad-Ahmed, A. M., M. A. Morris, et al. (2012). "Removal of Formaldehyde from Air Using Functionalized Silica Supports." Environmental Science & Technology **46**(24): 13354-13360.
Falconer, J. L. and J. A. Schwarz (1983). "Temperature-programmed desorption and reaction: applications to supported catalysts." Catalysis Reviews Science and Engineering **25**(2): 141-227.

Farnetti, E., R. D. Monte, et al. (2011). Inorganic and bioorganic chemistry-Volume II homogeneous and heterogeneous catalysis. Italy, Encyloppedia of life support system (EOLSS).

Faust, S. D. and O. M. Aly (1987). Adsorption Processes for water treatment. London, Butterworths.

Feng, X., G. Fryxell, et al. (1997). "Functionalized monolayers on ordered mesoporous supports." Science **276**(5314): 923-926.

Freundlich, H. (1926). Colloid and Cappilary chemistry. London, Methuen and Co.

Ganesan, V. and A. Walcarius (2004). "Surfactant templated sulfonic acid functionalized silica microspheres as new efficient ion exchangers and electrode modifiers." Langmuir **20**(9): 3632-3640.

Gates, B. C. (1991). Catalytic Chemistry. United States of America, John Wiely & Sons, Inc.

Giesche, H. (2006). "Mercury porosimetry: a general (practical) overview." Particle & Particle Systems Characterization **23**(1): 9-19.

Goertzen, S. L., K. D. Thériault, et al. (2010). "Standardization of the Boehm titration. Part I. CO2 expulsion and endpoint determination." Carbon **48**(4): 1252-1261.

Goldstein, J., D. E. Newbury, et al. (2007). Scanning Electron Microscopy and X-ray Microanalysis: Third Edition. New York, Springer.

Gorgulho, H. F., J. P. Mesquita, et al. (2008). "Characterization of the surface chemistry of carbon materials by potentiometric titrations and temperature-programmed desorption." Carbon **46**(12): 1544-1555.

Graham Hill and J. Holman (2011). CHemistry in context 6th Edtion Oxford, Nelson Thornes.

Gregg, S. J. and K. S. W. Sing (1982). Adsorption, Surface Area and Porosity 2nd Edition. London, Academic Press

Gupta, S. S. and K. G. Bhattacharyya (2006). "Adsorption of Ni (II) on clays." Journal of Colloid and Interface Science **295**(1): 21-32.

Gupta, V., B. Gupta, et al. (2011). "A comparative investigation on adsorption performances of mesoporous activated carbon prepared from waste rubber tire and activated carbon for a hazardous azo dye—Acid Blue 113." Journal of Hazardous Materials **186**(1): 891-901.

Haggerty, G. M. and R. S. Bowman (1994). "Sorption of chromate and other inorganic anions by organo-zeolite." Environmental Science & Technology **28**(3): 452-458.

Hall, T. (2010 March 23rd). Removal of metaldehyde and other pesticides. CIWEM Drinking Water Quality Conference on Emerging Contaminants and Advanced Treatment Technologies. London, WRc

Hall, T. (2011 June 7-8th). Treatment for Metaldehyde and Other Problem Pesticides. 4th Developments in Water Treatment and Supply Conference. Cheltenham, WRc**:** 7-8 June 2011.

Halling-Sørensen, B., S. Nors Nielsen, et al. (1998). "Occurrence, fate and effects of

pharmaceutical substances in the environment-a review." Chemosphere **36**(2): 357-393.

Halsey, G. (1948). "Physical adsorption on non-uniform surfaces." The Journal of Chemical Physics **16**(10): 931.

Hameed, B. (2009). "Evaluation of papaya seeds as a novel non-conventional low-cost adsorbent for removal of methylene blue." Journal of Hazardous Materials **162**(2): 939-944.

Hameed, B. and M. El-Khaiary (2008). "Equilibrium, kinetics and mechanism of malachite green adsorption on activated carbon prepared from bamboo by K_2CO_3 activation and subsequent gasification with CO_2." Journal of Hazardous Materials **157**(2): 344-351.

Hameed, B., J. Salman, et al. (2009). "Adsorption isotherm and kinetic modeling of 2, 4-D pesticide on activated carbon derived from date stones." Journal of Hazardous Materials **163**(1): 121-126.

Hanafiah, M. A. K. M., W. S. W. Ngah, et al. (2012). "Acid Blue 25 adsorption on base treated *Shorea dasyphylla* sawdust: Kinetic, isotherm, thermodynamic and spectroscopic analysis." Journal of Environment Science **24**(2): 261-268.

Hayashi, T., M. Kumita, et al. (2005). "Removal of acetaldehyde vapor with impregnated activated Carbons: Effects of steric structure on impregnant and acidity." Environmental Science & Technology **39**(14): 5436-5441.

Helfferich, F. (1995). Ion exchange. New York, Dover Publications.

Hendricks, D. (2011). Fundamentals of water treatment unit processes. United States of America CRC Press

Hill, T. L. (1949). "Physical Adsorption on Non‐Uniform Surfaces." The Journal of Chemical Physics **17**(1): 106-106.

Ho, Y.-S. and G. McKay (2000). "The kinetics of sorption of divalent metal ions onto sphagnum moss peat." Water Research **34**(3): 735-742.

Ho, Y. and G. McKay (1998). "A comparison of chemisorption kinetic models applied to pollutant removal on various sorbents." Process safety and environmental protection: transactions of the Institution of Chemical Engineers, Part B **76**(4): 332-340.

Ho, Y. and G. McKay (1998). "Sorption of dye from aqueous solution by peat." Chemical Engineering Journal **70**(2): 115-124.

Ho, Y. and G. McKay (1999). "Pseudo-second order model for sorption processes." Process Biochemistry **34**(5): 451-465.

Ho, Y. S. (2006). "Review of second-order models for adsorption systems." Journal of Hazardous Materials **136**(3): 681-689.

Ho, Y. S. and G. McKay (2000). "The kinetics of sorption of divalent metal ions onto sphagnum moss peat." Water Research **34**(3): 735-742.

Hong, S., C. Wen, et al. (2009). "Adsorption thermodynamics of Methylene Blue onto bentonite." Journal of Hazardous Materials **167**(1-3): 630-633.

Huo, S. H. and X. P. Yan (2012). "Metal–organic framework MIL-100 (Fe) for the

adsorption of malachite green from aqueous solution." Journal of Materials Chemistry **22**(15): 7449-7455.

Iftikhar, A. R., H. N. Bhatti, et al. (2009). "Kinetic and thermodynamic aspects of Cu (II) and Cr (III) removal from aqueous solutions using rose waste biomass." Journal of Hazardous Materials **161**(2-3): 941-947.

Iowa State University. (2014). "How the SEM works." Retrieved 14/02, 2014, from http://www.mse.iastate.edu/?page_id=3679&preview=true.

Jackson, R. E. (2004). "Recognizing emerging environmental problems: the case of chlorinated solvents in groundwater." Technology and Culture **45**(1): 55-79.

John C. Crittenden, R. Rhodes Trussell, et al. (2012). MWH's Water Treatment: Principles and Design, 3rd Edition. New York, John Wiley & Sons Inc.

Johnson, A. C., M. D. Jürgens, et al. (2008). "Do cytotoxic chemotherapy drugs discharged into rivers pose a risk to the environment and human health? An overview and UK case study." Journal of hydrology **348**(1): 167-175.

Kiselev, A. (1968). "Adsorption properties of hydrophobic surfaces." Journal of Colloid and Interface Science **28**(3): 430-442.

Kolpin, D. W., E. M. Thurman, et al. (1998). "The environmental occurrence of herbicides: the importance of degradates in ground water." Archives of Environmental Contamination and Toxicology **35**(3): 385-390.

Krätschmer, W., J. Rathouský, et al. (1999). "Adsorption of krypton at 77K on fullerene C_{60}, graphitized carbon black and diamond." Carbon **37**(2): 301-305.

Kruk, M., T. Asefa, et al. (2002). "Metamorphosis of ordered mesopores to micropores: periodic silica with unprecedented loading of pendant reactive organic groups transforms to periodic microporous silica with tailorable pore size." Journal of the American Chemical Society **124**(22): 6383-6392.

Kruk, M., M. Jaroniec, et al. (2000). "Characterization of the porous structure of SBA-15." Chemistry of Materials **12**(7): 1961-1968.

Kumar, K. V. and S. Sivanesan (2006). "Selection of optimum sorption kinetics: comparison of linear and non-linear method." Journal of Hazardous Materials **134**(1): 277-279.

Kuwata, K., M. Uebori, et al. (1983). "Determination of aliphatic aldehydes in air by liquid chromatography." Analytical Chemistry **55**(12): 2013-2016.

L.S. Pereira, Ian Cordery, et al. (2009). Coping with Water Scarcity: Addressing the Challenges. UK, Springer

Lagergren, S. (1898). "About the theory of so-called adsorption of soluble substances." Kungliga Svenska Vetenskapsakademiens Handlingar **24**(4): 1-39.

Langmuir, I. (1915). "CHEMICAL REACTIONS AT LOW PRESSURES. 1." Journal of the American Chemical Society **37**(5): 1139-1167.

Langmuir, I. (1916). "The Constitution and Fundamental Properties of Solids and Liquids.Part I. Solids. " Journal of the American Chemical Society **38**(11): 2221-2295.

Lee, C. R., H. S. Kim, et al. (2011). "Pseudo First Order Adsorption Kinetics of N719 Dye on TiO_2 Surface." ACS Applied Materials & Interfaces.

Li, Y. H., Z. Di, et al. (2005). "Adsorption thermodynamic, kinetic and desorption studies of Pb^{2+} on carbon nanotubes." Water Research **39**(4): 605-609.

Lindström, A., I. J. Buerge, et al. (2002). "Occurrence and environmental behavior of the bactericide triclosan and its methyl derivative in surface waters and in wastewater." Environmental Science & Technology **36**(11): 2322-2329.

Low, M. (1960). "Kinetics of Chemisorption of Gases on Solids." Chemical Reviews **60**(3): 267-312.

Lucci, P., D. Pacetti, et al. (2012). "Current Trends in Sample Treatment Techniques for Environmental and Food Analysis." Chromatography -The most Versatile Method of Chemical Analysis: 127.

Ma, J., Y. Z. Jia, et al. (2010). "Equilibrium models and kinetic for the adsorption of methylene blue on Co-hectorites." Journal of Hazardous Materials **175**(1-3): 965-969.

Margolese, D., J. Melero, et al. (2000). "Direct syntheses of ordered SBA-15 mesoporous silica containing sulfonic acid groups." Chemistry of Materials **12**(8): 2448-2459.

Marshall, J. (2013). Briefing paper on metaldehdye UK.

Mbaraka, I. K., D. R. Radu, et al. (2003). "Organosulfonic acid-functionalized mesoporous silicas for the esterification of fatty acid." Journal of Catalysis **219**(2): 329-336.

Michael Smith, J. M. (2007). March's Advanced Organic Chemistry: Reactions, Mechanisms, And Structure 6th Edition. New York, John Wiley & Sons.

Misono, M. (2013). Basis of Heterogeneous Catalysis. USA, Elsevier B.V.

Montgomery, J. M. (1985). Water treatment principles and design. New York, John Wiley &Sons, Inc.

Moreno-Castilla, C. (2004). "Adsorption of organic molecules from aqueous solutions on carbon materials." Carbon **42**(1): 83-94.

Mori, Y. and T. J. Pinnavaia (2001). "Optimizing organic functionality in mesostructured silica: direct assembly of mercaptopropyl groups in wormhole framework structures." Chemistry of Materials **13**(6): 2173-2178.

MSG. (2014). "Get Pelletwise-Metaldehyde Stewartship Group." Retrieved 14/03/2014, 2014, from http://www.getpelletwise.co.uk/.

Neagu, V., I. Untea, et al. (2003). "Retention of chromate ion by conventional and N-ethylpyridinium strongly basic anion exchange resins." Reactive and Functional Polymers **57**(2): 119-124.

Nemr, A. E. (2009). "Potential of pomegranate husk carbon for Cr (VI) removal from wastewater: Kinetic and isotherm studies." Journal of Hazardous Materials **161**(1): 132-141.

Nolte, I. (2012). "Toxicity of metaldehyde in the dog and cat." Praktische Tierarzt **93**(10): 886.

Norit (2010). Datasheet of activated carbon CNR115 http://www.norit.com/files/documents/CNR_115_rev9.pdf.

Norit. (2014). "Technical Datasheet of Norit activated carbon CA1." http://www.norit.com/products-and-services/products/norit-ca-1/.

Oickle, A. M., S. L. Goertzen, et al. (2010). "Standardization of the Boehm titration: Part II. Method of agitation, effect of filtering and dilute titrant." Carbon **48**(12): 3313-3322.

Organization, W. H. O. a. F. a. A. (1996). WHO/FAO data sheets on pesticides, Number 93: Metaldehdye. W. a. FAO. U.S., WHO and FAO.

Pal, A., K. Y.-H. Gin, et al. (2010). "Impacts of emerging organic contaminants on freshwater resources: review of recent occurrences, sources, fate and effects." Science of the Total Environment **408**(24): 6062-6069.

Parsons, S. (2004). Advanced oxidation processes for water and wastewater treatment, IWA publishing.

Parsons, S. A. and B. Jefferson (2006). Introduction to Potable Water Treatment Processes United Kingdoms, Blackwell.

Paul Otto Schallert, C. C. F. (1968). Process for purifying wet process phosphoric acid with ethyl ether, United States Patents 3,367,738.

Penczek, S., K. Kaluzynski, et al. (2007). "Addition of H3PO4 to diglycidyl ethers of bisphenol A: Kinetics and product structure." Journal of Applied Polymer Science **105**(1): 246-254.

Possanzini, M. and V. DiPalo (1995). "Determination of olefinic aldehydes and other volatile carbonyls in air samples by DNPH-coated cartridges and HPLC." Chromatographia **40**(3-4): 134-138.

Purolite. (2014). "Purolite International product infromation database ", from www.purolite.com.

Riaz, M., R. Nadeem, et al. (2009). "Pb (II) biosorption from hazardous aqueous streams using Gossypium hirsutum (Cotton) waste biomass." Journal of Hazardous Materials **161**(1): 88-94.

Richardson, J. A., S. L. Welch, et al. (2003). "Metaldehyde toxicoses in dogs." Compendium on Continuing Education for the Practicing Veterinarian **25**(5): 376-380.

Richardson, M. L. and J. M. Bowron (1985). "The fate of pharmaceutical chemicals in the aquatic environment." Journal of Pharmacy and Pharmacology **37**(1): 1-12.

Richardson, S. D. (2011). Encyclopedia of Environmental Health. Burlington MA, US, Elsevier.

Richardson, S. D. and T. A. Ternes (2005). "Water analysis: emerging contaminants and current issues." Analytical Chemistry **77**(12): 3807-3838.

Richardson, S. D. and T. A. Ternes (2011). "Water analysis: emerging contaminants and current issues." Analytical Chemistry **83**(12): 4614-4648.

Roop Chand Bansal, J., ean-Baptiste Donnet, et al. (1988). Activated Carbon. New York, Marcel Dekker Inc.

Rouquerol, J., D. Avnir, et al. (1994). "Recommendations for the characterization of porous solids (Technical Report)." Pure and Applied Chemistry **66**(8): 1739-1758.

Rožić, M., Š. Cerjan-Stefanović, et al. (2000). "Ammoniacal nitrogen removal from water by treatment with clays and zeolites." Water Research **34**(14): 3675-3681.

Salame, I. I. and T. J. Bandosz (2001). "Surface chemistry of activated carbons: combining the results of temperature-programmed desorption, Boehm, and potentiometric titrations." Journal of Colloid and Interface Science **240**(1): 252-258.

Sanches, S., M. T. Barreto Crespo, et al. (2010). "Drinking water treatment of priority pesticides using low pressure UV photolysis and advanced oxidation processes." Water Research **44**(6): 1809-1818.

Seiler, R. L., S. D. Zaugg, et al. (1999). "Caffeine and pharmaceuticals as indicators of waste water contamination in wells." Ground Water **37**(3): 405-410.

Selim, S. and J. N. Seiber (1973). "Gas chromatographic method for the analysis of metaldehyde in crop tissue." Journal of Agricultural and Food Chemistry **21**(3): 430-433.

Senthilkumaar, S., P. Varadarajan, et al. (2005). "Adsorption of methylene blue onto jute fiber carbon: kinetics and equilibrium studies." Journal of Colloid and Interface Science **284**(1): 78-82.

Sharpless, C. M. and K. G. Linden (2003). "Experimental and model comparisons of low-and medium-pressure Hg lamps for the direct and H2O2 assisted UV photodegradation of N-nitrosodimethylamine in simulated drinking water." Environmental Science & Technology **37**(9): 1933-1940.

Shen, J. G., R. G. Herman, et al. (2002). "Sulfonic acid-functionalized mesoporous silica: Synthesis, characterization, and catalytic reaction of alcohol coupling to ethers." Journal of Physical Chemistry B **106**(39): 9975-9978.

Shieh, F.-K., C.-T. Hsiao, et al. (2013). "A bioconjugated design for amino acid-modified mesoporous silicas as effective adsorbents for toxic chemicals." Journal of hazardous materials **260**: 1083-1091.

Siminiceanu, I., I. Lazau, et al. (2008). "Textural Characterization of a New Iron-Based Ammonia Synthesis Catalyst." Chemical Bulleten “Politehnica” University **53**(67): 1-2.

Sing, K. S. (1989). "The use of physisorption for the characterization of microporous carbons." Carbon **27**(1): 5-11.

Sing, K. S. W., D.H.Everett, et al. (1985). "Reporting physisorption data for gas/solid systems with special reference to the determination of surface area and porosity (Recommendations 1984)." Pure and Applied Chemistry, IUPAC Publications **57**(4): 603-619.

Sperling, M., A. Schoenfelder, et al. (2010). "Metaldehyde poisoning in a horse: an actual case report." Wiener Tierarztliche Monatsschrift **97**(11-12): 290-293.

Standley, L. J., R. A. Rudel, et al. (2008). "Wastewater‐contaminated groundwater as a source of endogenous hormones and pharmaceuticals to surface water ecosystems." Environmental toxicology and chemistry **27**(12): 2457-2468.

Steenbergen, V. M. (2004). "Toxicology brief: Taking the bait - Metaldehyde toxicosis." Veterinary Technician **25**(4): 259-261.

Stuart, M., D. Lapworth, et al. (2012). "Review of risk from potential emerging contaminants in UK groundwater." Science of the Total Environment **416**: 1-21.

Sundaram, C. S., N. Viswanathan, et al. (2008). "Defluoridation chemistry of synthetic hydroxyapatite at nano scale: equilibrium and kinetic studies." Journal of Hazardous Materials **155**(1-2): 206-215.

Tan, I., A. L. Ahmad, et al. (2008). "Adsorption of basic dye on high-surface-area activated carbon prepared from coconut husk: Equilibrium, kinetic and thermodynamic studies." Journal of Hazardous Materials **154**(1-3): 337-346.

Tao, B. and A. J. Fletcher (2013). "Metaldehyde removal from aqueous solution by adsorption and ion exchange mechanisms onto activated carbon and polymeric sorbents." Journal of Hazardous Materials **244**: 240-250.

The Council of The European Union (1998). Council Directive 98/83/EC on the quality of water intended for human consumption European Union, Ofiicial Journal of the European Comminities.

Thommes, M., R. Köhn, et al. (2002). "Sorption and pore condensation behavior of pure fluids in mesoporous MCM-48 silica, MCM-41 silica, SBA-15 silica and controlled-pore glass at temperatures above and below the bulk triple point." Applied surface science **196**(1): 239-249.

Thomson, J., F. Roddick, et al. (2002). "Natural organic matter removal by enhanced photo-oxidation using low pressure mercury vapour lamps." Water Supply **2**(5-6): 435-443.

Toepfer, B., A. Gora, et al. (2006). "Photocatalytic oxidation of multicomponent solutions of herbicides: reaction kinetics analysis with explicit photon absorption effects." Applied Catalysis B: Environmental **68**(3): 171-180.

Tsai, C.-T., Y.-C. Pan, et al. (2009). "A simple one-pot route to mesoporous silicas SBA-15 functionalized with exceptionally high loadings of pendant carboxylic acid groups." Chemical Communications(33): 5018-5020.

Tseng, R.-L., F.-C. Wu, et al. (2003). "Liquid-phase adsorption of dyes and phenols using pinewood-based activated carbons." Carbon **41**(3): 487-495.

Uc, V. H., J. R. Alvarez-Idaboy, et al. (2008). "Theoretical explanation of nonexponential OH decay in reactions with benzene and toluene under pseudo-first-order conditions." The Journal of Physical Chemistry A **112**(33): 7608-7615.

UK Environmetal Agency (2009). The determination of metaldehdye in waters using chromatography with mass spectrometric detection UK http://www.environment-agency.gov.uk/static/documents/Research/Metaldehy

de-226b.pdf.
United Nations World Water Assessment Program (2003). The World Water Development Report 1:Water for People, Water for Life UNESCO Paris France.
University of Hertfordshire (2012). Pesticide Properties Database-Metaldehyde. UK.
Valderrama, C., J. I. Barios, et al. (2010). "Kinetic evaluation of phenol/aniline mixtures adsorption from aqueous solutions onto activated carbon and hypercrosslinked polymeric resin (MN200)." Reactive and Functional Polymers **70**(3): 142-150.
Valderrama, C., J. Cortina, et al. (2007). "Kinetics of sorption of polyaromatic hydrocarbons onto granular activated carbon and Macronet hyper-cross-linked polymers (MN200)." Journal of Colloid and Interface Science **310**(1): 35-46.
Valderrama, C., X. Gamisans, et al. (2007). "Kinetics of polycyclic aromatic hydrocarbons removal using hyper-cross-linked polymeric sorbents Macronet Hypersol MN200." Reactive and Functional Polymers. **67**(12): 1515-1529.
Van Rhijn, W., D. De Vos, et al. (1998). "Sulfonic acid functionalised ordered mesoporous materials as catalysts for condensation and esterification reactions." Chemical Communications(3): 317-318.
Vermeulen, T. (1953). "Theory for irreversible and constant-pattern solid diffusion." Industrial & Engineering Chemistry Research **45**(8): 1664-1670.
Vinu, A., V. Murugesan, et al. (2004). "Adsorption of lysozyme over mesoporous molecular sieves MCM-41 and SBA-15: influence of pH and aluminum incorporation." The Journal of Physical Chemistry B **108**(22): 7323-7330.
Vulliet, E. and C. Cren-Olivé (2011). "Screening of pharmaceuticals and hormones at the regional scale, in surface and groundwaters intended to human consumption." Environmental Pollution **159**(10): 2929-2934.
Water England and Wales (2000). The water supply (water quality) regulations 2000, No. 3184. W. E. a. Wales. UK, Water England and Wales.
Weber, W. and J. Morris (1963). "Kinetics of adsorption on carbon from solution." Journal of the Sanitary Engineering Division **89**(17): 31-60.
World Health Organization. (2002). "The World Health Report: Reducing risks, Promoting Healthy Life ".
Young, D. M. and A.D.Crowell (1962). Physical Adsorption of Gases. London, Butterworths.
Yuan, L., W. Lin, et al. (2011). "A ratiometric fluorescent probe for specific detection of cysteine over homocysteine and glutathione based on the drastic distinction in the kinetic profiles." Chemical Communications **47** (2011), 6275-6277.
Zeidan, R. K., S. J. Hwang, et al. (2006). "Multifunctional Heterogeneous Catalysts: SBA‐15‐Containing Primary Amines and Sulfonic Acids." Angewandte Chemie International Edition **45**(38): 6332-6335.
Zeldowitsch, J. (1934). "Über den mechanismus der katalytischen oxydation von CO an MnO2'." Acta Physicochim URS **1**: 364-449.

Zhang, J., P. J. Lioy, et al. (1994). "Characteristics of aldehydes: concentrations, sources, and exposures for indoor and outdoor residential microenvironments." Environmental Science & Technology **28**(1): 146-152.

Zhao, D., J. Feng, et al. (1998). "Triblock copolymer syntheses of mesoporous silica with periodic 50 to 300 angstrom pores." Science **279**(5350): 548-552.

Outcomes of the Project

Bing Tao and Ashleigh J. Fletcher; Metaldehyde Removal from Aqueous Solution by Adsorption and Ion-exchange Mechanism onto Activated Carbon and Polymeric Sorbents , *Journal of Hazardous Materials*, 244-245 (2013) 240-250.

http://dx.doi.org/10.1016/j.jhazmat.2012.11.014

Bing Tao and Ashleigh J. Fletcher; Catalytic degradation and adsorption of metaldehyde from drinking water by functionalised mesoporous silicas and ion-exchange resin, *Separation and Purification Technology*, 124 (2014) 195–200.

http://dx.doi.org/10.1016/j.seppur.2014.01.013

Bing Tao and Ashleigh J. Fletcher; Development and Optimization of a Novel Dual-stage Method for Metaldehyde Remediation from Water, ready to submit for publication.